

Dissertation
submitted to the combined Faculties for Natural Science and
Mathematics of the Ruprecht-Karls University of Heidelberg, Germany
for the degree of
Doctor for Natural Science

Presented by:
Nadine Stephanie Winn
Diploma: Biology, Humboldt University of Berlin, Germany
Date and place of birth: 02.07.1975 in Berlin, Germany

The differential Role of Insulin-like Growth Factor-I Isoforms in Skeletal Muscle

Referees:

Dr. Claus Nerlov (EMBL-Monterotondo)

Prof. Dr. Herman Bujard (University of Heidelberg)

Abstract

Insulin-like growth factor-1 (IGF-1) has pleiotropic effects on various tissues during pre- and postnatal development by stimulating proliferation and differentiation, and plays a major role in hypertrophy and tissue remodeling in the fetal, perinatal, and adult organism. In skeletal muscle the role of IGF-1 is well established, but questions remain about the significance of the various isoforms that are produced from the single-copy IGF-1 gene. By the use of different promoters, differential splicing and post-translational modifications, at least six IGF-1 isoforms are generated from the IGF-1 gene, that differ in the N-terminal signal peptide (Class) and the C-terminal E-peptide. The aim of this work was to dissect the different roles of IGF-1 isoforms in skeletal muscle *in vitro* and *in vivo*. Cell culture experiments revealed that IGF-1Ea isoforms promoted myogenic differentiation and cell hypertrophy, resulting in enlarged myofibers, while IGF-1Eb isoforms instead did not show an effect on fiber size but on proliferation of myoblasts. Correlating with the results obtained *in vitro*, transgenic animals over-expressing IGF-1Ea isoforms showed pronounced muscle fiber hypertrophy, accompanied by an increase in force generation and strength, while IGF-1Eb isoforms showed very mild effects on muscle size and no changes in muscle strength, further implicating the Ea-peptide in the hypertrophic response. Analysis of the intracellular signals transduced by the different IGF-1 isoforms revealed a complex regulatory network, excluding certain pathways previously implicated in the induction of skeletal muscle hypertrophy in response to IGF-1. Preliminary analysis of regeneration in response to IGF-1 isoforms demonstrated that each isoform enhanced the regeneration process, suggesting that Eb-peptide-containing isoforms did so by stimulating the proliferation of satellite cells, while IGF-1Ea enhanced the growth of newly forming fibers. Class 2 IGF-1Eb was found to specifically induce a calcineurin isoform (CnA β 1) that has been linked to enhanced regeneration. In addition, this thesis describes the cloning of a Class 2 IGF-1En isoform that was previously not described in rodent species, but known to exist in humans. The present work constitutes the first evidence for different functions of IGF-1 isoforms *in vitro* and *in vivo*, provides an overview of their variable effects in skeletal muscle and a strong basis for future research into their specific functions.

Zusammenfassung

Der Insulin-ähnliche Wachstumsfaktor-1 (IGF-1) spielt sowohl in der Embryonalentwicklung, als auch während der postnatalen Entwicklungsphase eine wichtige Rolle. Neben der Fähigkeit Zellwachstum und Zelldifferenzierung zu stimulieren, hat IGF-1 eine wichtige Funktion bei Vorgängen wie Muskel Hypertrophie und Regeneration. Die wichtige Rolle von IGF-1 in der Skelettmuskulatur ist seit langem bekannt, aber dennoch verbleiben viele Fragen über die Funktion der verschiedenen Isoformen, die ausgehend vom IGF-1 Gen gebildet werden. Durch die Nutzung verschiedener Promoter, differentiellem Spleißen und post-translationalen Modifizierungen, werden verschiedene IGF-1 Präpro-Proteine gebildet, die sich in der Kombination ihrer N-terminalen Signal-Peptide (Klasse) und C-terminalen Extensions-Peptide unterscheiden. Die vorliegende Arbeit zielte auf eine gründlich Analyse der Rolle verschiedener IGF-1 Isoformen in der Skelettmuskulatur *in vitro* und *in vivo*. Experimente in Zellkultur ergaben, dass IGF-1Ea Isoformen einen beschleunigten Differenzierungsvorgang induzierten, was auch eine Vergrößerung der Muskelfasern zur Folge hatte. IGF-1Eb Isoformen hingegen, zeigten einen Effekt auf die Proliferierung der Myoblasten und nicht auf deren Größe. In Übereinstimmung mit den *in vitro* Daten, zeigten transgene Mäuse, die IGF-1Ea Isoformen (Klasse 1 IGF-1Ea (=mIGF-1) und Klasse 2 IGF-1Ea) überexprimieren, ausgeprägte Muskel Hypertrophie, die mit einer erhöhten Muskelkraft einhergingen. Im Gegensatz dazu zeigten IGF-1Eb transgene Tiere einen sehr milden Phänotyp, der weder mit Hypertrophie, noch mit erhöhter Muskelkraft einherging. Dies unterstreicht noch einmal eine Verbindung zwischen der Präsenz des Ea-Peptides und der Induktion eines hypertrophen Phänotyps. Die Analyse der intrazellulären Signaltransduktionswege ergab ein komplex reguliertes Netzwerk und führte zum Ausschluss von Signaltransduktionswegen, die in früheren Publikationen für die Induktion von IGF-1-induzierter Hypertrophie vorgeschlagen wurden. Die vorläufige Analyse der Regenerationsprozesse in Folge von Cardiotoxin-Injektionen demonstrierte, dass alle IGF-1 Isoformen diesen Prozess beschleunigen konnten. Die Resultate implizieren, dass IGF-1 Isoformen, die das Eb-Peptid beinhalten die Proliferation von Satellitenzellen stimulieren, während Klasse 2 IGF-1Ea die Größe der neu formenden Muskelfasern erhöhen. Klasse 2 IGF-1Eb zeigte zusätzlich eine spezifische Induzierung der Calcineurin Isoform CnA β 1, die bereits mit verbesserter Muskelregenerierung in Verbindung gebracht wurde. Ausserdem beschreibt diese Arbeit die Klonierung einer Klasse 2 IGF-En Variante, die bisher nicht in Nagern beschrieben wurde, aber im Menschen existiert. Die vorliegende Arbeit liefert die ersten Beweise, dass IGF-1 Isoformen *in vitro* und *in vivo* andere Effekte hervorrufen und ebnet damit den Weg für die Zukunft spezifischere Fragen stellen zu können.

Acknowledgements

First I would like to thank my supervisor Professor Nadia Rosenthal for giving me the possibility to do my PhD in her laboratory. I want to thank her for her support and guidance, for critical discussions and useful suggestions, and most importantly, for always believing in me. I greatly appreciate her positive attitude and her capability of cheering me up when I had lost faith in my work.

I also want to thank all the other members of my thesis advisory committee, Dr. Claus Nerlov, Dr. Carl Neumann, and Professor Dr. Bujard for their critical evaluation of the process of my work, for their suggestions and also for assuring that I always stayed on the right track. In addition, I thank Professor Dr. Bujard for providing me with the pBi-2 and pUHrtTA plasmids.

I also greatly appreciated the useful discussions and suggestions I had with Antonio Musaro, and overall I want to thank him for the MLC/mlGF- mice that I included for the comparative studies in this thesis and for the electrophysiological data on his animals that he kindly provided for further comparison. In the same line I thank Antonio and his PhD student Emanuele Rizzuto for the collaboration in the analysis of the physiologic muscle phenotype of my transgenic mouse lines.

I owe special thanks to Jose Gonzalez, who injected all my constructs, our caretaker Marco III, and over all Esfir Slonimsky for taking care of my mice and also myself in all the years I spent with her. Thank you for everything Esfir!

Obviously, I also thank all the other members in the lab: Both Ekaterinas, Pascal, and Bianca for helping and guiding me through the cell culture work, Michele for many useful discussions and for his amusing jokes, and Maria-Paola for many conversations and for always having an open ear for my questions. I also thank Paschalis, Catarina, Olivier and Lieve for sharing the fate of being a PhD student. In addition I thank Olivier for his help in solving mathematical riddles and Lieve for the profound search for spelling mistakes in my thesis. A very special thank you goes to Enrique for helping me with all the RT-PCR work and initial analysis of the Affymetrix data. Just as special are Faye and Tommaso who were there for me until the very end! Thank you Faye for critical reading of my thesis, useful suggestions and precious guidance! Above all thank you Tommaso for your help in the presentation of the Affymetrix data, formatting of the figures, thank you for always being so nice and ready to help out when the time was running too fast!

I also greatly appreciated the hospitality of Professor Miranda Grounds, who treated me like her own student during my stay in her lab and was always open for profound discussions about our favorite topic: IGF-1 and skeletal muscle. In addition, I thank her Postdoc Dr. Thea Shavlakadze, who guided me through the histological analysis of my mice. I will also not forget the fun times we spent together!

Craig, Mark, Elke, Tiago, I thank all of you for distractions, lots of fun times, coffees and all that other good stuff we did together. Without you guys, I would have gone crazy!

And last, but not least, I want to thank my parents and my brother, who always supported me in my plans, believed in me, and helped me wherever they could! The same is true for Clemens, who was there for me during the last two years, distracted me and cheered me up. And finally I want to thank my best friend Melanie, who came all the way from Berlin to be there with me in the last few days before submission. Thank you for comforting me Melanie!

Table of contents

Page		
Abstract	3
Zusammenfassung	4
Acknowledgements	5
Table of contents	7
List of figures	11
List of tables	13
1	Introduction	14
1.1	Skeletal muscle development and structure	14
1.1.1	Overview of muscle development.....	14
1.1.2	Development of skeletal muscle structure	16
1.1.3	Skeletal muscle fiber types.....	19
1.2	Physiological and pathological remodeling of skeletal muscle	20
1.2.1	Skeletal muscle hypertrophy	20
1.2.2	Skeletal muscle atrophy	21
1.2.3	Skeletal muscle aging	22
1.3	Skeletal muscle injury and regeneration	23
1.3.1	Myofiber necrosis	24
1.3.2	Revascularization.....	25
1.3.3	Inflammatory cell infiltration and phagocytosis.....	25
1.3.4	Skeletal muscle fibrosis and scar formation.....	26
1.3.5	Satellite cell activation and myofiber regeneration.....	26
1.3.6	Reinnervation.....	29
1.4	The Insulin-like growth factor system.....	29
1.4.1	The IGF-1 system.....	29
1.4.2.	Insulin and Insulin-like growth factor-1 gene and protein structure	33
1.4.2.1	Insulin versus Insulin-like growth factor-1	33
1.4.2.2	IGF-1 gene structure	34
1.4.2.3	Complexity of IGF-1 transcription	34
1.4.2.4	Transcription start sites in exon 1 and 2	34
1.4.2.5	Differential splicing at the 5'-end of IGF-1 RNA precursors.....	35
1.4.2.6	Alternative splicing at the 3'-end of IGF-1 precursors	36
1.4.2.7	Polyadenylation signals in IGF-1 in IGF-1 RNA precursors	37
1.4.2.8	Translation of Class 1 and Class 2 mRNAs	37

1.4.2.9	Processing of IGF-1 prepro-peptides.....	38
1.4.3	Expression of IGF-1 isoforms	39
1.4.4	Expression of IGF-1 isoforms in skeletal muscle	40
1.4.5	IGF-1 signaling in skeletal muscle	41
1.4.5.1	IGF-1 and IGF-2 receptors	42
1.4.5.2	Pathways downstream of the IGF-1 receptor.....	43
1.4.5.3	MAP-kinase signaling.....	43
1.4.5.4	PI(3)-kinase signaling.....	44
1.4.5.5	Calcineurin signaling	47
1.5	Skeletal muscle-specific IGF-1 transgenic mice	50
1.6	Significance of this work.....	52
2	Materials and methods.....	53
2.1	Molecular Biology	53
2.1.1	DNA gel electrophoresis.....	53
2.1.2	Extraction of DNA from agarose gels.....	53
2.1.3	Plasmid purification	53
2.1.4	Transfection of bacteria for plasmid amplification	53
2.1.5	Cloning of IGF-1 isoforms.....	54
2.1.5.1	Design of skeletal muscle-specific expression vectors	55
2.1.5.2	Design of doxycycline-inducible expression vectors	55
2.1.6	Cloning of an exon 4-5 splice variant-containing IGF-1 isoform.....	56
2.1.7	Cloning of probes for Northern blot.....	57
2.1.8	Preparation of DNA for generation of transgenic lines	58
2.1.9	Genomic DNA isolation from mouse-tail biopsies and genotyping	58
2.1.9.1	Genotyping of IGF-1 isoform transgenic mice.....	58
2.1.9.2	Genotyping of MLC/rtTA mice	58
2.1.9.3	Genotyping of pBi/Class 1 IGF-1Eb transgenic mice	58
2.1.10	Total RNA preparation from mouse tissues	59
2.1.11	Total RNA isolation from cultured cells	59
2.1.12	Combined reverse transcription (RT)-PCR	59
2.1.13	Reverse transcription	59
2.1.14	SYBR green/Taqman quantitative RT-PCR.....	60
2.1.15	Northern blot analysis.....	61
2.1.16	GeneChip analysis	62
2.2	Cell Biology	63
2.2.1	Established myoblast cell culture and transfections.....	63

2.2.2	Skeletal muscle primary cell culture	64
2.3	Biochemistry.....	64
2.3.1	Preparation of protein lysates from mouse skeletal muscle	64
2.3.2	Preparation of protein lysates from cultured cells	64
2.3.3	Preparation of protein lysates for luciferase assay.....	65
2.3.4	Immunoprecipitation	65
2.3.5	Western blot analysis	65
2.3.6	Generation of IGF-1 antibodies	67
2.3.7	Immunoenzymometric assay (IEMA)	68
2.4	Histochemistry.....	68
2.4.1	Processing of tissues for frozen and paraffin sections	68
2.4.2	Double immunohistochemistry.....	68
2.4.3	Haematoxin/Eosin staining	69
2.4.4	Trichrome staining.....	69
2.4.5	Nicotinamide Adenine Dinucleotide Nitro-blue Tetrazolium (NADH-TR) staining	69
2.5	Animals	70
2.5.1	Experimental procedures.....	70
2.5.2	Electrophysiology	71
2.6	Statistical analysis.....	72
3	Results	73
3.1	A rodent IGF-1 isoform containing a third E-peptide	73
3.2	Effects of IGF-1 isoform over-expression <i>in vitro</i>	75
3.2.1	Transient transfection of L6E9 cells with inducible IGF-1 constructs	76
3.2.2	Morphology of IGF-1 isoform transfected cells	78
3.2.3	Effects of IGF-1 isoforms of myoblast proliferation	79
3.2.4	Effects of IGF-1 isoforms on myoblast proliferation and differentiation	81
3.3	Effects of IGF-1 isoforms <i>in vivo</i>	83
3.3.1	Generation of transgenic mouse lines	83
3.3.2	Expression analysis of transgenic founder lines	84
3.3.3	Skeletal muscle-specific transgene expression of transgenic lines	86
3.3.4	Comparison of expression levels to MLC/mIGF-1 transgenic line.....	87
3.3.5	Influence of IGF-1 isoforms on endogenous IGF-1 isoform expression	90
3.3.6	Effects of IGF-1 isoforms on body weight and weight of visceral organs	92
3.3.7	Effects of IGF-1 isoform over-expression on serum IGF-1 levels.....	95
3.3.8	Skeletal muscle weight of IGF-1 isoform transgenic lines.....	97
3.3.9	Histological analysis of IGF-1 isoform transgenic skeletal muscle	98

3.3.10	Skeletal muscle physiology of IGF-1 isoform transgenic skeletal muscle.....	103
3.3.11	IGF-1 isoform-mediated signaling.....	107
3.3.11a	Activation of the IGF-1 receptor in IGF-1 isoform transgenic lines	107
3.3.11b	Affymetrix GeneChip analysis of IGF-1 isoform transgenic muscles	108
3.3.11c	Kinetwork™ Phospho-site screen.....	112
3.3.11d	The calcineurin pathway.....	117
3.4	Regeneration of IGF-1 isoform transgenic muscle.....	118
3.4.1	Histological analysis of regeneration in IGF-1 isoform transgenic mice	119
3.4.2	Changes in endogenous IGF-1 isoform expression in response to injury	121
3.4.3	Expression of calcineurin isoforms in response to injury.....	124
4	Discussion	127
4.1	The rodent En-peptide.....	127
4.2	Effects of IGF-1 isoforms on myoblast proliferation	129
4.3	Effects of IGF-1 isoforms on myoblast differentiation and muscle growth	130
4.3.1	<i>In vitro</i> effects of IGF-1 isoforms.....	130
4.3.2	<i>In vivo</i> effects of IGF-1 isoforms.....	132
4.4	IGF-1 signaling in response to different IGF-1 isoforms.....	135
4.5	Effects of IGF-1 isoforms on regeneration of skeletal muscle	139
4.6	Future perspectives.....	141
Appendix A: List of Abbreviations		144
Appendix B: Affymetrix analysis.....		147
Appendix C: Ingenuity Pathway Analysis.....		155
Bibliography		161

List of figures

Figure 1.1	Fate map of a somite.....	14
Figure 1.2	Signaling in myogenesis.....	15
Figure 1.3	MyoD and myf-5 signaling in the development of epaxial and hypaxial muscle.....	16
Figure 1.4	Primary and secondary myogenesis.....	17
Figure 1.5	Skeletal muscle structure.....	19
Figure 1.6	Satellite cell activation in response to injury.....	27
Figure 1.7	Regenerating tibialis anterior.....	28
Figure 1.8	IGF-1 gene and protein structure.....	35
Figure 1.9	Overview of IGF-1/IGF-1R signaling.....	44
Figure 2.1	Cloning of IGF-1 isoforms from mouse liver.....	54
Figure 2.2	Schematic representation of skeletal muscle-specific expression cassette.....	55
Figure 2.3	Schematic representation of the skeletal muscle adapted “tet-on” system.....	56
Figure 2.4	IGF-1 antibodies.....	67
Figure 2.5	Electrophysiological analyses of skeletal muscle.....	72
Figure 3.1	Cloning and preliminary characterization of the rodent En-peptide.....	74
Figure 3.2	Expression analysis of transiently transfected L6E9 cells.....	77
Figure 3.3	Morphology of IGF-1 isoform transfected L6E9 cells.....	79
Figure 3.4	Effects of IGF-1 isoforms during growth.....	80
Figure 3.5	Effects of IGF-1 isoforms during differentiation.....	82
Figure 3.6	Northern blot analysis of transgene expression of founder lines.....	84
Figure 3.7	Northern comparison of transgenic founder line expression levels.....	85
Figure 3.8	Skeletal muscle-specific transgene expression.....	86
Figure 3.9	Comparison of selected lines to MLC/mlGF-1 transgenic line.....	87
Figure 3.10	Over-expression of IGF-1 transgenes.....	88
Figure 3.11	Protein expression of IGF-1 transgenes.....	89
Figure 3.12	Expression of endogenous Isoforms (1).....	91
Figure 3.13	Expression of endogenous isoforms (2).....	92
Figure 3.14	Effect of IGF-1 isoform expression on body weight.....	93
Figure 3.15	Effect of IGF-1 isoform expression on weight of visceral organs.....	94
Figure 3.16	Effect of IGF-1 isoform expression of total circulating IGF-1 levels.....	96
Figure 3.17	Skeletal muscle weight of IGF-1 isoform transgenic lines.....	97
Figure 3.18	Histological analysis of MLC/Class 2 IGF-1Ea muscles.....	99
Figure 3.19	Histological analysis of MLC/Class 1 IGF-1Eb muscles.....	101
Figure 3.20	Histological analysis of MLC/Class 2 IGF-1Eb muscles.....	103
Figure 3.21	Functional analysis of IGF-1 isoform transgenic muscles (1).....	104
Figure 3.22	Functional analysis of IGF-1 isoform transgenic muscles (2).....	105
Figure 3.23	mRNA expression and activation of IGF-1R.....	108
Figure 3.24	Distribution of regulated genes by cellular localization.....	110
Figure 3.25	Kinetworks TM Phospho-site screen.....	115
Figure 3.26	The calcineurin pathway in IGF-1 isoform transgenic skeletal muscle.....	118
Figure 3.27	Histological analysis of CTX-injected skeletal muscle.....	120
Figure 3.28	Expression of endogenous IGF-1 isoforms in WT CTX-injected muscle ...	122
Figure 3.29	Influence of IGF-1 isoform transgenes on endogenous IGF-1	

	isoform expression after CTX-injury.....	123
Figure 3.30	Expression of calcineurin isoforms in CTX-injured transgenic muscle.....	125
Figure 4.1	Vertebrate 5'-donor splice site comparison.....	128
Figure C1	Example of an IGF-1 network constructed with Ingenuity	155
Figure C2	MLC/Class 1 IGF-1Ea overlay of regulated genes in the IGF-1 network...	156
Figure C3	MLC/Class 1 IGF-1Eb overlay of regulated genes in the IGF-1 network...	157
Figure C4	MLC/Class 2 IGF-1Ea overlay of regulated genes in the IGF-1 network...	158
Figure C5	MLC/Class 2 IGF-1Eb overlay of regulated genes in the IGF-1 network...	159

List of tables

Table 1	List of primary antibodies used for immunoprecipitation	65
Table 2	List of primary antibodies used in Western blot analysis	66
Table 3	List of secondary antibodies used in Western blot	66
Table 4	List of kinases screened by the Kintworks™ Phospho-site screen	114
Table B1	MLC/Class 1 IGF-1Ea list of up-and down-regulated genes	147
Table B2	MLC/Class 1 IGF-1Eb list of up-and down-regulated genes	148
Table B3	MLC/Class 2 IGF-1Ea list of up-and down-regulated genes	149
Table B4	MLC/Class 2 IGF-1Eb list of up-and down-regulated genes	150
Table B5	List of up-and down-regulated genes in response to Class 1 isoforms.....	151
Table B6	List of up-and down-regulated genes in response to Class 2 isoforms	152
Table B7	List of up-and down-regulated genes in response to Ea isoforms	153
Table B8	List of up-and down-regulated genes in response to Eb isoforms	154
Table C1	List of Ingenuity gene abbreviations	160

1 Introduction

Recent studies on the role of insulin-like growth factor-1 (IGF-1) isoforms in skeletal muscle growth and differentiation have implicated IGF-1 as an important mediator of anabolic pathways and also provided new insights into the function of these signaling molecules in muscle homeostasis. Many studies suggest promising new avenues for systemic as well as local intervention in the defects associated with many muscle pathologies. Since IGF-1 levels decline with age in both humans and rodents, this growth factor has also been considered a promising therapeutic agent in staving off advancing muscle weakness during aging.

The introduction to this thesis is crucial to understand the work presented later on and aims to give an overview of development and structure of the skeletal muscle system, as well as a detailed description of the IGF-1 system and its role in skeletal muscle.

1.1 Skeletal muscle development and structure

1.1.1 Overview of muscle development.

Skeletal muscle development results from a cascade of events leading to mesoderm formation (reviewed in [1-3]). The mesoderm is subdivided into four compartments: axial, paraxial, intermediate and lateral plate mesoderm. In the developing embryo, the paraxial mesoderm, which is located between axial structures (neural tube and notochord), and lateral structures (intermediate and lateral mesoderm), gives rise to the somites (reviewed in [4]), which are the main source of all skeletal muscle cells in vertebrates. In response to positive and negative signals from the notochord, the neural tube, and the dorsal ectoderm, the somite develops into three distinct cellular compartments: dermamyotome (DM), myotome and sclerotome. These compartments subsequently give rise to distinct cell fates (Figure 1.1).

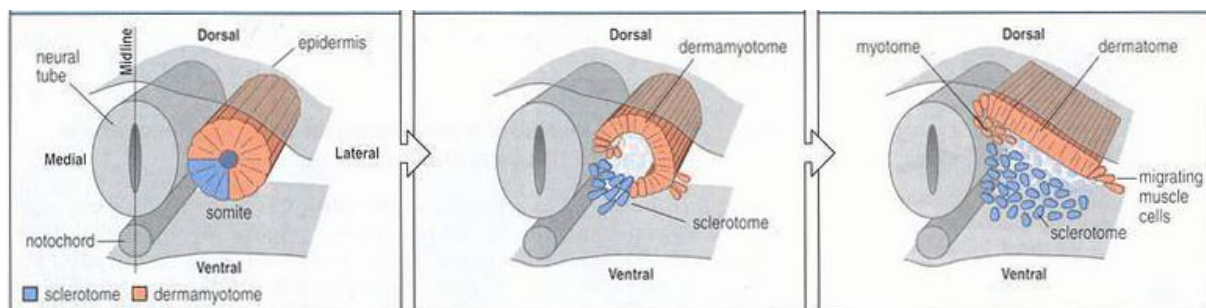


Figure 1.1: Fate map of a somite. The ventral medial portion of the somite (blue) gives rise to the sclerotome and dermamyotome. While the sclerotome cells migrate to form the cartilage of the vertebrae, the dermamyotome forms the dermatome and the myotome, which give rise to the dermis, all the trunk muscles, as well as to the muscle cells that migrate into the limb bud. [5]

The sclerotome arises in response to positive signals from the notochord, such as sonic hedgehog (Shh), and gives rise to the axial skeleton and ribs, while the dermamyotome forms in response to positive signals from the dorsal neural tube and the notochord, as well as from the overlying ectoderm. Shh from the notochord acts together with basic fibroblast growth factor (bFGF) and members of the Wnt family, such as Wnt-1 and Wnt-3a from the dorsal neural tube, and Wnt-4, Wnt-6, and Wnt-7a from the surface ectoderm to induce the formation of the dermamyotome (reviewed in [6]). The dermamyotomal cells, while maintained in an undifferentiated state by negative signals from the lateral plate and surface ectoderm (e.g. bone morphogenic protein-4 (BMP-4), Notch, and Msx-1), continue to proliferate and give rise to the myotome and the dermis [7, 8] (Figure 1.2). The dermamyotome can further be classified into medial and lateral components, which develop into two lineages of adult muscle, epaxial (axial) myotome and hypaxial myotome. While the epaxial myotome forms the muscles of spinal column and face, the hypaxial myotome gives rise to the muscles of the limbs and body wall [9].

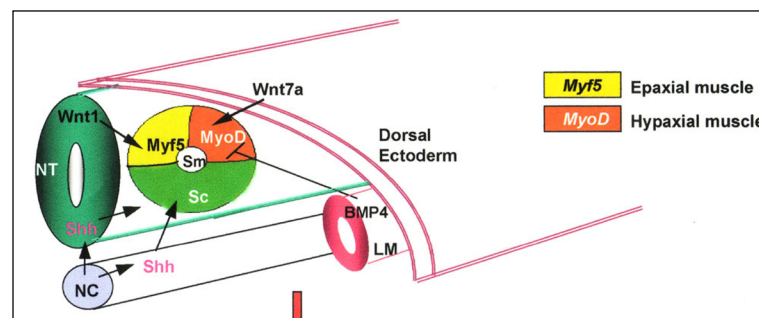


Figure 1.2: Signaling in myogenesis. Signals from the notochord (NC), the neural tube (NT), and the lateral mesoderm (LM) give rise to the sclerotome (Sc), the epaxial and the hypaxial muscles. Shh – sonic hedgehog; Sm – somite.

Myogenic identity is acquired as a result of the activation of the myogenic determination factors (MDFs), members of the basic helix-loop-helix (bHLH) family of transcription factors, which include myf-5, MyoD, myogenin, and MRF-4 (myogenic regulatory factor). Due to their ability to activate muscle-specific gene expression programs when over-expressed in transfected non-muscle cell types [10, 11], the MDFs are considered to be key factors of myogenesis. Their important role has been confirmed by transgenic, knock-out, and knock-in mouse models over the last decade [12-17].

By interacting with ubiquitous bHLH proteins, known as E-proteins [18], and other myogenic transcription factors, such as the members of the myocyte enhancing factor (MEF) family, MDFs mediate the activation of genes encoding structural and regulatory muscle-specific proteins, such as myosin light chain (MLC), α -actin, troponin I, troponin T, muscle creatine kinase (MCK), and the different subunits of the acetylcholin receptor (AChR) [11].

Activation of the MDFs is dependant on the signals from the neural tube, notochord and dorsal ectoderm. While Wnt-1, derived from the neural tube, has been shown to activate myf-5 expression in the epaxial myotome, Wnt-7a from the dorsal ectoderm activates MyoD and promotes the formation of the hypaxial muscles [19] (Figure 1.3).

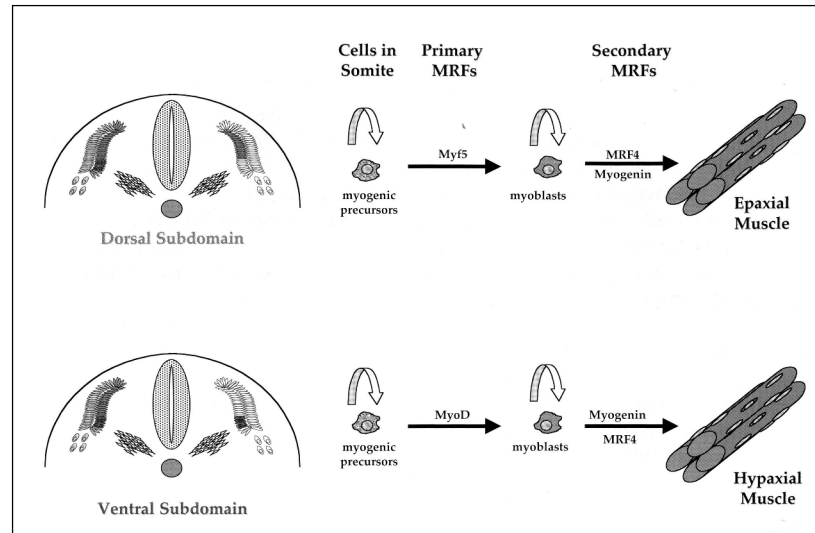


Figure 1.3: MyoD and myf-5 signaling in the development of epaxial and hypaxial muscle. Positive signals from the axial structures induce expression of the primary MRFs in the myotome. MyoD expression in the ventral myotome leads to activation of the secondary MRFs, MRF4 and myogenin and finally to epaxial muscle, while myf-5 expression also leads to activation of the secondary MRFs, but to the development of hypaxial muscle. From Palmer et al. [20]

In vitro studies also revealed a role of IGF-1, IGF-2, and insulin in promotion of somite myogenesis [21], showing that the IGFs and insulin interact synergistically with Shh, bFGF and transforming growth factor- β 1 (TGF- β 1) to stimulate high levels of muscle development. The detection of insulin, IGF-2, insulin receptor, and IGF-1 receptor mRNAs in both the neural tube and the somites, and the detection of IGF-1 transcripts in the entire embryo but not in the neural tube or somites, support the role of these molecules as early myogenic signals during embryogenesis [21].

1.1.2 Development of skeletal muscle structure

The embryonic development of the hypaxial limb and trunk muscles occurs in two temporally distinct phases of so-called primary and secondary myogenesis during which muscle precursor cells migrate into the limb, where they form the muscle mass [22] (Figure 1.4). In the first wave of primary myogenesis, which corresponds to the onset of muscle formation in the embryo, certain mesenchymal cells in each myotome differentiate into long mononucleated muscle precursors (myoblasts). After a period of proliferation, myoblasts start to fuse into primary myofibers by forming progressively elongated multinucleated cells. It is

only after myoblast fusion that the myofibers start to synthesize the contractile proteins necessary for muscle function. The second wave of myogenesis is the result of proliferation and differentiation of previously quiescent myoblasts which use the primary myofibers as a scaffold for formation of the secondary myofibers. (Figure 1.3 and 1.4)

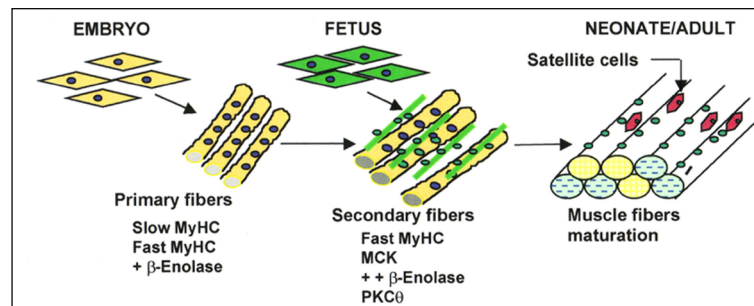


Figure 1.4: Primary and secondary myogenesis. Primary myofibers, expressing markers like slow myosin heavy chain (MyHC), fast MyHC and β-enolase, act as a scaffold for the development of secondary myofibers, which express markers like fast MyHC, muscle creatine kinase (MCK), β-enolase and protein kinase C (PKC). In the mature muscle a small pool of satellite cells is present, located between the sarcolemma and the basal lamina of the muscle fiber.

At the endpoint of muscle development, skeletal muscle tissue is mainly composed of very long multinucleated myofibers (Figure 1.5A). The cytoplasm of the myofiber is usually referred to as sarcoplasm and the plasma membrane as sarcolemma. Outside the sarcolemma lies the basement lamina (specialized extracellular matrix rich in laminins). Multiple elongated myonuclei are arranged at the periphery of the myofiber immediately beneath the sarcolemma. The sarcoplasm is filled with specialized contractile proteins arranged in myofibrils (Figure 1.5A). Mononucleated cells located between the sarcolemma and the basement lamina are called satellite cells (due to their geographical location) or myoblasts (due to their function) (Figure 1.5A). Satellite cells represent a reserve of muscle precursor cells for the mature myofibers and facilitate muscle growth and repair [23, 24].

The major cellular component of the myofiber is the myofibril, which is formed by an assembly of contractile filaments. Under the light microscope, myofibrils have a striated appearance, which contributes to the striations of the entire myofiber. Thick filaments form the so-called A band (A stands for anisotropic, because it can rotate polarized light) and have a greater density than thin filaments, which form the I band (I for isotropic since I bands cannot rotate polarized light). At both ends of the A band lays a zone of even higher density, the Z disc, which marks the region where thin and thick filaments meet. The interval between two Z discs is called the sarcomere. The dense A band consists of myosin-containing thick filaments and has a less dense central part (since the ends of thin myofilaments do not reach here), referred to as H zone. The H zone is bisected with a so-called M line. The I band

consists of three filaments (not shown): actin-containing thin filaments that span the I-band and overlap with myosin-containing thick filaments in the A-band; nebulin-containing filaments that extend to the same length as actin filaments and titin-containing filaments that span half of the sarcomere. The actin, titin and nebulin filaments are anchored to the Z-discs. Striation of myofibrils is due to a regular repetition of a basic contractile unit, the sarcomere [25, 26] (Figure 1.1B).

The sarcomeric and cytoskeletal proteins are linked to the sarcolemma and to molecules in the basement lamina by two main classes of membrane associated molecules: integrins (reviewed in [27, 28]) and the dystrophin-associated protein complex (DPC) (reviewed in [29, 30]). Both integrin $\alpha 7$ (the main integrin in mature muscle) and DPC bind to molecules in the basement lamina (laminin 2) and provide for the structural integrity of myofibers during contraction. The DPC represents an assembly of at least three protein complexes: 1) the cytoplasmic, dystrophin-containing complex; 2) the dystroglycan complex; and 3) the sarcoglycan-sarcospan complex (Figure 1.5C).

Linkage between the membrane complexes at the myofiber surface and sarcomeric proteins within the muscle cells involves many cytoskeletal proteins including actin, α -actinin, desmin and spectrin [26]. Desmin forms a 3D scaffold around the Z-disks of sarcomeres and interconnects the entire contractile apparatus with the sarcolemmal skeleton, the nuclei and other organelles (reviewed in [28]).

Individual myofibers are covered with an interstitial connective tissue referred to as endomysium (Figure 1.5A). The endomysium represents a dynamic complex of many extracellular matrix components (reviewed in [28]) and contains different structures and cells: blood and lymphatic vessels; nerve branches; fibroblasts; mast cells and macrophages. The myofibers are arranged in bundles ensheathed with the so-called perimysium. These bundles of myofibers are further assembled into the whole muscle covered with the epimysium [31] (Figure 1.5A). Muscles are attached by connective tissue and tendons to the bones of the skeleton.

Skeletal muscle depends upon a signal (action potential) from a motor neuron to become activated and contract. The axon of a motor neuron extends from the cell body located in the spinal cord or the brainstem, to the muscle, where it branches and each axon terminal attaches to the surface of a myofiber at a neuromuscular junction called the synapse (reviewed in [32]).

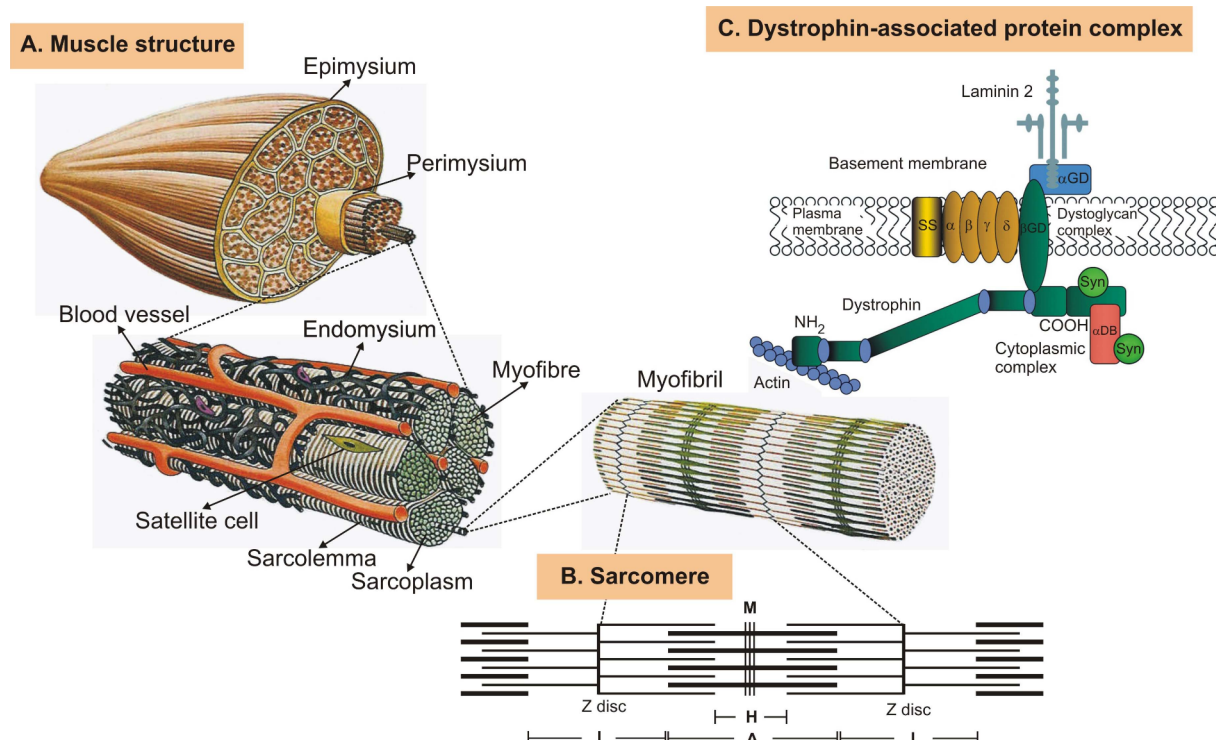


Figure 1.5 Skeletal muscle structure. **A** Skeletal muscles consist of myofibers arranged in bundles. The connective tissue of skeletal muscle is composed of three sheaths: epimysium covers the whole muscle, perimysium covers the bundles of the myofibers and endomysium covers each individual myofiber. Satellite cells are located between the basement lamina (not shown) and the sarcolemma of the myofiber. The sarcoplasm of the myofiber is filled with striated myofibrils. A segment of the myofibril located between two Z lines represents a sarcomere, the structural unit of the myofiber **B** A sarcomere contains parallel arrays of contractile filaments arranged in a central dark A band (Anisotropic in polarized light) flanked by two lighter I bands (Isotropic in polarized light). The dark A band consists of myosin-containing thick filaments and has a less dense central part (since the ends of thin myofilaments do not reach here), referred to as H zone. The H zone is bisected with a so-called M line. The I band consists of three filaments (not shown): actin-containing thin filaments that span the I-band and overlap with myosin-containing thick filaments in the A-band; nebulin-containing filaments that extend to the same length as actin filaments and titin-containing filaments that span half of the sarcomere. The actin, titin and nebulin filaments are anchored to Z-discs. Z-discs form borders on each side of the sarcomere. They are precisely aligned and laterally associated with cytoskeletal proteins intermediates, such as desmin and plectin.

1.1.3 Skeletal muscle fiber types

Terminally developed skeletal muscle groups contain populations of heterogeneous fibers. Skeletal muscle fibers differ in their metabolic activity, which is mainly defined by the expression of different myosin heavy chain (MyHC) isoforms and their capacity to catalyze hydrolysis of adenosine triphosphate (ATP). ATP hydrolysis is required for muscle contraction and the kinetics of the ATP splitting reaction are directly related to the physiological parameters of the myofiber contraction. Slow-twitch fibers contain myosin isoforms which split ATP at a low rate and are characterized by slow contraction (therefore slow-twitch, also referred to as type I myofibers). Fast-twitch (type II) fibers instead, contain myosin isoforms which split ATP at a high rate are characterized by fast contraction (fast-twitch myofibers, also referred to as type II myofibers). The splitting rate of ATP is also different among fast type myofibers and further distinguishes the speed of their contraction (type IIA, IIX, and IIB, in order of increasing rates of contraction) (reviewed in [33]). Slow-

twitch myofibers contain many mitochondria, high levels of oxidative enzymes (e.g. succinic dehydrogenase) and are characterized by oxidative metabolism (breakdown of glucose to 38 molecules of ATP, H₂O, and CO₂). Slow fibers contract very slowly, but show high endurance, while fast fibers contract more rapidly, but are easily fatigued. Fast-twitch myofibers contain relatively low numbers of mitochondria, low levels of oxidative enzymes and high levels of glycolytic enzymes: these myofibers are characterized by glycolytic metabolism (breakdown of glucose to lactic acid). Due to their morphological appearance, slow and fast-twitch myofibers are also referred to as red and white myofibers respectively.

Adult mammalian muscles contain mixtures of all four types of myofibers, characterizing a certain muscle by their composition and spatial organization. While the muscles of the limbs, such as the quadriceps and gastrocnemius, are mainly composed of fast fibers and function in the production of power and force, the diaphragm and latissimus dorsi contain a higher percentage of slow fibers and show a higher endurance.

1.2 Physiological and pathological remodeling of skeletal muscle

The heterogeneous population of muscle fibers that characterizes adult skeletal muscle confers to it a considerable degree of plasticity (reviewed in [34]). This property makes the muscle capable to respond to a wide range of external and internal factors, such as physical activity, injury, stimulation by motor neurons, oxygen and nutrient supply, and changes in hormone levels. By remodeling the cytoarchitecture and/or changing of protein composition the muscle can adapt to environmental demands and maintain its functionality. Beneficial remodeling can result in skeletal muscle hypertrophy in response to increased physiological loading (compare 1.2.1), while detrimental remodeling, caused by disuse, aging, or systemic diseases results in skeletal muscle atrophy (compare 1.2.2).

1.2.1 Skeletal muscle hypertrophy

The term “skeletal muscle hypertrophy” describes an increase of the diameter/size of individual myofibers, and is associated with increased content of myofibrillar protein. Normally, skeletal muscle develops hypertrophic fibers as a compensatory response to increased physiological loading *in vivo*. Postnatal muscle growth, including hypertrophy, depends on activation, proliferation and subsequent fusion of satellite cells with existing myofibers. Fusion of activated satellite cells into the growing (hypertrophying) myofibers can result in a proportional increase of the protein and DNA content of the myofiber (i.e. protein to DNA ratio of the myofiber remains constant) [35]. However, there are different modes of

hypertrophy, demonstrated by the fact that hypertrophy can also result from increased fiber diameter, without an increase in the number of nuclei, which might be determined by structural aspects of the muscle [36]. The importance of satellite cell proliferation for muscle hypertrophy has been shown by a study where γ -irradiation, which eliminates satellite cell proliferation completely, blocked compensatory hypertrophy of the extensor digitorum longus (EDL) muscle in rats [37]. However, other studies provide evidence, that hypertrophy can be uncoupled from DNA synthesis and show that increase of myotube and myofiber size can occur in the absence of satellite cell proliferation in tissue culture [38-40] and *in vivo* [41, 42]. In summary, muscle hypertrophy could be due to both processes: increased anabolism within the differentiated myofibers as well as activation and proliferation of satellite cells.

Various signals trigger compensatory growth of skeletal muscles. Growth-inducing muscular activity (e.g. increased physiological loading) causes changes in the biophysical (temperature, contraction induced strain, cell damage) and biochemical (intramuscular oxygen concentrations, sarcoplasmic calcium concentrations, levels and availability of hormones, locally produced growth factors and cytokines) parameters in muscles (reviewed in [43]). Changes in these variables initiate intracellular signal transduction pathways, which regulate differential gene expression and facilitate responses of the muscle cells. Intracellular signaling pathways responsible for skeletal muscle hypertrophy are discussed in detail in section 1.4.5.

1.2.2 Skeletal muscle atrophy

Atrophy of skeletal muscle is accompanied by a reduction of the diameter/size of individual muscle cells, and is caused by the rapid loss of myofibrillar proteins associated with dramatic changes in the biochemistry and enzymatic activity of skeletal muscle. These processes result (among other effects) in reduced capacity to synthesize new protein and up-regulation of pathways leading to increased protein breakdown. Two common causes of dramatic myofiber atrophy are muscle disuse [44] and denervation [45], however skeletal muscle atrophy also occurs secondary to different pathological conditions, such as heart failure [46], fasting [47], burn injury [48], sepsis [49], glucocorticoid treatment [50], diabetes [51], cancer [52] and AIDS [53]. Myofiber atrophy is a serious problem encountered in aging individuals (reviewed [32, 54]). Physiological reasons for muscle atrophy vary: in starvation and diabetes, glucocorticoids and low insulin levels are essential for muscle wasting [55-57], whereas in pathological inflammatory conditions, muscle wasting is caused by high levels of pro-inflammatory cytokines, such as tumor necrosis factor- α (TNF- α) and such muscle wasting is termed cachexia (reviewed in [58]).

Enhancement of overall proteolysis linked to the induction of the ubiquitin-proteasome protein degradation pathway is a common characteristic of atrophying muscle [59]. Two main genes (atrogenes) up-regulated in atrophic states are ubiquitin ligases MAFbx (muscle atrophy F box or atrogin-1) and MuRF-1 (muscle RING finger-1) [59, 60]. The expression pattern of atrogenes appears to be common for the catabolic states induced by different factors: e.g. fasting, diabetes mellitus, renal failure and tumor implantation [59].

IGF-1 has been shown to block skeletal muscle atrophy in several experimental models, such as the treatment of muscle cell cultures with the catabolic glucocorticoid dexamethasone [39, 61-63], angiotensin II-induced muscle atrophy *in vivo* [64], and chronic heart failure-induced atrophy of skeletal muscle [46].

1.2.3 Skeletal muscle aging

Muscle aging involves many processes involved in disuse or disease-induced atrophy, and is accompanied by an alteration of the heterogeneity of muscle fibers and therefore in muscle plasticity [65]. Hallmarks of aging skeletal muscle are restriction of adaptability, decline in muscle mass and function, as well as quality (innervation patterns, contractility, capillary density, and endurance), leading to a decrease in muscle strength and force output. This process is known as muscle wasting or sarcopenia of old age [66], common in both old humans and animals, and is accompanied by an early decrease in protein synthetic rates and a subsequent increase in protein degradation [67]. In addition, senescent muscles are characterized by a selective reduction in muscle fiber size, shift in fiber composition [68], modulation in gene expression [69] and numerous metabolic and physiological alterations (reviewed in [70]). In particular, selective loss of the most powerful fast glycolytic (type IIB) fibers over fast glycolytic oxidative fibers (type IIA and IIX) or slow fibers (type I) [68], leads to the decrease in the force-generating capacity, as the remaining fibers exhibit restricted contractile options in terms of speed and power output, although being energetically more efficient than type IIB fibers.

Changes in gene expression involve the up-regulation of the myogenic determination factors MyoD and myogenin and the muscle-specific genes, such as AChR, MLC, and MCK that are activated by these MDFs [69]. MyoD and myogenin are expressed at high levels in muscles of newborn mice, but decline continuously during postnatal life, until they are not detectable anymore in the adult animals. Thus, their up-regulation in senile muscle might be a compensatory mechanism to maintain the muscle phenotype in aged muscle. However these compensatory mechanisms fail to preserve muscle function and senescent muscles undergo wasting processes.

One of the highlights of age-related alterations of cellular metabolism is the accumulation of oxidatively modified proteins, lipids, and nucleic acids. As a result of an aerobic metabolism, reactive oxygen species (ROS) are produced throughout an organism's life. The key enzymes protecting the cell against the damaging effects of ROS, such as catalase, superoxide dismutase (SOD) and glutathione peroxidase, have been reported to decrease in their activities with increasing age (reviewed in [71]), leading to free radical-mediated oxidative damage of muscle tissue [72]. Mutations in genes coding for these antioxidant enzymes have also been connected to neurodegenerative diseases, such as familial amyotrophic lateral sclerosis (ALS), where mutated SOD1 is thought to contribute to severe degeneration of motor neurons [73]. In fact, transgenic mice over-expressing a mutant form of SOD1 develop age-dependent motor neuron degeneration, skeletal muscle weakness, and paralysis and die at the age of five to six months [74].

Finally, it has been demonstrated that the expression of anabolic hormones, like growth hormone (GH) and IGF-1, decline with age [75]. This might contribute to the progress of muscle atrophy in senescence and limit the reparative and regenerative abilities of skeletal muscle. This assumption is supported by muscle-specific viral mediated over-expression of IGF-1 and in a transgenic mouse model which over-expresses IGF-1 exclusively in skeletal muscle (MLC/mIGF-1) [76, 77]. Both studies used the same IGF-1 isoform, Class 1 IGF-1Ea (compare section 1.4.2), which is the isoform that is normally expressed in skeletal muscle and was therefore termed mIGF-1 (muscle IGF-1). Both reports showed that muscle mass and strength, as well as fiber type distribution in old animals was maintained at levels similar to those of younger adults. In addition, Musaro et al. discovered that even in aged muscle, the mIGF-1 transgenic mice retained the proliferative response to muscle injury characteristic of younger animals [77]. mIGF-1 has also been shown to protect against free radical-induced damage and muscle degeneration in double transgenic SOD1/ mIGF-1 animals [78], further supporting a beneficial role for IGF-1 as a survival factor.

1.3 Skeletal muscle injury and regeneration

Skeletal muscle tissue has a high potential for regeneration following injury. Under normal physiological conditions, muscle injury can result from physical exercise and especially eccentric (lengthening) contractions [79, 80]. The exercise-induced injury (or micro-injury [81]) is initially caused by the increased strain on the myofibers and involves damage to myofiber ultrastructure, basement lamina and capillaries. Myofiber damage activates an inflammatory response and regeneration [79]. The recovery of myofibers follows a similar

pathway after injuries resulting from eccentric contractions [82-84], ischemia after grafting [85, 86], physical muscle damage [87, 88], chemical damage (e.g. cardiotoxin injection) [89], and muscle disease [87].

Use of the various experimental models shows that regeneration of skeletal muscle is a sequential process, which involves muscle necrosis, revascularisation, infiltration of inflammatory cells, phagocytosis of necrotic tissue, and activation, proliferation and fusion of muscle precursor cells to form new myofibers. Ultimately, successful functional reinnervation is essential for restoration of the physiological parameters of regenerated muscle.

1.3.1 Myofiber necrosis

Muscle injury, muscle transplantation or myopathologies like Duchenne muscular dystrophies (DMD) and polymyositis are characterized by necrosis of myofibers followed by myofiber regeneration. The term “necrosis” refers to the irreversible breakdown of the sarcolemma and all sarcoplasmic structures. Necrosis can occur through the whole length of the myofiber or else only part of the myofiber can degenerate (segmental necrosis). Segmental myofiber necrosis is common in muscular diseases such as DMD [87] and has been shown to be attenuated by transgenic over-expression of mIGF-1 in dystrophic muscles, where mIGF-1 reduced myofiber breakdown and led to a less severe necrotic phenotype [90, 91].

Necrosis of whole myofibers is seen after grafting of the intact whole muscles [85, 86] or minced muscles [92, 93], where the blood and nerve supply is completely disrupted. Injection of cardiotoxin (a snake venom) or other myotoxins also results in almost entire degeneration of the myofibers, however cardiotoxin spares satellite cells, blood vessel supply and innervation [89]. There are many experimental models of segmental necrosis and these include crush injury [88, 94], cut injury [95], and localized chemical injury [96]. Segmental damage of the myofibers is followed by formation of super-contracted bands of myofibrils, which delineate the structurally normal parts of the myofiber, usually located on both sides of the injury site [97]. To minimize the extent of myofiber necrosis after injury the undamaged stumps of the original myofiber are rapidly sealed off with newly formed sarcolemma [97]. In the course of necrosis, the basement lamina of the myofiber can degenerate or remain relatively intact and retain the appearance of a scaffold [89, 98]. Persisting basement lamina around necrotic sarcoplasm can be seen in transplanted whole muscle grafts [85] and cardiotoxin-injected muscles [89]. Severe mechanical injury, like crush [88] or muscle mincing [93] disrupts the basement lamina along with the other muscle structures located in the injury site.

1.3.2 Revascularization

Muscle necrosis can occur in the presence of blood vessel supply (e.g. cardiotoxin injection) or in conditions of ischemia. Ischemic muscle degeneration occurs in transplanted whole or minced muscle grafts due to the loss of vascular connections [85, 99, 100]. The efficiency of new blood vessel formation is a critical event for the successful regeneration of transplanted grafts [99-102]. If big muscles are transplanted without vascular anastomoses, the central core of the transplants fails to revascularize and becomes fibrotic [103-105]. On the contrary, muscles transfected with exogenous vascular endothelial growth factor (VEGF), which stimulates vascular growth, regenerate faster after transplantation than non-transfected muscles [102]. In rat whole muscle grafts, the original vascular network degenerates one day after grafting and only the basement lamina of blood vessels is maintained. Revascularization of the muscle grafts in rats begins two days [99] and in mice three days [101] after transplantation. The first blood vessels, which grow into the muscle grafts from the host tissue are sinusoidal thin-walled endothelial tubes with large lumens. Capillaries sprout from these tubes approximately one day after entering the transplant. Sprouting capillaries often utilize the basement lamina of degenerated capillaries to grow towards the avascular center of the graft. Grafted EDL muscle become fully revascularized in rats by six days [99], and in mice by eight days [101] after transplantation.

1.3.3 Inflammatory cell infiltration and phagocytosis

The regeneration process is accompanied by an inflammatory reaction, during which distinctive populations of macrophages infiltrate the affected tissue [106]. Necrotic muscle is rapidly infiltrated by polymorphonuclear leukocytes (neutrophils) and macrophages, which mediate cellular destruction and phagocytosis of degenerating myofibers [85, 88, 96]. Neutrophils can exacerbate muscle injury by damaging uninjured myofibers via generating reactive oxygen species [107]. In necrotic muscle, which remains in its bed and maintains a more or less intact blood vessel supply (e.g. cardiotoxin injection, crush or cut injury, exercise-induced damage), massive inflammatory cell infiltration is seen by 24 hours after damage [84, 88, 89, 96]. In muscles of exercised rats (downhill running on treadmill), the numbers of neutrophils start to increase by two hours after the exercise and peak by 24 hours and numbers of macrophages are significantly increased by 24 and 48 hours after exercise [84]. The detailed time-course of inflammatory cell infiltration was studied in the experimental model of segmental necrosis caused by localized chemical damage [96], where it was shown that neutrophils enter the injury site as early as three hours after injury. By six hours the injured segment is infiltrated with many polymorphonuclear leukocytes and occasional macrophages. The number of infiltrating macrophages and other phagocytic cells increase by 24 hours after injury and these cells carry out active destruction and elimination

of degenerating myofiber debris [96]. A second and later wave of macrophage infiltration is thought to deliver a number of growth factors and cytokines involved in promoting the regeneration process (reviewed in [108]). However, recent studies discuss the concept that muscle itself plays an active part in the interaction with the immune system (reviewed in [109, 110]). Human satellite cells, for example, were shown to release factors that attract macrophages and monocytes most efficiently upon satellite cell activation [111], raising the possibility that activated satellite cells themselves could signal for macrophage invasion upon injury.

1.3.4 Skeletal muscle fibrosis and scar formation

The inflammatory response to muscle injury eventually leads to the attraction of fibroblasts to the site of injury, recruited by a combination of cytokines, which are secreted by platelets, macrophages and other cellular sources. Fibroblasts secrete high amounts of TGF- β and are believed to be the major source of collagen and glycoproteins, which take part in remodeling of the extracellular matrix, reducing the level of vascularity, and finally in replacing the connective tissue with scar tissue (reviewed in [112]). Even though the formation of fibrotic tissue is a crucial step during skeletal muscle regeneration and provides early support for the rejoining of damaged myofibers, it can also lead to restriction of regeneration in pathologic conditions, where gradual replacement of muscle tissue with adipose and scar tissue ultimately leads to muscle paralysis. One such example is dystrophic muscle, which undergoes repetitive rounds of muscle damage and repair, resulting in exhaustion of the regenerative capabilities of the muscle tissue and leads to massive scar formation. This condition could be attenuated by the supplemental expression of the mIGF-1 transgene described by Musaro et al. [77] in a mouse model of DMD, the *mdx* mouse. mIGF-1 over-expression by the dystrophic muscles was sufficient to increase the regeneration capacity by reducing the extent of fibrotic tissue formation [90], suggesting that improved healing can be achieved by modulating the inflammatory response and thereby reducing the formation of scar tissue (reviewed in [110]).

1.3.5 Satellite cell activation and myofiber regeneration

Skeletal muscle is a post-mitotic tissue, which limits its ability to effectively repair or to regenerate. Therefore an external source of mitotically active cells is required for changes in muscle fiber volume and number. This source is provided by a population of quiescent mononucleated myogenic cells known as satellite cells [23]. These cells retain their mitotic capacity and serve as a pool of myoblasts in postnatal life. Molecular markers used to identify quiescent satellite cells are M-cadherin [113], c-Met [114], CD34 and Myf5 [114],

syndecan-3, and syndecan-4 [115]. In Pax7 null mice, which lose satellite cells during postnatal development, muscle regeneration is impaired [116].

During muscle regeneration, satellite cells become activated, proliferate and fuse with each other to form multinucleated new muscle cells (myotubes). Myotubes further fuse with each other, but also with surviving parts of the myofibers (if such remain) to repair or replace the damaged myofiber (reviewed in [117]) (Figure 1.6 and 1.7).

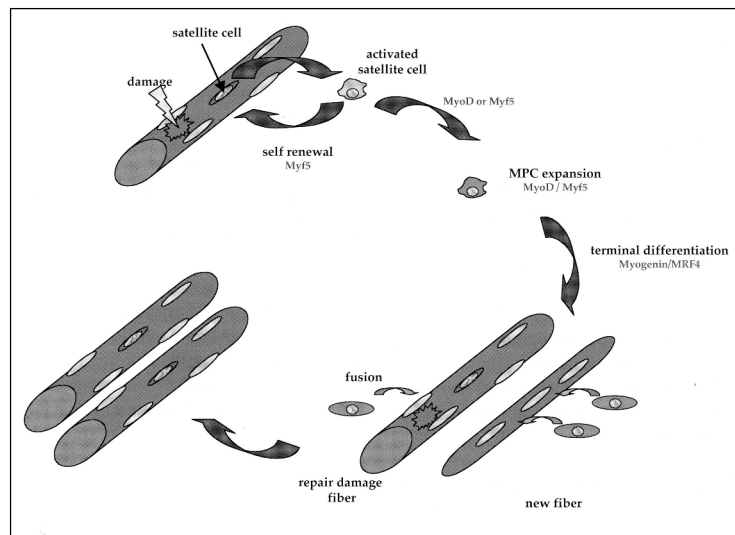


Figure 1.6: Satellite cell activation in response to injury. In response to muscle damage, muscle satellite cells are activated and either MyoD or myf-5 expression is up-regulated prior to proliferation. Subsequently, most proliferating satellite cells express both primary MRFs. Expression of the secondary MRFs, myogenin and MRF4, is coincident with satellite cell differentiation and fusion to existing fibers or to form new fibers. From Palmer et al. [20]

If spared from degeneration, the basement lamina of the necrotic myofibers serves as a scaffold for new muscle formation and myoblasts proliferate and fuse into the myotubes along its inner surface [85, 98]. Regenerated myotubes develop their own basement lamina and the original one is removed via diffusion or disintegration [85]. Fusion of some myotubes can also occur outside any basement lamina [85].

Although satellite cells have long been considered a distinct myogenic lineage responsible for postnatal growth, repair, and maintenance of skeletal muscle, recent research indicates that they are not the only source of undifferentiated progenitors in skeletal muscle (reviewed in [110]). Much attention has been focused on the involvement of a muscle-derived stem cell-like population, which can be isolated from adult skeletal muscle on the basis of Hoechst dye exclusion [118-120] and is considered to be distinct from the myogenic lineage [118] and even from mesenchymal cells [121]. Even though these cells do express some markers of the hematopoietic lineage, such as CD34, and Sca-1, their exact origin is still under investigation [119, 120, 122]. Studies using bone marrow transplantation experiments

suggest that hematopoietic stem cells indeed can contribute to skeletal muscle regeneration [123, 124]. Notably, the bone marrow contains a heterogeneous population of cells and many studies further selected a so-called side population (SP) of cells (reviewed in [125]) on the basis of various cell-surface markers (reviewed in [110]). Studies describing the transplantation of SP cells that have been isolated from the bone marrow or from skeletal muscle, could demonstrate active participation of those cells in regeneration-induced myotube formation [118, 120, 123, 126]. Nevertheless, apart from two specific muscles in the body (panniculus carnosus and extensor digitorum longus), the general frequency of incorporation of these cells into the myogenic lineage was too low to be significant for muscle replacement [126, 127]. Thus, despite the recent focus on alternative stem cell sources for muscle regeneration [128, 129], it appears that satellite cells remain to be the main source of myoblasts in postnatal muscle [24].

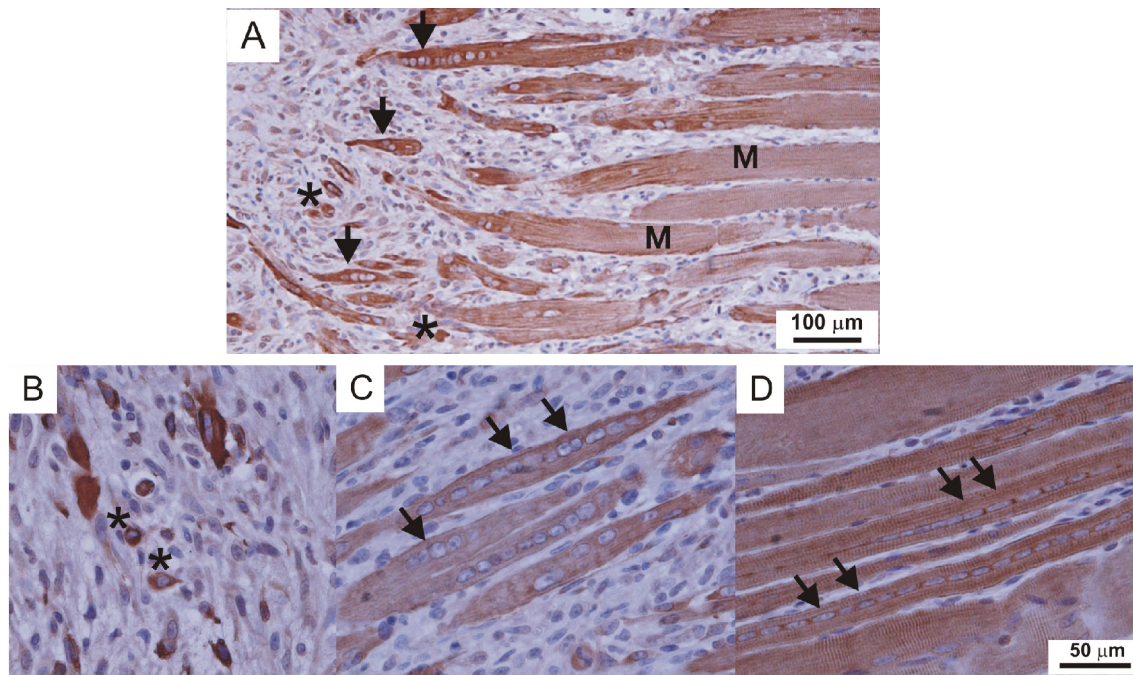


Figure 1.7 Regenerating tibialis anterior (TA). Longitudinal view of the regenerating TA muscle of a mouse seven days after crush injury immunostained with an antibody against desmin (brown) to show muscle cells. **A** Low power view of the crush zone showing fusion of myoblasts (*) and myotubes (arrows) to the ends of the damaged myofibers (M). **B-D** High power view of myoblasts (* on **B**), fusing myotubes (arrows on **C**) and newly formed young myofibers with central nucleation (arrows on **D**). *Kindly provided by Thea Shavlakadze.*

However, the relatively low involvement of stem or progenitor cells in muscle regeneration might be explained by the lack of proper attraction signals and the right environment for the homing of circulating stem cells to regenerating skeletal muscle. Muscle-specific over-expression of mIGF-1, for example, did not only increase the number of bone marrow-derived stem cells to the site of injury in lethally irradiated mice, but also in mice that have not been irradiated [130], indicating that the presence of mIGF-1 enhanced the recruitment of

these cells (reviewed in [110]). Since differentiation of attracted stem cells into components of the host tissue has been linked to the presence of tissue-specific signals and growth factors [131], mIGF-1 might also provide the right environment for integration of circulating stem cells into the injured muscle.

1.3.6 Reinnervation. Successful reinnervation is a key factor for restoration of functional parameters of regenerated muscle. Early events of regeneration, which involve revascularization, activation of satellite cells and their fusion into new myotubes and myofibers, do not require innervation. In the transplanted whole muscle grafts, which are disconnected from the nerve supply, myofibers are successfully restored. However, establishment of the functional reinnervation is crucial for histochemical differentiation of myofiber types and restoration of the final functional mass of the transplanted muscle [132].

1.4 The insulin-like growth factor system

1.4.1 The IGF-1 system

The Insulin-like growth factor (IGF) system consists of three peptide hormones (Insulin, IGF-1 and IGF-2), cell surface receptors (insulin receptor, IGF-1 receptor and the IGF-2 receptor) and six IGF binding proteins (IGFBP-1, -2, -3, -4, -5, and -6). Recently IGFBP-7 has been identified as an annotated gene, provided by Genome Informatics, but information about the role of this potential IGF-binding protein is still missing.

The insulin receptor is a main mediator of the biological functions of insulin, while the IGF-1 receptor mainly mediates cellular responses of IGF-1 and IGF-2. It is believed that the IGF-2 receptor does not have a major role for IGF signal transduction, but it is responsible for reducing IGF-2 levels during fetal development (reviewed in [133]).

In the circulation and in the extracellular milieu, IGFs can exist in an unbound form or form binary complexes with specific IGF binding proteins (IGFBP). The six IGFBPs have been characterized: they serve as carrier molecules for IGFs, extend their half-life and modulate their actions [134, 135]. In the circulation, IGFBP-3 and IGFBP-5 can form a ternary complex with IGF and an approximately 85-kDa leucine-rich glycoprotein known as the acid-labile subunit (ALS) [136, 137]. Unlike binary complexes, ternary complexes cannot pass through capillaries to tissues, and therefore ALS further extends the half-life of IGFs due to its stabilizing effect and creates a circulating reservoir of IGFs. IGFBPs can inhibit or potentiate IGF effects and can also act independently from IGFs [138]. *In vitro* studies suggest that IGFBP-2, -4 and -6 largely inhibit IGF-1 actions, IGFBP-5 enhances IGF-1 action and IGFBP-1 and -3 can be either inhibitory or stimulatory (reviewed in [139]). Transgenic over-

expression of IGFBP-1 [140], IGFBP-2 [141], IGFBP-3 [142], and IGFBP-6 [143] *in vivo* has an inhibitory effect on somatic growth of mice. Ubiquitous over-expression of IGFBP-5 from early development also results in inhibition of the whole body growth and muscle development, but increases the brain growth in transgenic mice [144]. These *in vitro* and *in vivo* data indicate that actions of IGFBPs are very complex and their precise function in regulating IGF bioavailability in tissues has yet to be fully elucidated.

Recent data suggest the existence of another level of regulation of IGF bioavailability as there is evidence that molecules like glycoproteins [145, 146], metalloproteases [147], and glycosaminoglycans [148] can also modulate IGF function. Vitronectin is a multifunctional glycoprotein found in plasma and extracellular matrix. Although vitronectin is structurally unrelated to IGFBPs, it has been shown to bind directly to IGF-2, although only minimal direct binding of IGF-1 to vitronectin occurs [149]. *In vitro* studies show that IGFBPs (IGFBP-2, -3, -4 and, -5) enhance binding of IGF-1 to vitronectin [145], which has a functional significance. For example, IGF-1 in complex with vitronectin and IGFBP-5 increases protein synthesis in cultured skin keratinocytes and enhances migration of these cells [146] and also of human breast carcinoma cell [145]. Metalloproteases (such as ADAM12) can cleave IGFBP-3 and -5, which would diminish their affinity for IGF ligands [147]. Glycosaminoglycans can increase the availability of IGF-1 to the receptors by inhibiting formation of IGF-1 and IGFBP complexes. For example, heparin dissociates IGF-1 from IGFBP-5 and inhibits formation of IGF-1:IGFBP-5 and IGF-1:IGFBP-3 complexes [148]. Inhibition of IGF-1:IGFBP-5 complex formation has also been shown for sulphated glycosaminoglycans (heparan sulphate and dermatan sulphate) [148]. These various binding possibilities illustrate the complexity of molecules that regulate IGF-1 function.

Local and systemic functions of IGF-1 are essential for normal growth and development. IGF-1 is produced by a wide range of tissues. About 75% of circulating IGF-1 is derived from the liver. However IGF-1 is also expressed locally in other tissues and is supposedly released into the bloodstream to contribute to the other 25% of circulating IGF-1. Exactly which tissues release IGF-1 into the bloodstream is not known, however muscle and fat tissues are the likely candidates. Expression of IGF-1 gene gives rise to multiple isoforms of pre-processed IGF-1, which differ by signal and termination peptides, and can exert different biological functions. The complexity of IGF-1 isoforms is discussed in detail in section 1.4.2 and reviewed in [150, 151].

Like other multifunctional growth factors, the insulin-like growth factors show pleiotropic effects on various tissue types. Early investigations into the biological actions of IGF-1 led to

the formulation of the somatomedin hypothesis [152], according to which the effects of GH on cartilage are not due to a direct interaction of GH with the target tissue, but are mediated by somatomedin-C, later identified as IGF-1 [153]. The idea was that growth was determined by GH acting primarily on the liver, which was thought to be the only source of IGF-1. This in turn stimulated the synthesis of IGF-1, which was then released into the circulation and transported to the main target organs, such as cartilage, bone, and muscle, thus acting in an endocrine mode. This hypothesis turned out to be an oversimplification of a complex biological problem, since GH has direct growth effects of its own [154-156]. In the early 1980s, D'Ercole et al. additionally discovered that IGF-1 was also expressed in extrahepatic tissues [157]. This evidence for local IGF-1 production suggested that IGF-1 had an additional autocrine/ paracrine effect, which was supported by subsequent investigations into the tissue distribution of IGF-1 mRNAs and their response to GH. An analysis of postnatal (up to six months) growth curves of mutant mice, which lack the GH receptor gene, the IGF-1 gene or both, showed that all these mutant strains displayed dwarfism; while mice lacking the IGF-1 gene were born with weight deficiency, in GH receptor knockout mice dwarfism was observed starting from postnatal day ten. At two weeks of age all mutant mice showed obvious growth retardation in the order GH receptor knockout>IGF-1 knockout>GH receptor/IGF-1 double knockout [158]. Several important conclusions derive from this study: GH is not involved in embryonic and early (at least up to postnatal day 10) postnatal growth regulation in mice; IGF-1 by itself makes more significant contribution to total weight than GH alone (35% versus 14%); overlapping GH/IGF1 function makes a 34% contribution; and body growth unrelated to the GH/IGF1 axis is estimated to account for ~ 17% of weight [158]. It is suggested that IGF-2 could be the major contributor for GH/IGF-1 unrelated growth [159].

Further evidence for the essential role of the distinct components of the IGF system *in vivo* has been gained by generation of gene knockout mice, which carry null mutations for one or more components of the IGF system or GH/IGF axis (reviewed in [160]). While disruption of the IGF-2 gene revealed that IGF-2 is an important regulator of embryonic, but not of postnatal growth [161], disruption of the IGF-1 gene showed that normal expression of IGF-1 is critical for normal growth and tissue development pre- and postnatally. Mice deficient in IGF-1 show a severe growth deficit, and are born with a birth-weight approximately 60 % of WT neonates, which is due to a decrease in organs, muscle, and bone mass [162]. Depending on the genetic background, greater than 95 % of the dwarf IGF-1^(-/-) mice die shortly after birth due to respiratory failure, while a small percentage survives and reaches adulthood [163]. Surviving IGF-1^(-/-) mutants are infertile, show delayed bone development and grow with a retarded rate, only reaching 30 % of normal weight as adults, compared to WT animals [164].

Mice with a targeted deletion of the IGF-1 receptor gene are affected even more profoundly and die immediately after birth due to respiratory failure. They show a more severe growth deficiency, reaching only 45% of normal size, which is due to a generalized decrease in tissue cell number (hypoplasia) of the organs, the skin, and all skeletal muscle groups in the embryo. In addition, a delay in ossification and changes in architecture of the spinal cord and brain, potentially secondary to diminished numbers of non-neuronal cells [163], were observed.

The Cre/loxP recombination technique was used to produce mice with partially (more or less severely) abrogated expression of the IGF-1 gene. These studies revealed that IGF-1 affects postnatal growth in a gene dosage dependent manner [165]. In particular, compared to controls, mice with single-copy recombination of the IGF-1 locus showed ~19% and ~15% of the weight reduction at three and six weeks of age respectively, whereas the weight of the mice with homozygous IGF-1 gene recombination at the same ages was reduced by ~28% and ~32%. These latter mice survived due to the incomplete recombination of the IGF-1 gene locus [165].

Although studies carried out using conventional gene knockout and Cre/LoxP recombination mouse models shed light on the growth regulatory role of IGF-1 during embryonic and postnatal development, they do not distinguish between systemic and local actions of this growth factor. Other studies looked at the effect of circulating IGF-1 on postnatal growth by knocking out the IGF-1 gene specifically in liver using Cre/loxP recombination [166, 167]. Such abrogation of IGF-1 gene expression specifically in liver caused a 75% reduction of circulating IGF-1, but did not affect the postnatal growth of mice. Based on these observations, it was suggested that the endocrine function of IGF-1 for postnatal growth is minimal and that circulating IGF-1 might have its function in negative feedback effects on GH secretion, an effect that has been described earlier (reviewed in [133, 168]. In fact, the observation that GH levels are increased in the liver-IGF-1-deficient mice (LID-mice) [166] supports this suggestion. In addition, there is evidence that circulating IGF-1 plays an important role as a component of overall insulin action in peripheral tissues, as the LID-mice display muscle-specific insulin insensitivity [169].

However, it later became clear that the importance of circulating IGF-1 for somatic growth was underestimated (reviewed in [159, 168]). In mice with liver specific IGF-1 gene recombination, such recombination was induced at 24 [166] and ten [167] days after birth. During the time the body measurements were obtained (at 53 days after birth [166] and one

to six weeks after birth [167]), the levels of IGF-1 in blood serum might have been decreasing gradually and were maintained at the level sufficient for normal growth (reviewed in [159]). Also, pups receive IGF-1 with the mother's milk for up to three weeks of age, which could have masked any effect of IGF-1 gene recombination. In addition, further characterization of the liver specific IGF-1 knockout mice showed that there was a dramatic decrease of IGFBPs in the circulation and in fact levels of unbound free IGF-1 were similar in the knockout and control mice [168]. A subsequent study [158], which shows that the overlapping contribution of GH/IGF-1 for somatic growth in mice is about 34%, further supports the importance of the endocrine function of IGF-1 for somatic growth, since systemic IGF-1 is considered to be the main mediator of GH effects.

1.4.2 Insulin and Insulin-like growth factor-1 gene and protein structure

1.4.2.1 Insulin versus insulin-like growth factor-1

In humans, the insulin gene is a single-copy gene and consists of three exons and two introns and is transcribed into a mature mRNA of 465 nucleotides coding for prepro-insulin. The insulin precursor contains a 24 amino acid signal peptide, a 30 amino acid A-chain, a 31 amino acid C-chain, and a 21 amino acid B-chain. Processing of the precursor leads to removal of the signal peptide and to an additional protein splicing event, where a specific protease removes the C-domain, which results in generation of the mature insulin protein containing 21 amino acids of the A-chain and 30 amino acids of the B-chain connected by two disulfide bonds.

Unlike the insulin gene, the single-copy IGF-1 gene locus encodes multiple precursor proteins, which vary in the N-terminal signal peptide sequence and the C-terminal E-domain amino acid sequences (discussed in detail below). The unprocessed precursor peptides undergo post-translational protease cleavage to generate mature IGF-1, a 70 amino acid single chain polypeptide with three intra-chain disulfide bridges. Mature IGF-1 differs from insulin by retention of the C-domain, by a short extension of the A-domain to include a novel domain D, and by the presence of variable C-terminal Extension peptides (E-peptides) (Figure 1.8 C). IGF-1 shares 62% homology with pro-insulin and 48% homology with insulin [170, 171]. Among mammalian species the primary structure of IGF-1 is highly conserved: canine [172], bovine [173], ovine [174], porcine [175], and human [170] IGF-1s are identical, whereas rat [176] and mouse [177] IGF-1s differ from human by three and four amino acids respectively and there is only one amino acid difference between these rodent IGF-1s.

Apart from the full length IGF-1, two other protein products are thought to be produced by post-translational cleavage of IGF-1 precursor protein and these have been identified in the human brain ([178]). A truncated IGF-1 isoform (-3N:IGF-1) lacks the first three amino acids from the NH₂-terminal end of the B domain, has low binding affinity to IGFBPs, and displays enhanced biological (neurotrophic) effects, which are mediated through the IGF-1 receptor [179, 180]. Another product from this post-translational modification of IGF-1 precursor protein is the tripeptide glycyl-prolyl-glutamate (GPE), which corresponds to the amino terminal end of mature IGF-1 [178]. In the central nervous system GPE modulates neurotransmitter release via N-methyl-D-aspartate type of glutamate receptor.

1.4.2.2 IGF-1 gene structure

The human and rodent single-copy IGF-1 gene contains six exons, separated by five introns [176, 181-184] and spans >70 kb of genomic DNA [176, 183] (Figure 1.8A). Exons 1 and 2 contain multiple transcription start sites and encode distinct, mutually exclusive 5'-untranslated regions (5'-UTRs) of IGF-1 precursor mRNAs as well as different parts of the signal peptide sequences of IGF-1 precursor polypeptides [176, 185-187]. Exon 3 encodes 52 amino acids: the initial 27 amino acids precede a start of a B domain of mature IGF-1 and comprise the terminal part of the signal peptide; the rest of the 25 amino acids comprise the B domain of mature IGF-1. The remainder of the coding information for the mature IGF-1 peptide (rest of domain B and domains C, A, D) resides in exon 4. Rat exon 4 also contains 16 codons corresponding to the amino-terminal portion of the E-domain. Exon 5 and exon 6 each encode distinct E-peptides, termination codons, and 3'-UTRs.

1.4.2.3 Complexity of IGF-1 transcription

The IGF-1 gene underlies a complex regulation and gives rise to a heterogeneous pool of IGF-1 mRNAs (Figure 1.8). Such heterogeneity results from several events (or combination of these events): use of alternative promoters and transcription start sites located in the leader exons (exon 1 and exon 2) [176, 182, 185-187]; alternative post-transcriptional exon splicing [176, 177, 185-188]; and use of different polyadenylation sites [189, 190]. These multiple IGF-1 mRNAs transcripts encode different isoforms of the IGF-1 precursor peptide, which undergo further post-translational cleavage to release the biologically active mature IGF-1. Every aspect of the complex regulation of the IGF-1 gene will be discussed in detail below.

1.4.2.4 Transcription start sites in exon 1 and 2

Using RNase protection and primer extension procedures multiple transcription initiation sites have been identified in association with the activity of each promoter [185, 186, 191,

192]. Exon 1 transcription can occur from at least four distinct sites in the rat and human genes (Figure 1.8 C): a minor site is located at ~382 bp (start site one), two major sites located at ~343 bp and ~245 bp (start site two and start site three respectively) and a minor start site locate at ~40 bp position (start site four) upstream of the 3'-end of exon 1 [185-187]. Simmons et al. have also identified two additional minor transcription start sites located at the ~361 bp and ~353 bp positions upstream of the 3'-end of exon 1, however their use is thought to be insignificant [186]. Compared to the dispersed pattern of exon 1 start sites, transcription initiation for exon 2 is more localized (Figure 1.8 C). The most upstream and the most rarely used start site is located at ~770 bp (start site 1) upstream to its 3'-end. Two downstream start sites are located at ~50 bp (start site 2) and ~70 bp (start site 3) upstream to the 3'-end of the exon 2. The length and structure of the different 5'UTRs generated by the usage of different promoters and transcription start sites within exon 1 and 2 has been shown to affect the efficiency of translation initiation [187], in particular, translational efficiency of IGF-1 mRNA *in vitro* and *in vivo* is inversely proportional to the length of the 5'-UTR [187].

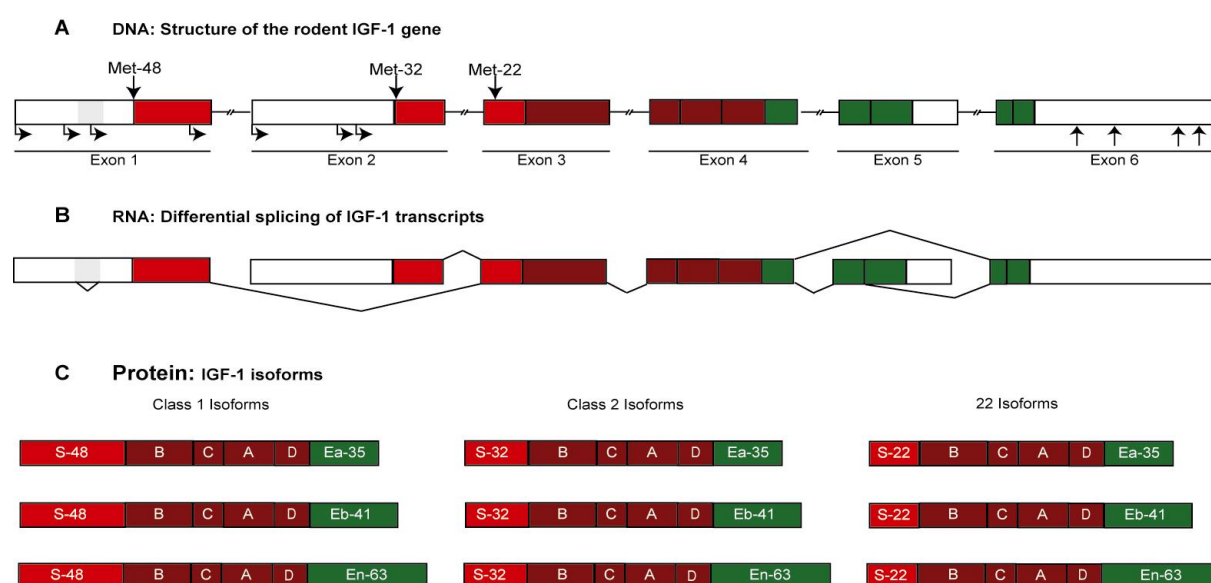


Figure 1.8 Structure of the rodent IGF-1 gene and protein. Colored boxes represent the open reading frames, which code for the different IGF-1 precursor peptides. **A** Genomic structure of the IGF-1 gene. Multiple transcription start sites in exon 1 and 2 are indicated by horizontal arrows. AUG Translation initiation codons are located at indicated positions –48 in exon1, –32 in exon 2 and –22 in exon 3 and encode the specific N-terminal part of the different signal peptides of IGF-1 precursors (red boxes). The mature IGF-1 peptide of 70 amino acids (dark red boxes) is translated from exon 3 and 4, while exon 4 also codes for the N-terminal part of the E-peptide (green). Exon 5 and 6 encode different C-terminal parts of the E-peptide. Poly(A) addition signals are indicated by vertical arrows. **B** Differential splicing of precursor RNA on the 5'- and 3'-end of the IGF-1 gene. **C** The different IGF-1 isoforms.

1.4.2.5 Differential splicing at the 5'-end of IGF-1 RNA precursors

Heterogeneity of IGF-1 gene transcripts is further determined by differential splicing of exons at the 5'-end of precursor mRNA (Figure 1.8 B). Transcripts initiated at exon 1 are spliced to produce mRNAs, which contain exon 1, but lack exon 2 and will be referred to as Class 1

transcripts, whereas transcripts initiated at exon 2 give rise to mRNAs which contain exon 2, but lack exon 1 and are therefore termed Class 2 [186, 187, 193, 194]. In addition, transcripts initiated at start sites one and two of exon 1 can undergo a post-transcriptional splicing (exon 1 spliced variant), which results in the removal of a 186 base long sequence (including a major transcription site three) and introduces further complexity in heterogeneity of IGF-1 mRNAs [191]. In rodents about 20% of liver IGF-1 transcripts are subject to this modification [191].

1.4.2.6 Alternative splicing at the 3'-end of IGF-1 RNA precursors

Additional splicing at the 3'-end of the IGF-1 gene adds further complexity to the variety of IGF-1 transcripts and IGF-1 isoforms translated from these transcripts. In rat and mouse liver two splice variants have been identified [176, 177, 188]. When exon 4 is spliced to exon 6, 19 amino acids are added to the common 16 amino acids encoded by exon 4, thus generating a 35 amino acid long E-peptide, termed Ea-peptide (Figure 1.8 C). A second E-peptide, in rodents known as the Eb-peptide, is translated when a 52 base fragment, derived from exon 5, is included and spliced to exon 6. This insertion encodes 17 codons and causes a frame shift in the reading frame, thereby introducing an earlier in-frame stop codon in the exon 6 sequence. The Eb-peptide contains 41 amino acids, with exon 4 coding for 16 amino acids, exon 5 for 17 amino acids, and exon 6 for eight amino acids [177, 188] (Figure 1.8 C). In murine species, exon 6 encodes the 3'-UTR for both the Ea-peptide and the Eb-peptide which basically only differ in the presence or absence of the 52 base insertion derived from exon 5 (Figure 1.8 B). An important difference between the two E-peptides described in rodents is the presence of two potential N-linked glycosylation sites in the Ea variant which are absent from the Eb variant of the E-peptide [188]. An *in vitro* study revealed that both glycosylation sites were N-glycosylated and that both sites are probably used [195], suggesting that this post-translational modification is involved in a biological action of the IGF-1 isoform.

In contrast to rodents, three mRNA splice variants with alternatively spliced 3'-end have been described in humans. Similarly to rodents, splicing of exon 4 to exon 6 generates mRNAs encoding for the 35 amino acid Ea-peptide [196], which shares 91% homology with the rodent Ea-peptide [177], but only contains one of the two glycosylation sites described for the rodent Ea-peptide [171]. Other than in rodents, the human Eb-peptide is encoded by exon 4 and exon 5, with exon 5 coding for the stop codon and a unique 3'-UTR [181, 197]. The human exon 4-5 splice variant encodes for an Eb-peptide of 77 amino acids with the common 16 amino acids coming from exon 4 and an additional 61 amino acids from exon 5. Even though termed Eb-peptide as well, there is no homology between the human and

mouse Eb-peptide [177]. The third E-peptide splice variant in humans instead, which has been termed Ec-peptide, is the counterpart of Eb in mouse and rat, and is generated by splicing exon 4 to exon 5 to exon 6. In contrast to rodents, the insertion derived from exon 5 contains only 49 base pairs. This produces a third possible E-peptide of 40 amino acids, which shares 72% homology with the rat Eb-peptide sequence [198].

The possible existence of the exon 4-5 splice variant, which codes for the Eb-peptide in humans, was also predicted in rats [176], but since it was not detected in liver using Northern blot techniques, it was assumed that this splice variant does not exist in rodents. However, in the course of this thesis, I recently succeeded in cloning the exon 4-5 splice variant from mouse liver mRNA (compare section 3.1). The mouse exon 4-5 splice variant encodes a 63 amino acid sequence of E-peptide (16 aa encoded by exon 4 and 47 encoded by exon 5), while the human counterpart (Eb-peptide in humans) encodes a 77 amino acids E-peptide (16 aa from exon 4 and 61 from exon 5) and there is only 57% homology between these two sequences. Most importantly predicted from the mouse sequence, the mouse exon 4-5 splice variant does not contain a nuclear and nucleolar localization signal, which has been described for the human Eb-peptide and has been shown to direct this human IGF-1 isoform to the nucleolus [199].

1.4.2.7 Polyadenylation signals in IGF-1 RNA precursors

Finally another level of IGF-1 post-transcriptional regulation is added by the existence of at least four polyadenylation sites in the 3'-UTRs of the rodent and human IGF-1 mRNAs, encoded by exon 6 [176, 190]. The use of several different polyadenylation sites creates size heterogeneity of rodent IGF-1 mRNAs and gives rise to three main IGF-1 transcript sizes: 0.8-1.2, 1.5-2.1, and 7.5 kb [189]. The largest 7.5 kb IGF-1 mRNAs have a long (6.7-6.2 kb) 3'-UTR, whereas the smaller 0.8-1.2 and 1.5-2.1kb IGF-1 mRNAs have a shorter (1.4-1.2 and 0.5-0.2 kb) 3'-UTR. It has been shown *in vitro* and *in vivo* that the half-life of IGF-1 mRNAs is inversely proportional to the length of their UTRs with the longest transcript of 7.5 kb having the shortest half-life [200].

1.4.2.8 Translation of Class 1 and Class 2 mRNAs

Both leader exons encode their own 5'-UTR and contain multiple in-frame AUG translation initiation codons [201]. By usage of alternate promoters and transcription start sites three distinct signal peptides can be generated from the IGF-1 gene (Figure 1.8). Exon 1 contains four AUG translation initiation codons. The most upstream AUG codon initiates a putative 14 amino acid open reading frame (ORF), but no evidence for translation of this ORF exists. The following two AUG codons are immediately followed by UGA stop codons and might

function in regulation of translation initiation of the most downstream AUG at position – 48 relative to the mature IGF-1 coding region. Three of the four described transcription initiation sites in exon 1 are located upstream of the Met-48 translation start codon and polypeptide precursors translated from these mRNAs contain a signal peptide of 48 amino acids [186, 187]. Transcription start site four is located downstream of Met-48 codon and mRNAs initiated from this site encode a 22 amino acid signal peptide derived from exon 3 (which encodes a translation initiation codon at position -22 relative to the coding sequence of mature IGF-1) [187]. However, mRNAs that are translated from one of the three most upstream transcription start sites could theoretically also be translated from the -22 start codon, but *in vitro* studies have shown that in mRNAs containing two translation start sites, preference is given to the upstream one [187]. Translation of the mRNAs initiated at transcription start site one has not been studied, since the amount of these transcripts in rat liver is negligible [187]. Human exon 1 contains an additional AUG codon at a – 25 position relative to the IGF-1 coding region that is translated into a 25 amino acid signal peptide [196].

Exon 2 contains a single in-frame AUG translation start codon at position -32 relative to the mature IGF-1 coding sequence and all three transcription start sites reported for exon 2 are located upstream of this codon. Therefore exon 2 mRNAs can give rise to IGF-1 precursor peptides translated either from the Met-32 or the Met-22 codons, while again preference is given to the more upstream one [186, 187]. Throughout this thesis isoforms with the shortest (22 amino acid) signal peptide are termed 22-IGF-1.

In summary, rodent IGF-1 precursor peptides translated from Class 1 and Class 2 mRNAs can give rise to three different signal peptides of 48, 32 or 22 amino acids, which have been shown to be cleaved normally during post-translational processing *in vitro* [187]. The 48 and 32 amino acid signal peptides generated from Class 1 and Class 2 mRNAs respectively, contain the same C-terminal 27 amino acids, which are encoded by exon 3, but differ at their N-terminus, with exon 1 coding for 21 unique amino acids and exon 2 coding for 5 unique amino acids.

1.4.2.9 Processing of IGF-1 prepro-peptides

It has been suggested that alternate splicing and differential promoter usage at the 5'-end of IGF-1 transcripts that leads to the generation of different signal peptides could affect the precise N-terminal cleavage site of the signal peptide [202] at a position three amino acids downstream of the usual cleavage site to produce the N-terminal truncation of the B-domain of mature or pro-IGF-1 [203, 204]. The cleavage of three N-terminal amino acids (gly-pro-glu)

results in the above mentioned -3N:IGF-1 (also referred to as des (1-3) IGF-1) peptide and the tripeptide glycyl-prolyl-glutamate (GPE) [180].

Different signal peptides have also been shown to be implicated in determination of glycosylation of the rodent Ea-peptide *in vitro* [186]. Simmons et al. could show that co-translational processing of IGF-1 precursors with 22 and 32 amino acid signal peptides leads to glycosylation of the Ea-peptide, whereas co-translational processing of IGF-1 precursors with a 48 amino acid signal peptide is not associated with glycosylation of the Ea-peptide.

1.4.3 Expression of IGF-1 isoforms

In rat liver, ~75% of total IGF-1 synthesis is accounted by exon 1 transcription [191], from which the vast majority of the transcripts (~ 70% of total liver IGF-1 mRNA synthesis) initiate from start sites two and three and the minority of the transcripts (~ 5% of total liver IGF-1 mRNA) initiate at the start site four [191]. Abundance of transcripts initiated at the most upstream promoter (start site one) of exon 1 is extremely low [191]. Almost 90% of exon 2 transcripts initiate from the second start site in exon two [191]. During postnatal development and in adult rats expression of exon 2 transcripts is more GH-dependent than expression of exon 1 transcripts [205, 206]. Exon 2 transcripts appear later in postnatal development than exon 1 transcripts, increasing especially at the onset of GH-dependent linear growth, and their appearance coincides with that of circulating IGF-1 [191]. Expression of exon 1 and exon 2 transcripts has also been studied in extrahepatic tissues of adult rats [207] and, similar to liver, in kidney and brain most of the exon 1 transcripts initiate from start sites two and three. However in testis, lung, muscle and stomach, transcription initiates primarily from start site three. Transcription in heart occurs only from start site three. The presence of the transcripts initiated at start site four is also detected in all these tissues, however at low levels [207]. Exon 2 transcripts are detected in testes, lung, kidney and stomach, however at much lower absolute levels than in liver. Exon 2 transcripts are undetectable in heart, brain and muscle [207].

IGF-1 mRNAs encoding the Ea form of the E-peptide are the major transcripts found in extrahepatic tissues, where they represent 95% of the total IGF-1 mRNA. In liver, IGF-1 transcripts coding for the Ea-peptide were also detectable and represent 88% of total IGF-1 mRNA [208]. Transcripts encoding the Eb form of the E-peptide (which contain the exon 5 derived insertion), in contrast, are more abundant in liver [208], although also detectable in extrahepatic tissues to a low extent. As demonstrated for Class 2 transcripts, Lowe et al. showed that IGF-1 mRNA levels encoding the Eb-peptide were somewhat more sensitive to GH in liver than in other tissues.

Taken together, these results led to the hypothesis that Class 2 IGF-1Eb represents the endocrine form of IGF-1, as transcripts encoding the Class 2 signal peptide and the Eb-peptide are regulated by GH and primarily found in liver, which is thought of as the main source of circulating IGF-1. Transcripts coding for the Class 1 signal peptide and the Ea-peptide, in contrast, are expressed in all tissues and are less GH responsive and therefore might encode the autocrine/paracrine form of IGF-1.

1.4.4 Expression of IGF-1 isoforms in skeletal muscle

The predominant IGF-1 mRNA variant expressed in skeletal muscle is initiated with exon 1 (Class 1) and carries the information for the Ea-peptide on the 3'end (exon 4-6 splice variant). This mRNA therefore codes for the Class 1 IGF-1Ea isoform of IGF-1 [77]. In muscles subjected to damage or exercise transcripts encoding an IGF-1Eb isoform (exon 4-5-6 splice variant on the 3'-end of the mRNA) are up-regulated and the isoform as well as the isolated E-peptide translated from this mRNA has therefore also been called mechano growth factor (MGF) [209-211]. The signal peptide included in the transcripts giving rise to MGF has not been specified. Expression of MGF-containing IGF-1 transcripts has also been detected in resting muscles of rats and humans however at a much lower levels than that of Class 1 IGF-1Ea [210, 212]. A study on C2C12 myogenic cells suggests different roles for Class 1 IGF-1Ea and IGF-1Eb isoforms: while both isoforms increase myoblast proliferation, IGF-1Eb further prolongs proliferation and appears to block differentiation of myoblasts, whereas Class 1 IGF-1Ea promotes their fusion [213]. The same study suggests that other than Class 1 IGF-1Ea, which acts through the IGF-1 receptor (IGF-1R), MGF (either the IGF-1Eb or the isolated Eb-peptide) might act through another, yet undefined, receptor and initiate a signaling pathway which is different from the one initiated by Class 1 IGF-1Ea [213].

It is important to point out that these tissue culture experiments employed a predicted synthetic MGF peptide [213], and as yet there is no evidence for the presence or function of isolated Eb-peptide (MGF protein) *in vivo*. However, involvement of IGF-1Eb/MGF in myoblast proliferation is also supported by *in vivo* studies on humans [210] and rats [214]. Robust up-regulation of IGF-1Eb mRNA (in the range from 2 to 864%) was observed within 2.5 hours after high resistance exercise in young men, with no significant changes in Class 1 IGF-1Ea mRNA levels [210]. Rapid up-regulation of IGF-1Eb was seen in rat muscles after stretch or bupivacaine injury, where the peak of IGF-1Eb mRNA preceded that of Class 1 IGF-1Ea. However, it should be pointed out that in these experiments the absolute mRNA levels of Class 1 IGF-1Ea were always much higher ($\sim 10^3$ folds) than those of MGF [210, 214].

1.4.5 IGF-1 signaling in skeletal muscle

IGF-1 plays a central role in the control of muscle development, growth and differentiation, as well as in maintenance of skeletal muscle, both in culture and in live animals. IGF-1 shares many anabolic functions with insulin, like stimulation of amino acid uptake and incorporation into proteins, DNA and RNA synthesis, and regulation of glucose uptake [215, 216]. All members of the IGF family (IGF-1, IGF-2, and insulin) were also shown to be potent stimulators of cell proliferation, which is consistent with their anabolic effects (reviewed in [134, 215, 217]). The metabolic actions of IGF-1 differ from the metabolic effects of insulin, as IGF-1 stimulates whole body protein metabolism by increasing protein synthesis, as well as by inhibition of protein proteolysis [218, 219], while insulin acts primarily by inhibiting protein breakdown. In addition, insulin primarily acts as a hormone of intermediary metabolism, while IGF-1 primarily functions as a growth, survival and differentiation factor.

The IGFs are unique among other growth factors, as they are capable of promoting proliferation as well as differentiation of skeletal muscle cells, two processes that are mutually exclusive. Other growth factors act as mitogens while they inhibit differentiation (reviewed in [216]). IGF-1, in contrast, has been shown to promote both responses, but in a temporally separated manner, first acting upon myoblast replication and subsequently promoting myogenic differentiation [220-222].

In vitro studies on fibroblasts also established IGF-1 as a progression factor of the cell cycle (reviewed in [133, 215]). So-called competence factors, like epidermal growth factor (EGF), fibroblast growth factor (FGF), and platelet-derived growth factor (PDGF), were shown to stimulate quiescent cells to enter the G₁ phase of the cell cycle, while IGF-1 effected progression from G₁ to S-phase and therefore was termed G₁-progression factor [223]. Although this view could not be supported in more recent *in vivo* studies [224, 225], as IGF-1 null animals displayed a normal progression through G₁- and S-phase, it nevertheless is believed that IGF-1 may be important for timely progression through later phases of the cell cycle. This is suggested by the finding that the IGF-1 null mice exhibited a severe retardation in G₂/M-phase transit [225].

The intracellular signaling pathways which mediate the pleiotropic effects of IGF-1 are complex and inter-connected, however in broad terms, three main pathways can be identified downstream of the activated IGF-1 receptor: mitogen activated protein kinase (MAP-kinase) signaling, mainly linked to myoblast proliferation; phosphatidylinositol 3-kinase (PI(3)-kinase) signaling involved in muscle differentiation and survival and essential for muscle hypertrophy and prevention of muscle atrophy; and calcineurin signaling important for myoblast

differentiation and possibly involved in hypertrophic muscle growth. These pathways are shown in Figure 1.9 and are discussed in detail below.

1.4.5.1 IGF-1 and IGF-2 receptors

The IGF-1 receptor (IGF-1R) is a heterotetrameric transmembrane glycoprotein, which is similar in topography and sequence to the insulin receptor and shares ~50% amino acid identity [226]. Both receptors belong to the family of ligand-activated receptor tyrosine kinases and are $\alpha_2\beta_2$ heterotetramers with subunits of almost identical size. In case of the IGF-1R, a single prepro-protein is translated and after co-translational cleavage of the signal peptide and post-translational glycosylation, the protein is cleaved to generate an α - and a β -subunit. These are connected by disulfide bonds to form a $\alpha\beta$ half receptor. The mature IGF-1R consists of two $\alpha\beta$ half receptors that are linked together by disulfide bonds between the α -subunits.

The α -subunits of the insulin and IGF-1 receptor contain the ligand binding domains, which specifically bind to their cognate ligands, despite the structural similarities between insulin and the IGFs. The IGF-1R has the highest affinity for IGF-1, but also binds to IGF-2 with several-fold lower affinity and to insulin with more than 100-fold lower affinity. Insulin receptors have the highest affinity for insulin, bind IGF-1 with a 100-fold lower affinity, and do not bind to IGF-2 [134, 227].

The β -subunits of the holoreceptor contain a short extracellular domain, a membrane-spanning region, and a large intracytoplasmic domain. The cytoplasmic portion carries a highly conserved tyrosine kinase catalytic domain and sites for tyrosine and serine phosphorylation. In response to ligand binding, both insulin and IGF-1 receptors are capable of autophosphorylation by an intramolecular *trans*-reaction. The tyrosine kinase of one β -subunit phosphorylates residues on the other β -subunit of the $\alpha_2\beta_2$ holoreceptor [228-230]. Due to their high degree of similarity in structure and sequence, the insulin and IGF-1 receptor can form receptor hybrids that consist of $\alpha\beta$ dimers of the IGF-1R connected via disulfide bonds to $\alpha\beta$ dimers of the insulin receptor [231, 232]. This hybrid receptor, which is found in several tissues [233] shows a high affinity to IGF-1 and binds insulin with much lower affinity [234].

Unlike the insulin and IGF-1 receptor, the IGF-2 receptor is not a tyrosine kinase, but a monomeric membrane-spanning receptor with a large extracellular domain, which is responsible for ligand binding. The IGF-2R is not considered to have a major role in IGF

signal transduction, but is primarily believed to be responsible for reducing the levels of IGF-2 during fetal development [235, 236]. Moreover IGF-2R functions also as the cation-independent mannose-6-phosphate receptor [237], which plays a major role in transporting lysosomal enzymes between intracellular compartments.

1.4.5.2 Pathways downstream of the IGF-1 receptor

The biological actions of both, IGF-1 and IGF-2 are mediated by the type 1 IGF-receptor (IGF-1R). Upon ligand binding, the intracellular kinase domain becomes activated and in turn autophosphorylates the receptor (Figure 1.9). This autophosphorylation event leads to the recruitment of endogenous substrates, of which the insulin receptor substrate (IRS) proteins-1 and the src-homology containing protein (SHC), an adaptor protein with src-homology 2 domains (SH2), play a major role [238, 239]. In addition, it was shown that IRS-2 can compensate for IRS-1 and may provide an alternate pathway to IRS-1 signal transduction [215]. These docking proteins bind to the juxtamembrane domain of the IGF-1R, where they are phosphorylated by the IGF-1R and thereby enabled to recruit other substrates that in turn activate different signal cascades [240, 241]. Several other docking proteins that are recruited to an activated IGF-1R have been described (reviewed in [215, 238]) and these provide a mechanism to activate distinct signaling cascades in a tissue- and cell-specific manner. Since the expression pattern of these proteins varies between tissues and throughout development, they might provide an explanation for the multiple functions of IGF-1. Multiple other proteins, such as the adaptor proteins Nck or the Src-like kinase Fyn, are likely to be involved in the specificity of responses to IGF-1.

In muscle cells, IGF-1R is responsible for initiating several signal transduction pathways, which might occur independently or overlap. It is important to point out that most of the work done to unravel the intracellular signaling pathways induced by IGF-1 has been carried out in tissue culture and to what extent this information translates to more complex *in vivo* situations remains to be elucidated.

1.4.5.3 MAP-kinase signaling

It is suggested that MAP-kinase signaling is involved as the major pathway for IGF-1-mediated cell proliferation [242]. Recruitment of the docking protein SHC to the activated receptor leads to the association of SHC with the growth factor receptor-bound protein 2 (Grb2) via their SH2 domains. Grb2 is an adaptor protein which recruits the GTP-exchange factor Sos (Sons of sevenless) via an additional SH3 domain. The interaction between Grb2 and Sos results in the recruitment of the small G-protein Ras, and in the transition of the inactive Ras-GDP to active Ras-GTP. Activated Ras induces sequential activation of Raf-1,

MAP-kinase kinase (MAPKK), and a family of MAP-kinases, namely Erk1, Erk2 (extracellular regulated kinase), Jun kinase, and p38 MAP-kinase (reviewed in [215]) (Figure 1.9). MAP-kinases are thought to phosphorylate transcription factors, which increases their ability to induce expression of molecular markers of cell cycle progression, like c-jun, c-fos, cyclin D1, and cdk4 (reviewed in [215]). Cyclin D1 and cdk4 are the regulatory and catalytic components of a holoenzyme playing a critical role in mediating the phosphorylation of the retinoblastoma protein (Rb). Upon phosphorylation, Rb releases E2F, a transcription factor essential for activating the transcription of many proteins involved in the cell cycle. Also IRS-1 is able to recruit Grb2 and thereby activates the MAP-kinase pathway. Inactivation of the MAP-kinase pathways by using the specific inhibitor PD098059 in L6A1 myogenic cells induced a ~90% reduction of IGF-1 stimulated proliferation [242]. Apart from cell proliferation, the MAP-kinase pathway may also play a role in myotube formation [243].

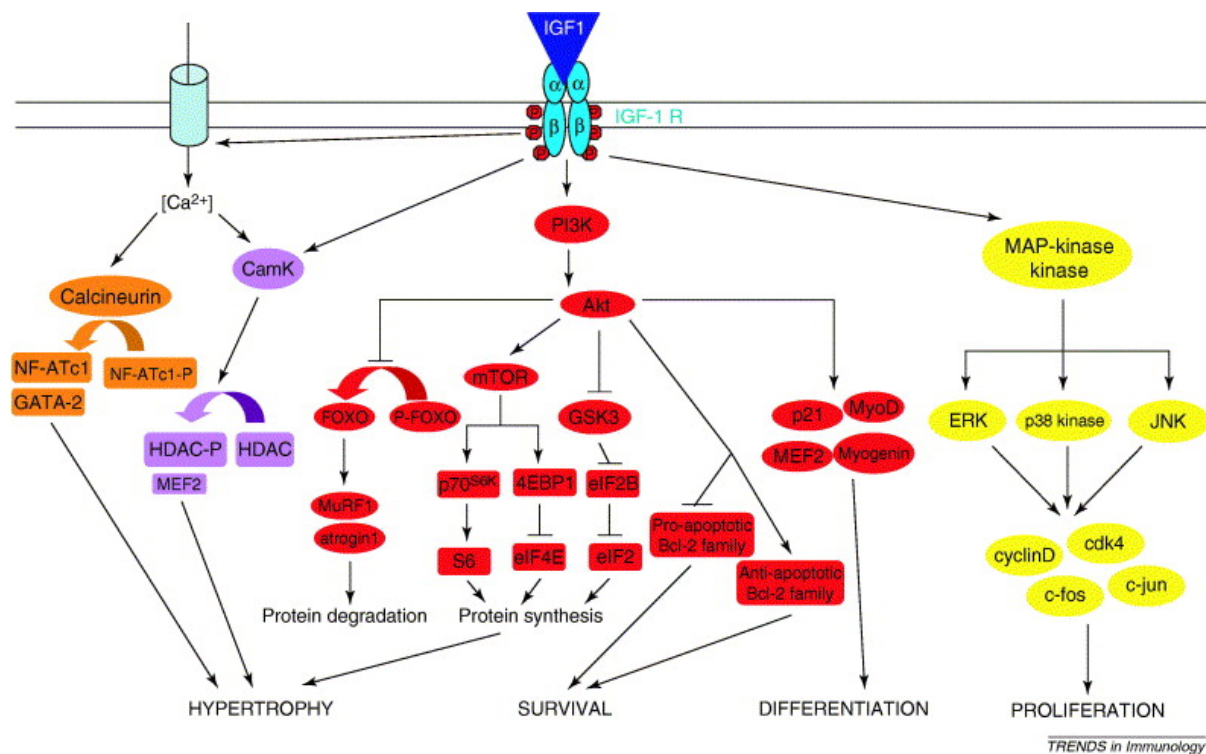


Figure 1.9 Overview of IGF-1/IGF-1R signaling. Binding of IGF1 ligand to the IGF-1R can result in downstream activation of the calcineurin (orange), CamK (purple), PI3K (red) and MAP-kinase (yellow) pathways. Explanations are given in the text. (From Mourkioti et al., 2005).

1.4.5.4 PI(3)-kinase signaling

The pathway downstream of PI(3)-kinase has been linked to differentiation and survival of skeletal muscle cells, as well as to hypertrophic growth and prevention of muscle atrophy. Upon IGF-1R activation, IRS-1 can also interact with the PI(3)-kinase, a heterodimer composed of a 110 kDa catalytic subunit and an 85 kDa regulatory subunit containing a SH2 domain. The p85 regulatory subunit directly binds to activated IRS-1 [244], is phosphorylated

and thereby activated as well. p85 is also capable of binding directly to the IGF-1R [245]. Activated PI(3)-kinase phosphorylates inositol phospholipids, which are required to induce several downstream targets, such as the serine/threonine kinase Akt, also known as the protein kinase B (Figure 1.9).

In the myogenic response to IGF-1, the PI(3)-kinase has been shown to play a critical role [242, 246-248]. During the muscle differentiation process, myoblasts exit the cell cycle in response to the two skeletal muscle-specific MDFs, MyoD and myf-5. Both MyoD and myf-5 are expressed in myoblasts prior to the onset of muscle differentiation [249, 250] and induce the expression of the third MDF, myogenin, as well as members of the MEF family which interact with the MDFs to activate many muscle specific structural genes, such as neonatal myosin, MCK, and β -enolase [251, 252].

PI(3)-kinase together with its downstream effector Akt has been implicated in activating factors involved in muscle differentiation and muscle cell survival, most importantly an early member of the MDF family, MyoD. MyoD induction consequently leads to up-regulation of p21 [253, 254], a cyclin-dependant protein kinase inhibitor, which blocks progression through the cell cycle [255, 256]. An increase in p21 is associated with an ongoing decline in cyclin-dependant kinase activity indicating the involvement of both MyoD and p21 in the critical transition from the proliferative to the differentiative phase.

One of the most important effects of IGF-1 in stimulating myogenesis is its ability to activate expression of the myogenin gene via the PI(3)-kinase and direct translocation of Akt into the nucleus (reviewed [215, 257]). Myogenin is the member of the MDFs which is most directly associated with terminal myogenic differentiation [14, 15], and is an obligatory part of myogenesis stimulation by IGF-1 [258]. The PI(3)-kinase pathway has also been shown to induce the transcription of MEF2, a myocyte enhancer factor, which acts together with the MDFs to activate muscle specific structural genes [259]. This is likely to be the way, by which the PI(3)-kinase pathway mediates the IGF-1 induced activation of myogenin, as MEF2 is essential for activating myogenin expression and later muscle differentiation genes. Tamir et al. also revealed that the MAP-kinase p38 is involved in regulating transcriptional activity of MEF2, but by using another, as yet unidentified signal transduction pathway [259].

Activation of the PI(3)-kinase/Akt pathway is crucial for regulation of protein synthesis in skeletal muscle cells and muscle hypertrophy [39, 61, 260]. There are multiple targets activated downstream of PI(3)-kinase/Akt. For example, a micro array analysis shows that treatment of C2C12 myotubes with IGF-1 (which results in their hypertrophy [39, 61])

regulates at least 242 genes and LY294002 (a specific inhibitor for PI(3)-kinase)) blocks 89.1% of the changes induced by IGF-1 [60]. IGF-1 induced hypertrophy of C2C12 myotubes as well as hypertrophy of the plantaris muscle in rats following functional overload is concomitant with increased phosphorylation and activation of Akt [39, 60, 61]. Muscle-specific expression of constitutively active Akt in mice results in profound myofiber hypertrophy and decreased fat deposition [260]. Such muscle hypertrophy is obtained in conditional transgenic mice (when the transgene is expressed in blastocytes), as well as when the transgene expression is induced in adult mice using tamoxifen-dependent recombination [260].

Activated Akt can lead to up-regulation of protein synthesis in at least two ways: regulation of enzymes involved in carbohydrate metabolism, namely phosphorylation and inhibition of glycogen synthase-serine kinase 3 α (GSK-3 α) (PI(3)-kinase/Akt/GSK-3 α pathway) and phosphorylation of molecules downstream of Akt and its target mTOR (target of rapamycin) (PI(3)-kinase/Akt/mTOR pathway) [39, 61]. It has been shown that activation of mTOR is concomitant with phosphorylation and activation of p70^{S6K}, which stimulates protein synthesis and phosphorylation of PHAS-1/4E-BP1 (phosphorylated heat- and acid-stable protein-1), which releases it from the inhibitory complex with translation initiation factor eIF4E, thereby permitting binding of eIF4E to eIF4D and promoting protein synthesis [39, 61]. Specific blocking of PI(3)-kinase/Akt/mTOR pathway with rapamycin (specific inhibitor of mTOR), almost completely (by 95%) prevents hypertrophic growth of skeletal muscle *in vivo* [61] and blocks all but 1% of the genes activated by IGF-1 through PI(3)-kinase/Akt pathway [60]. However, a recent report by Song et al. raised the possibility for an alternative, Akt-independent pathway mediating skeletal muscle hypertrophy downstream of the PI(3)-kinase, since it demonstrated activation of phosphoinositide-dependent protein kinase (PDK-1), mTOR, and p70^{S6K} without affecting Akt activity in the hypertrophic muscles of transgenic animals over-expressing Class 1 IGF-1Ea (mIGF-1) specifically in skeletal muscle [261].

Activation of PI(3)-kinase/Akt signaling can counteract protein degradation in catabolic states and reduce myofiber atrophy [60, 61, 63, 262]. Micro array analysis confirms that in C2C12 myotubes, IGF-1 and dexamethasone (which causes myotube atrophy) inversely regulate a number of genes including atrophy related MAFbx [60]. Atrophying muscle is characterized by down-regulation of the PI(3)-kinase/Akt pathway which results in up-regulation of atrophy related genes via dephosphorylation (activation) of Foxo transcription factors and their translocation into the nucleus [60, 262]. It has been shown that Foxo3 can directly activate transcription from the atrogin-1(MAFbx) promoter *in vivo* and in cell culture and induce muscle atrophy [262]. Activated Akt phosphorylates Foxo transcription factors on multiple

sites, leading to the exclusion of phosphorylated Foxo proteins from the nucleus and inhibition of their transcriptional functions [263]. Treatment of atrophying myotubes with IGF-1 prevents activation of Foxo transcription factors and suppresses expression of atrogens [63, 262] (Figure 1.9). The anti-atrophic effect of IGF-1 is dependent on PI(3)-kinase/Akt activation, since transfection of myotubes with constitutively active PI(3)-kinase [63] or Akt [63, 262] blocks up-regulation of atrophy related genes. Suppression of atrogens by activated PI(3)-kinase/Akt pathways has also been demonstrated by *in vivo* experiments. For example, transfection of constitutively active Akt, blocked atrogen-1 promoter activity in the muscles of food-deprived (catabolic state) mice [262] and injection of IGF-1 into a short-term denervated muscle decreased expression of MAFbx and MuRF-1 and reduced myofiber atrophy [63]. Denervation-induced atrophy can also be reduced by expression of constitutively active Akt [61]. Taken together these data indicate a protective effect of the PI(3)K/Akt pathway on myofiber atrophy in different catabolic states.

The PI(3)-kinase/Akt pathway, also plays a role in inhibiting apoptosis by interacting with members of the Bcl-2 family (B-cell lymphoma) of proteins [264, 265], which have been shown to either inhibit or stimulate apoptosis (reviewed in [266, 267]). Following IGF-1-mediated stimulation, activated Akt can either lead to inhibition of pro-apoptotic Bcl-2 members and BAD at the earlier stage of apoptosis, and caspase 9 at later stages (reviewed in [257]), or to up-regulation of anti-apoptotic Bcl-2 members [268-270].

Although it is clear that the Akt pathway is the main pathway by which the activated IGF-1R exerts its anti-apoptotic affect, there is evidence that the IGF-1R has alternative pathways. One alternative pathway is the MAP-kinase pathway [271, 272], originating, at least in part, from another major substrate of the IGF-1R, the SHC proteins [273]. A third pathway has been identified by Peruzzi et al. [272], which depends on the mitochondrial translocation of Raf-1 and the phosphorylation of BAD. Recent work by Jin et al. shows that Raf-1 translocation to the mitochondria and phosphorylation of BAD is mediated by p21-activated kinase-1 (Pak1), which phosphorylates Raf-1 at Ser-338/Ser-339 inducing an interaction with Bcl-2 and thereby the dissociation of Bcl-2 and BAD [274]. The same group shows that these signals are specific to Pak1, since Src activates Raf-1 by phosphorylating residues Tyr-340/Tyr-341 and this leads to activation of the MAP-kinase pathway.

1.4.5.5 Calcineurin signaling

This pathway is likely to account for several biological functions of IGF-1: muscle cell differentiation, muscle hypertrophy (although the results are controversial), and conversion of myofibers from slow to fast type. Calcineurin is a cytoplasmic serine-threonine phosphatase

which consists of a catalytic (A) subunit and a regulatory (B) subunit [275]. Three CnA genes have been described, giving rise to CnA α , CnA β , and CnA γ isoforms. While CnA α and β are ubiquitously expressed, CnA γ is only expressed in brain and testis. CnA β mRNA is subject to differential splicing, giving rise to CnA β 1 and β 2 [276]. Due to the insertion of an intron, this isoform of CnA β lacks the auto-inhibitory domain. Calcineurin is activated by increased intracellular Ca²⁺ levels and causes dephosphorylation and nuclear translocation of cytoplasmic NF-ATc (nuclear factor of activated T cells) family members, which in combination with other transcription factors activate transcription [277] (Figure 1.9). The immunosuppressant drugs cyclosporin A (CsA) and FK-506 are specific inhibitors of calcineurin activity [275]. In skeletal muscle cells, downstream targets for calcineurin involve NF-ATc1, zinc finger transcription factor GATA-2 and MEF family members [278-280].

Involvement of calcineurin-mediated signaling in differentiation of skeletal muscle cells has been shown in experiments where transfection of mouse primary myoblasts with viral vector carrying the active calcineurin gene triggered differentiation (assessed by induction of myogenic markers myogenin and embryonic MyHC) and occasional fusion of these cells in proliferation media. Such differentiation occurred only in the presence of adequate Ca²⁺ levels in the media, was independent of NF-ATc1 activity and was blocked by CsA [281]. In general, addition of CsA to pre-differentiated myoblasts results in significantly fewer myotubes indicating the importance of calcineurin signaling for differentiation [39]. It is suggested that calcineurin serves as a downstream mediator for IGF-1-induced myoblast differentiation [282]. Transfection of L6E9 rat myogenic cells (which otherwise do not express endogenous IGF-1) with the MLC/mlIGF-1 transgene (where the gene coding for Class 1 IGF-1Ea isoform of IGF-1 is driven by MLC1/3 promoter and is expressed only after differentiation) enhanced differentiation assessed by induction of differentiation markers [278] and expression of dominant negative calcineurin A or treatment with CsA (the same day when the cells were transferred to differentiation media) blocked IGF-1 mediated differentiation.

In skeletal muscle cells, pathways activated by over-expression of calcineurin coincide with those activated during physical over-load and normally lead to muscle hypertrophy [280]. However, the role of the calcineurin mediated signaling pathway in skeletal muscles hypertrophy is not conclusively established and controversy exists in the published reports. It has been suggested that at least in tissue culture, IGF-1 might induce skeletal muscle hypertrophy through calcineurin in association with GATA-2 and NF-ATc1 [279, 282]. These downstream targets overlap with the mediators of calcineurin activity in cardiomyocytes [275], where calcineurin plays a central role in hypertrophy.

Two studies link the hypertrophic action of IGF-1 to calcineurin signaling:

In one study, transfection of C2C12 myoblasts with plasmid encoding the IGF-1 gene (isoform not indicated) induced mobilization of Ca^{2+} within the cell, increased activation of calcineurin and resulted in nuclear translocation of the transcription factor NF-ATc1 [279]. This was concomitant with myotube hypertrophy and a switch to a glycolytic phenotype and both of these phenotypic responses were inhibited by CsA and FK506 [279]. Similarly, treatment of C2C12 cultures with human recombinant IGF-1 (250ng/ml) resulted in activation of calcineurin and myotube hypertrophy. However, the timing for IGF-1 treatment appears to be critical and myotube hypertrophy occurred only when IGF-1 was added to proliferating cultures or at the time of differentiation, but not one day after [279]. The same group suggested the involvement of calcineurin signaling in IGF-1-induced muscle hypertrophy *in vivo*, based on increased calcineurin activity after local injection of a plasmid carrying the IGF-1 gene into the latissimus dorsi muscle of the rat [279]. This study did not directly examine the effect of exogenous IGF-1 expression on myofiber hypertrophy (myofiber size), but concluded that muscle hypertrophy had occurred based on the presence of centrally nucleated myofibers [279]. It is now recognized that in transgenic mice, formation of the centrally nucleated myofibers might be an indication of an abnormal myogenesis rather than a hypertrophic growth [283]. Notably, the *in vitro* findings of both studies could not be supported by an *in vivo* approach [284], suggesting that additional signals are required *in vivo* to support sustained skeletal muscle hypertrophy.

In another study, endogenous IGF-1 (Class 1 IGF-1Ea isoform) expression under the MLC1/3 promoter (induced when cells are switched to the differentiation programme) in L6E9 cell cultures resulted in myotube hypertrophy concomitant with enhanced accumulation of CnA and GATA-2 transcripts. GATA-2 protein was associated with nuclear complexes containing calcineurin and NF-ATc1 which was extensively dephosphorylated [282].

Involvement of the calcineurin signaling pathway in IGF-1-induced skeletal muscle hypertrophy was questioned by later studies which consider Akt signaling as the principle hypertrophic pathway [39, 61]. These authors proposed that in the earlier studies by Musaro et al. [282, 285] and Semsarian et al. [279] inhibition of IGF-1-induced myotube hypertrophy by CsA could have been due to inhibition of myoblast differentiation and fusion, since CsA was applied to undifferentiated myoblasts. Moreover, it has been suggested that in C2C12 myotubes it is the Akt pathway that is responsible for the hypertrophic action of IGF-1 and can even antagonize calcineurin signaling [39]: administration of IGF-1 (10 ng/ml) to fusing myotubes at day 2 of differentiation caused hypertrophy concomitant with hyperphosphorylation (inactivation) of NF-ATc1, which indicated that IGF-1 might be

inhibiting calcineurin activity [39]. Moreover, addition of IGF-1 blocked the calcium-dependent dephosphorylation and nuclear translocation of NF-ATc1 induced by calcium ionophore (a standard method for activating calcineurin [286]). Treatment of differentiated C2C12 cultures with CsA did not prevent IGF-1-induced hypertrophy, however CsA inhibited differentiation when added to pre-differentiated cultures. It was also shown that calcineurin activity is decreased in functionally overloaded rat plantaris muscle (*in vivo*) and treatment with calcineurin inhibitors cyclosporin A and FK506 do not prevent increase in muscle mass and myofiber size [61].

Disparities in the reports on IGF-1 signaling pathways indicate the complexity and multifunctional nature of these pathways and underline that many open questions still remain in this field.

1.5 Skeletal muscle-specific IGF-1 transgenic mice

In the past years various transgenic approaches, using different IGF-1 isoforms, raised many questions regarding the isoform specificity of IGF-1 function. The Schwartz laboratory [287] generated a transgenic mouse over-expressing a human IGF-1 isoform initiated by exon 1 and including the Ea-peptide (Class 1 IGF-1Ea), driven in skeletal muscle and heart under the control of the α -skeletal actin promoter. Over-expression of this isoform resulted in mild skeletal muscle hypertrophy and initially physiologic hypertrophy in the heart, which later became maladaptive, pathologic cardiac hypertrophy. Additionally, the human IGF-1 isoform was detected in the circulation, presumably secreted from heart and skeletal muscle where it was synthesized.

An unpublished study by Chris Goddard in South Australia used the mature human IGF-1 under the control of the rat skeletal α -actin promoter (Rsk α -actin/hIGF-1) (reviewed in [151]). This expression construct was designed to contain a synthetic translation initiation signal from the rat somatostatin gene, lacking IGF-1 gene-derived signal sequences and distinguishing this mouse from the other lines described here, where native IGF-1 signal sequences were used. This mouse did not show skeletal muscle hypertrophy and levels of circulating hIGF-1 were strongly increased.

More specific restriction of the IGF-1 transgene to skeletal muscle was achieved in the MLC/mlIGF-1 transgenic line, where a Class 1 IGF-1Ea isoform was driven by the skeletal muscle-specific MLC1/3 promoter and enhancer. No increase of circulating IGF-1 was detected in the initial description of this mouse line [77]; however significant circulating IGF-1

has subsequently been observed (the present study). Over-expression of Class 1 IGF-1Ea (named mIGF-1) caused pronounced myocyte hypertrophy and rescued the muscle from age-related muscle atrophy. In addition, the hypertrophic muscles retained the proliferative response to muscle injury, normally seen in younger animals [77], protected dystrophic fibers from necrosis and enhanced regeneration by recruitments of stem cells [90, 130]. The mIGF-1 transgene also protected motor neurons from degeneration in a model of ALS [78] and enhanced regeneration of the affected muscle. The same transgene was restricted to cardiac muscle using the α MyHC promoter (MyHC/mIGF-1) and showed similar beneficial effects in the transgenic hearts, with physiological hypertrophy returning to control levels by six months of age, enhanced regeneration in response to cardiotoxin injections, and myocardial infarction (Santini M.P., manuscript submitted). The presence of circulation IGF-1 was not assessed in this study.

An additional transgenic mouse, generated in the Rosenthal laboratory (unpublished data), which differed from the above-mentioned MLC/mIGF-1 mouse by carrying a shorter 5'-UTR and an as yet unidentified C-terminal sequence, demonstrated a dramatically different phenotype. No skeletal muscle hypertrophy was seen, but instead the transgene caused a mild cardiac hypertrophy, accompanied by an up-regulation of the glucose-sensitive transporter Glut-4 in cardiac and skeletal muscle. In addition, the transgene was detectable in the circulation.

Another study [288], using a human IGF-1 isoform under the control of the cardiac muscle-specific α MyHC promoter, reported cardiomegaly, mediated by an increased number of cells in the heart. These authors also detected human IGF-1 in the circulation, causing site effects by increasing the size of several organs, especially brain and kidney. Notably, the isoform used contained the human Eb-peptide, which corresponds to an En-peptide described in the present work (compare section 1.4.2.6). The same group reported that in this mouse model IGF-1 prevented activation of cell death in the viable myocardium after infarction, thereby limiting ventricular dilation and pathological cardiac hypertrophy [289].

These studies provide a few examples of the diverse phenotypes obtained by over-expression of different IGF-1 isoforms, and highlight the need for a comprehensive characterization of the different isoforms and their normal physiologic function.

1.6 Significance of this work

As outlined above, the IGF-1 gene has a complex expression pattern that results in the production of different N-terminal pre-peptide and C-terminal E-peptide combinations, generated by alternate promoter usage, differential splicing and post-translational modification. The complexity of the IGF-1 gene has complicated the analysis of the circulating and/or localized protein products generated from the single-copy IGF-1 gene and the specific functions of these IGF-1 isoforms have not been systematically described, although their existence had been documented in the early days of IGF-1 research about 20 years ago. The assignment of specific functions to these isoforms is still under debate. Some insight into the role of IGF-1 in skeletal muscle has been gained by supplemental over-expression of IGF-1 using transgenic mice, but the combination of different IGF-1 isoforms with various regulatory sequences to drive transgene transcription has generated discrepancies in the literature (compare section 1.5). The distinct phenotypes of these mice imply differences in the action of the various IGF-1 isoforms and underline the importance of choosing comparable conditions for a comprehensive characterization of IGF-1 isoform function. Parameters such as the choice of promoter, and signal peptide, can alter IGF-1 availability and localization and therefore complicate interpretation and comparison of different IGF-1 transgenic mouse lines.

The approach taken in this thesis aimed for a complete characterization of the four main IGF-1 isoforms and their differential function in skeletal muscle *in vitro* and *in vivo*. Over-expressing these isoforms in the similar manner by driving them from the same regulatory sequences was a crucial prerequisite in the design of this project to allow the comparison between IGF-1 isoform-induced effects. This work will have major implications for the development of IGF-1-based therapies in different disease conditions of skeletal muscle, a region of research which has been given much focus in the past years.

2 Materials and Methods

2.1 Molecular Biology

2.1.1 DNA gel electrophoresis

For small fragments (100-200 bps) low electroendosmosis agarose (Roche, # 1685660) was used and dissolved to a percentage of 1.3-1.5 (w/v) in standard 1x Tris-acetate-EDTA (TAE) buffer. For bigger fragments normal agarose (Invitrogen, #15510-027) was dissolved in standard 1x Tris-borate-EDTA (TBE) buffer. Agarose was melted, cooled down, and 2 µl of ethidium bromide (10 mg/ml) were added per 100 ml of agarose solution. Depending on the gel size, gels were run at a voltage between 60 and 150 V with constant current.

2.1.2 Extraction of DNA fragments from agarose gels.

DNA fragments were excised from agarose gels of the appropriate percentage using a 70%UV lamb and purified using QIAquick Gel Extraction Kit (QIAGEN #28704) according to the instructions. After purification, DNA was ethanol-precipitated (1/10 volume 5 M Na-acetate; 2.5 volumes 100% ethanol), washed in 70% ethanol and dissolved in the appropriate amount of sterile H₂O. All isolated fragments were stored at -20°C until needed.

2.1.3 Plasmid purification

All plasmids were isolated by using QIAGEN plasmid purification Kits (QIAprep[®] Spin Miniprep Kit #27106; Endofree[®] Plasmid Maxi Kit #12362) according to the manufacturer's instructions. Purified plasmids were eluted with sterile H₂O and stored at -20°C.

Concentration of the DNA was determined by spectrophotometric measurement of the absorbance (A) at 260 nm and 280 nm.

2.1.4 Transformation of bacteria for plasmid amplification

Competent E.coli XL-1/blue cells were used for plasmid amplification. Cells were made competent by growing them in LB medium to an OD of 0.5 to 0.6, followed by centrifugation at 1000 x g for 10 min and re-suspended in 1/10 volume of freshly made transformation storage buffer (TSB) (LB broth pH6.5, 10% polyethylene glycol (PEG), 5% dimethyl sulfoxide (DMSO), 10mM MgCl₂, 10mM MgSO₄). After a 10 min. incubation step on ice, the cells were flash-frozen in liquid nitrogen and stored at -80°C. Chemical transformation was performed by incubating the ligation reaction in 1x KCM buffer (0.5M KCl, 0.15M CaCl₂, 0.25M MgCl₂) for 20 min on ice and 10 min at room temperature (RT). Cells were then plated on LB-plates containing 0.5 mM isopropyl-thio-β-galactoside (IPTG), 80µg/ml X-Gal, and 100µg/ml

ampicillin and incubated over night at 37°C. Recombinant clones were identified by color screening and analytical restriction digests.

2.1.5 Cloning IGF-1 isoforms

All IGF-1 isoforms were cloned from three-month-old mouse liver by reverse transcription PCR following the manufacturer's instructions (Promega Access RT-PCR System #A1260) and cloned into pGEM®-T Easy vectors based on A/T-cloning (Promega pGEM®-T Easy Vector System I #A1360). Specific primers were designed for amplification of Class 1 (Figure 2.1A) and 2 (Figure 2.1B) isoforms containing either the Ea or the Eb-peptides (**Class 1 IGF-1Ea**: forward 5'-CTCGATAACTTTGCCAGAAG-3', reverse 5'-CCTCCTACATTCTGTAGGTCTTG-3'; **Class 1 IGF-1Eb**: forward 5'-CTCGATAACTTTGCCAGAAG-3', reverse 5'-CCTGCACTTCCTCTACTTGTG-3'; **Class 2 IGF-1Ea**: forward 5'-AGTTTTGTGTTACCTCGGCC-3', reverse 5'-CCTCCTACATTCTGTAGGTCTTG-3'; **Class 2 IGF-1Eb**: forward 5'-AGTTTTGTGTTACCTCGGCC-3', reverse 5'-CCTGCACTTCCTCTACTTGTG-3').

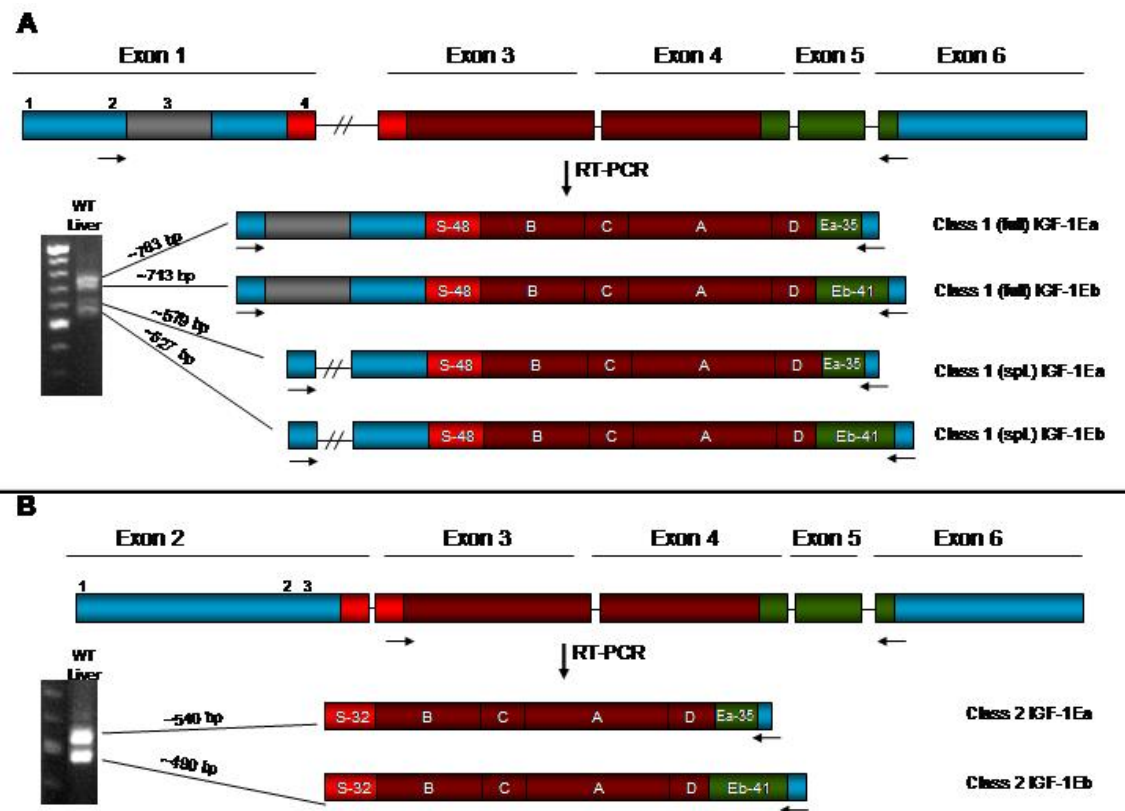


Figure 2.1 Cloning of IGF-1 isoforms from mouse liver. Primer positions are indicated by black arrows. mRNA sequences amplified by the different primer pairs are colored according to the protein domains they encode. Red: signal peptide; dark red: mature IGF-1; green: E-peptides; blue: 5' and 3' UTRs; grey: 186 bp region in exon 1, which can be spliced out in 20% of total mRNA population in liver (compare 1.3.2). **A** Class 1 IGF-1 isoforms **B** Class 2 IGF-1 isoforms

2.1.5.1 Design of skeletal muscle-specific expression vectors

All isoforms were cloned into an expression vector carrying the MLC 1/3 promoter and enhancer sequences and the SV40 poly(A) signal (pMex). The MLC regulatory sequences provide skeletal muscle-specific expression of the IGF-1 isoforms (Figure 2.2).

Primers were designed to generate 5'-SacI and 3'-Sall restriction sites for each isoform and inserts were amplified by PCR from the different pGEM[®]-T Easy/IGF-1 isoform plasmids and gel-purified (**Class 1 IGF-1**: forward 5'-GAGCTCATCTCGATAACTTTGCCAGA AG-3'; **Class 2 IGF-1**: forward 5'-GAGCTCATAGTTTTGTGTTACCTCGGCC-3'; **Ea-coding**: reverse 5'-GTCG ACCCTCCTACATTCTGTAGGTCTTG-3'; **Eb-coding**: reverse 5'-GTCGACCCTGCACTTCCTCTA CTTGTG-3'). IGF-1 isoforms 22-IGF-1Ea (463 bp) and 22-IGF-1Eb (489 bp) were cloned from plasmids pGEM[®]-T Easy/Class 1 IGF-1Ea and pGEM[®]-T Easy/Class 1 IGF-1Eb with primers generating 5'-SacI and 3'-Sall restriction sites (**22-IGF-1**: forward 5'-GAGCTCAT GAAAATCAGCAGCCTTCCAAC-3'). All primers were purchased from Invitrogen.

The PCR fragments, as well as the pMex vector were sequentially digested with first SacI and then Sall (NEB #R0156, #R0138), gel-purified, and ligation was carried out over night at 16°C. All constructs were sequenced to ensure sequence integrity and linearized by EcoRI (NEB #R0101) digest.

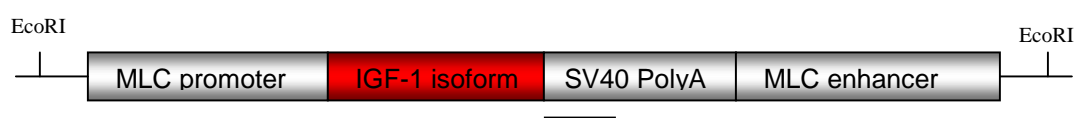


Figure 2.2 Schematic representation of skeletal muscle-specific expression cassette. Regulatory sequences of the pMex-derived expression cassette are shown in silver boxes, position of the cloned IGF-1 isoform is shown as a red box. Start of the surrounding region is shown by a black line. Position of EcoRI restriction sites are indicated by vertical lines. The black line marks the position of the SV40-probe used for Northern blot characterization of the transgene expression.

2.1.5.2 Design of doxycycline-inducible expression vectors

To achieve inducible IGF-1 isoform expression, we applied the “tet-on” system [290, 291], kindly provided by Professor Herman Bujard from the Centre of Molecular Biology Heidelberg (ZMBH) of the University of Heidelberg. This inducible system consists of two expression cassettes, one encoding a modified tetracycline repressor protein (reverse tetracycline trans-activator (rtTA)) under the transcriptional control of the human CMV promoter and enhancer, and the second one driving expression of the gene of interest by the rtTA-responsive target promoter. The regulatory region with a bidirectional promoter pBi-1 consists of a heptamized tet-operator sequence flanked by two divergently orientated human CMV minimal promoters ($P_{\min-1}$ and $P_{\min-2}$). $P_{\min-1}$ controls expression of the luciferase gene *luc** [292] followed by SV40 late poly(A) signal. $P_{\min-2}$ is followed by a multiple cloning site and the rabbit β -globin intron/poly(A) signal and would drive expression of a selected gene of choice upon induction with the tetracycline derivate doxycycline [293].

For the purpose of driving tet-inducible IGF-1 transcription, all IGF-1 isoforms have been cloned into the pBi-2 vector by PCR-mediated generation of 5'-NheI and 3'-EcoRV restriction sites (**Class 1 IGF-1**: forward 5'-GCTAGCCTCGATAACTTTGCCAGAAG-3'; **Class 2 IGF-1**: forward 5'-GCTAGCAGTTTTGTGTTACCTCGGCC-3'; **22-IGF-1**: forward 5'-GCTAGCGAAAATCAGCAGCCTTCCAAC-3'; **Ea-coding**: reverse 5'-GATATCCCTCCTACATTCTGTAGGTC-3'; **Eb-coding**: reverse 5'-GATATCCCTGCACTTCCTCTACTTG-3' (Figure 2.3A).

All primers were purchased from Invitrogen.

Fragments and pBi/IGF-1 isoform vectors were double-digested with NheI and EcoRV (NEB #R0131, #R0195), gel-purified, and ligated over night at 16°C. All constructs were sequenced by the EMBL sequencing service prior to use. For injection of pBi/Class 1 IGF-1B, the plasmid was linearized by digestion with AseI (NEB #R0526).

To generate the skeletal muscle-specific rtTA expression cassette, the rtTA sequence was amplified from the original pUHRtTA 62-1 vector by PCR. For cloning the rtTA2^SM2 sequence into the pMex vector, primers were designed to include 5'-SacI and 3'-Sall restriction sites (forward 5'-GAGCTCATATGTCTAGACTGGACAAGAGC-3'; reverse 5'-GTCGACTTACTTAGTTACCCGGGGAGC-3') (Figure 2.3B). The amplified insert was gel-purified and subsequently the different inserts and the pMex vector were sequentially digested with first SacI and then Sall. After gel-purification, ligation was performed over night at 16°C. Integrity of the construct was confirmed by sequencing. For generation of transgenic rtTA mice, the construct was linearized by EcoRI digest.

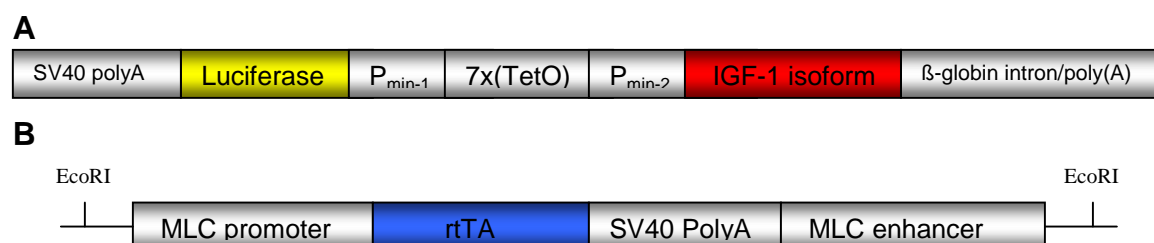


Figure 2.3 Schematic representation of the skeletal muscle adapted “tet-on” system. Regulatory sequences of both constructs are shown in silver boxes. **A** Inducible pBi/IGF-1 isoform expression cassette. Upon binding of doxycycline activated rtTA molecules to the TetO sequence, transcription of luciferase (yellow box) is driven by P_{min-1}, while P_{min-2} regulates transcription of a given IGF-1 isoform (red box). **B** By regulatory sequences of the MLC promoter and enhancer, rtTA (blue box) transcription is restricted to skeletal muscle.

2.1.6 Cloning of an exon 4-5 splice variant-containing IGF-1 isoforms

In an attempt to clone the mouse IGF-1 isoform coding for the Eb-peptide described in humans (compare section 1.4.2.6), mouse liver total RNA was prepared as described in 2.1.10. To exclusively isolate messenger RNA, the OLIGOTEX mRNA Midi Kit (QIAGEN #70042) was used according to the instructions. Combined RT-PCR was carried out with 1µg of mRNA as described in section 2.1.12, using specific primers to amplify Class 1- and Class

2-derived sequences on the 5'-end and two different reverse primers that bind to sequences 5-25 bp and 118-136 bp downstream of the 5'-splice site normally used for generation of the exon 4-5-6 splice variant encoding for the rodent Eb-peptide (corresponds to the human Ec-peptide). Primer sequences were: **Class 1 IGF-1**: forward 5'-CTCGATAACTTTGCCAGAAG-3', **Class 2 IGF-1**: 5'-AGTTTTGTGTTACCTCGGCC-3', **Exon 5 (5-25)**: reverse 5'-ATCCCTGTTC CCGCATGTC-3', **Exon 5 (118-136)**: reverse 5'-CCTTCTGGGTGTGTCTTTGG-3'. Expected fragment size for Class 1 IGF-1 mRNAs combined with the (5-25) exon 5 primer were 776 bp for mRNAs containing the full exon 1 5'-UTR and 590 bp for Class 1 IGF-1 mRNAs containing the spliced exon 1 5'-UTR (compare section 1.4.2). Class 1 IGF-1 mRNAs amplified with the (118-136) exon 5 reverse primer were expected to yield fragments of 888 bp for Class 1 mRNAs containing the full exon 1 sequence and 702 bp for those containing the spliced exon 1 5'-UTR. Amplification with Class 2 IGF-1 and (5-25) exon 5 primer was expected to yield a single fragment of 501 bp, while the combination of Class 2 IGF-1 primer and the further downstream (118-136) exon primer, was expected to amplify a fragment of 613 bp.

2.1.7 Cloning of probes for Northern blots

Probes for endogenous IGF-1 isoform detection were generated by combined reverse transcription PCR (compare 2.1.12), using 1 µg of total RNA from mouse liver. Specific primers used were:

186-exon 1 probe (spans a 186bp region in exon 1 5'UTR, which is spliced in 20% of total IGF-1 mRNA population in mouse liver (compare 1.4.2.5), therefore detects all mRNAs generated from transcription start sites one, two, and three, but not the Class 1 transgenes, as they do not contain this region): forward 5'-GTGAGGATTTTCTCTAAATCC-3', reverse 5'-GAAATGAATTGGTGGGCAG-3'. **Exon 2 probe** (spans 81 bps of exon 2 sequence): forward 5'-AGTTTTGTGTTACCTCGGCC-3', reverse 5'-GGTGCGGTCATTTTGGTAGG-3'. **Eb-probe** (spans the entire 52 bps of exon 5): forward 5'-TCCCCGTCCCTATCGACAAAC-3', reverse 5'-CTTTCCTTCTCCTTTGCAGCTTC-3'. **IGF-1R probe** (spans 339 bps of IGF-1R mRNA): forward 5'-CTACTGGAAGATCCGCCATTC-3', reverse 5'-GTGGTGGAGGTGAAACGGAG-3'. **SV40-probe** (spans 185bp of the most 5'-end of the SV40 poly(A) signal sequence): forward 5'-GATCTTTGTGAAGGAACCTTAC-3', reverse 5'-ATTCCACCACTGCTCCCATTC-3'. **Gata-2 probe** (spans 700 bps of Gata-2 mRNA): kindly provided by Antonio Musaro from the University of Rome, La Sapienza.

All probe fragments were cloned into pGEM[®]-T Easy vectors. For probe generation, plasmids were EcoRI-digested, gel-purified and quantified by gel-electrophoresis using a quantitative DNA-Ladder (MassRuler[™] DNA Ladder, Mix, ready-to-use; MBI Fermentas #SM0403). All primers were purchased from Invitrogen.

2.1.8 Preparation of DNA for generation of transgenic mice

All constructs selected for generation of transgenic lines were linearized as indicated above. The digestion products were run on ethidium bromide-free gels, excised and gel-isolated. For further purification, isolated fragments were ethanol precipitated by adding 1/10 volume of 5M sodium acetate and 2.5 volumes 100% ethanol, left for up to 1 hour at -20°C, washed in 70% ethanol, dried and re-suspended in injection buffer (10mM Tris-HCl, pH 7.5; 0.25 mM EDTA, pH 8.0). All injections were performed by the transgenic service of the EMBL-Monterotondo.

2.1.9 Genomic DNA isolation from mouse-tail biopsies and genotyping

Genomic DNA was isolated from mouse tail biopsies, taken from three-weeks-old pups. Tail biopsies were digested over night at 65°C proteinase K (PK) (Roche #11961799)-containing digestion buffer (0.5µg/µl PK, 10mM Tris-HCl pH 9.0, 50mM KCl, 0.1% Tris-ton®X-100), followed by a 30 min incubation at 95°C to inactivate PK. Samples were centrifuged at high speed for 15 min and without any further purification, 2 µl aliquots were used for all genotyping PCR reactions.

2.1.9.1 Genotyping of IGF-1 isoform transgenic mice

To ensure presence of the different IGF-1 transgenes, primers were designed to recognize all IGF-1 isoforms by choosing a forward primer located in exon 4 and a reverse primer located in the SV40 Poly(A) signal sequence adjacent to the 3'-end of the IGF-1 coding sequence (forward: 5'-ACTGACATGCCCAAGACTC AG-3'; reverse: 5'-ATTCCACCACTGC TCCCATTC-3'; Invitrogen). Band sizes were 283 bp for fragments containing the exon 4-6 splice variant (coding for the Ea-peptide) and 335 for fragments containing the exon 4-5-6 splice variant (coding for the Eb-peptide).

2.1.9.2 Genotyping of MLC/rtTA transgenic mice

Presence of the rtTA transgene was determined using primers amplifying a region within the SV40 poly(A) signal (forward 5'-GATCTTTGTGAAGGAACCTTAC-3', reverse 5'-ATTCCA CCACTGCTCCCATTC-3'; Invitrogen). A 185 bp fragment confirmed the transgenic background of the analyzed mice.

2.1.9.3 Genotyping of pBi/Class 1 IGF-1Eb transgenic mice

Presence of the inducible expression cassette was confirmed by PCR using primers specific for the luciferase gene (forward 5'-GCGAGAATCTGACGCAGGC-3', reverse 5'-CCGC TAGAGGATGGAACCG-3'), amplifying a fragment of 600 bp. Primers were purchased from Invitrogen.

2.1.10 Total RNA isolation from mouse tissues

Total RNA was isolated from frozen tissue following the standard TRIzol protocol (Invitrogen #15596-026). All equipment used was previously treated with RNase ZAP (Ambion #9780;0782). Tissues were homogenized (Biospec Products, Model 985379) in the appropriate amount of TRIzol (50-100 mg of tissue per 1 ml of TRIzol). RNA was separated using the appropriate amount of chloroform, precipitated with isopropanol, and washed in 75% ethanol. RNA was dissolved in 20-50µl of sterile water and stored at -80°C until used. The concentration of the RNA samples was determined by spectrophotometric measurement of the absorbance (A) at 260 nm and 280 nm.

2.1.11 Total RNA isolation from cultured cells

For RNA isolation, plates were washed twice with sterile phosphate-buffered saline (PBS) and scraped in 1ml of sterile PBS. Scraped cells were centrifuged for 5 min at 4°C and 1.100x g, washed in 5 ml of sterile PBS and the pellet was stored at -80°C if not processed immediately. For total RNA isolation the SV Total RNA Isolation System (Promega #Z3100) was used according to the manufacturer's instructions.

2.1.12 Combined reverse transcription (RT) PCR

Combined reverse transcription PCR was performed using the Access RT-PCR System (Promega #A1260), according to the manufacturer's instructions.

1µg of total RNA was used in each reaction and combined with specific primers. Other than suggested by the kit's instructions, the mixture of RNA, primers, and water was incubated on 94°C for 2 min to avoid any secondary mRNA structures. RT-PCR was performed (Reverse transcription: 45 min 48°C, 94°C for 2 min, PCR: 40x (94°C for 30 sec; 57°C for 1 min; 68°C for 2 min), 68°C for 7 min, 4°C for ever), and reaction products were stored at -20°C.

2.1.13 Reverse Transcription

For reverse transcriptions, the Ready-To-Go T-primed First-Strand Kit was used according to the manufacturer's instructions (Amersham, # 27-9263-01). 1µg of total RNA was used in every reaction and brought up to 33µl with sterile H₂O. The samples were first incubated at 65°C for 5 min and then left at 37°C for 5 min. The reaction tubes supplied by the kit were incubated at 37°C for the same time. Subsequently, the RNA/H₂O mix was transferred to the Ready-To-Go reaction tube and left at 37°C. After 10 min of incubation, the tube content was mixed by flicking the tube mildly and left for 1 hour at 37°C. Every reaction was then brought up to 200µl with sterile H₂O and cDNAs were stored at -20°C until needed.

2.1.14 SYBR green/Taqman quantitative RT-PCR

1µg of RNA was used for reverse transcription using Ready-To-Go T-primed First-Strand Kit described in section 2.1.13. Taqman real time PCR was performed on 1µl of cDNA using 10 µl of the Taqman Universal PCR Master Mix (Applied Biosystems #4304437), 1µl of each appropriate primer (10mM), and 2µl of the Taqman probe (2mM) in a total reaction volume of 20 µl. When SYBR green quantitative PCR was performed the same reaction conditions were applied, but without adding a Taqman probe. Duplicated samples were incubated at 95° for 3 min, followed by 45 cycles of amplification (2 min 50°C, 10 sec 95°C, 20 sec 60°C, 30 sec 72°). Results for each molecule were normalized to ubiquitin expression (forward 5'-TGGCTATTAATTATTCGGTCTGCAT-3', reverse 5'-GCAAGTGGCTAGAGTGCAGAGTAA-3'). Specific primers used for analysis of transgenic IGF-1 isoform expression levels were:

Endogenous IGF-1 isoform expression:

Class 1 IGF-1Ea (recognize Class 1 IGF-1Ea AND Eb): forward 5'-ATTTAAGATCTGCCTCTGTGACTTCTT-3', reverse 5'-TCTTGTTTCCTGCACTTCCTCTACT-3'; probe: 5'-TTTACTTCAACAAGCCC-3'. This is an major groove binding (MGB) probe and was labeled with FAM. **Class 1 IGF-1 Eb** (recognize Class 1 IGF-1Eb): forward 5'-ATTTAAGATCTGCCTCTGTGACTTCTT-3', reverse 5'-TCTTGTTTCCTGCACTTCCTCTACT-3'; probe: 5'-TCTCCTTTGCAGCTTC-3'. This is a MGB probe and was labeled with VIC. VIC probes can be run with FAM probes in the same tube and with SYBR green. FAM probes can not be run with SYBR green in the same tube. **Class 2 IGF-1Ea** (recognize Class 2 Ea AND Eb): forward 5'-TGTGTAAACGACCCGGACCTA-3', reverse 5'-TCTTGTTTCCTGCACTTCCTCTACT-3'; probe: 5'-TTTACTTCAACAAGCCC-3'. This is an MGB probe and labeled with FAM. **Class 2 IGF-1Eb** (recognize Class 2 IGF-1Eb): forward 5'-ATTTAAGATCTGCCTCTGTGACTTCTT-3', reverse 5'-TCTTGTTTCCTGCACTTCCTCTACT-3'; probe: 5'-TCTCCTTTGCAGCTTC-3'. This is a MGB probe and labeled with VIC.

All primers can be used with SYBR green, which will recognize any double stranded DNA present. SYBR green is compatible with VIC but not FAM-labeled probes. All primers and probes were designed by Leanne Felkin (Harefield Heart Science Centre, Imperial College London, UK) and conditions set up by Leanne Felkin and Enrique Lara-Pezzi (HHSC, ICL, UK / EMBL-MR).

Since Class 1 and Class 2 IGF-1Ea primer and probe sets recognize both Class 1/2 IGF-1 Ea and Eb, values for the IGF-1Eb versions were subtracted from values for IGF-1Ea expression to calculate expression levels for Class 1 or 2 IGF-1Ea.

Calcineurin isoform expression:

CnAα (200): forward 5'-CAAGGCGATTGATCCCA-3', reverse 5'-TCGAAGCACCTCTGTTA-3';
CnAβ1 (229): forward 5'-AGAAGGTGAAGACCAGT-3', reverse 5'-AGCAAGTTGCATAACAT

ATT-3'; **CnA β 2** (300 bp): forward 5'-AGGCTATTGAGGCTGAAA-3', reverse 5'- CGGATCTC AGAAAGCAC -3'. All RT-PCRs for calcineurin were done with SYBR green.

Primers used for regeneration analysis:

Pro-Collagen 1: forward 5'-GTAAGTTCGTCGCTAGCAACA-3', reverse 5'-CCTTTGTCAGAAT ACTGAGCAGC-3'; **TGF- β 1**: forward 5'-CCGAAGCGGACTACTAT-3', reverse 5'-GTAACGCC AGGAATTGT-3'; **TNF- α** : forward 5'-GCAAGCTTCGCTCTTCTGTCTACTGAACTTCGG-3', reverse 5'-GCTCTAGAATGAGATAGCAAATCGGCTGACGG-3'; **MCP-1**: forward 5'-CACCAGCAAGATGA TCC-3', reverse 5'-ATAAAGTTGTAGGTTCTGATCTC-3'; **Rantes**: forward 5'-ACCATCATCCTCA CTGC-3', reverse 5'-GATGTATTCTTGAACCCACT-3'; **IL-10**: forward 5'-CCAAGCCTTATCGGA AATG-3', reverse 5'-TGGCCTTGTAGACACC-3'

2.1.15 Northern blot analysis

For separation of RNA samples a 1.3% agarose gel containing 1x MOPS and 7% formaldehyde (Sigma #F-8775) was prepared. 10-15 μ g of RNA were brought to 5 μ l with sterile water and mixed with 15 μ l of freshly prepared RNA loading buffer (1 volume of bromophenol blue-xylene cyanole dye solution (Sigma B-3269), 4 volumes of formamide (Sigma #F-7508), and 1 μ l of ethidium bromide [10mg/ml] per 100 μ l of solution). Samples were incubated at 65°C for 10 min, chilled on ice and loaded. Gels were run at 80 V and photographed under a UV lamp to ensure RNA integrity.

Gels were rinsed four times five min in sterile H₂O, while the nylon membrane (GeneScreen Plus NEF976, NENTM Life Science Products) was hydrated in sterile H₂O and incubated in 10xSSC for 15 min. The Transfer Apparatus was built following standard protocols and performed over night. Membranes were rinsed in 2xSSC after transfer, UV-cross linked (UV-Stratalinker 1800, Stratagene), and baked at 80°C for 1-2 hours.

For hybridization, Northern blots were re-hydrated in 2xSSC and pre-hybridized (50% formamide, 1M NaCl₂, 10% dextran sulfate, 1%SDS) for at least 4 hours at 42°C.

Preparation of radiolabeled probes. All probes for Northern blots were labeled by using the Megaprime DNA labeling system (Amersham #RPN1604) according to the manufacturer's instructions. This system is based on the use of random sequence hexanucleotides to prime DNA synthesis on denatured template DNA. 25-50ng of DNA and 5 μ l of radiolabeled [α ³²P] dGTP (3000Ci/mmol) (Amersham) were used in each labeling reaction. For isolation of the hot probe the G-50 Sephadex Quick Spin Columns for radiolabeled DNA purification (Roche #11273973001) were used following the manual's instructions.

Hybridization of Northern blots. Prior to use, the hot probe was mixed with 150 μ l of salmon sperm DNA per 15 ml of hybridization solution, heated at 95°C for 5 min, and chilled on ice for 5 min. The mixture was then added directly to the pre-hybridization solution. Hybridization was carried out over night at 42°C.

blots were rinsed once in 0.2M SSC, washed in washing buffer (0.2M SSC, 0.5% SDS) for 10 min at RT, for 20 min at RT, and for 30 min at 60°C. The solution was changed after each washing step. The filters were then wrapped in saran wrap and exposed to a phosphorimager screen for 3 hours and if needed over night.

Removal of probes from Northern blots. To remove hybridization probes, the membrane was boiled in stripping solution (1% SDS, 0.1x SSC, 0.015M NaCl) for 10 min. To verify probe removal, the membrane was wrapped in plastic wrap and exposed to a phosphorimager screen for 3 hours.

2.1.16 GeneChip analysis

Two one-month-old male transgenic mice and two negative littermates from each transgenic line were sent for Affymetrix GeneChip analysis performed by the EMBL Genomics Core Facility. Total RNA from the quadriceps muscle of each mouse was isolated following the TRIzol protocol described in section 2.1.10. Further purification was achieved by using the QIAgen RNeasy Midi Kit (QIAgen #75142) according to the manual's instructions. To ensure integrity of the RNA, 2µg of each sample were run on a formaldehyde gel (1.3% agarose, 1x MOPS, 7% formaldehyde). Functionality of the RNA samples was determined by reverse transcribing 1µg of each sample (Ready-To-Go T-primed First-Strand Kit compare 2.1.13) and performing PCR with β -tubulin-specific primers (forward 5'-CTGGGCTAAAGGCCAC-3', reverse 5'-AGACACTTTGGGCGAG-3').

Micro array analysis. Two transgenic and two control RNA samples from each animal model were hybridized to Affymetrix MO430-2 Mouse Genome Array chips. The screen returned 22626 probe set signals. With the great help of Tommaso Nastasi those data sets were then analyzed as follows. In order to reduce variances due to the background of each transgenic model, we calculated the average values and variability of the total eight control mice analyzed, and excluded the probe-sets that did not show consistent signal among the different wildtype controls. We also excluded probe-sets that showed a low signal or high variability in all of the sample groups analyzed, i.e. wildtype (WT) and the four IGF1 isoform transgenic samples. This initial filtering returned 15333 probe sets valid for analysis. For every transgenic model we selected all the probe sets that either showed an increase or decrease by 1.9 fold, compared to WT values. Within this pool of genes we then identified the probe sets that showed increase (or decrease) by 1.9 fold only in the model under focus and a signal ratio of 1.3 or less (or -1.3 or more) in the other 3 models (unique probe sets). The distribution of the selected genes by cellular localization was performed by using the Gene Ontology database information available for the different probe sets at the Affymetrix website (www.affymetrix.com). Pathway analysis was performed using a trial account on the

Ingenuity Pathway Application server, based on the proprietary knowledge database of this company (www.ingenuity.com).

For the comparison of genes whose altered expression could be relevant for a Class- or E-peptide-specific IGF1 function, the reduced filtered array of 15333 probe sets was analyzed as follows. We grouped the four samples by either Class or E-peptide feature (2 Class groups and 2 E-peptide groups); a cut off value of fold-induction of 1.3 was set for either up-regulated or down-regulated genes; all the genes that resulted up-regulated in both samples of the analyzed group AND down-regulated or unchanged in the opposing group OR the genes that resulted down-regulated in the analyzed group AND up-regulated or unchanged in the opposing group were selected.

2.2 Cell Biology

2.2.1 Established myoblast cell cultures and transfection

L6E9 and C2C12 cells were plated and extended in growth medium (GM: 20% fetal bovine serum (FBS) (Gibco #10270-106), 2mM L-glutamine (Gibco #25030-024), 1mM Na-pyrovate (Gibco #11360-039), 10mM HEPES (Gibco #15630-056), 1x penicillin/ streptomycin (Gibco #15140-122) in Dulbecco's Modified Eagle Medium (DMEM) (Gibco #41965-039)). L6E9 cells were differentiated in differentiation medium (DM), containing 1% albumin (Sigma #A-8806), 2mM L-glutamine, 1mM Na-pyrovate and 1x penicillin/ streptomycin. C2C12 cells were differentiated in DM containing 2% horse serum (Gibco #26050-088), 2mM L-glutamine, 1mM Na-pyrovate, 10mM HEPES and 1x penicillin/ streptomycin.

Transient transfections of L6E9 cells were done with LipofectamineTM 2000 (Invitrogen #11668-019), using a modified protocol: the cells were plated at a concentration of 200.000 cells/ml the day before the experiment. Prior to transfection, cells were washed three times in plain DMEM and incubated in DMEM containing 10% FBS, 2mM L-glutamine and 1mM Na-pyrovate for at least 30 min before transfection. For transfection of one 10 cm plates a total of 24µg of DNA was used as suggested by the protocol and diluted in 1.5ml of DMEM only substituted with 1mM Na-pyrovate and 2mM L-glutamate. For the double-transfections with the two necessary plasmids of the tet-on system (compare section 2.1.5.2) a ratio of 1 (pBi/IGF-1 isoform x): 3 (pUHrtTA) was used. For every 10 cm plate 60µl of LipofectamineTM were diluted in DMEM containing 1mM Na-pyrovate and 2mM L-glutamine and both solutions were incubated for 5 min at RT. The solutions were then combined, incubated for another 20 min at RT and added to the pre-incubated plates for at least 5 hours. After the transfection incubation, the medium was exchanged with DMEM containing 10% FBS, 2mM L-glutamine, 1mM Na-pyrovate, 10mM HEPES and 1µ/ml doxycycline and the plates were incubated over night. After about 12 hours, the medium was exchanged with doxycycline-substituted (1µg/ml)

DM. The preparation of RNA and protein samples is described in sections 2.1.11 and 2.3.2 respectively.

2.2.2 Skeletal muscle primary cell cultures

Whole legs from 2-5 days old pups were incubated in penicillin/ streptomycin/ gentamycin (400µg/ml) (GIBCO #15750-045) for 15 min. All skeletal muscle groups from 4-6 legs were removed carefully and chopped into small pieces. Enzymatic desegregation was achieved by 30 min incubation at 37°C each in first collagenase (1mg/ml) (Sigma #C-5138) and then collagenase/ dispase (1mg/ml) (Sigma #C-3180) solutions. Enzymatic reactions were stopped by adding the appropriate amount of horse serum (GIBCO #26050-088). The solution was filtered twice to remove cell debris (70µm and 40µm cell strainer filters (Falcon #352350 and #352340)) and then centrifuged (10 min at 1100 rpm). The cell pellet was dissolved in the appropriate amount of GM (20% horse serum, 3% chicken embryo extract (ICN #2850145), 1mM Na-pyrovate, 2mM L-glutamine, XM HEPES, 1x penicillin/ streptomycin and 0.8µg/ml gentamycin (Gibco #15750-045) in DMEM) and pre-plated twice for 30 min each to reduce the number of fibroblasts. Cells were plated in 3cm petri dishes and left over night in GM. Medium was changed to DM (5% horse serum, 4mM L-glutamine, 10mM HEPES and 1x penicillin/ streptomycin) after 24 hours to induce differentiation of the myoblasts.

2.3 Biochemistry

2.3.1 Preparation of protein lysates from mouse skeletal muscle

Frozen tissues were homogenized using a 2 ml tissue grinder (WHEATON #358003) at 4°C in the appropriate amount of lysis buffer (20mM Tris pH 7.5, 5mM MgCl₂, 150mM NaCl, 1% SDS, 1mM NaVO₄, 1mM NaF, 1mM PMSF; for 5ml of final lysis buffer, one tablet of Complete Mini Protease Inhibitors (Roche #11836170001) was added). For immunoprecipitation, a milder lysis buffer was used (20mM Tris pH 7.5, 5mM MgCl₂, 150mM NaCl, 1% NP40, 0.1% TritonX, 1mM NaVO₄, 1mM NaF, 1mM PMSF; for 5ml of final lysis buffer, one tablet of Complete Mini Protease Inhibitors was added). Samples were sonicated for 20-30 sec, centrifuged (10 min at 4°, 14.000 rpm), and protein concentration of the supernatant was determined by Bradford assay (Bio-Rad Protein Assay Dye Reagent Concentrate #500-0006). All protein extracts were stored at -80°C until needed.

2.3.2 Preparation of protein lysates from cultured cells

Cultured cells were washed twice in sterile PBS and scraped in the appropriate volume of lysis buffer (20mM Tris pH 7.5, 5mM MgCl₂, 150mM NaCl, 1% SDS, 1mM NaVO₄, 1mM NaF,

1mM PMSF; for 5ml of final lysis buffer, one tablet of Complete Mini Protease Inhibitors was added). Lysates were sonicated for 20-30 sec, centrifuged for 10 min at 4°C and 14.000 rpm, and protein concentration of the supernatant was determined by Bradford assay. Protein extracts were stored at -80°C until needed.

2.3.3. Preparation of protein lysates from cultured cells for luciferase assay

For detection of luciferase in protein lysates the Promega Luciferase Assay System (#E1500) was used according to the manufacturer's instructions. Cells were washed twice in sterile PBS, scraped in 300µl 1x lysis buffer (provided by the Assay System), and after transfer into a suitable tube incubated on ice for 12 min. Luciferase activity was measured immediately or samples were frozen at -20°C until needed. The measurements were done on 5µl of 1:500 diluted protein lysates for 10 seconds.

2.3.4 Immunoprecipitation

Protein extracts were prepared as described in section 2.3.1 and immediately used for immunoprecipitation. The appropriate amount of protein A (Sigma #P-3391) was left to swell in 1ml of PBS for 10 min at RT and centrifuged for 30 seconds at 4°C and maximum speed. Supernatant was removed and PBS was added for equal distribution of protein A to the desired number of tubes. 1 ml of lysis buffer stock solution (without inhibitors) was added and left for 10 min for equilibration. After centrifugation for 30 seconds, 4°C and maximum speed, the supernatant was removed and 150µl of lysis buffer stock solution substituted with the appropriate amount of antibody (diluted according to the manufacturer's description) (compare table 1) were added and incubated rotating over night at 4°C. 2-4mg of protein sample were added to the pre-incubated tubes and left rotating for 1.5 hours at 4°C. Samples were washed four times with 1ml of lysis buffer stock solution. 30µl of 2x SDS-loading buffer (100mM Tris pH 6.8, 4% SDS, 20% glycerol, bromophenol blue) without DTT were added to each sample and specimens were frozen at -20°C until used for Western blot analysis.

Primary Antibody	Description	Company
Anti-IGF-1Receptor β	Rabbit polyclonal	Cell Signaling #3027

Table 1 List of primary antibodies used for immunoprecipitation.

2.3.5 Western blot analysis

For SDS-page, proteins were diluted in 2xSDS sample buffer (100mM Tris pH 6.8, 4% SDS, 20% glycerol, bromophenol blue), denatured by boiling for 5 min and subjected to gel-electrophoresis. If immunoprecipitated samples were used, DTT to a final concentration of 2mM was added to each sample prior to boiling. Proteins were electrophoretically transferred

onto a polyvinylidene difluoride (PVDF) membrane (Amersham), which has been activated for 10 seconds in methanol (Fluka #65542) and equilibrated in transfer buffer (14.45g Glycin, 3g Tris-baze, 0.75g SDS, ad 800ml with H₂O and 200 ml methanol) prior to transfer. Transfer was carried out in a wet transfer apparatus for 1.5 hours at 100V. After transfer membranes were left in methanol for 10 seconds, dried and incubated in blocking solution (5% non-fat powder milk (Roth #T145.2)) dissolved in TBST buffer (20mM Tris pH 7.5, 140mM NaCl, 0.1% Tween20) for 1 hour up to over night. Primary and secondary antibodies were diluted in blocking solution to the dilutions indicated by the company if not otherwise specified (Tables 2 and 3). Membranes were washed 3 to 4 times in TBST buffer between primary and secondary antibody incubations. To detect specific bands the enhanced chemiluminescence system (ECLTM) Western Blotting Detection Reagent (Amersham #RPN2106) was used, followed by the exposure to HyperfilmTM ECL films (Amersham #RPN3103K).

Primary Antibody	Description	Company
Anti-IGF-1	Goat polyclonal	R&D Systems
Anti-phospho histone H3	Rabbit polyclonal	Cell Signaling
Anti-histone H3	Rabbit polyclonal	Cell Signaling
Anti-phospho Akt	Mouse monoclonal	BD Pharmingen
Anti-PKB α /Akt	Mouse monoclonal	BD Pharmingen
Anti-phospho SAPK/JNK	Rabbit polyclonal	Cell Signaling
Anti-JNK1	Rabbit polyclonal	Santa Cruz
Anti-phospho p44/42 MAPK	Mouse monoclonal	Cell Signaling
Anti-p44/42 MAPK	Rabbit polyclonal	Cell Signaling
Anti-phospho p38 MAPK	Rabbit polyclonal	Cell Signaling
Anti-p38 (C-20)	Rabbit polyclonal	Santa Cruz
Anti-myogenin (Clone FD5)	Mouse monoclonal	Santa Cruz
Anti-MEF2C	Rabbit polyclonal	Cell Signaling
Anti-phospho S6 ribosomal protein	Rabbit polyclonal	Cell Signaling
S6 ribosomal protein	Rabbit polyclonal	Cell Signaling
Anti-mouse IGFBP-5	Rat monoclonal	R&D Systems
Anti- α -tubulin	Mouse monoclonal	Sigma
Anti-Phosphotyrosine Clone 4G10	Mouse monoclonal	Upstate

Table 2 List of primary antibodies used in Western blot analysis

Secondary Antibody	Description	Company
Donkey-anti-rat IgG	Polyclonal	Jackson IR

ECL Anti-rabbit IgG	Polyclonal	Amersham
ECL Anti-mouse IgG	Polyclonal	Amersham
Rabbit Anti-goat IgG HRP	Polyclonal	Chemicon

Table 3 List of secondary antibodies used in Western blot analysis

2.3.6 Generation of IGF-1 antibodies

Since IGF-1 isoform-specific antibodies are not available yet, we tried to raise Ea- and Eb-peptide-specific antibodies. Antigenic peptide sequences were selected (**pan-IGF-1** (to recognize mature IGF-1): VDECCFRSCDLRRLE; **Ea-peptide**: EVHLKNTSRGSAG; **Eb-peptide**: KKTKLQRRRKGSTFE) and synthetic peptides were produced by Sigma-Genosys. Generation of polyclonal rabbit antisera was also done by Sigma-Genosys. We received four bleedings for each injected rabbit (two rabbits per peptide) that were tested by ELISA (data not shown) and Western blot (data not shown). Pan-IGF-1 and Ea-specific antibodies failed to give a specific signal in western blot analysis, while Eb-specific antibodies detected Eb-peptide-containing isoforms specifically (Figure 2.4). In a second attempt, the same synthetic peptides were used to raise monoclonal antibodies by the EMBL Monoclonal Antibodies Core facility. No positive clones were received for the Ea- and Eb-peptide injections, but two positive clones were obtained for pan-IGF-1 (Figure 2.4)

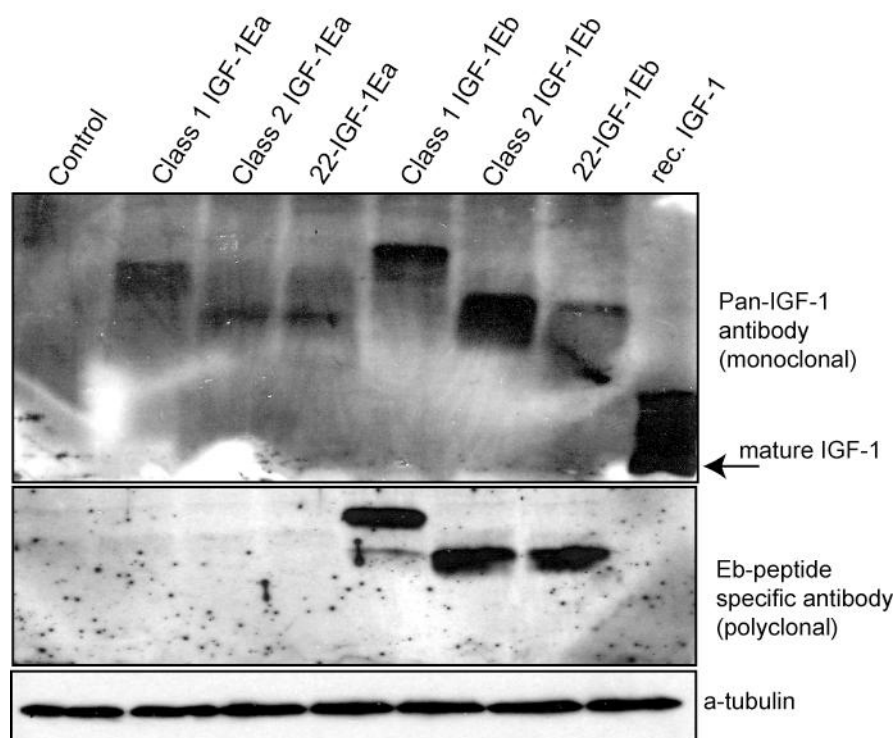


Figure 2.4 Generation of IGF-1 antibodies. 50µg of protein from IGF-1 isoform transfected cells were separated by SDS-page and transferred for Western blot analysis. The upper panel shows one of two obtained positive clones of an antibody directed against mature IGF-1. This antibody therefore detects each IGF-1 isoform. The lower panel shows detection of only Eb-peptide containing isoforms with a polyclonal antibody directed against the Eb-peptide.

2.3.7 Immunoenzymometric assay (IEMA)

To determine circulating IGF-1 levels, the OCTEIA Rat/Mouse IGF-1 IEMA for the quantitative determination of IGF-1 in rat and mouse serum or plasma was used (iDS, AC-18F1) according to the instructions. Sampling of blood and isolation of serum is described in 2.5.1. Results were calculated by logarithmic plotting of the mean absorbance of each calibrator (provided by the kit) on the ordinate against concentration of rat IGF-1 on the abscissa. Values for controls (provided by the kit) and the unknown samples were read from the calibration curve in ng/ml.

2.4 Histochemistry

2.4.1 Processing of tissues for frozen and paraffin sections.

Tissues collected for frozen sections were excised and frozen as described in section 2.5.1. Transverse sections of the mid belly region of the frozen muscle were cut on a cryostat, collected onto SuperFrost®Plus glass slides (Menzel-Glaeser), air-dried, and stored at -80°C until used.

Tissues sampled for paraffin sections were removed as described in section 2.5.1, fixed in 4% paraformaldehyde (Sigma #P6148) for 30 min, washed in 2 x 5 min in 1x PBS, and dehydrated by incubation in ethanol solutions of increasing percentage (2x30 min in 50%, 2x30 min in 70%, 1x30 min in 95%, and 2x30 min in 100% ethanol). Tissues were washed 3x15 min in xylene (Riedel-de Haen #33817), incubated in a 1:1 paraffin wax/xylene mix at 60°C for 30 min, and after six changes of paraffin wax (1 hour per incubation), tissues were embedded in fresh paraffin wax and left over night to dry. Sections were cut at a thickness of 8µm.

2.4.2 Double Immunohistochemistry

The VECTOR® M.O.M. Immunodetection Kit (VECTOR Laboratories #BMK-2202) was used according to the instruction manual. Frozen muscle sections (8µm) were equilibrated to room temperature, re-hydrated in PBS, and incubated for 1 hour in M.O.M Mouse Ig blocking reagent. Sections were washed twice for 2 min in PBS and incubated for 20 min in working solution of M.O.M diluent, which was removed afterwards. The primary type IIB myosin antibody was a kind gift from Miranda Grounds and applied as an undiluted supernatant over night at 4°C. Slides were equilibrated to room temperature and washed twice for 2 min in PBS. Pan-laminin (Sigma #L-9393), diluted 1:200 in M.O.M. diluent, was applied as the second primary antibody and incubated at 37°C for 1 hour, followed by two PBS washing

steps for 2 min each. The secondary antibody biotin-conjugated goat anti-mouse IgM (Sigma #B-9265) was diluted 1:250 in M.O.M. diluent, and incubated for 1 hour at RT. Sections were washed twice for 5 min in PBS. Anti-type IIB myosin antibody was detected by incubation with streptavidin ALEXA 488 (Molecular Probes #S-11223), diluted 1:3000 in 0.1% BSA, and Pan-laminin was visualized by incubation with goat anti-rabbit ALEXA 594 (Molecular Probes #A-11012), diluted 1:250 in 0.1% BSA. Incubation was carried out for 1 hour at RT, followed by two 5 min washing steps in PBS. Nuclei were stained with HOECHST for 2 min. Slides were washed twice for 5 min in PBS and mounted with Aqua-Mount (Lerner Laboratories #13800).

2.4.3 Haematoxin/Eosin Staining

Paraffin sections were incubated in xylene for 3 min, re-hydrated with 1 min ethanol washes of decreasing percentage (100%, 70%, 50%), washed in dH₂O, and incubated in Harris Haematoxin solution (Sigma-Aldrich #HHS16) for 1 min. Slides were washed in dH₂O, treated with acidic alcohol (1% HCl, 70% ethanol) for 30 seconds, washed again in dH₂O, and left in 1% eosin solution for 30 sec. After a dH₂O wash, sections were transferred to 95% ethanol (30 seconds), 100% ethanol (1-2 min), and then left in xylene for at least 3 min until mounted (Eukitt quick hardening mounting medium, Fluka #03989).

2.4.4 Trichrome Staining

Paraffin sections were deparaffinized by three 5 min washes in xylene, followed by 3 min ethanol washes of decreasing percentage (100%, 95%, 80%, and 70%). Sections were then fixed for 15 min at 56°C in Bouin's solution (Sigma-Aldrich #HT10-1-32) and washed in running tap water. Nuclear staining was achieved by 5 min incubation in Weighert's iron haematoxin solution (Sigma-Aldrich #HT 1079-1Set). Slides were washed in dH₂O and stained 5 min in Biebrich scarlet-acid fuchsin (Sigma-Aldrich #HT 1079-1Set) and washed again. After 10 min incubation in phosphotungstic/ phosphomolybdic acid solution, sections were stained for collagen (5 min) in aniline blue (Sigma-Aldrich #HT 1079-1Set), then treated with 1% acetic acid for 2 min, and washed in dH₂O. Sections were then dehydrated by ethanol washes of increasing percentage (70%, 80%, 95%, and 100%), cleared in xylene for 3min, and mounted (Eukitt quick hardening mounting medium).

2.4.5 Nicotinamide Adenine Dinucleotide Nitro-Blue Tetrazolium (NADH)-TR Staining

Histochemistry with NADH was used to differentiate fast, intermediate, and slow fibers [294]. Frozen muscle sections (8µm) were incubated in NADH-TR solution (1 volume NADH solution (Sigma #N-8129): 1 volume nitro blue tetrazolium (NBT) solution (Sigma #N-6876))

for 30 min at 37°C, followed by 3 washes in distilled deionized water (ddH₂O) and 3 changes of increasing (30, 60, 90%) and decreasing acetone solutions (30 seconds each) to remove unbound NBT. Slides were rinsed with ddH₂O and mounted with Aqua-Mount (Lerner Laboratories #13800).

Morphometric analysis was performed on digital images taken by a camera (Nikon DXM 1200F) connected to a Leica PM RBE microscope. Non-overlapping images were taken of the entire cross-sectional area of the muscle using ImagePro Plus 4.0 (Microsoft) software and tiled to reconstitute the whole image of the muscle. CSA of fast, intermediate, and slow fibers was measured by tracing individual myofibers using ImagePro Plus 4.0 or MetaMorphTM (Universal Imaging Corporation). Fast, intermediate, and slow fibers were measured in the whole muscle section from four individual mice of each transgenic line and genotype.

2.5 Animals

Animals were housed in individual ventilated cages and maintained on a 12 hour light/dark regime with free access to standard chow and drinking water. All experiments were performed according to the EMBL ethical committee. In all cases the FVB strain of mice was used.

2.5.1 Experimental procedures

Dissection of mice. Animals were sacrificed by asphyxiation with CO₂ and cervical dislocation. The body weight was determined and tissues were removed and weighted.

For RNA and protein analysis, tissues were snap-frozen in liquid nitrogen, and then stored at -80°C until needed. For preparation of frozen sections, tissues were cut transversely in the central area, mounted onto tragacanth gum (Sigma #G-1128), and snap-frozen in liquid nitrogen-quenched isopentane (BDH #294526G). For paraffin sections, tissues were fixed in 4% paraformaldehyde for 30 min. and processed as described in 2.4.1. If blood samples were taken, animals were sacrificed by asphyxiation with CO₂. The chest was opened and blood samples were taken directly from the heart and kept at 4°C over night. Blood serum was separated by centrifugation of blood samples (4°C, 14.000rpm for 20 min.). Serum samples were stored at -80°C until needed.

Cardiotoxin injections. Three-month-old mice were anesthetized by injecting the appropriate amount of 2.5% avertine (2,2,2-Tribromoethanol; Sigma-Aldrich #T48402), which was determined by the body weight of the animal. The left leg was shaved and 5µl of 10µM

cardiotoxin (Latoxan #L8102) was injected in five different points in the TA muscle (total of 25µl) and in eight different points in the quadriceps muscle (total of 40µl). Cardiotoxin is a specific inhibitor of the protein kinase C isolated from *Naja nigricollis* snake venom and leads to depolarization of skeletal muscle fibers [295]. The right leg was used as a control. Animals were sacrificed after two, five, and ten days. The TA muscle was used for paraffin sections, while the quadriceps was removed for RNA and protein analysis.

2.5.2 Electrophysiology

For the *in vitro* analysis of the mechanic properties of IGF-1 isoform transgenic skeletal muscle, an isometric protocol described below was applied. All experiments have been performed by Emanuele Rizzuto from the University of Rome, La Sapienza (Group of Antonio Musaro).

The muscle to be tested was vertically mounted in a temperature controlled chamber (30°C), where it was immersed in a continuously oxygenated Krebs-Ringer bicarbonate buffer solution. One end was linked to a fixed clamp while the other end was connected to the lever-arm of an ASI 300b Dual-Mode actuator/transducer with a non-compliant nylon wire. The protocol is based on the appropriate electrical stimulation that is achieved by keeping the excised muscle in the bathing solution, which is connected to a couple of electrodes, and by the simultaneous acquisition of the evoked force. The muscle was initially stimulated with three 0.5ms single pulses (twitch) and subsequently with three trains of 0.1ms pulses performed at a typical summation frequency (120Hz pulses for 0.6s for the EDL muscles, 30Hz pulses for 1s for the soleus muscles). To evoke tetanic force the muscle was then stimulated with two trains of 0.1ms pulses (180Hz pulses for 0.6s for the EDL muscles, 60Hz pulses for 1s for the soleus muscles). Finally the muscle was subjected to a series of closer trains of pulses to induce isometric fatigue (120Hz pulses for EDL and 60Hz pulses for soleus for 0.4s every just 1s).

During the first twitch we measured twitch force and contraction time (Figure 2.5 A), while during the first train of pulses at tetanic frequency the maximum force was acquired (Figure 2.5 B). Dividing this value of force for the weight of each muscle we obtained the values for the specific force (N/g). Finally, during the fatigue stimulation we measured the skill of the muscle to resist to repeated stimulations measuring the time (*fatigue time*) it needs to half the value of its own maximum force (Figure 2.5 C).

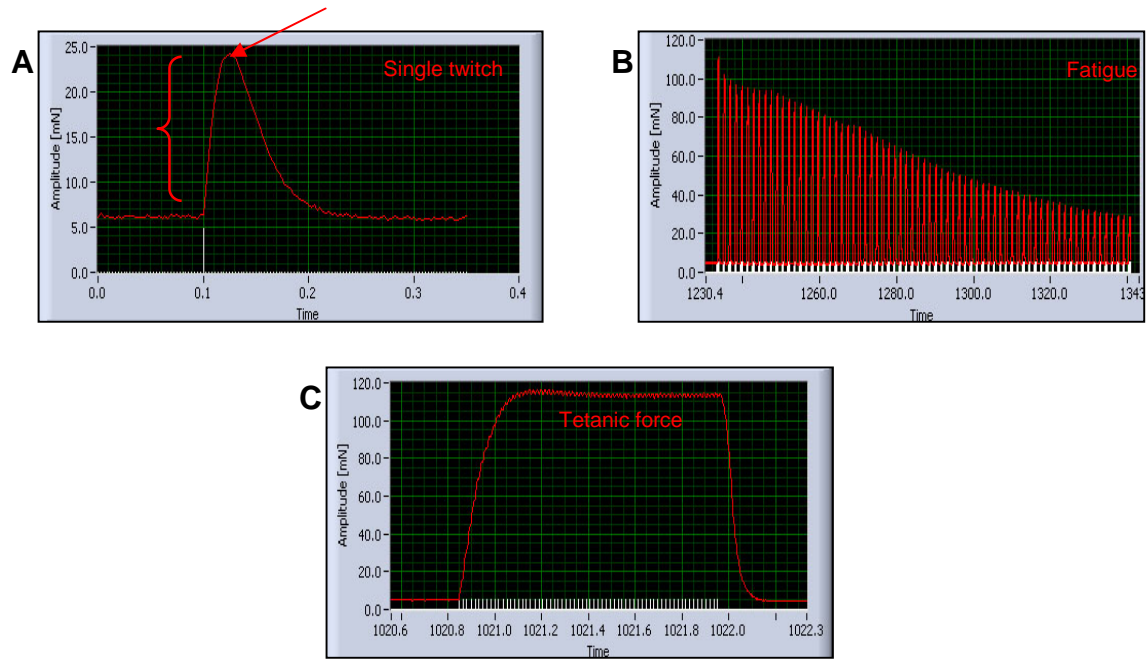


Figure 2.5 Electrophysiological analyses of skeletal muscle. **A** Measurement of maximal twitch force (red arrow) and contraction time (red parenthesis) by single pulse stimulation **B** Measurement of the maximal force (titanic force) by pulse train stimulation **D** Measurement of the fatigue time (time the muscle needs to half its maximum force) by pulse train stimulation

2.6 Statistical analysis

Statistical analysis was performed using the student's *t* test (tail 2, type 2) and differences were considered significant when p-value was <0.05.

3 Results

3.1 A rodent IGF-1 isoform containing a third E-peptide

In rodents, two 3' splice variants have been described, encoding different E-peptides. The rodent and human Ea-peptides share extensive homology, whereas the second rodent E-peptide (Eb) corresponds to the Ec peptide in human nomenclature (discussed in section 1.4.2.6). The possible existence of an exon 4-5 splice variant, which encodes a third E-peptide in humans (confusingly named Eb-peptide), was also predicted in rats [176], but since it was not detected in rat liver using Northern blot analysis, it was assumed that the human Eb splice variant does not exist in rodents (compare section 1.4.2.6). This section describes the cloning of a mouse Class 2 IGF-1 isoform containing the exon 4-5 splice variant, which we term En-peptide.

Forward primers were designed to bind to exon 1 or 2, thereby amplifying Class 1 or Class 2 isoforms, and reverse primers were designed to bind to two different regions in the intron sequence downstream of the 52 bp region (bp 5-25 and 118-136) that until now was considered to represent rodent exon 5 (section 2.1.6). By choosing such primer pairs, Class 1 and Class 2 isoforms containing the exon 4-5 splice variant were expected to be amplified. Since liver is the one tissue in the body that is known to express all IGF-1 isoforms, total RNA isolated from three-months-old mouse liver was chosen for RT-PCR (Figure 3.1A). RT-PCR with the primer pair Class 1 and (5-25) did not yield any fragments, while primer pairs Class 1 and (118+136) amplified four fragments, but only one showed the expected size (702 bp). RT-PCR performed with primers for Class 2 and (5-25) yielded two fragments with one being of the expected size (501 bp), and primers for Class 2 and (118-136) amplified one 613 bp fragment (Figure 3.1 A). DNA fragments of expected sizes were sub-cloned and sequenced. Analysis of the sub-cloned sequences revealed that the 702 bp fragment obtained from RT-PCR with Class 1 and (5-25) and the 501 bp fragment from RT-PCR with Class 2 and (5-25) were unspecific, while the 613 bp fragment amplified with Class 2 and (118-136) primers represented a Class 2 IGF-1 isoform encoding the third E-peptide described in humans (human Eb-peptide). To avoid more confusion in the nomenclature of IGF-1 isoforms and E-peptides, we termed this third rodent version Enew-peptide (En-peptide). The En-peptide could only be amplified together with the Class 2-specific primers, suggesting that no Class 1 IGF-1En isoforms are expressed in the liver.

Analysis of the mRNA sequence of the En-peptide revealed a TAG stop codon 141 bp downstream of the exon 5 start as well as four AATATA polyadenylation signals (458, 569, 2888, and 5178 bp downstream of the exon 5 start respectively). No consensus AATAAA polyadenylation signals could be predicted. Further characterization is needed to identify the functional poly(A) addition sites of the exon 5-encoded 3'-UTR for this splice variant.

The mouse exon 4-5 splice variant encodes a 63 amino acid En-peptide sequence (16 aa encoded by exon 4 and 47 aa encoded by exon 5), while the human counterpart (Eb-peptide in humans) encodes a 77 amino acid E-peptide (16 aa from exon 4 and 61 aa from exon 5) and there is only 57% homology between the common N-terminal 63 amino acids of those two sequences. Most importantly, the predicted amino acid sequence encoded by the mouse exon 4-5 splice variant does not contain a GKKK signal for proteolytic cleavage and peptidyl C-terminal amidation, which has been shown to be used in human Eb-peptides to generate the IGF-1B(103-124) E₁amide (IBE₁) [296]. Synthetic IBE₁ has been shown to have mitogenic effects on normal and malignant human bronchial epithelial cells and to bind to specific high-affinity receptors [296]. In addition, the mouse exon 4-5 splice variant lacks a nuclear and nucleolar localization signal (KKGK), which has also been described for the human Eb-peptide and has been shown to direct this human IGF-1 isoform to the nucleolus [199] (Figure 3.1 B). Further analysis will therefore be necessary to determine whether the rodent En variant is functionally equivalent to the longer human Eb variant.

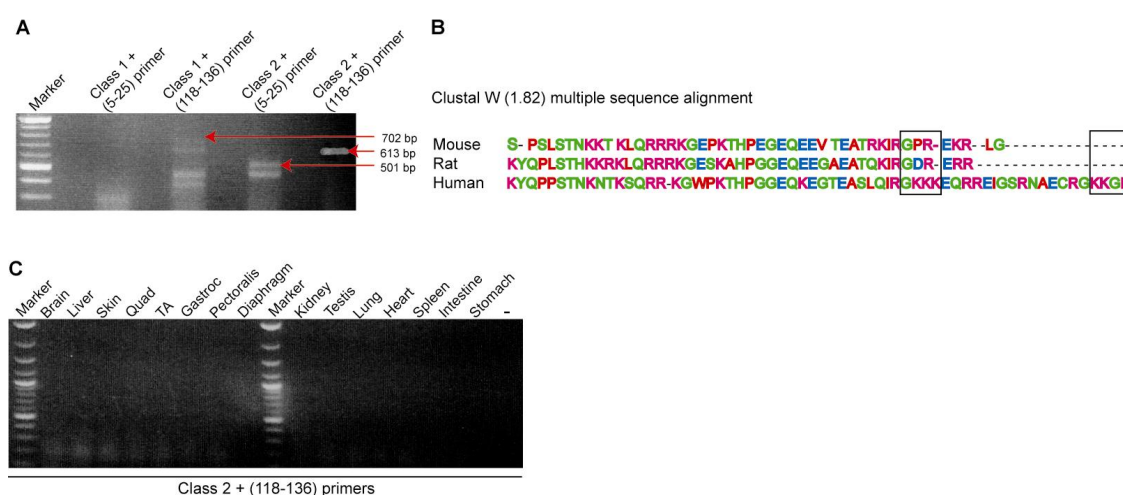


Figure 3.1 Cloning and preliminary characterization of the rodent En-peptide. **A** Cloning of an exon 4-5-containing IGF-1 mRNA. 1 µg of mRNA isolated from mouse liver was used for RT-PCR. Fragments of the expected size are indicated by a red arrow. **B** Comparison of IGF-1 exon 5 -encoded human, rat and mouse amino acid sequences. Peptide sequences shown to be important in the human Eb-sequence are indicated. **C** Expression pattern of the Class 2 IGF-1En isoform in mouse tissues. 1 µg of total RNA was used for RT-PCR.

To evaluate the expression of the mouse Class 2 IGF-1En isoform, RT-PCR was performed (Figure 3.1 C). Total RNA was isolated from mouse brain, liver, skin, kidney, testis, lung, heart, spleen, intestine, and stomach, as well as from the skeletal muscles quadriceps, gastrocnemius, pectoralis, and the diaphragm. Using this approach, no specific signals could be detected in any of the tissues analyzed for expression. In contrast to the RT-PCR performed for initial amplification of this isoform, where mRNA was used, expression analysis was performed with total RNA. Even in liver mRNA, expression of the Class 2 IGF-1En isoform was very weak, which might be the reason why amplification from total RNA gave a negative result.

Since identification of this isoform was not the focus of this thesis no further experiments were performed, which are clearly needed for deeper characterization of this isoform and its significance.

3.2 Effects of IGF-1 isoform over-expression *in vitro*

In the past decades, numerous studies on the effects of IGF-1 on skeletal muscle cell proliferation and differentiation have been performed in tissue culture [215, 297]. Established cell lines that have been very useful for such studies are C2C12 cells, a myoblast cell line isolated from mouse satellite cells, and L6E9 cells, a sub-clone of the parental rat neonatal myogenic line, which does not express endogenous IGF-1. The L6E9 cell line also lacks expression of other myogenic regulator proteins, such as MyoD, but does express the IGF-1 receptor. The L6E9 cell line is therefore especially useful for studying the effects of single IGF-1 isoform over-expression. An earlier study described the stable transfection of L6E9 cells with the Class 1 IGF-1Ea isoform (mIGF-1), which resulted in myotube hypertrophy, accompanied by the activation of the neonatal myosin heavy chain (MyHC) isoform (L6E9 cells normally only express the embryonic MyHC isoform). Expression of the mIGF-1 isoform also increased expression of myogenin, muscle creatine kinase, β -enolase, and IGFBP-5, and activated the MEF2C gene, which is normally silent in this cell line [278]. Stably transfected cells described in this study, expressed the mIGF-1 transgene under the control of the MLC promoter, which is only activated upon differentiation, thereby restricting the analysis to the post-mitotic effects of IGF-1. In contrast, the system applied in the present work drives transcript expression from an inducible hCMV promoter, which allows the analysis of the IGF-1 isoform actions at all stages of development. The effects of IGF-1 isoforms on proliferation and differentiation of L6E9 cells are described in this section.

3.2.1 Transient transfection of L6E9 cells with inducible IGF-1 constructs

To test the differential function of IGF-1 isoforms *in vitro*, the “tet-on” system described in section 2.1.5.2 was applied. In an initial test experiment, cells were double-transfected with the original pBi-2 vector (only coding for luciferase) and the original pUHrtTA 62-1 plasmid to determine the induction efficiency of this inducible system (described in section 2.2.1). Results shown in Figure 3.2 A demonstrate the functionality of the system. Highest induction was achieved in growth medium (GM), where luciferase activity was increased 3152-fold. Throughout the four days of differentiation, luciferase activity decreased but was still sufficiently induced (464-fold at day 1, 138-fold at day 2, 70-fold at day 3, and 64-fold at day 4). The decrease of luciferase signal in the subsequent days is most likely due to a dilution effect of the transfected plasmids. Since no genome-integration appears in transient transfections, the plasmids are not equally inherited by daughter cells and therefore become diluted with ongoing cell replication in GM.

In order to test the effect of inducible IGF-1 isoforms on L6E9 proliferation and differentiation, cells were double-transfected with plasmids encoding the different IGF-1 isoforms and luciferase driven by the inducible tetO/ hCMV $P_{\text{min-1}}$ and $P_{\text{min-2}}$ promoter (pBi/IGF-1 isoform X) on the one hand, and the rtTA protein under control of the human CMV promoter (pUHrtTA) on the other hand (described in section 2.1.5.2). Control cells were transfected with the empty pBi-2 vector and pUHrtTA (mock control). Luciferase and IGF-1 isoform expression was induced five hours after transfection by addition of the tetracycline derivate doxycycline (1 µg/ml) to the medium. Cells were kept in GM for 24 hours after doxycycline-induction and then shifted to differentiation medium (DM) for four days. Expression of the IGF-1 isoforms throughout the experiment was confirmed by RT-PCR (Figure 3.2 B). Further confirmation of IGF-1 transgene expression was achieved by monitoring luciferase expression throughout the experiment, which also allowed for a comparison of IGF-1 isoform expression levels. Results shown in Figure 3.2 C show that luciferase activity was strongest shortly after doxycycline induction in GM (4012-fold in mock controls, 1072-fold in Class 1 IGF-1Ea cultures, 2068-fold in Class 2 IGF-1Ea, 1823-fold in 22-IGF-1Ea, 903-fold in Class 1 IGF-1Eb, 2589-fold in Class 2 IGF-1Eb, and 1435-fold in 22-IGF-1Eb transfected cells). Due to differences in transfection efficiency, a high variation has to be taken into account, but all of the differently transfected cultures continued to demonstrate a sufficiently high level of IGF-1 transgene-induction, even though total values decreased after shift to DM (ranging from 139-fold to 489-fold at day one, from 78-fold to 346-fold at day two, from 74-fold to 277-fold at day three, and from 59-fold to 746-fold at day four). However, induction levels at all time points were considered sufficient to study IGF-1 isoform induced differences.

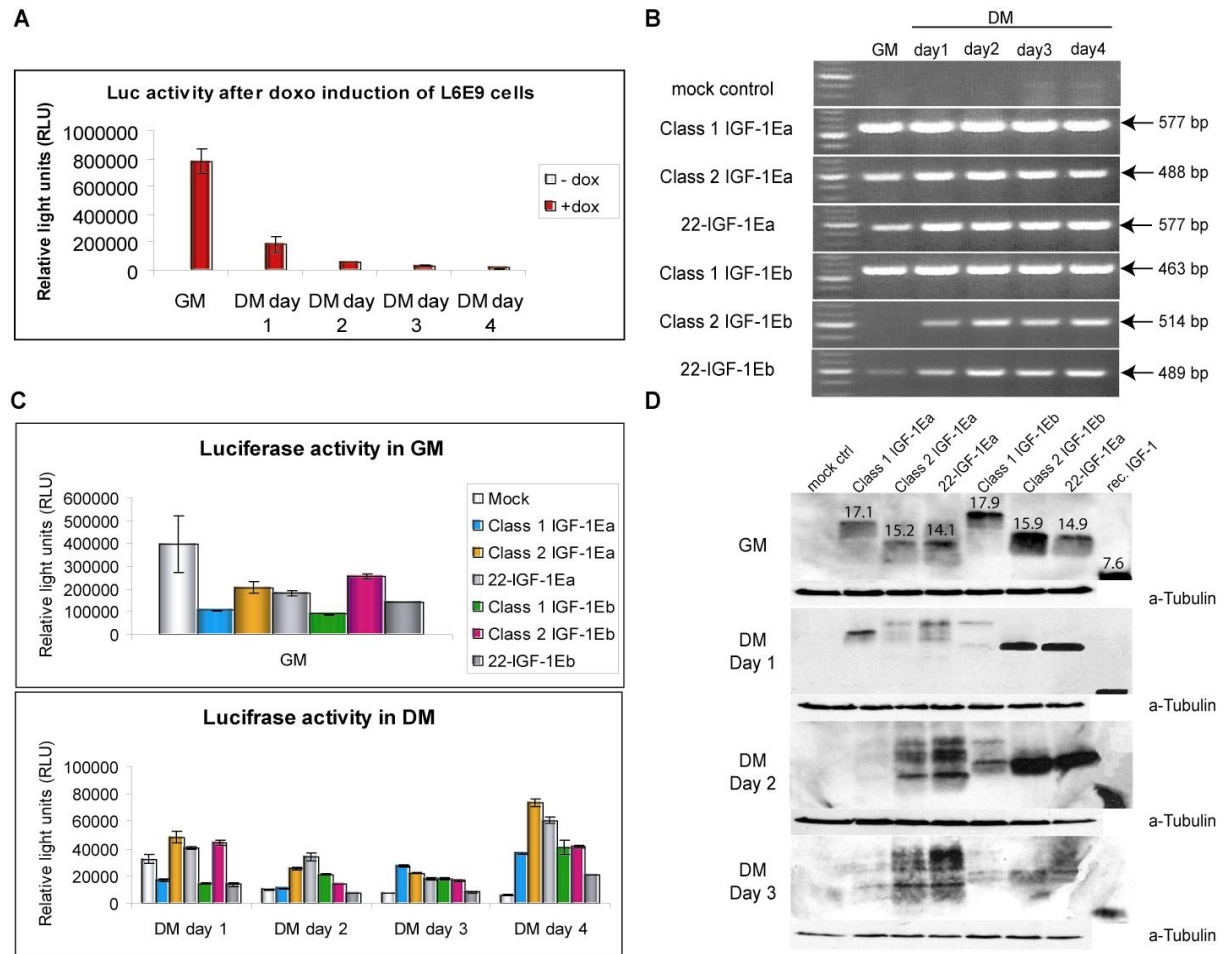


Figure 3.2 Expression analyses of transiently transfected L6E9 cells. **A** Pattern of luciferase activity in control transfected L6E9 cells. **B** RT-PCR analysis on 1µg of total RNA isolated from differently transfected cells at all time points. **C** Luciferase activity in IGF-1 isoform transfected L6E9 cells. Luciferase assay was performed on 5µl of 1:500 dilutions of protein lysates prepared for every time point. Measurements were done for 10 seconds. **D** Western analysis of IGF-1 isoform expression. 50µg of protein were loaded for each sample. Molecular weights (kDa) of prepro IGF-1 isoforms are indicated above the appropriate band.

Results obtained by Western blot analysis show that in comparison to the mock control, where IGF-1 protein was not detectable, all transfected cultures over-expressed IGF-1 protein at all time points surveyed (Figure 3.2 D). Interestingly IGF-1 protein was detected in unprocessed form during growth (GM) and appeared to be processed only upon shift to DM, shown by the appearance of multiple bands corresponding to the different processed forms of IGF-1 (with signal- and E-peptide, without signal-, but with E-peptide, and in case of Ea-peptides containing isoforms, two additional bands are detected, most likely representing glycosylated versions of these isoforms). Notably, at no stage of proliferation and differentiation were the IGF-1 isoforms processed to the mature form of IGF-1 (7.6kDa), which was loaded as a positive control (Figure 3.1D last lane: recombinant mouse IGF-1 (Bio Trend #C-25019-FC)).

In summary, doxycycline-induced expression of IGF-1 isoforms in double-transfected L6E9 cells was confirmed by measuring luciferase activity, RT-PCR, and Western analysis and was considered sufficient to further analyze the phenotype of the IGF-1 transfected cells.

3.2.2 Morphology of IGF-1 isoform transfected cells

Morphology of IGF-1 isoform transfected cells was observed during all stages of proliferation and differentiation (Figure 3.3). In GM, cells did not show any differences in morphology (data not shown). Upon shift to DM, cell morphology was documented after 24 hours (day one), 48 hours (day two), and 72 hours (day three). At day one of differentiation, cells started to elongate as a first sign of differentiation. However, in comparison to the mock control cells, cells transfected with Class 1 IGF-1Ea showed an enhanced number of elongated cells, while cells transfected with the other five IGF-1 isoforms had less effect on the differentiation process, indicated by the overall appearance of only few elongated fibers (Figure 3.3 A). Most importantly, cultures transfected with IGF-1 isoforms containing the Eb-peptide appeared to be more confluent at day one in DM, suggesting a delay in cell-cycle exit (see section 3.2.3 below).

At day two of differentiation, all the differently transfected cultures displayed elongated myocytes (data not shown). At this point cells transfected with Class 1 IGF-1Ea already displayed small myofibers, indicating that myocytes started to fuse, again pointing towards an enhancement of the differentiation process (data not shown).

Three days after shift to DM, myofibers were formed in all transfected cell cultures (Figure 3.3 B). Control transfected cells showed very poor fusion and fibers were thin and small. Cultures transfected with IGF-1 isoforms containing the Ea-peptide, overall Class 1 IGF-1Ea and Class 2 IGF-1Ea, showed the formation of large myofibers, while fibers in cultures transfected with 22-IGF-1Ea and the three Eb-containing IGF-1 isoforms were rather thin and more comparable to the size of mock control fibers.

Taken together, transient transfection of L6E9 cells with six different IGF-1 isoforms resulted in an enhanced differentiation of Class 1 IGF-1Ea-transfected cells that culminated in the formation of hypertrophied myofibers. Cells transfected with Class 2 IGF-1Ea showed normal differentiation kinetics but nevertheless showed an increased size of differentiated fibers after day three of differentiation. 22-IGF-1Ea-transfected cells instead showed fibers that were comparable to control fibers, indicating that this IGF-1 isoform does not induce a hypertrophic response. L6E9 cultures transfected with the Eb-peptide containing isoforms of IGF-1 showed a delay in the differentiation process and the formation of normally sized

muscle fibers, suggesting that IGF-1 isoforms containing the Eb-peptide do not play a role in mediating IGF-1 induced hypertrophy.

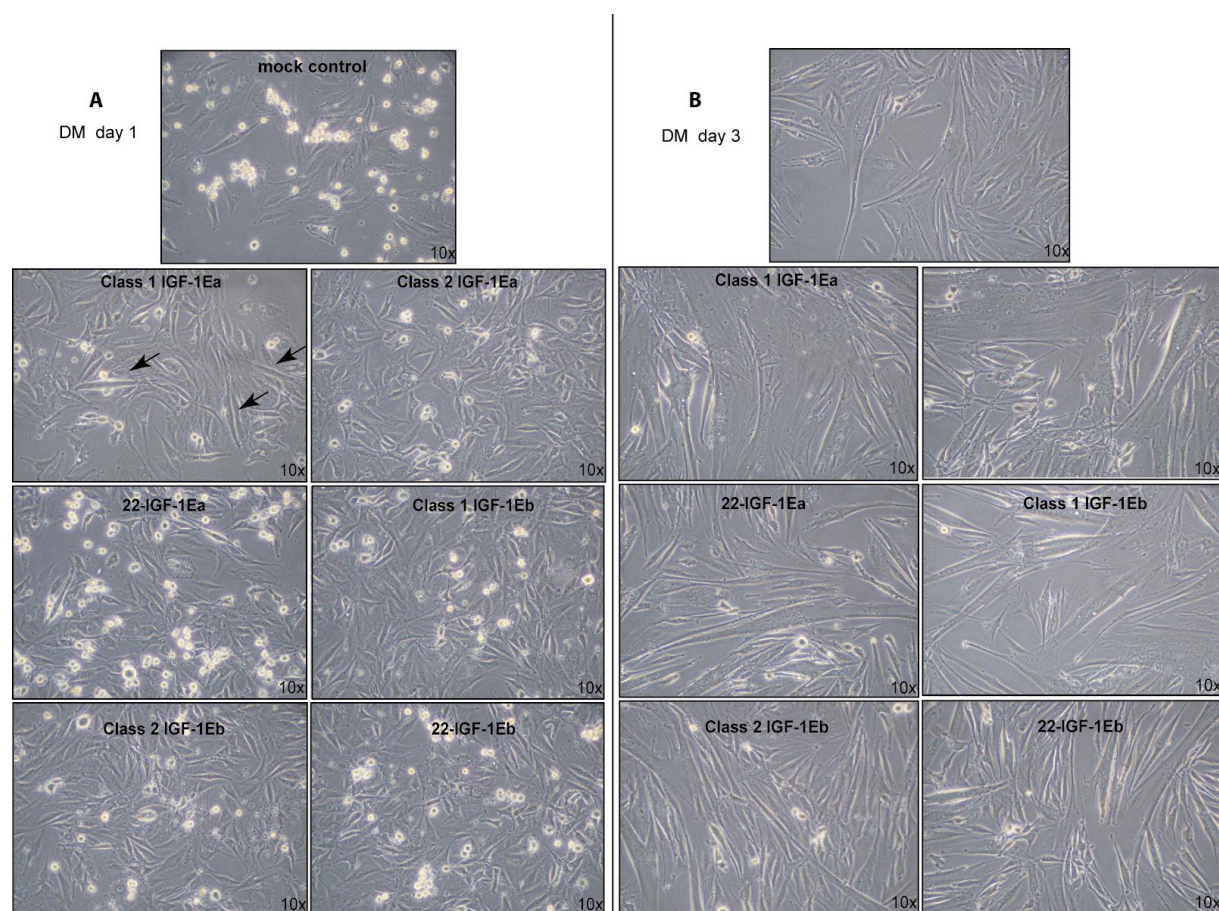


Figure 3.3 Morphology of IGF-1 isoform transfected L6E9 cells. Pictures were taken 24 hours (A) and 72 hours (B) after shift to differentiation medium. A After 1 day in DM, cells transfected with the Class 1 IGF-1Ea isoform showed the enhanced elongation of cells (indicated by black arrows), while cells transfected with the other 5 isoforms were less efficient in starting the differentiative response. B At day 3 of differentiation cultures transfected with Class 1 IGF-1Ea and Class 2 IGF-1Ea showed enlarged fibers, while 22-IGF-1Ea as well as the three IGF-1 isoforms containing the Eb-peptide did not show an effect on fiber size.

3.2.3 Effects of IGF-1 isoforms on myoblast proliferation

To compare the proliferative state of IGF-1 isoform transfectants during growth, levels of phosphorylated histone H3 were analyzed (Figure 3.4 A). Phosphorylation of histone H3 is tightly correlated with chromosome condensation during mitosis and meiosis [298] and serves as a marker for cells undergoing mitosis. The mock control as well as the 22-IGF-1Ea samples were slightly overloaded as shown by total levels of H3 protein and therefore showed a stronger signal for phospho H3. Taking this in account, transfection with Class 1 IGF-1Ea and Class 2 IGF-1Ea samples resulted in decreased amounts of phosphorylated H3, while samples isolated from cultures over-expressing 22-IGF-1Ea, Class 1 IGF-1Eb, Class 2 IGF-1Eb, and 22-IGF-1Eb showed slightly higher levels of histone H3 phosphorylation when compared to mock controls. These findings suggest that expression of

Class 1 IGF-1Ea and Class 2 IGF-1Ea had weaker effects on proliferation of L6E9 cells, while isoforms containing the Eb-peptide as well as 22-IGF-1Ea might stimulate proliferation.

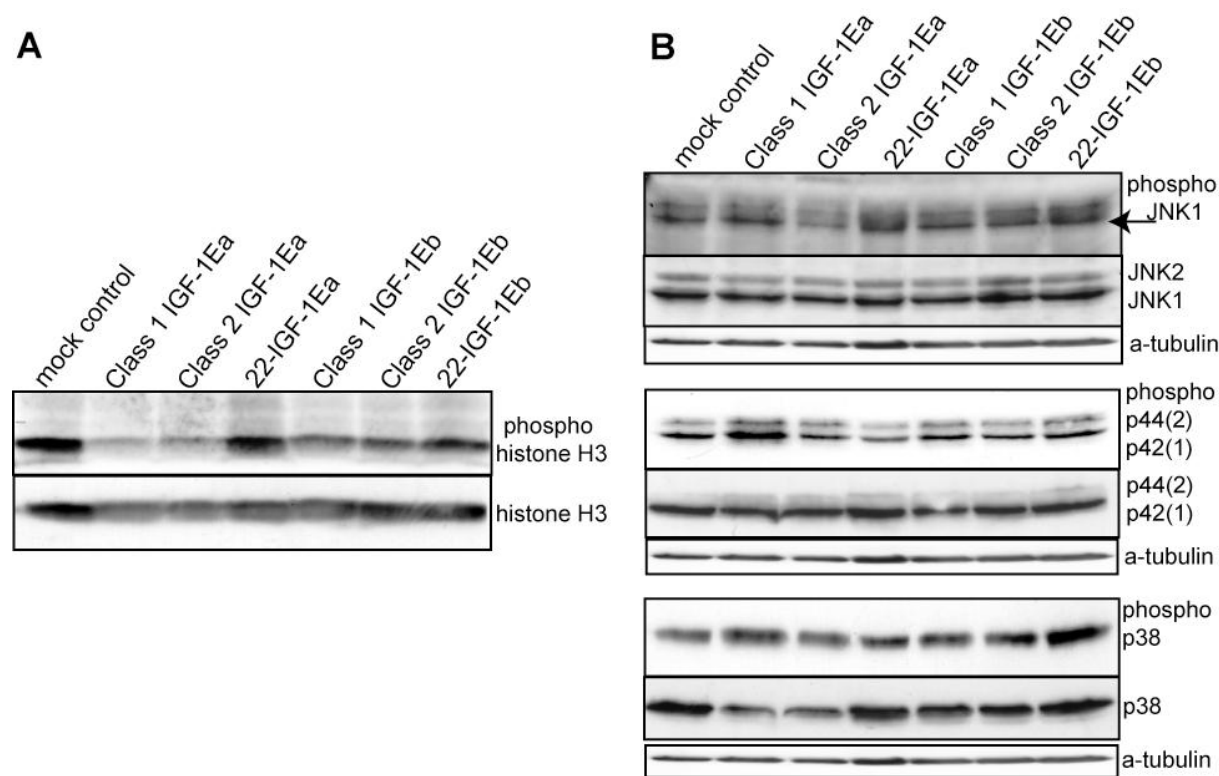


Figure 3.4 Effects of IGF-1 isoforms during growth. 50µg of every protein sample were used for Western blot analysis. **A** Histone H3 phosphorylation was lower in Class 1IGF-1Ea and Class 2 IGF-1Ea cultures, while Eb-containing IGF-1 isoforms and the 22-IGF-1Ea showed increased phosphorylation . **B** Activation level of MAP-kinases JNK1, Erk1 and 2 and p38. Class 2 IGF-1Ea cultures showed lower levels of phsopho-JNK1 and Class 1 IGf-1Ea cells up-regulated phosphorylation of ERk1 and 2. The other isoforms did not induce changes in MAP-kinase phosphorylation.

One of the major pathways that has been implicated in mediating the proliferative response to IGF-1 is the MAP-kinase pathway. A cascade of events can ultimately lead to phosphorylation-mediated activation of the MAP-kinases SAPK/JNK1, ERK 1 and 2, and p38 (section1.4.5). To determine eventual differences in activation of these kinases in response to the different IGF-1 isoforms, their level of phosphorylation was analyzed by Western blot (Figure 3.4 B). Phosphorylation of SAPK/JNK1 was unchanged in samples from all transfected cultures but Class 2 IGF-1Ea, where levels were slightly decreased. Phosphorylation levels of phospho-Erk1 and 2 were up-regulated in Class 2 IGF-1Ea samples, while samples from cultures transfected with the other five isoforms did not show any differences. Finally analysis of p38 phosphorylation showed no major differences among the IGF-1 isoform transfected samples and the mock control.

In summary, analysis of histone H3 phosphorylation revealed a weaker effect of Class 1 IGF-1Ea and Class 2 IGF-1Ea on proliferation, while the level of phospho-H3 was slightly

increased in samples from 22-IGF-1Ea, Class 1 IGF-1Eb, Class 2 IGF-1Eb, and 22-IGF-1Eb transfected cells. Analysis of MAP-kinase activation revealed subtle changes for samples transfected with the Class 1 IGF-1Ea and the Class 2 IGF-1Ea isoforms, showing decreased phospho-JNK1 levels in Class 2 IGF-1Ea cultures and increased phospho-Erk1 and 2 levels in Class 1 IGF-1Ea cultures.

3.2.4 Effects of IGF-1 isoforms on myoblast maturation and differentiation

To monitor effects of IGF-1 isoform expression on the differentiation process, cells were analyzed for the necessary expression of the myogenic determination factor myogenin, as well as the myocyte enhancing factor MEF2C (compare section 1.1.1) (Figure 3.5 A upper panel). While not detectable in GM (data not shown), myogenin was induced in all transfected cultures after 24 hours in DM. Induction was stronger in all IGF-1 transfected cells compared to the mock control, an effect that is well described (reviewed in [297]). However, subtle differences in the degree of induction in response to different IGF-1 isoforms were noted. Class 1 IGF-1Ea showed the strongest up-regulation of myogenin protein, confirming the enhanced elongation of cells transfected with this isoform. Class 2 IGF-1Ea and Class 1 IGF-1Eb also showed increased up-regulation of myogenin when compared to the other IGF-1 isoforms, while 22-IGF-1Ea, Class 2 IGF-1Eb and 22-IGF-1Eb showed rather mild induction of myogenin. However, after two days of differentiation all IGF-1 isoform transfected cells showed similar levels of myogenin, which were still higher in comparison to the mock control. To further confirm normal progression of differentiation, protein levels of MEF2C were analyzed (Figure 3.5 lower panel). In comparison to the control cells, where MEF2C is not detectable at day one, all IGF-1 isoform transfected cells similarly induced MEF2C. With ongoing differentiation, levels further increased at day two, when also the control cells start expressing low levels of MEF2C.

To efficiently promote growth, the level of protein translation must increase. One of the pathways implicated in IGF-1 mediated stimulation of growth is the PI(3)-kinase pathway (compare section 1.4.5.4). To investigate effects of IGF-1 isoform expression on induction of the PI(3)-kinase pathway, activation of the downstream target Akt was analyzed (Figure 5.5 B upper panel). In comparison to the control cells, which activated Akt mildly, induction was much stronger in cells transfected with the IGF-1 isoforms. Among the different IGF-1 isoforms there was no difference in Akt activation, indicating that the six IGF-1 isoforms uniformly are capable of activating Akt.

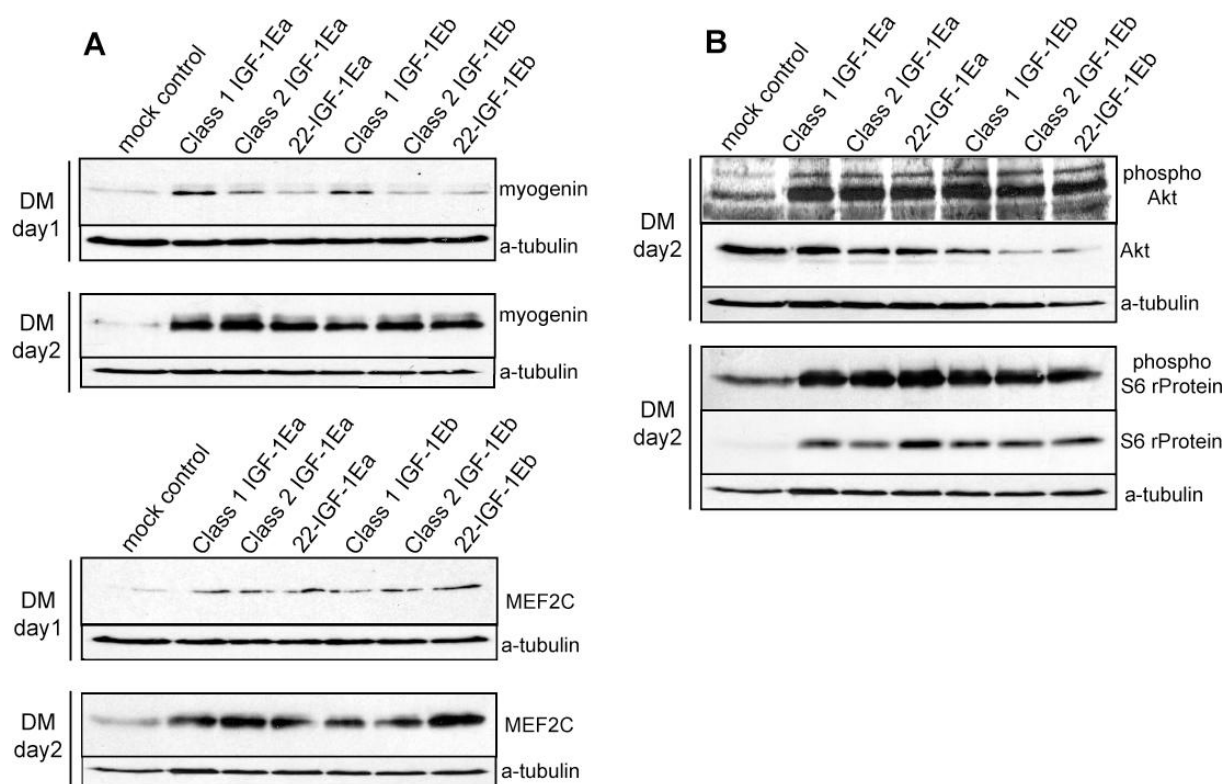


Figure 3.5 Effects of IGF-1 isoforms during differentiation. 50 μ g of every sample were used for Western analysis. **A** upper panel: Induction of myogenin by IGF-1 isoforms. Lower panel: Induction of MEF2C by IGF-1 isoforms. **B** upper panel: Activation of Akt in IGF-1 isoform transfected cells. Lower panel: phosphorylation of S6 ribosomal protein in IGF-1 isoform expressing cells.

One of the downstream effectors of the PI(3)-kinase/Akt pathway is the p70 S6-kinase (p70^{S6K}), which phosphorylates the S6 ribosomal protein upon activation. Phosphorylation of the S6 ribosomal protein in turn is directly correlated with an increase in translation. To investigate if IGF-1 isoforms can lead to phosphorylation of S6 ribosomal protein similarly, levels of phospho-S6 ribosomal protein were determined (Figure 3.5 lower panel). As seen for Akt activation, all isoforms up-regulated induction of phosphorylation equally when compared to control cells. This further suggests that all of the isoforms similarly stimulate the PI(3)-kinase pathway.

In summary, all IGF-1 isoforms uniformly induced expression of myogenin and MEF2C, even though subtle differences were seen for myogenin induction, where Class 1 IGF-1Ea showed the strongest induction, further implicating this isoform in enhancement of the differentiation process. Activation of the PI(3)-kinase pathway, determined by phosphorylation of the downstream targets Akt and S6 ribosomal protein, showed uniform up-regulation compared to the controls, but no differences among the different IGF-1 isoforms.

3.3 Effects of IGF-1 isoform over-expression *in vivo*

To gain insight into the role of the different IGF-1 isoforms in skeletal muscle *in vivo*, the six main IGF-1 isoforms were cloned into an expression vector containing the regulatory sequences from the MLC 1/3 promoter and enhancer (described in section 2.1.5.1). The MLC 1/3 promoter is exclusively activated in mouse skeletal muscle starting at embryonic day E9.5 and persisting into adulthood, thereby providing post-mitotic and skeletal muscle-specific transgene expression throughout the life of the transgenic animal.

A crucial aspect of this thesis is the ability to compare the effects of over-expression of IGF-1 isoforms. Only by driving the transgene from the same regulatory sequences and in the same tissue, conclusions can be drawn about differential effects of IGF-1 isoforms. Three transgenic mouse lines over-expressing IGF-1 specifically in skeletal muscle have been generated in the past years (compare section 1.5), but since different regulatory sequences have been used to drive transgene expression, a profound comparison has been difficult (reviewed in [151]). In addition, the choice of the IGF-1 isoform used for over-expression has not always been clearly defined and adds another crucial parameter in understanding the phenotype of IGF-1 transgenic mice.

The present work aimed to provide an overview of the phenotype seen in transgenic animals that over-express the main IGF-1 isoforms driven from the same regulatory elements. This approach allows the comparison of IGF-1 isoform effects *in vivo* for the first time.

3.3.1 Generation of transgenic mouse lines

All expression constructs were generated as described in section 2.1.5.1 and sequenced before injection to ensure integrity of every IGF-1 isoform sequence. Vectors were digested to completion with EcoRI to linearize the expression cassette and eliminate plasmid sequences. All injections have been performed by the transgenic service of the EMBL-Monterotondo.

One positive founder was born for the transgenic lines MLC/Class 1 IGF-1Ea (founder A) and MLC/22-IGF-1Ea (founder A). For the Line MLC/Class 2 IGF-1Ea (founders A-D) and MLC/Class 2 IGF-1Eb (founders A-D) four positive founders were obtained, three were generated for MLC/22-IGF-1Eb (founders A-C), and injection of MLC/Class 1 IGF-1Eb yielded two positive founder lines (founders A and B). Each positive founder was mated to WT mice and female and male offspring for each transgenic founder of every line were analyzed for transgene expression.

3.3.2 Expression analysis of transgenic founder lines

Expression of IGF-1 isoform transgenes was surveyed by Northern blot analysis. Since the transgenic IGF-1 isoforms are of mouse origin, a probe specific for the most 5'-end of the SV40 poly(A) signal was used to exclusively detect the transgenic mRNAs (compare section 2.1.5.1) Total RNA was isolated from three-months-old male and female quadriceps muscles.

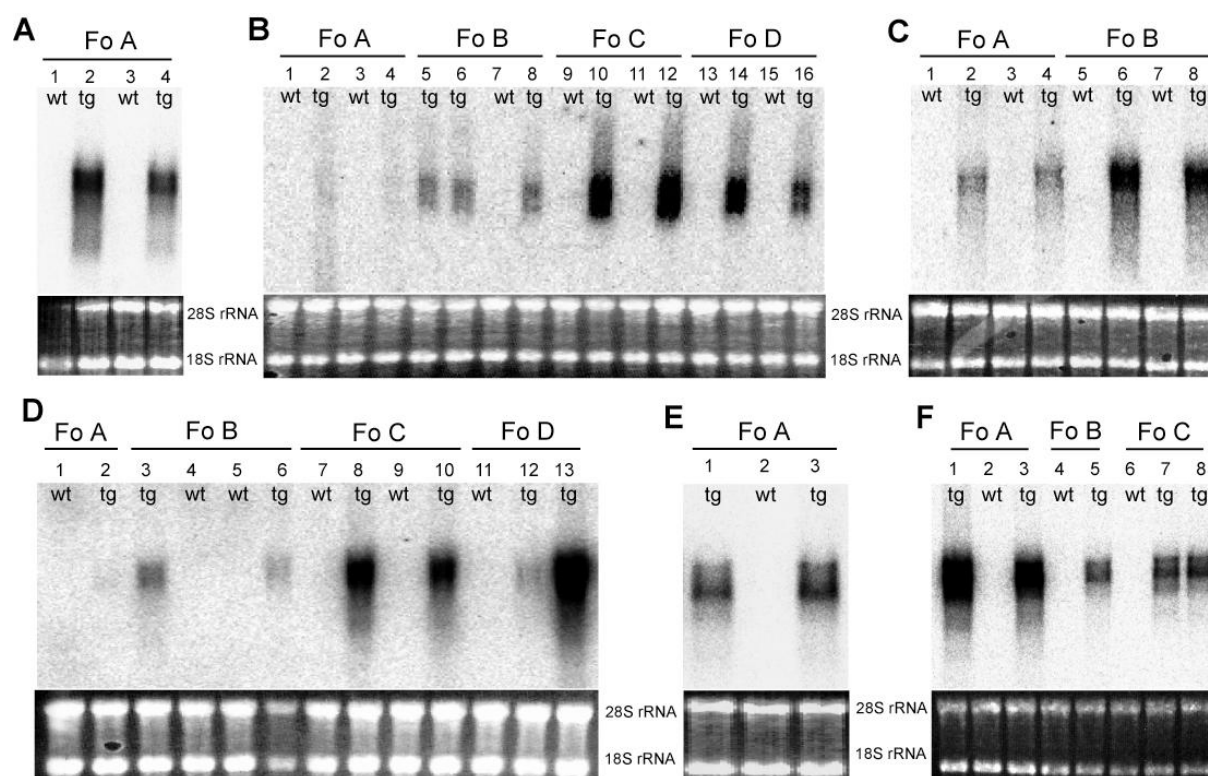


Figure 3.6: Northern blot analysis of transgene expression of founder (Fo) lines. 10 µg of total RNA from female and male three-months-old quadriceps muscles were used for Northern analysis and probed with a SV40-specific probe A MLC/Class 1 IGF-1Ea founder. **A** Lanes 1 and 2 are female; lanes 3 and 4 are male samples. **B** MLC/Class 2 IGF-1Ea. Lanes 1, 2, 5, 6, 9, 10, 13, and 14 are female, lanes 3, 4, 7, 8, 11, 12, 15, and 16 are male samples. **C** MLC/Class 1 IGF-1Eb founders A and B. Lanes 1, 2, 5, and 6 are female; lanes 3, 4, 7, and 8 are male samples. **D** MLC/Class 2 IGF-1Eb founders A-D. Lanes 3, 4, 7, 8, 11, and 12 are female; lanes 1, 2, 5, 6, 9, 10, and 13 are male samples. **E** MLC/22-IGF-1Ea founder A. Lane 1 is female; lanes 2 and 3 are male samples. **F** MLC/22-IGF-1Eb founders A-C. Lanes 1, 6, and 7 are female; lanes 2, 3, 4, 5, and 8 are male samples.

For line MLC/Cass 1 IGF-1Ea only one founder was available for expression analysis (Figure 3.6A) and therefore further analysis was performed on MLC/Class 1 IGF-1Ea founder A. Line MLC/Class 2 IGF-1Ea founders C and D showed the highest transgene expression, while founders A and B showed moderate to low expression (Figure 3.6B). Due to their high transgene expression level, founders C and D were kept for further analysis. The two founders obtained for line MLC/Class 1 IGF-1B expressed moderate (founder A) and high (founder B) levels of the transgene (Figure 3.6C) and both founders were further analyzed. Among founders A to D of line MLC/Class 2 IGF-1Eb founders C and D showed the strongest transgene expression, while founder B expresses low levels of the transgene and

founder A showed only traces of a positive signal (Figure 3.6D). Founder C and D were therefore chosen for further analysis. The single founder A for line MLC/22-IGF-1Ea showed moderate to high expression of the transgene (Figure 3.6E) and was further analyzed. The three founders obtained for line MLC/22-IGF-1Eb showed high (founder A) and moderate (founders B and C) transgene expression (Figure 3.6F). Founder A was kept due to highest transgene expression and since founder C gave a slightly stronger signal than founder B, it was kept as well.

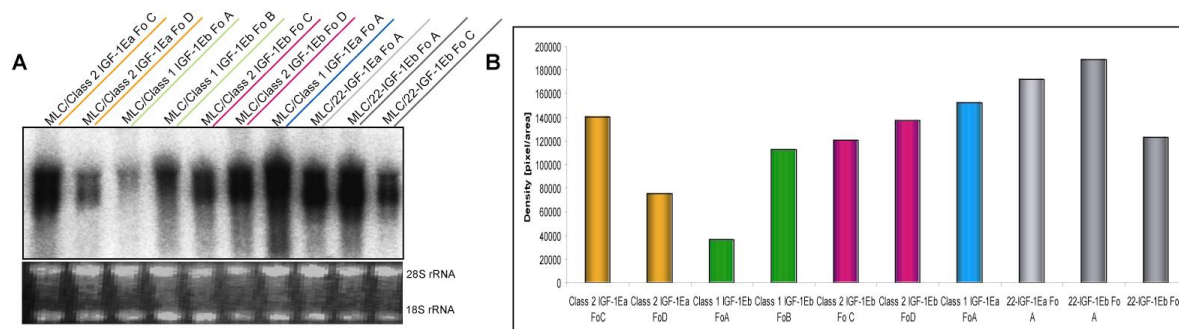


Figure 3.7: Northern comparison of transgenic founder line expression levels. 10µg of total RNA from quadriceps muscle of male mice were used and probed with a SV40-specific probe. **A** Northern comparison of all selected founder lines for each IGF-1 isoform transgenic line. **B** Density of IGF-1 isoform transgene bands detected with Northern analysis (A)

For a better comparison of the transgene expression level among the different founders of each line, total RNA isolated from three-month-old male quadriceps muscles of each selected founder was analyzed by Northern blot using the previously described SV40-specific probe (Figure 3.7 A). The results were analyzed by using the Radames software to screen the density (pixel/area) of the bands detected by Northern blot (Figure 3.7 B). Highest expression was detected for line MLC/22-IGF-1Ea founder A (172476 pixel/area) and MLC/22-IGF-1Eb founder A (188542 pixel/area), followed by comparably high expression in lines MLC/Class 2 IGF-1Ea founder C (140161 pixel/area), MLC/Class 1 IGF-1Eb founder B (112511 pixel/area), founders C (120636 pixel/area) and D (137135 pixel/area) of line MLC/Class 2 IGF-1Eb and MLC/22-IGF-1Eb founder C (123382 pixel/area). Expression of MLC/Class 2 IGF-1Ea founder D and MLC/Class 1 IGF-1Eb founder A was low compared to the other founders (30918 and 36675 pixel/area respectively). Based on this comparison, primary founders were selected for each line to perform further analysis. Primary founders of each line were: Founder A for line MLC/Class 1 IGF-1Ea, founder C for MLC/Class 2 IGF-1Ea, founder A for line MLC/22-IGF-1Ea, founder B for line MLC/Class 1 IGF-1Eb, founder D for line MLC/Class 2 IGF-1Eb and founder A for line MLC/22-IGF-1Eb.

3.3.3 Skeletal muscle-specific transgene expression of transgenic lines

The next crucial step in the analysis of the transgenic founder lines was to determine if the IGF-1 transgenes were expressed in a skeletal muscle-specific manner. For this purpose total RNA of distal organs (heart, brain, liver, kidney, and spleen), as well as different skeletal muscle groups (quadriceps, gastrocnemius, diaphragm, and tibialis anterior (TA)) of male and female (data not shown) WT and transgenic three-month-old mice of each selected founder was isolated and analyzed by Northern blot using the previously described SV40-specific probe. Figure 3.8 A-F shows the results for the highest expressing founder of all six transgenic lines that were selected based on the expression analysis described in section 3.3.2. Results obtained for the second selected founders were similar (data not shown). No signal was detectable in any WT tissue and non-muscle transgenic tissue. Specific bands were exclusively found in the skeletal muscle groups of all transgenic lines, confirming expected expression of the transgenic IGF-1 isoforms. Due to the expression pattern of the MLC promoter, transgene expression was highest in the fast IIB fibers, although lower levels are also expressed in fast IIX and IIA fibers. Therefore fast muscles like the quadriceps, gastrocnemius, and TA, showed higher IGF-1 isoform transgene expression than the diaphragm that does not express IIB fibers and consequently only expressed the transgene at low levels.

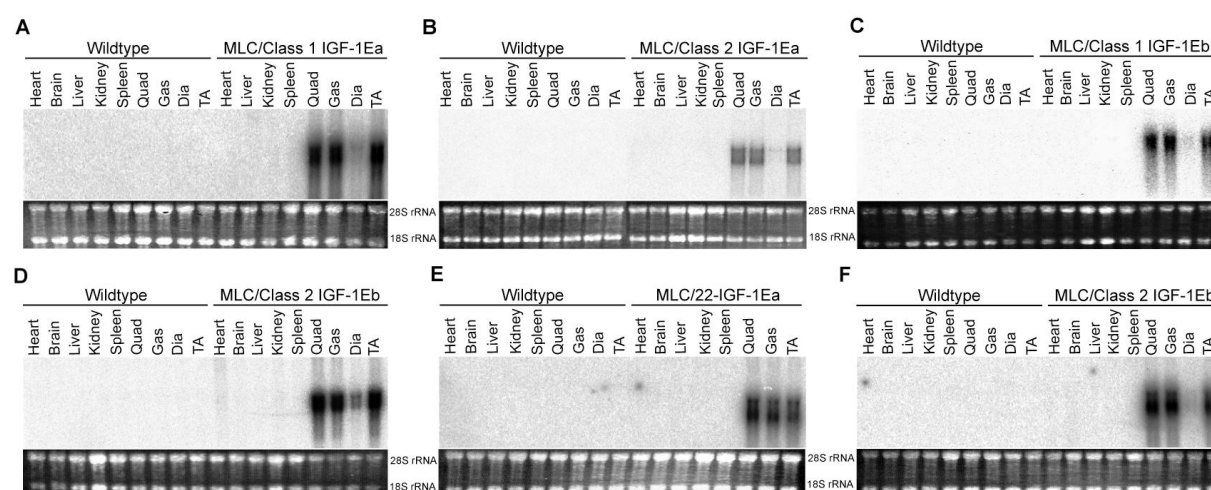


Figure 3.8: Skeletal muscle-specific transgene expression. 10µg of total RNA were run for every sample and probed with a SV40-specific probe. Transgenic tissues of different lines were compared to WT littermates. A MLC/Class 1 IGF-1Ea founder A. B MLC/Class 2 IGF-1Ea founder C. C MLC/Class 1 IGF-1Eb founder B. D MLC/Class 2 IGF-1Eb founder D E MLC/22-IGF-1Ea founder A. F MLC/22-IGF-1Eb founder A.

For deeper phenotypic analysis of the IGF-1 isoform transgenic mouse lines, priority was given to the founder that expressed highest levels of the transgene and to the four isoforms mainly expressed in WT animals, namely MLC/Class 1 IGF-1Ea, MLC/Class 2 IGF-1Ea, MLC/Class 1 IGF-1Eb, MLC/Class 2 IGF-1Eb.

During preliminary analysis it became clear though that the MLC/Class 1 IGF-1Ea line was problematic. The mice were aggressive and didn't breed well, which led to loss of this line. Since no second founder was available, the previously well described MLC/mIGF-1 line, generated by Antonio Musaro [77] was used for further comparative work. This line carries the same transgene as used for generating the MLC/Class 1 IGF-1Ea line (Class 1 IGF-1Ea), but of rat and not of mouse origin, and contains the same MLC 1/3-derived regulatory sequences to drive transgene expression. From now on this line will be referred to as MLC/mIGF-1.

3.3.4 Comparison of expression levels to MLC/mIGF-1 transgenic line

For further work including the MLC/mIGF-1 transgenic line, the expression level of each of the selected founders for every line chosen had to be compared again.

Final comparison was done by Northern blot, quantitative real time RT-PCR, and Western blot (Figures 3.9 and 3.10). Results obtained by Northern blot experiments using of 10µg of total RNA from one-month-old quadriceps probed with the previously described SV40 probe (Figure 3.9 A) were analyzed with the Radames software to determine the density of bands detected by Northern analysis (Figure 3.9 B). This analysis revealed highest expression for MLC/Class 2 IGF-1Ea (125627 pixel/area) and MLC/Class 2 IGF-1Eb (171052 pixel/area), followed by MLC/mIGF-1 (92482 pixel/area). Lowest transgene expression levels were detected for line MLC/Class 1 IGF-1Eb (57838 pixel/area).

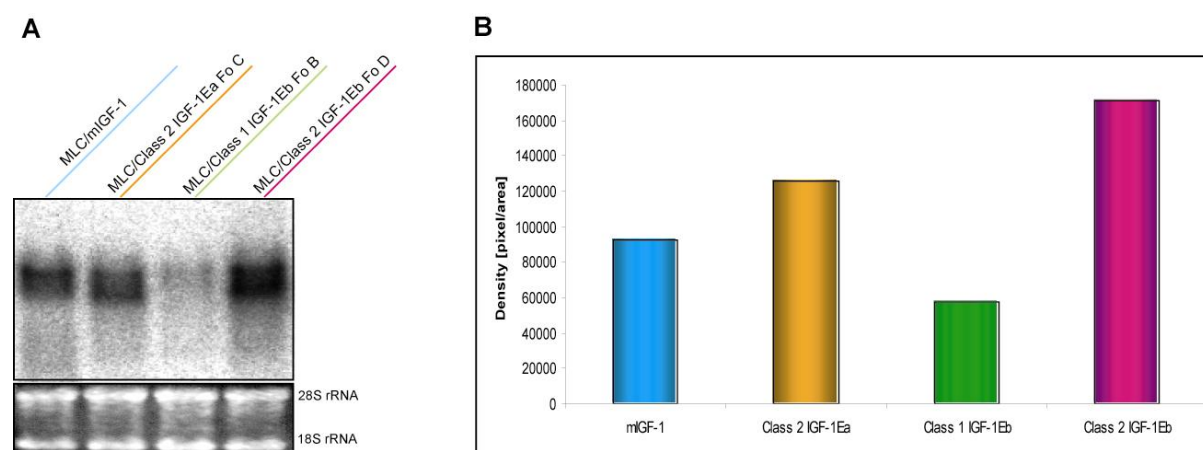


Figure 3.9 Comparison of selected lines to MLC/mIGF-1 transgenic line. 10µg of total quadriceps RNA from male one-month-old animals was used for Northern analysis and probed with a SV40-specific probe. **A** Comparison of selected founder lines to MLC/mIGF-1. **B** Density of IGF-1 isoform transgene bands detected with Northern analysis (**A**).

For quantification in relation to WT total IGF-1 levels and specific IGF-1 isoform levels, quantitative real time RT-PCR was performed on RNA isolated from three-months-old quadriceps muscle of three WT mice and three transgenic mice of each line. To determine

total IGF-1 levels in WT quadriceps muscle, the WT values obtained by quantitative RT-PCR for every isoform were added (3301.2 molecules/ng). Values for the specific isoform over-expressed were then related to this value to gain the total fold-increase over the WT (Figure 3.10 A). With this type of analysis MLC/mIGF-1 animals (181-fold) and MLC/Class 2 IGF-1Ea (52-fold) showed the highest increase, while MLC/Class 1 IGF-1Eb (8-fold) and MLC/Class 2 IGF-1Eb (2-fold) instead, showed a rather mild increase. However, if values obtained for the different over-expressed IGF-1 isoforms were related to the WT expression level of the corresponding endogenous isoform, the level of induction was more comparable (Figure 3.10 B). Line MLC/mIGF-1 showed a 227-fold increase, MLC/Class 1 IGF-1Eb a 190-fold increase, and MLC/Class 2 IGF-1Ea displayed a 364-fold increase. Since the Class 2 IGF-1Eb isoform was not detectable in WT quadriceps muscles, the fold-increase over the WT was much higher for this transgene (6280-fold) (Figure 3.10 C). The discrepancies in the expression levels of the IGF-1 transgenes observed with the different methods are most likely due to naturally occurring differences in expression level between different animals of the same transgenic line.

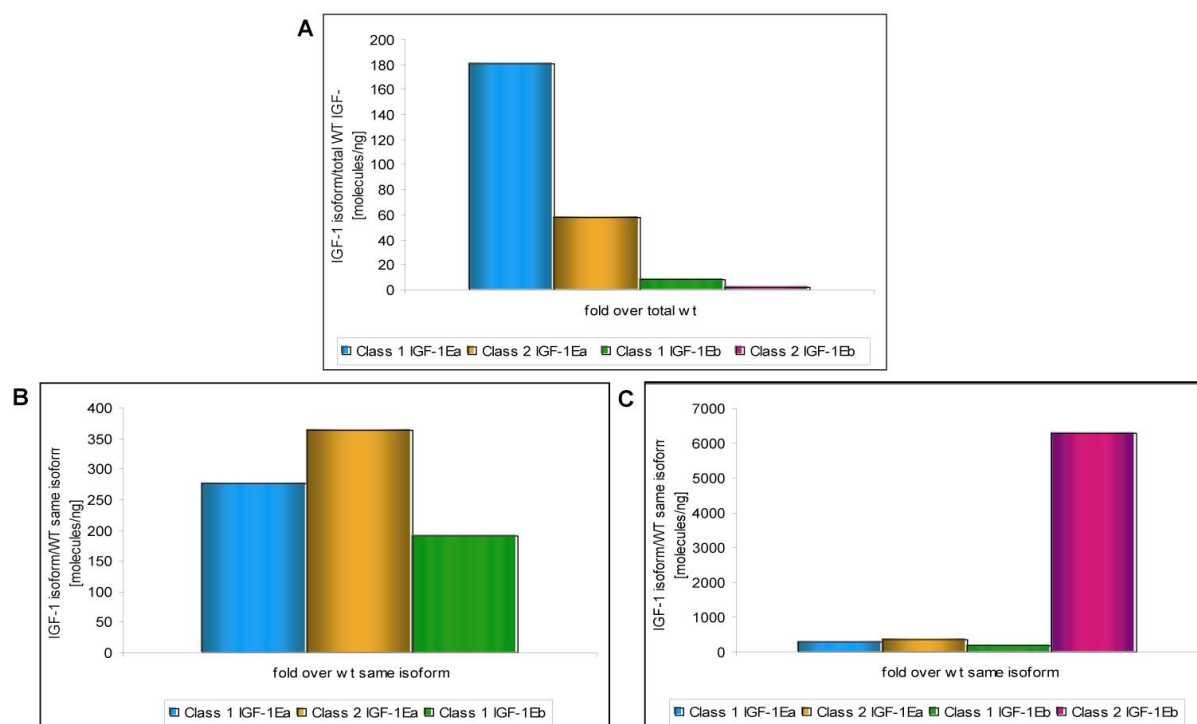


Figure 3.10 Over-expression of IGF-1 isoform transgenes. The level of IGF-1 isoform over-expression was compared by quantitative RT-PCR. **A** Fold over-expression of IGF-1 isoforms in relation to WT total IGF-1 level. **B** Fold over-expression of isoforms with the wt expression level of the same isoform as a reference. For a better overview the graph was prepared without MLC/Class 2 IGF-1Eb. **C** Fold over-expression over wt levels of the same isoform with MLC/Class 2 IGF-1Eb

To relate the mRNA expression level to the protein levels detected in the transgenic muscles, as well as to confirm proper protein expression of the transgenic IGF-1 isoforms, Western blot analysis was done on quadriceps protein lysates of one-month-old and six-months-old

WT and transgenic animals for each IGF-1 isoform (Figure 3.11). The antibody used for both experiments was directed against the mature IGF-1 sequence and therefore detected all the differently processed forms of IGF-1, represented by the multiple bands detected. As observed *in vitro*, isoforms containing the Ea-peptide showed two additional bands, most likely reflecting glycosylated forms of those IGF-1 variants. Most importantly, all isoforms were processed to the mature IGF-1 *in vivo*. Due to detection of multiple bands, quantification was performed by combining the densities of each detected band for every sample. These values are not absolutely accurate, since the Radames software used for detection and quantification of the single bands, did not detect bands of very low intensity. However, this analysis is still accurate enough to allow the determination of expression levels.

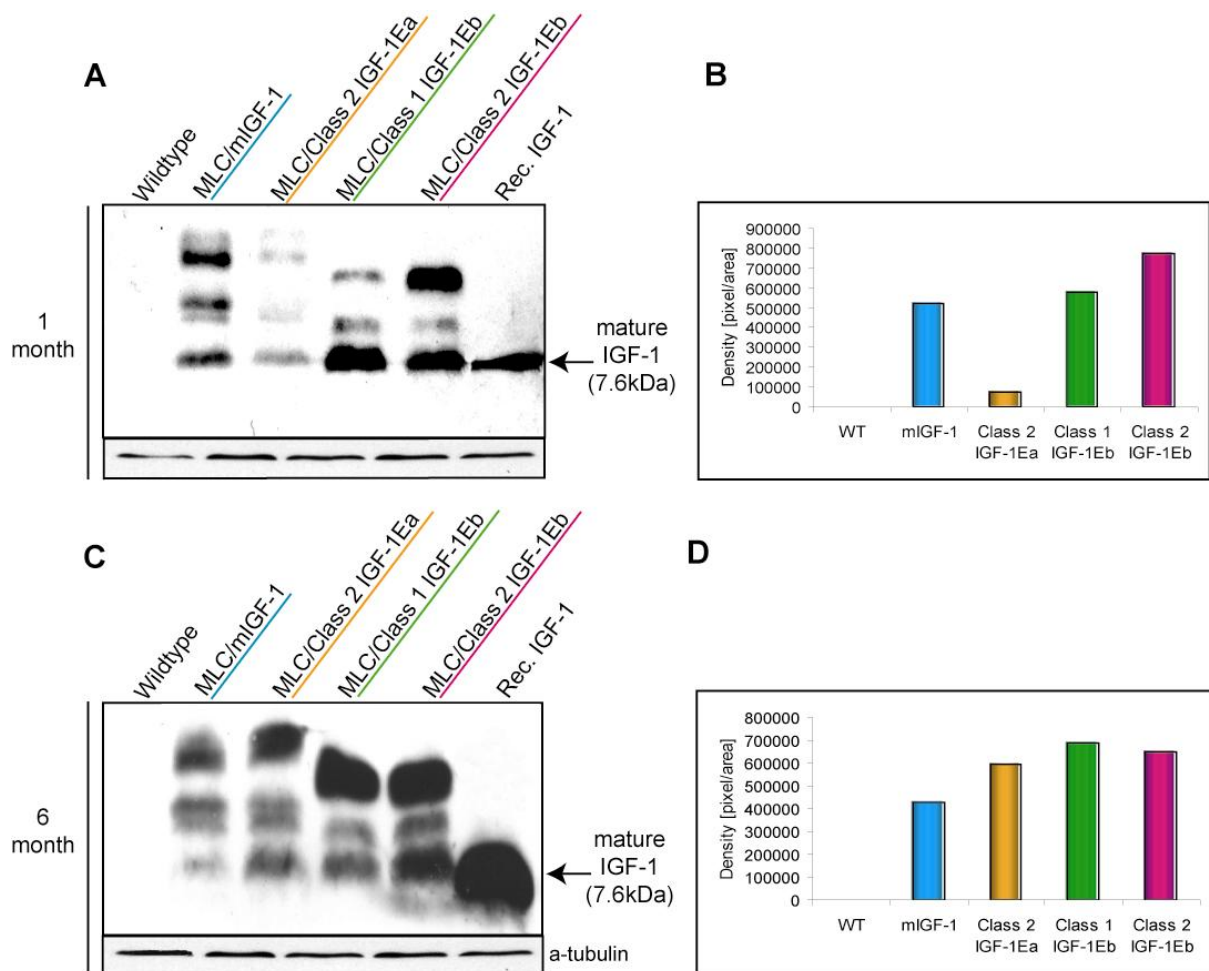


Figure 3.11 Protein expression of IGF-1 isoform transgenes. 50µg of protein from male quadriceps muscle from one-month (A) and six-months-old mice (C) were used for Western analysis with an antibody to detect all IGF-1 isoforms. Band density was determined using the Radames software for one-month-old (B) and six-month-old samples (D).

At one month of age, no IGF-1 was detected in the WT sample, while MLC/mlIGF-1 (521705 pixel/area), MLC/Class 1 IGF-1Eb (579348 pixel/area), and MLC/Class 2 IGF-1Eb (773249

pixel/area) showed comparable high levels of IGF-1 protein expression. The signal detected for MLC/Class 2 IGF-1Ea (75805 pixel/area) instead, was quite low (Figure 3.11 A and B). However, the different IGF-1 isoform transgenic lines showed comparable levels of IGF-1 protein expression at six months of age (Figure 3.11 C and D), while no IGF-1 was detectable in the WT sample. These results confirm that all IGF-1 isoform transgenic lines express the IGF-1 protein to a comparable extent. Variations seen in one-month and six-months-old animals most likely reflect normally occurring differences in expression between different animals of the same line, since these differences were also seen by analysis of transgenic mRNA. Notably, the quite dramatic differences seen in the fold-increase of transgenic mRNA in reference to total WT levels in the different mouse lines are not reflected in the IGF-1 protein expression of these animals. This observation raises the question if there is a limit or threshold for IGF-1 protein translation that is not overcome by higher transcription levels.

In summary, comparison of IGF-1 isoform transgene expression on the transcriptional level revealed variable differences among the lines, depending on which method was used. However, despite these differences, expression of IGF-1 protein determined by quantification of results obtained by Western blot analysis showed comparable expression of the different IGF-1 isoforms.

3.3.5 Influence of IGF-1 isoforms on endogenous IGF-1 isoform expression

To investigate if the over-expression of IGF-1 isoforms influenced the endogenous IGF-1 isoform expression levels, primers were designed for quantitative RT-PCR, allowing amplification of the full-length isoforms, thereby providing reliable evidence for endogenous IGF-1 isoform expression levels. The screening for endogenous IGF-1 isoform expression in each transgenic mouse line was carried out on total RNA from three-months-old quadriceps muscle, isolated from three WT and three transgenic mice from each line. While MLC/Class 2 IGF-1Ea and MLC/Class 2 IGF-1Eb did not have any influence on the expression of endogenous IGF-1 isoforms (Figure 3.12 C and D), the over-expression of rat Class 1 IGF-1Ea in MLC/mIGF-1 animals up-regulated endogenous Class 2 IGF-1Ea 6.7-fold ($p=0.04$) without affecting other endogenous IGF-1 isoforms (Figure 3.12 A). MLC/Class 1 IGF-1Eb transgenic samples showed a 7.7-fold induction of endogenous Class 1 IGF-1Ea ($p=0.03$), while other IGF-1 isoforms were unchanged (Figure 3.12 B). The values of each isoform were always compared to the WT expression levels of the corresponding isoform.

To confirm these results, Northern blot analysis was performed with probes designed to bind to specific sequences of the differentially spliced exons (section 2.1.7). Transgenic lines

over-expressing Class 1 isoforms (derived from exon 1) were analyzed with a probe directed against exon 2 sequences, while lines over-expressing Class 2 isoform (derived from exon 2) were analyzed with a probe recognizing the 186 bp 5'-UTR exon 1 sequence, which is subject to a splicing event in 20% of the total IGF-1 mRNA in the liver. By choosing the probe in this region, the majority of endogenous exon 1-derived Class 1 transcripts were detected. Over-expressed isoforms containing the Ea-peptide (exon 4-6 splice variant) were analyzed with a probe derived from exon 5 (giving rise to the specific part of the Eb-encoding sequence). Generation of a probe allowing the detection of the exon 4-6 sequence was not possible, since the sequences giving rise to the Ea-peptide are also contained in the exon 4-5-6 splice variant giving rise to the Eb-peptide.

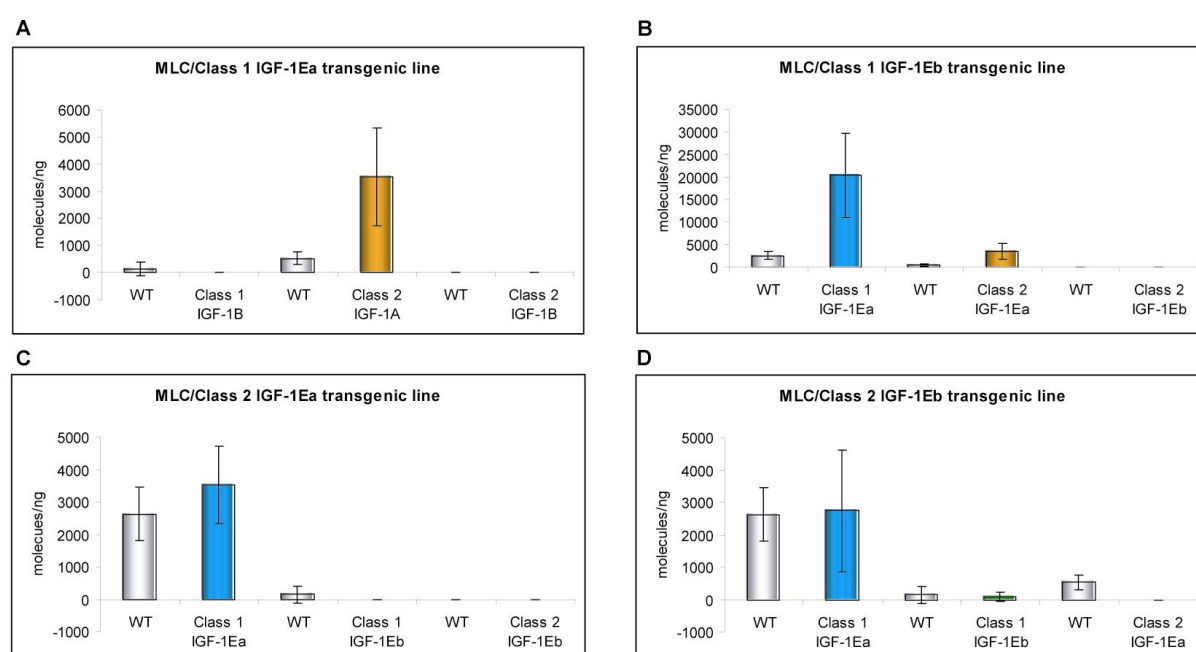


Figure 3.12 Expression of endogenous isoforms (1). Quantitative RT-PCR was used to assess if the over-expression of IGF-1 isoforms had an effect on the expression of endogenous isoforms. The transgenic line analyzed is indicated on top of the graph. **A** Results for line MLC/mIGF-1 show significant up-regulation of endogenous Class 2 IGF-1Ea transcripts ($p=0.04$), while other isoforms were not affected. **B** Line MLC/Class 1 IGF-1Eb samples showed significantly more Class 1 IGF-1Ea transcripts ($p=0.03$), but no changes for other isoforms. No effect on endogenous isoform expression was seen in lines MLC/Class 2 IGF-1Ea and Class 2 IGF-1Eb (C and D). The values of each isoform were always compared to the WT levels of the same isoform.

Results obtained with an exon 2-specific probe confirmed the slight skeletal muscle-specific up-regulation of a Class 2 isoform in response to the Class 1 IGF-1Ea (mIGF-1) transgene (Figure 3.13 A), while Northern blot analysis with an exon 5-specific probe to detect exon 4-5-6 splice variants giving rise to the Eb-peptide, confirmed no changes for Eb-encoding mRNAs (Figure 3.13 B). To monitor endogenous Class 1 isoform transcription in MLC/Class 2 IGF-1Ea animals, the 186 exon 1-, and the exon 5-specific probes were used. Both experiments confirmed no changes for those isoforms (Figure 3.13 C and D). Since the exon 4-6 splice variant that gives rise to the Ea-peptide cannot be specifically detected, Northern

analysis for MLC/Class 1 IGF-1Eb was restricted to the exon 2-specific probe for Class 2 mRNA detection. Results shown in Figure 3.13 E confirm no changes for Class 1 IGF-1Eb transcripts. MLC/Class 2 IGF-1Eb analysis instead was restricted to detection of class 1 IGF-1 mRNAs and showed no changes in comparison to the WT samples (Figure 3.13 F), again confirming results obtained by quantitative RT-PCR.

Taken together, these results revealed that the Class 1 IGF-1Ea transgene present in MLC/mIGF-1 animals up-regulated endogenous Class 2 IGF-1Ea transcripts without affecting the expression of other endogenous isoforms. In contrast, the MLC/Class 1 IGF-1Eb transgene up-regulated endogenous Class 1 IGF-1Ea, even though this could not be confirmed by Northern blot analysis due to lack of a suitable probe. No effects on endogenous IGF-1 isoforms were seen in lines MLC/Class 2 IGF-1Ea and MLC/Class 2 IGF-1Eb.

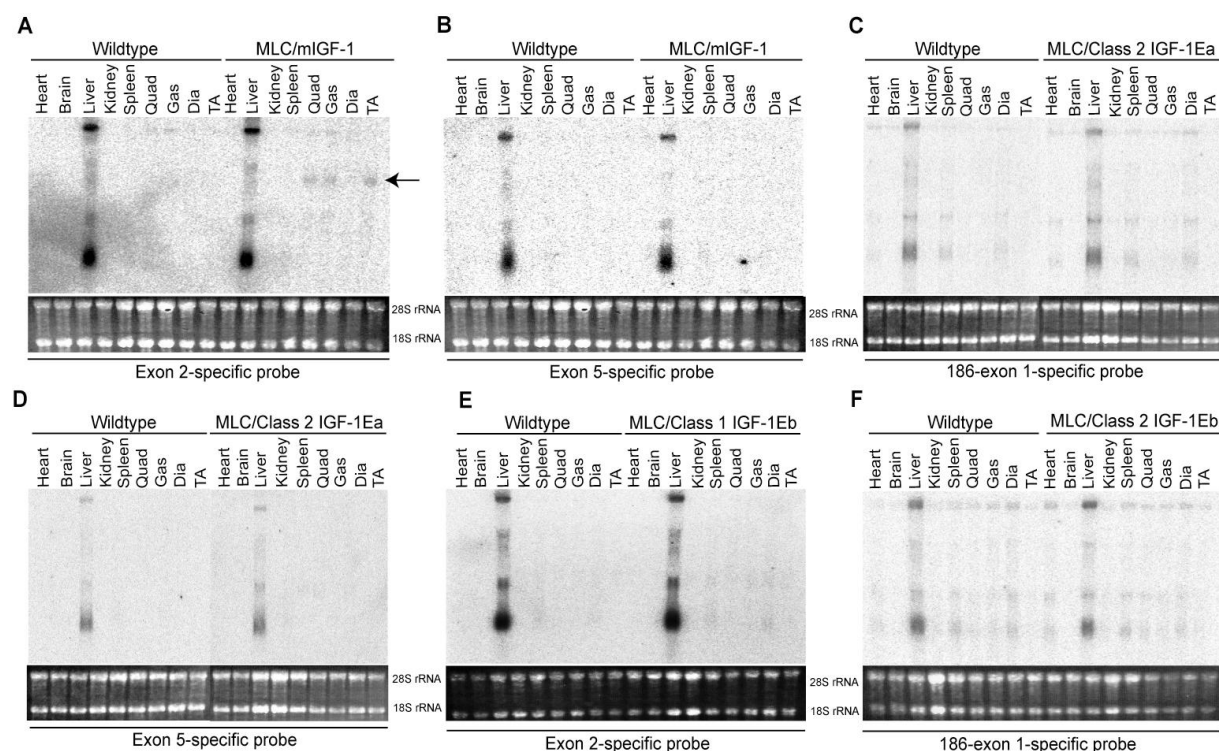


Figure 3.13 Expression of endogenous IGF-1 isoforms (2). 10µg of total RNA from three-month-old male quadriceps muscle from WT and transgenic mice were analyzed with the specific probes indicated. **A** MLC/mIGF-1 samples probed with an exon 2-specific probe showed mild induction of exon 2-containing transcripts specifically in the transgenic skeletal muscle groups (indicated with an arrow). **B** MLC/mIGF-1 samples probed hybridized with an exon 5-specific probe revealed no changes. **C** No changes in MLC/Class 2 IGF-1Ea samples probed with the 186 exon 1-specific probe. **D** MLC/Class 2 IGF-1Ea derived samples screened with the exon 5-specific probe were also unchanged. **E** MLC/Class 2 IGF-1Eb samples analyzed with an exon 2-specific probe were negative. **F** MLC/Class 2 IGF-1Eb samples probed with the 186 exon 1-specific probe showed similar levels to WT samples.

3.3.6 Effects IGF-1 isoform on body weight and weight of visceral organs

A previous study on a transgenic mouse line over-expressing IGF-1 in skeletal muscle (SIS2) reported an increase in body weight and an effect on the size of visceral organs such as the

spleen [299]. This IGF-1 transgenic line over-expressed a human Class 1 IGF-1Ea isoform under the control of the avian skeletal α -actin promoter (SIS2 mice), which restricted the transgene expression to skeletal muscle and heart. In contrast, the primary characterization of the MLC/mlIGF-1 transgenic mouse line, also over-expressing the Class 1 IGF-1Ea isoform, but exclusively in skeletal muscle, did not show an effect on the total body weight, and the weight of distal organs was not assessed in these animals [77]. Since the transgene expression in these animals is controlled by different promoters and therefore the expression pattern is different, a direct comparison is difficult. In addition the first, but not the second study reported the presence of transgenic human IGF-1 in the circulation, which might cause the increased weight of the spleen. It is therefore crucial to determine if these parameters are influenced in the IGF-1 isoform transgenic mice described here.

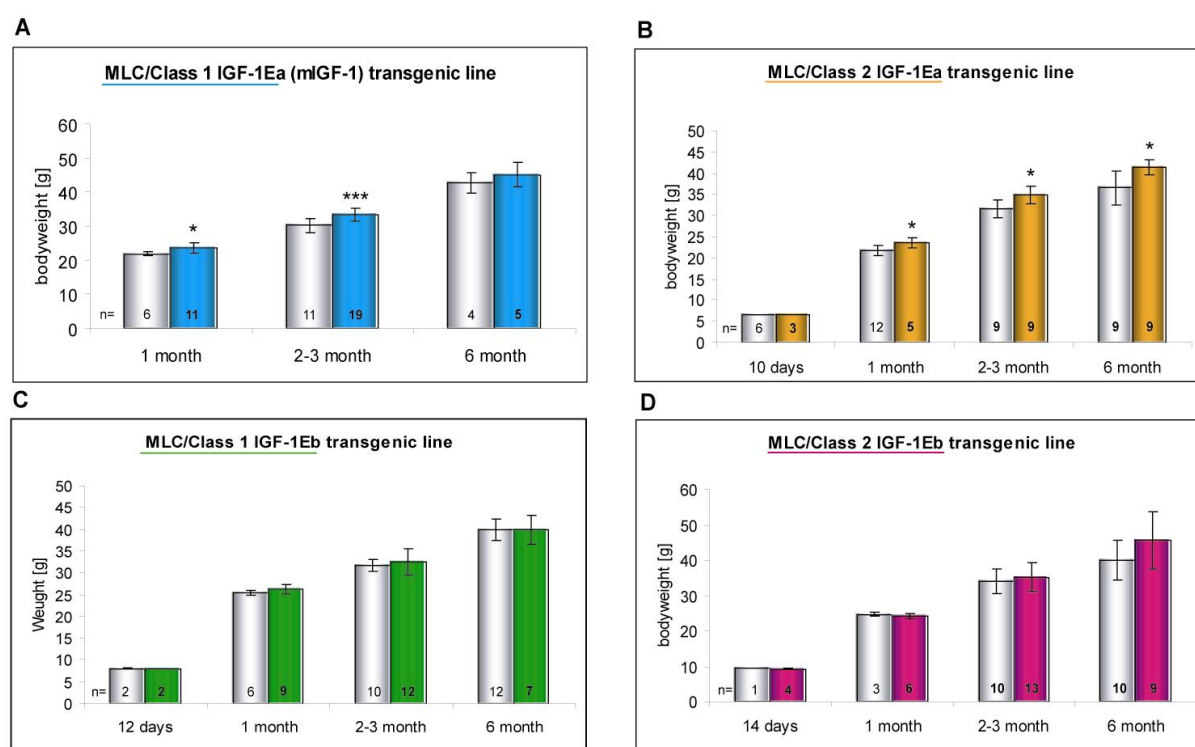


Figure 3.14 Effect of IGF-1 isoform over-expression on body weight. Number of animals is indicated at the bottom of the columns. All measurements were performed on male animals. **A** MLC/mlIGF-1 animals show significantly elevated body weight by 1 ($p=0.01$) and 2-3 months of age ($p=0.0001$). **B** MLC/Class 2 IGF-1Ea mice are significantly heavier at all ages analyzed ($p=0.01$ for all). **C** MLC/Class 1 IGF-1Eb and MLC/Class 2 IGF-1Eb (**D**) do not have an effect on body weight.

On the bases of over-expressing the different IGF-1 isoforms under the same conditions, the effect of IGF-1 isoform over-expression on the over all body weight and the weight of visceral organs of the transgenic animals was monitored throughout life of the transgenic mice and their WT littermates. Results shown in Figure 3.14 demonstrate a significant ($p<0.05$) effect on the overall body weight for lines MLC/mlIGF-1 and MLC/Class 2 IGF-1Ea. MLC/mlIGF-1 body weight was increased by 8% at one month of age ($p=0.01$), 11% at two-three months

($p=0.0001$), and by 6% at six months of age, even though at six months, values no longer reached significance ($p=0.3$) (Figure 3.14A). MLC/Class 2 IGF-1Ea animals showed a similar increase up to two-three months of age (9% at one month ($p=0.01$), 11% at two-three months ($p=0.01$)), but in contrast to MLC/mIGF-1 mice, the 14% increase measured at six months of age for MLC/Class 2 IGF-1Ea animals was still significant ($p=0.01$) (Figure 3.14B). MLC/Class 1 IGF-1Eb and MLC/Class 2 IGF-1Eb instead, did not show any significant changes in body weight throughout all ages analyzed ($p>0.05$) (Figure 3.14C and D).

To exclude an effect of IGF-1 isoform over-expression on visceral organs, also the weight of visceral organs (heart, brain, liver, kidney, and spleen) was monitored throughout life of the transgenic animals. All weight values were normalized for body weight and results are shown in Figure 3.15 A-D. None of the transgenic lines showed a significant increase in any of the organs monitored ($p>0.05$).

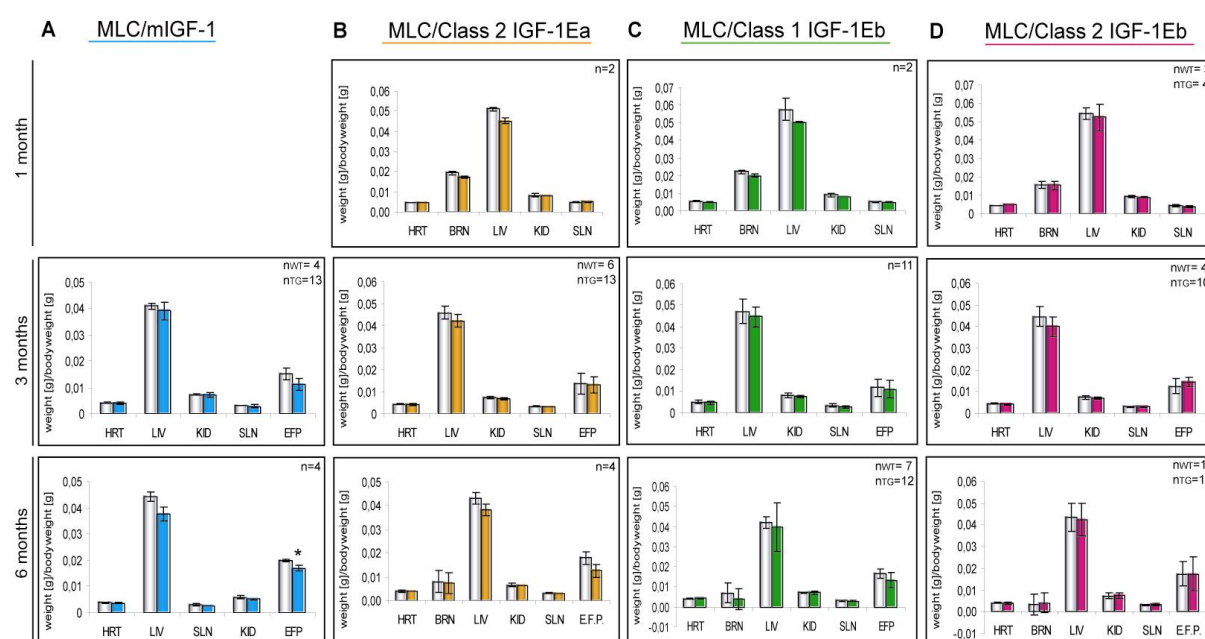


Figure 3.15 Effect of IGF-1 isoform over-expression on the weight of visceral organs. Tissue weights were taken from male transgenic mice (1, 3, and 6 months of age) and their negative littermates. The number of animals is indicated in every diagram. All organ values were normalized for bodyweight. **A** MLC/mIGF-1 animals did not show any effect on the weight of visceral organs. Only the weight of the EDP was significantly increased at 3 ($p=0.006$) and 6 months of age ($p=0.03$). MLC/Class 2 IGF-1Ea (**B**), MLC/Class 1 IGF-1Eb (**C**), and MLC/Class 2 IGF-1Eb animals (**D**) did not show an effect of the weight of distal organs.

To determine whether IGF-1 isoform over-expression had an effect on fat deposition, as reported for male SIS2 mice, which deposited less fat between five and ten weeks of age [299], measurements of the epididymis fat pat (EFP) of male mice were included. The EFP is the only well defined fat pat in the organism and is therefore well suited for comparison. However, these measurements do not necessarily reflect the total fat content of the animal. Only MLC/mIGF-1 animals (over-expressing the same Class 1 IGF-1Ea isoform as the SIS2

mice, but of rat and not of human origin) showed significant changes, reflected in a 26% decrease ($p=0.006$) at three months of age and a 15% decrease ($p=0.03$) at six months of age. None of the other transgenic lines showed an influence on fat deposition in the EFP ($p>0.05$).

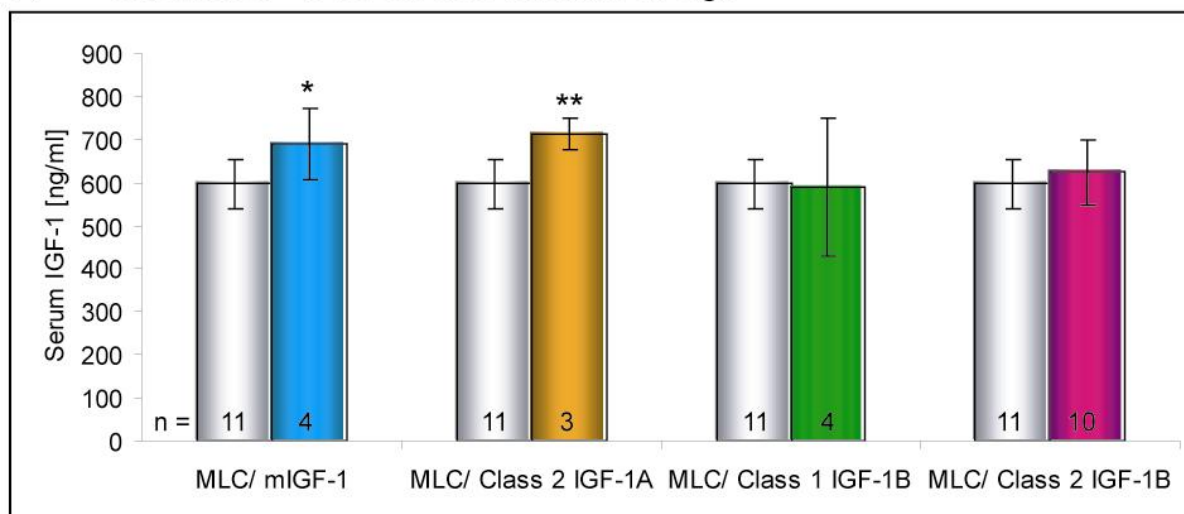
In summary, both IGF-1 isoforms that contain the Ea-peptide showed an effect on overall bodyweight, which was significant for MLC/mIGF-1 up until three months, while MLC/Class 2 IGF-1Ea showed a significant increase at all ages surveyed. IGF-1 isoforms containing the Eb-peptide in contrast, did not show any changes in bodyweight. None of the transgenic lines showed an influence on the weight of visceral organs, and only MLC/mIGF-1 showed a significant decrease of fat deposition in the EFP.

3.3.7 Effects of IGF-1 isoform over-expression on serum IGF-1 levels

A next crucial step in defining the phenotype of the different IGF-1 isoform over-expressing mice was to determine if the IGF-1 transgenes influenced the levels of circulating IGF-1. Previously generated transgenic mice over-expressing IGF-1 have been reported to secrete IGF-1 transgenes to the circulation (reviewed in [300]), a side effect that ideally should be avoided in a therapeutic setting, since it could lead to metabolic changes and/or effects on other organ systems in the body. This is especially important considering IGF-1 as a potential drug for curing muscle diseases.

None of the assays to determine serum concentrations of IGF-1 available to date distinguish between IGF-1 isoforms or between rat and mouse IGF-1. Since all transgenic lines analyzed in this work over-express transgenes of rat (MLC/mIGF-1) or mouse origin (MLC/Class 2 IGF-1Ea, MLC/Class 1 IGF-1Eb, and MLC/Class 2 IGF-1Eb), total IGF-1 concentrations in the blood serum of male transgenic mice of three and six months of age were compared to total IGF-1 concentrations in the blood serum of age-matched WT animals of the same gender (Figure 3.16). At the age of three months, MLC/mIGF-1 and MLC/Class 2 IGF-1Ea mice showed modest, but still significantly elevated serum IGF-1 levels (16% increase in MLC/mIGF-1 serum samples ($p=0.02$) and 19% in MLC/Class 2 IGF-1Ea samples ($p=0.005$)). Total serum levels of IGF-1 were unchanged in lines MLC/Class 1 IGF-1Eb and MLC/Class 2 IGF-1Eb (Figure 3.16 A). At the age of six months MLC/mIGF-1 serum samples showed a 7.4% increase in total circulating IGF-1 concentrations, which is not significant ($p>0.05$), while total circulating IGF-1 levels of MLC/Class 2 IGF-1Ea mice showed a similar increase noticed in three-months-old animals (24% increase ($p=0.0001$))(Figure 3.16 B). MLC/ Class 1 IGF-1Eb and MLC/Class 2 IGF-1Eb showed no effect on serum IGF-1 levels (Figure 3.16 B).

A Serum IGF-1 levels at 3 months of age



B Serum IGF-1 levels at 6 months of age

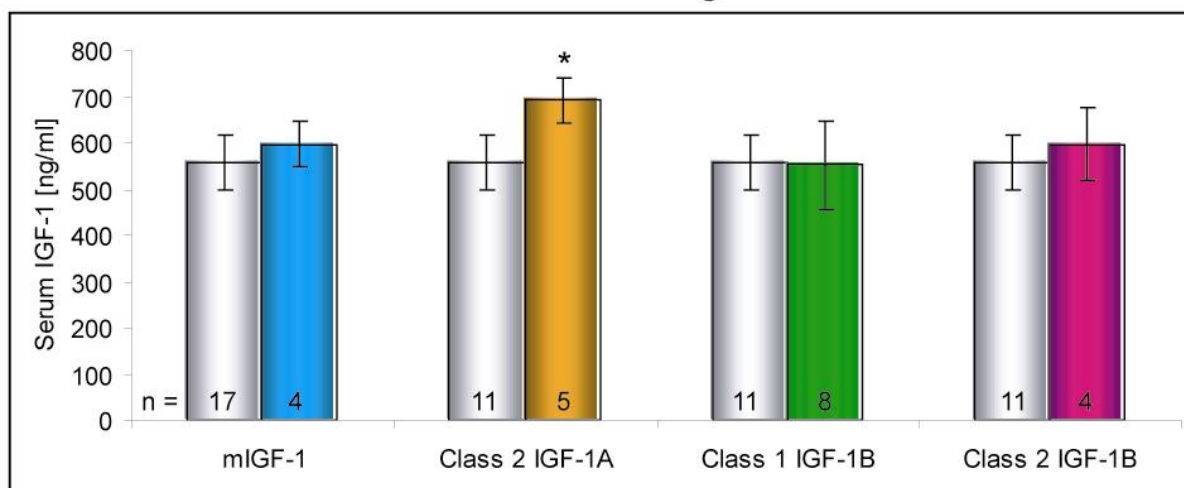


Figure 3.16 Effect of IGF-1 isoform expression on total circulating IGF-1 levels. All blood samples were taken from male transgenic mice and age matched WT animals (the number of animals is indicated on the bottom of the columns). **A** At 3 month of age MLC/mIGF-1 and MLC/Class 2 IGF-1Ea showed significantly elevated IGF-1 levels in the serum ($p=0.02$ and $p=0.005$ respectively), while serum levels of MLC/Class 1 IGF-1Eb and MLC/Class 2 IGF-1Eb levels were unchanged. **B** By the age of six months, only MLC/Class 2 IGF-1Ea levels were significantly increased ($p=0.0001$) and MLC/mIGF-1 total circulating IGF-1 levels were still elevated (7.4%). MLC/Class 1 IGF-1Ea and MLC/Class 2 IGF-1Eb showed no change.

In summary, over-expression of both Eb-peptide-containing versions of IGF-1 did not show any effect on total levels of IGF-1 in the blood serum, while the two isoforms including the Ea-peptide induced an increase of total serum IGF-1: MLC/Class 2 IGF-1Ea mice showed consistently significant increases at three and six months of age, while MLC/mIGF-1 IGF-1 serum levels were only significantly increased by the age on three months, even though still elevated by six months of age.

3.3.8 Skeletal muscle weight of IGF-1 isoform transgenic lines

The first step in analyzing the skeletal muscle phenotype of the different IGF-1 isoform transgenic mouse lines was to determine changes in the weight of different skeletal muscle groups. The weight of the quadriceps (abbreviated “quad”), gastrocnemius (abbreviated “gas”), tibialis anterior (TA), extensor digitorum longus (EDL), and soleus (abbreviated “sol”) muscles was measured in male mice of one, three, and six months of age and compared to age-matched WT animals of the same gender. All values were normalized for body weight and are shown in Figure 3.17.

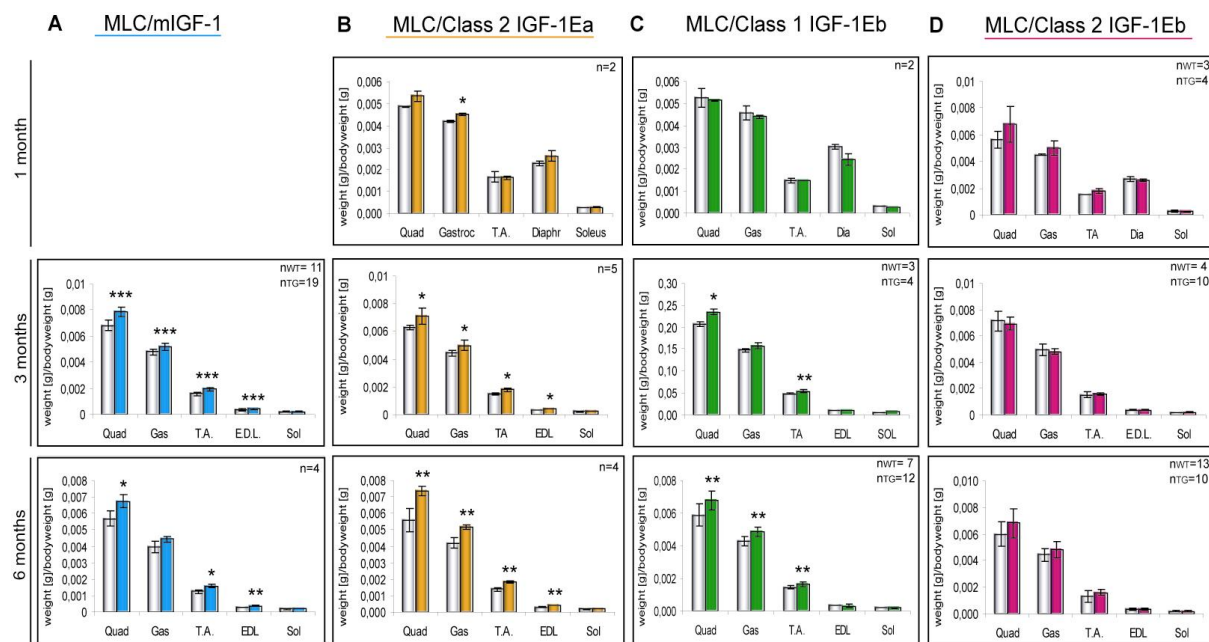


Figure 3.17 Skeletal muscle weights of IGF-1 isoform transgenic lines. One-, three-, and six-months-old male mice were used for skeletal muscle weight measurements. The number of mice is indicated on the top right corner of every graph. All values were normalized for bodyweight. **A** MLC/mlGF-1 fast skeletal muscle groups showed a significant weight increase ($p < 0.0002$ for all) at three and six months, soleus weight was not changed. **B** MLC/Class 2 IGF-1Ea fast muscle groups were increased in weight at three months and six months of age ($p < 0.007$ for all), while values at one months were elevated, but apart from gastrocnemius not significant. The weight of the slow soleus muscle was not influenced. **C** MLC/Class 1 IGF-1Eb one-month-old samples did not show any changes, while the weight of quad and TA showed a significant increase ($p < 0.03$) at three months. By the age of six months, all fast muscles but the EDL were significantly increased in weight ($p = 0.01$). **D** Line MLC/Class 2 IGF-1Eb samples showed elevated skeletal muscle weight at one and six months of age, while three-month-old samples were unchanged. None of the values reached significance.

MLC/mlGF-1 animals showed a significant increase of all fast muscles at three months of age (quad 16%, gas 9%, TA 22%, EDL 30% ($p < 0.0002$ for all)), which was maintained at similar levels at six months of age (quad 18%, gas 12%, TA 26%, EDL 32% ($p < 0.02$ for all)), while the weight of the soleus, a slow muscle, was unchanged at all times (Figure 3.17A). At one month of age, MLC/Class 2 IGF-1Ea mice displayed a modest increase of the fast muscles quadriceps (5%) and gastrocnemius (7%), which was only significant for the gastrocnemius muscle ($p = 0.03$). The weight of TA, diaphragm, and soleus were not

significantly changed (Figure 3.17B). At three months of age the skeletal muscle weight was significantly increased in all fast muscle groups (quad 13%, gas 12%, TA 19%, EDL 24% ($p < 0.007$ for all)), reaching even higher levels at six months of age (quad 32%, gas 23%, TA 32%, EDL 33% ($p < 0.007$ for all)). The soleus muscle weight did not significantly change at any age, but showed a tendency for a modest weight gain (Figure 3.17B).

The increase of skeletal muscle weight in MLC/Class 1 IGF-1Eb animals was rather mild at all ages surveyed. At one month of age, no significant changes were found for the analyzed skeletal muscle groups (Figure 3.17C). By the age of three months, quadriceps (11%) and TA (9%) weights are significant in their weight increase ($p < 0.03$), while gastrocnemius (4%) and EDL (7%), values did not reach significance. The weight of the soleus muscle was unchanged (Figure 3.17C). At six months of age, all fast skeletal muscle groups but the EDL showed a significant but modest weight increase (quad 14%, gas 12%, and TA 12% ($p < 0.01$)). Weights of EDL and soleus were not significantly altered.

Results for the MLC/Class 2 IGF-1Eb transgenic animals revealed increased but not significant weights for fast skeletal muscle groups at one month of age (quad 20%, gas 11%, TA 15%), while measurements of three-months-old mice showed no significant differences for any of the muscles measured (Figure 3.17D). By the age of six months, fast muscle weights were increased (quad 13%, gas 8%, TA 20%, and EDL 7%), but again did not reach significance. Soleus muscle weight was not influenced at any age.

Taken together, lines MLC/mIGF-1 and MLC/Class 2 IGF-1Ea showed the most prominent increase of skeletal muscle mass, which was consistently significant at three and six months of age. Lines MLC/Class 1 IGF-1Eb and MLC/Class 2 IGF-1Eb instead showed only modest and highly variable changes in muscle weight, many which fall below the level of statistical significance.

3.3.9 Histological analysis of IGF-1 isoform transgenic skeletal muscle

To determine whether the increase in skeletal muscle weight of IGF-1 isoform transgenic mice can be correlated to an increase of muscle fiber size, histological analysis of the skeletal muscle of IGF-1 isoform transgenic lines was carried out on four six-months-old male animals for each line and compared to age-matched WT mice of the same sex. As a measurement of increased muscle fiber size, the cross-sectional area (CSA) of slow, intermediate, and fast fibers was determined for the entire TA, EDL, and soleus muscles. 12 μ m frozen sections were stained for NADH-TR (section 2.4.5), which allows the differentiation between fast, intermediate, and slow fibers based on the intensity of the

staining (slow fibers stain dark blue due to a higher content of mitochondria, fast fibers stain very light blue due to a low content of mitochondria, and intermediate fibers stain light blue due to a higher mitochondria content than fast fibers but a lower content than slow fibers) (Figures 3.18 A, 3.19 A, and 3.20 A, upper panel). To confirm identity of the fast type IIB fibers, double-immunohistochemistry was performed with antibodies against type IIB myosin and laminin (Figures 3.18 A and 3.20 A, lower panel). MLC/mlGF-1 animals were not analyzed for CSA in the present work, since the CSA phenotype has already been analyzed elsewhere [77]. The data published by Musaro et al. demonstrated an overall increase in the CSA of fibers in the quadriceps but not the soleus muscle, with an increased diameter specifically of the fast fibers. The composition of fibers of the fast EDL muscle showed a significant decrease in the fast IIA fibers, while the percentage of type IIB fibers was modestly, but not significantly increased.

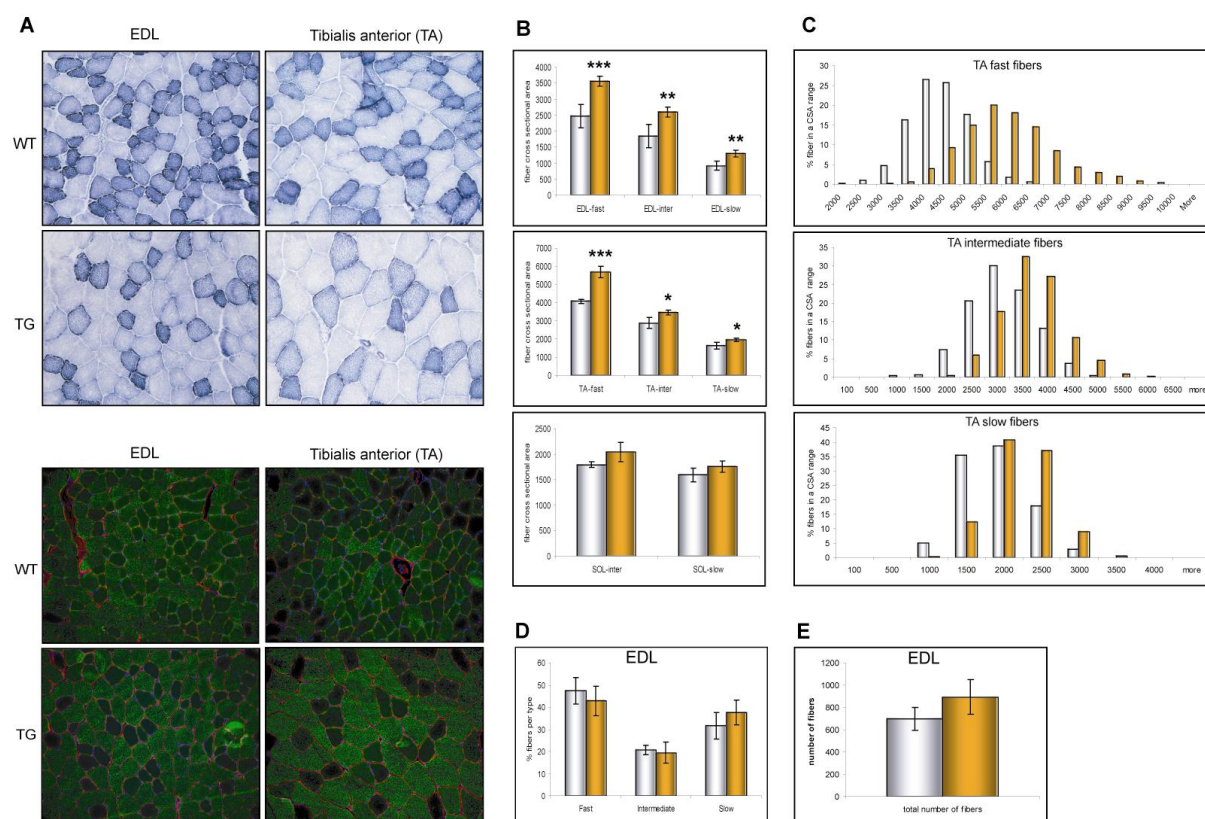


Figure 3.18 Histological analysis of MLC/Class 2 IGF-1 Ea muscles. Six-month-old transgenic mice were compared to littermates of the same sex (n=4 for both). **A** Representative pictures of EDL and TA sections stained with NADH-TR (upper panel). Identity of fast IIB fibers was confirmed with antibodies against type IIB myosin and laminin (lower panel). **B** CSA analysis of EDL and TA fast, intermediate, and slow fibers. **C** Size distribution of different fiber types of the TA muscle. **D** Fiber type composition of the EDL muscle. **E** Analysis of the total number of fibers in the EDL muscle.

Analysis of the MLC/Class 2 IGF-1Ea transgenic line revealed a significant increase of fast, intermediate, and slow fibers in both fast muscles analyzed, the EDL (fast: 44%, $p=0.003$, intermediate: 40%, $p=0.004$, and slow: 41%, $p=0.02$) and the TA (fast: 39%, $p=0.0002$,

intermediate: 20%, $p=0.02$, and slow: 20%, $p=0.02$). The slow soleus muscle showed a mild increase in CSA (13.5% for intermediate and 10% for slow fibers), which was not significant (Figure 3.18 B). Analyzing the data for the distribution of fibers of a certain CSA range as shown in figure 3.18 C for the TA as an example, clearly shows that the normal size distribution of fibers in the muscle was maintained, but in presence of the MLC/Class 2 IGF-1Ea transgene, the curve was dramatically shifted towards bigger fibers. This effect was most pronounced in the fast fibers, where the transgene is predominantly expressed, but also visible for intermediate and slow fibers. The same shift was seen for the EDL muscle (data not shown). These findings indicate that the transgene affects not only the fast fibers, where the MLC promoter is most active, but also the intermediate and the slow fibers, where it is less active or not active at all. This paracrine effect of IGF-1 over-expression was not described for the MLC/mIGF transgene [282], which is most likely due to a different type of analysis.

To determine if the presence of the Class 2 IGF-1Ea transgene influenced the composition of fibers within the muscle, the number of fast, intermediate, and slow fibers was counted in the EDL muscle and did not show a significant change (fast fibers: $47\pm6\%$ in the WT, $43\pm6\%$ in the transgenic; intermediate fibers: $20\pm2\%$ in the WT, $19\pm4\%$ in the transgenic; slow fibers: $31\pm6\%$ in the WT, $37\pm6\%$ in the transgenic) (Figure 3.18 D), indicating that the transgene did not induce any changes in fiber composition, which was reported for the MLC/mIGF-1 transgenic line [282].

To rule out the possibility that the increase of skeletal muscle weight could also be due to an increase in fiber number (hyperplasia), the total number of fibers was counted in the EDL muscle of WT and transgenic animals. Results shown in Figure 3.18 E did not show a significant difference in the total number (695 ± 101 in the WT and 892 ± 156 in the transgenic EDL), providing the definite evidence that the increase of the wet weight in MLC/Class 2 IGF-1Ea transgenic animals (section 3.3.8) was due to hypertrophy of the muscle fibers.

In contrast to line MLC/Class 2 IGF-1Ea, the CSA was not significantly changed in any of the muscles analyzed for line MLC/Class 1 IGF-1Eb (Figure 3.19 B). However, a modest increase was noted for all fiber types in the EDL muscle (fast: 4.5%, intermediate: 4.8%, and slow: 12%) and for the fast fibers in the TA muscle (6%). When analyzed for size distribution, the TA muscle (Figure 3.19 C), as well as the EDL muscle (data not shown) showed a modest shift towards a higher percentage of bigger fibers.

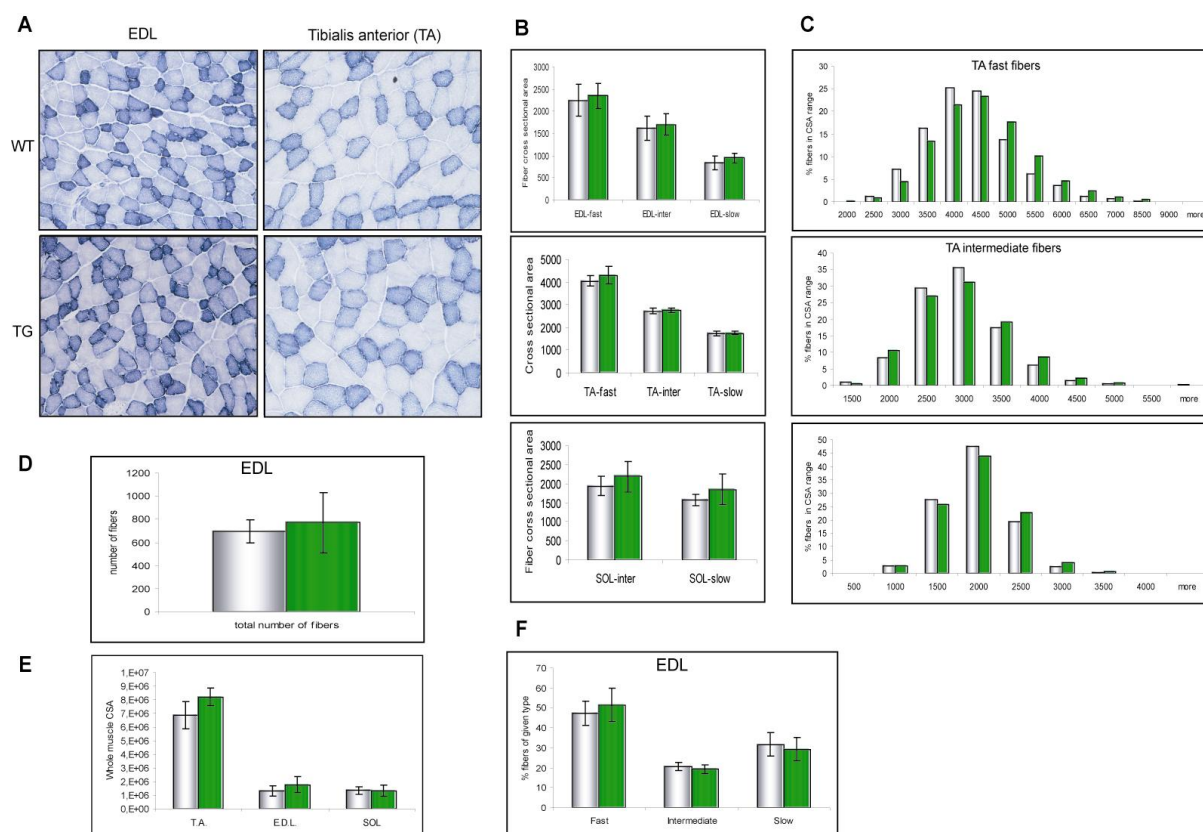


Figure 3.19 Histological analysis of MLC/Class 1 IGF-1Eb muscles. Six-months-old mice were compared to littermates of the same sex ($n=4$ for both). **A** Representative pictures of EDL and TA sections stained with NADH-TR. **B** CSA analysis of EDL and TA fast, intermediate, and slow fibers. **C** Size distribution of different fiber types of the TA muscle. **D** Total number of fibers of the EDL muscle. **E** Whole muscle CSA of TA, EDL, and soleus. **F** Fiber type composition of the EDL muscle.

Since the analysis of wet skeletal muscle weight described in section 3.3.8 demonstrated a significant increase for both the EDL and TA muscle, the total number of fibers was counted in the EDL muscle to determine if a higher number of fibers could account for this weight increase. Results shown in Figure 3.19 D, demonstrate that there was no change between the total number of fibers between the WT and transgenic EDL muscle (771 ± 101 in the WT and 694 ± 260 in the transgenic). Thus, the weight increase could not be correlated to a higher amount of fibers in the muscle.

To determine whether the shift towards a higher percentage of big fibers in the EDL and TA was sufficient to account for the CSA increase of the whole muscle, this parameter was determined as well and showed a 19% increase for the TA CSA, a 36.5% increase for the EDL and no change for the soleus (Figure 3.19 E). None of these changes reached significance, but generally indicate that a small increase in individual fiber size can account for an increase of the whole muscle CSA, without affecting the mean values for fiber-specific CSA.

Finally, the analysis of fiber composition in the EDL of the MLC/Class 1 IGF-1Eb transgenic animals showed no changes (fast: 47±6% in the WT, 51±8% in the transgenic; intermediate: 20±2% in the WT, 19±2% in the transgenic; slow: 31±6% in the WT, and 29±6% in the transgenic) (Figure 3.19 F).

A similar analysis of the MLC/Class 2 IGF-1Eb transgenic muscles revealed that the CSA of EDL fast and slow fibers was significantly increased (fast 32%, $p=0.04$ and slow 19%, $p=0.01$), while intermediate fibers were not affected. The TA instead did not show a significant increase in any of the fiber types, even though a very moderate elevation was detectable (fast: 8.4%, intermediate: 4%, and slow: 4.4%) (Figure 3.20 B). A slight increase of the CSA was also seen in the soleus muscle, with intermediate fibers being 10% and slow fibers being 25% increased, but due to a high standard deviation, values did not reach significance (intermediate: 1933±264 μm^2 in the WT, 2129±178 μm^2 in the transgenic; slow: 1550±250 μm^2 in the WT and 1928±206 μm^2 in the transgenic) (Figure 3.20 B). The analysis of the fiber size distribution revealed that despite of the non-significant increase of fiber CSA in the TA muscle, a shift towards a higher percentage of bigger fibers was induced in presence of the Class 2 IGF-1Eb transgene (Figure 3.20 C). A similar shift was noted for fibers of the EDL muscle (data not shown). The shift was much less pronounced than seen for MLC/Class 2 IGF-1Ea fibers and more comparable to line MLC/Class 1 IGF-1Eb.

Measurements of skeletal muscle weight of MLC/Class 2 IGF-1Eb mice described in section 3.3.8, did not show a significant increase of skeletal muscle wet weight, even though the TA and EDL muscle weights were elevated (20% TA and 7% EDL at six months of age).

To exclude a hyperplastic response to Class 2 IGF-1Eb over-expression, the total number of EDL fibers was determined and as seen for the other transgenic lines, did not show a significant change (695±101 in the WT and 703±129 in the transgenic) (Figure 3.20 D). Thus, the increased amount of big fibers in the TA and EDL, which at least in the EDL muscle also resulted in a significant increase of CSA, accounts for the elevation of muscle weight. The investigation of changes in the distribution of fibers in the EDL muscle did not show any significant changes (fast: 47±6% in the WT, 36±5%, in the transgenic, intermediate: 20±2% in the WT, 22±4% in the transgenic, slow: 32±6% in the WT and 40±2% in the transgenic).

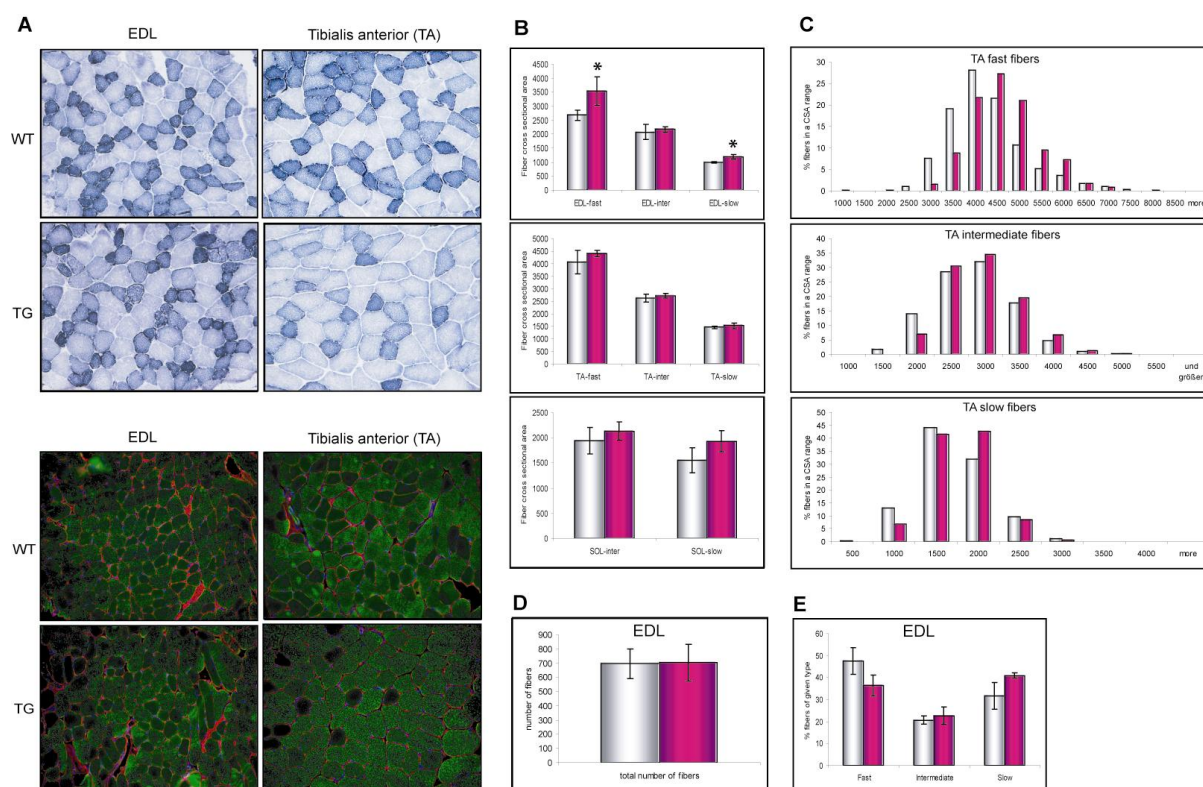


Figure 3.20 Histological analysis of MLC/Class 2IGF-1 Eb muscles. Six-month-old transgenic mice were compared to littermates of the same sex (n=4 for both). **A** Representative pictures of EDL and TA sections stained with NADH-TR (upper panel). Identity of fast IIB fibers was confirmed with antibodies against type IIB myosin and laminin (lower panel). **B** CSA analysis of EDL and TA fast, intermediate, and slow fibers. **C** Size distribution of different fiber types of the TA muscle. **D** Fiber type composition of the EDL muscle. **E** Analysis of the total number of fibers in the EDL muscle.

In summary, the histological and morphometric analysis of three of the transgenic lines, showed a consistent increase in the CSA of all skeletal muscle fiber types in the EDL and TA muscle of MLC/Class 2 IGF-1Ea animals. The CSA of soleus fibers was unchanged. In contrast to these findings, MLC/Class 1 IGF-1Eb and MLC/Class 2 IGF-1Eb showed a milder phenotype, with a modest shift towards a higher percentage of bigger fibers, which did not reach significance in the MLC/Class 1 IGF-1Eb animals, and were only just significant for MLC/Class 2 IGF-1Eb EDL fast and slow muscle fibers. The CSA of the soleus muscle was also not significantly changed in these animals. None of the transgenic lines analyzed showed an effect on the total number of fibers in the EDL muscle and no changes were seen in the fiber distribution of this muscle.

3.3.10 Skeletal muscle physiology of IGF-1 isoform transgenic skeletal muscle

In order to translate the changes seen in the skeletal muscle phenotype of the different IGF-1 transgenic lines into functional performance of these muscles, the EDL and soleus muscles were analyzed for their physiological properties. This work was done in collaboration with Antonio Musaro (University of Rome, La Sapienza). The protocol used is described in detail in section 2.5.2. Male WT animals (n=4) were compared to transgenic animals at 2.5 months

of age (MLC/Class 2 IGF-1Ea n=5, MLC/Class 1 IGF-1Eb n=3, MLC/Class 2 IGF-1Eb n=4). Analysis of MLC/mIGF-1 animals (n=4 for WT and transgenic animals) was done separately on six-months-old mice and the results were kindly provided by Antonio Musaro for comparison. Measurement of the single twitch force (F_{twitch}), the tetanic force (F_{max}), and the specific force (F_{spec}) allow conclusions about the muscle strength and force generation. The measurements of the time the muscle needs to reach the peak of F_{twitch} (T_{response}) reflects the contraction speed and is related to the muscle fiber composition, which also determines the time the muscle needs to reach half the tetanic force (T_{fatigue}). The analysis of these parameters was analyzed in the EDL muscle as an example of a predominantly fast muscle, and in the soleus, as an example for a slow muscle.

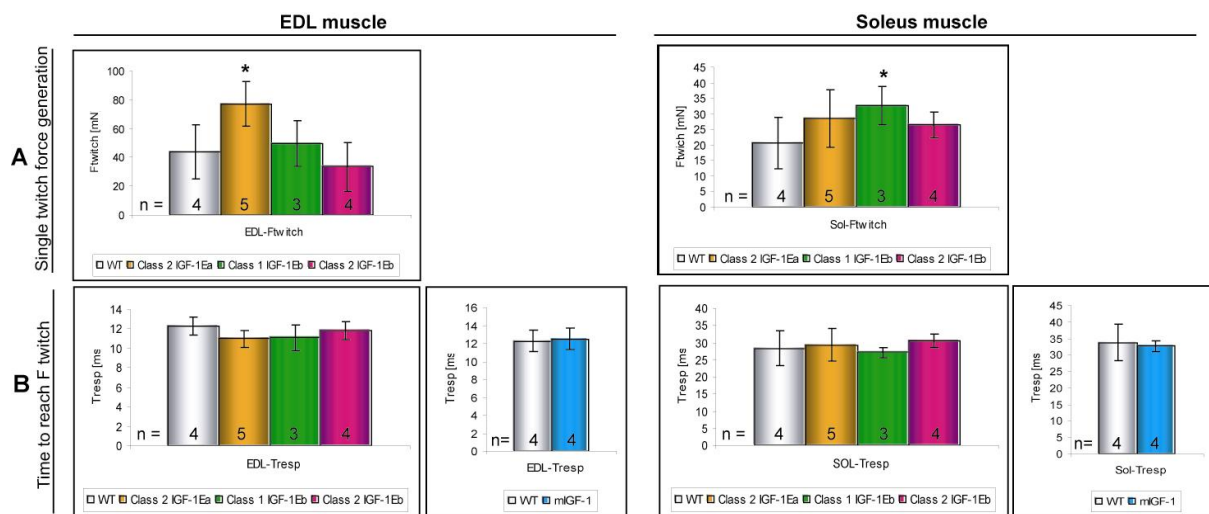


Figure 3.21 Functional analyses of IGF-1 isoform transgenic muscles (1). Two and a half months-old animals of male sex were analyzed for EDL and soleus electrophysiological properties. MLC/mIGF-1 animals were analyzed at six month of age and are therefore shown separately. The number of animals from each line is indicated at the bottom of each column. **A** EDL single twitch force generation (F_{twitch}) is shown in the left panel and was only significant for MLC/Class 2 IGF-1Ea ($p=0.01$). Soleus F_{twitch} is shown in the left panel and was significantly increased in MLC/Class 1 IGF-1Eb ($p=0.04$). Data for MLC/mIGF-1 was not available. **B** EDL contraction speed (F_{resp}) is shown in the left panel and showed a significant change for MLC/Class 2 IGF-1Ea ($p=0.04$), while soleus F_{resp} shown in the right panel, was unchanged.

Analysis of the single twitch force F_{twitch} in the EDL muscle revealed a significant increase for MLC/Class 2 IGF-1Ea animals (76%, $p=0.01$), while MLC/Class 1 IGF-1Eb (12%) and MLC/Class 2 IGF-1Eb (23%) showed an increase that was not significant (Figure 3.21 A left panel). Data to determine this parameter for MLC/mIGF-1 was unfortunately not available. The EDL contraction speed (T_{response}) was slightly decreased in MLC/Class 2 IGF-1Ea (9%) and Class 1 IGF-1Eb (9%) animals, while unchanged in MLC/mIGF-1 (12 ± 1.2 ms in the WT and 12 ± 1.2 ms in the transgenic) and MLC/Class 2 IGF-1Eb animals (12 ± 0.9 ms in the WT and 12 ± 0.9 ms in the transgenic) (Figure 3.21 B left panel). Measurements of the maximal force (tetanic force) F_{max} of the EDL muscle showed the most dramatic increase for line MLC/Class 2 IGF-1Ea (101% ($p=0.003$)). MLC/mIGF-1 transgenic EDL muscles also showed

a significant increase of 54% ($p=0.01$), while values for MLC/Class 1 IGF-1Eb and MLC/Class 2 IGF-1Eb were not significant due to high variability of the measurements. However, the tetanic force was increased by 43% and 24% respectively (Figure 3.22 A left panel). The time the different muscles needed to reach half their EDL tetanic force F_{\max} (T_{fatigue}) was decreased by 30% in MLC/Class 2 IGF-1Ea muscles, MLC/Class 1 IGF-1Eb T_{fatigue} was decreased by 39% and a decrease of 23% was measured in MLC/Class 2 IGF-1Eb EDL muscles. The high variability of the WT samples makes this decrease very unreliable and therefore none of the values were significant (Figure 3.22 B left panel). Values measured for line MLC/mIGF-1 were not changed at all (WT: 18.1 ± 1.6 ms, transgene: 17.1 ± 1.7 ms). Finally, the specific force F_{spec} for every muscle was calculated by dividing the tetanic force F_{\max} by the weight of the muscle measured. EDL specific force was increased by 43% in MLC/Class 2 IGF-1Ea samples and both MLC/Class 1 IGF-1Eb and MLC/Class 2 IGF-1Eb showed an increase of 25%, without being significant in any of these animals. MLC/mIGF-1 did not show any changes in EDL specific force (WT: 15.5 ± 6 N/g, transgenic: 15.4 ± 2.4 N/g) (Figure 3.22 C left panel).

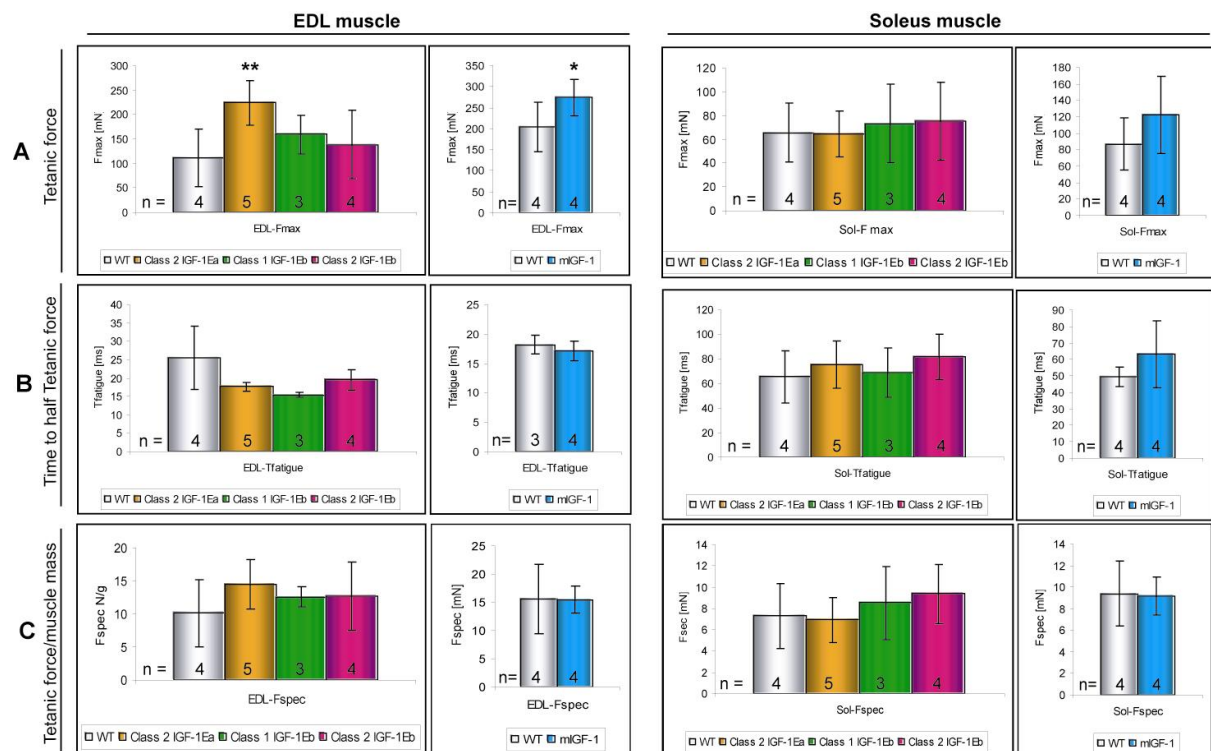


Figure 3.22 Functional analyses of IGF-1 isoform transgenic muscles (2). Two and a half months-old animals of male sex were analyzed for EDL and soleus electrophysiological properties. MLC/mIGF-1 animals were analyzed at six month of age and are therefore shown separately. The number of animals from each line is indicated at the bottom of each column. **A** EDL tetanic force (F_{\max}) is shown in the left panel and was significant for MLC/Class 2 IGF-1Ea ($p=0.003$) and MLC/mIGF-1 ($p=0.01$). Soleus F_{\max} is shown in the right panel and was unchanged in all transgenic lines. **B** The time the EDL muscle needed to half F_{\max} (T_{fatigue}) is shown in the left panel and was not significantly changed in any of the samples. Results for the soleus muscle are shown in the right panel and were unchanged as well. **C** The specific force F_{spec} was calculated by dividing F_{\max} by the weight of each analyzed muscle. Results for EDL (left panel) and soleus (right panel) were not significantly influenced by the presence of different IGF-1 isoform transgenes.

The same measurements were performed on the soleus to evaluate the effect of IGF-1 isoform over-expression on the overall physiological performance of a slow muscle. The single twitch force F_{twitch} of the soleus muscle of the different IGF-1 isoform transgenic lines showed a non-significant increase of 37% in Line MLC/Class 2 IGF-1Ea and 27% in MLC/Class 2 IGF-1Eb, while the 57% increase observed in MLC/Class 1 IGF-1Eb soleus was significant ($p=0.04$) (Figure 3.21 A right panel). The soleus contraction speed (T_{response}) did not show any transgene-induced changes (MLC/mlIGF-1: WT 34 ± 5 ms, transgenic 33 ± 1.6 ms; MLC/Class 2 IGF-1Ea: WT 28 ± 5 ms, transgenic 29 ± 4 ms; MLC/Class1 IGF-1B: WT 28 ± 5 ms, transgenic 27.1 ± 1.4 ms; MLC/Class 2 IGF-1Eb: WT 28 ± 5 ms, transgenic 30.6 ± 1.9 ms) (Figure 3.21 B right panel). The assessment of the maximal force (tetanic force) F_{max} in the soleus muscle revealed no changes for MLC/Class 2 IGF-1Ea (WT: 65 ± 24 mN transgenic: 64 ± 19 mN), MLC/Class 1 IGF-1Eb (WT: 65 ± 24 mN transgenic: 73 ± 33 mN), and MLC/Class 2 IGF-1Eb (WT: 65 ± 24 mN transgenic: 75 ± 33 mN). MLC/mlIGF-1 samples instead showed a 40% increase, but due to a very high variability, this value did not reach significance (86 ± 31 mN in the WT and 122 ± 47 mN in the transgenic) (Figure 3.22 right panel). The time the different muscles needed to reach half the tetanic force F_{max} (T_{fatigue}) was not significantly changed for MLC/Class 2 IGF-1Ea (WT: 65 ± 21 ms, transgenic: 75 ± 18 ms), MLC/Class 1 IGF-1Eb (WT: 65 ± 21 ms, transgenic: 69 ± 20 ms), and MLC/Class 2 IGF-1Eb (WT: 65 ± 21 ms, transgenic: 81 ± 18 ms). MLC/mlIGF-1 animals showed a 27% increase, but the variability was too high to reach significance (Figure 3.22 B right panel). Finally, the specific force F_{spec} , calculated by dividing the tetanic force F_{max} by the weight of the muscle, did not show any differences in any of the transgenic mice analyzed (MLC/mlIGF-1: WT 9.4 ± 3 N/g, transgenic 69.2 ± 1.8 N/g; MLC/Class 2 IGF-1Ea: WT 7 ± 3 N/g, transgenic 6.9 ± 2 ; MLC/Class 1 IGF-1Eb: WT 7 ± 3 N/g, transgenic 8.5 ± 3.5 ; MLC/Class 2 IGF-1Eb: WT 7 ± 3 N/g, transgenic 9.4 ± 2.8 N/g) (Figure 3.22.C right panel).

In summary, the electrophysiological analysis of the different IGF-1 isoform transgenic lines for the parameters related to force generation and strength (single twitch force (F_{twitch}), tetanic force (F_{max}), and specific force (F_{spec})), revealed a significant increase for the EDL muscle of MLC/Class 2 IGF-1Ea animals, and at least the maximal force generation was significantly increased in the EDL muscle of MLC/mlIGF-1. These findings correlate to the increased muscle mass and fiber CSA of these two transgenic lines (described in section 3.3.8 and 3.3.9) and establish a functional hypertrophy for MLC/Class 2 IGF-1Ea, that is even more pronounced than previously described for line MLC/mlIGF-1 [77]. In contrast, force-related parameters were not significantly changed in lines MLC/Class 1 IGF-1Eb and MLC/Class 2 IGF-1Eb, which correlates to the much milder increase in muscle mass and fiber CSA in these two transgenic lines (sections 3.3.8 and 3.3.9). Parameters correlated to the fiber

composition, T_{response} and T_{fatigue} in the EDL muscle were not significantly changed in any of the transgenic lines, confirming that the overall fiber composition was not affected by any of the transgenes. Analysis of these parameters in the soleus muscle of the IGF-1 isoform transgenic lines did not reveal any significant changes for none of the lines, but MLC/Class 1 IGF-1Eb, which showed a significant increase of the single twitch force F_{twitch} .

3.3.11 IGF-1 isoform-mediated signaling

In the past years at least three different pathways have been shown to be activated by IGF-1 (compare section 1.4.5). In the present work, several routes were taken to gain an overview of the signal transduction pathways that might mediate the different phenotypes seen in the distinct IGF-1 isoform transgenic lines. A first step in this analysis was to determine the activation level of the IGF-1 receptor (section 3.3.11a). In a next step, two high throughput screens were applied to gain a broad overview of candidate molecules involved in the IGF-1 isoform mediated response: Affymetrix GeneChip analysis (section 3.3.11b), and the Kinetworks™ Phospho-site screen done by Kinexus (section 3.3.11c). While Affymetrix analysis yielded some insight on the genes that might be differentially regulated by IGF-1, the Kinexus analysis provided an overview of the IGF-1 isoform-induced and phosphorylation-mediated activation of key kinases involved in IGF-1 signaling. Note, that the Affymetrix analysis and the Kinetworks™ Phospho-site screen were performed on mice from Line MLC/Class 1 IGF-1 Ea and not MLC/mIGF-1, since this analysis was performed early in the characterization of the transgenic lines. Finally, the involvement of the calcineurin pathway was investigated, since this pathway has been implicated in mediating the hypertrophic phenotype induced by the mIGF-1 (Class 1 IGF-1Ea) transgene [77, 282] (section 3.3.11d).

3.3.11a Activation of the IGF-1 receptor in IGF-1 isoform transgenic lines

To date it is well established that IGF-1 exerts its function by binding to the IGF-1 receptor (IGF-1R). To determine if all IGF-1 isoforms had an effect on the expression level of IGF-1R mRNA, Northern blot analysis was performed with total RNA isolated from the gastrocnemius muscle of one-month-old male WT and transgenic mice (Figure 3.23 A). No changes were seen between expression levels of WT and transgenic samples, indicating that transcriptional regulation was not affected by over-expression of the different IGF-1 isoforms.

To determine if the IGF-1R was regulated by phosphorylation, immunoprecipitations (IP) were performed with an antibody against the β -subunit of the IGF-R. Protein samples were prepared from six-months-old male mice of WT and transgenic background and 1.3 mg of protein were used for immunoprecipitations. For Western blot analysis the whole IP reaction

was used for SDS-page and transfer and phosphorylation of the IGF-1R β -subunit was detected with an anti-phosphotyrosine antibody (for details see section 2.3.4). Results presented in Figure 2.23 B clearly show the activation of the IGF-1R in all of the transgenic samples when compared to WT samples. Density analysis of the specific bands (Radames software) revealed that the strongest phosphorylation was seen in response to both Class 2 IGF-1 isoforms, Class 2 IGF-1Ea and Class 2 IGF-1Eb (Figure 3.23 C).

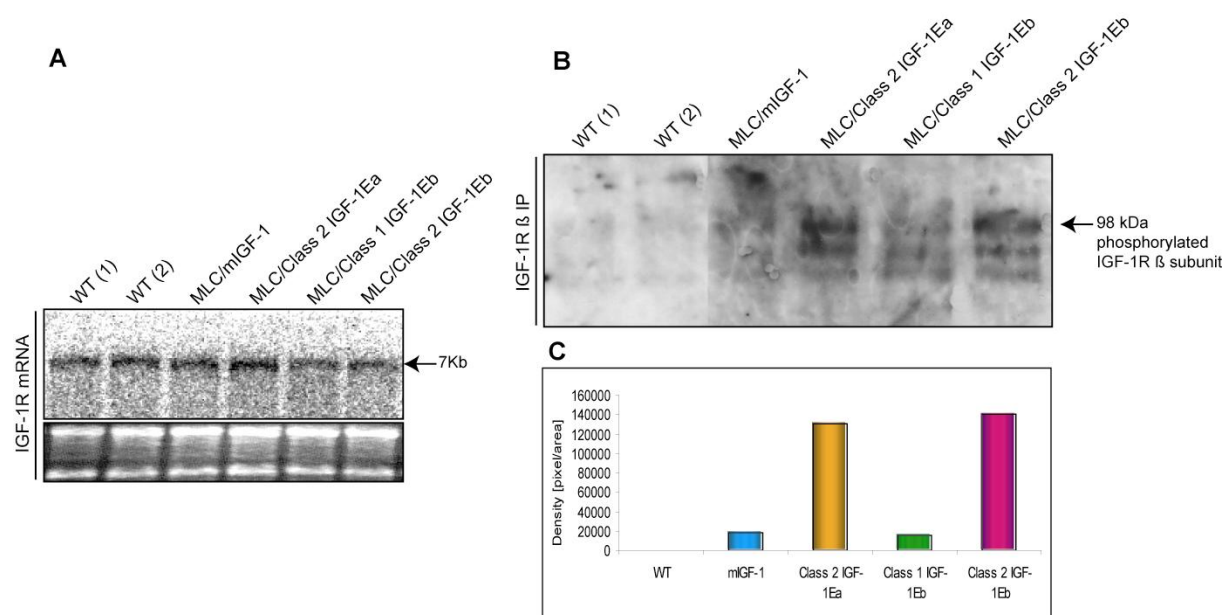


Figure 3.23 mRNA expression and activation of IGF-1R. **A** Northern blot analysis of IGF-1R expression. 10 μ g of total RNA from one-months-old male quadriceps muscle from WT and transgenic mice were used and the IGF-1R mRNA was detected with an IGF-1R-specific probe. Levels of expression did not show any changes induced by any of the transgenes. **B** Immunoprecipitation of the β -subunit of the IGF-1R. 1.3mg of protein per sample was immunoprecipitated with an IGF-1R β -specific antibody. Western blot analysis was performed with an anti-phosphotyrosine antibody to detect the phosphorylation of the intracellular IGF-1R β -subunit. All transgenes activated the IGF-1R. **C** Density graph for phospho-IGF-1R-specific bands. Activation of IGF-1R was strongest in Class 2 IGF-1 transgenes.

Taken together, these results show that IGF-1R mRNA not influenced by over-expression of different IGF-1 isoforms, while activation of the IGF-1R β -subunit was seen in all IGF-1 isoform transgenic lines. These findings proof that over-expressed IGF-1 isoforms are all capable of activating the receptor, even though the extent of activation is variable, with Class 2 IGF-1 isoforms showing the strongest effect.

3.3.11b Affymetrix GeneChip analysis of IGF-1 isoform transgenic muscles

Gene array analysis represents a powerful tool for gaining an overview of changes in the transcriptional regulation in response to a certain stimulus. Affymetrix GeneChip analysis was applied in this work in an attempt to understand IGF-1 isoform-induced alterations in RNA expression patterns.

Affymetrix analysis has been performed on the quadriceps muscle of WT and transgenic mice for each IGF-1 transgenic line (n=2 for each) and a large set of data was obtained. A crucial aspect of analyzing the Affymetrix data is to choose a reliable way of finding interesting candidate genes among the 22626 probe sets that returned a positive signal. The strategy for reducing the data sets is described in section 2.1.16. To further decrease the number of genes to an acceptable amount of candidates we chose a cut off of 1.9-fold up- or down-regulated. Notably, this excludes genes that are not regulated to such an extent, but nevertheless might have an important role. But this drawback has to be accepted to allow evaluation the data. However, it might be useful in the future to re-evaluate the data under different conditions.

Using such a cut off, the filtered genes can be grouped under several criteria, such as the sub-cellular localization, the molecular function, the involvement in disease states and many more, depending on the interest of research. We chose to group by sub-cellular localization to gain an overview of regulated genes with a function in a certain compartment of the cell. This can provide an idea about the nature of IGF-1 isoform-mediated effects. Figure 3.24 A-D shows the pooled up-or down-regulated genes for each IGF-1 isoform transgenic line.

This kind of sorting of genes demonstrates that almost half of the genes regulated by each IGF-1 isoforms can be correlated to organelle function, while only a very small percentage of those genes can be connected to a function in the mitochondria. An almost equal amount of genes is related to a function in the extracellular matrix and the cytosol, while IGF-1 isoforms regulated only a very small percentage of genes with a nuclear function. Class 1 IGF-1Eb did not regulate any nuclear genes. Between the different isoforms, no major differences were seen when analyzing the data in this way. A selection of genes that were found to be up- or down-regulated in this analysis is listed in tables B1-B4 in the appendix of this thesis (page145-148). These gene lists identify genes that were up-or down-regulated in response to one specific isoform (highlighted with bold font) and represent those candidate genes, which might play an important role in the IGF-1 isoform-mediated response. The regulation of these genes has not been confirmed in the present thesis, but an involvement of these candidates as downstream targets of an IGF-1-mediated response is planned for the future.

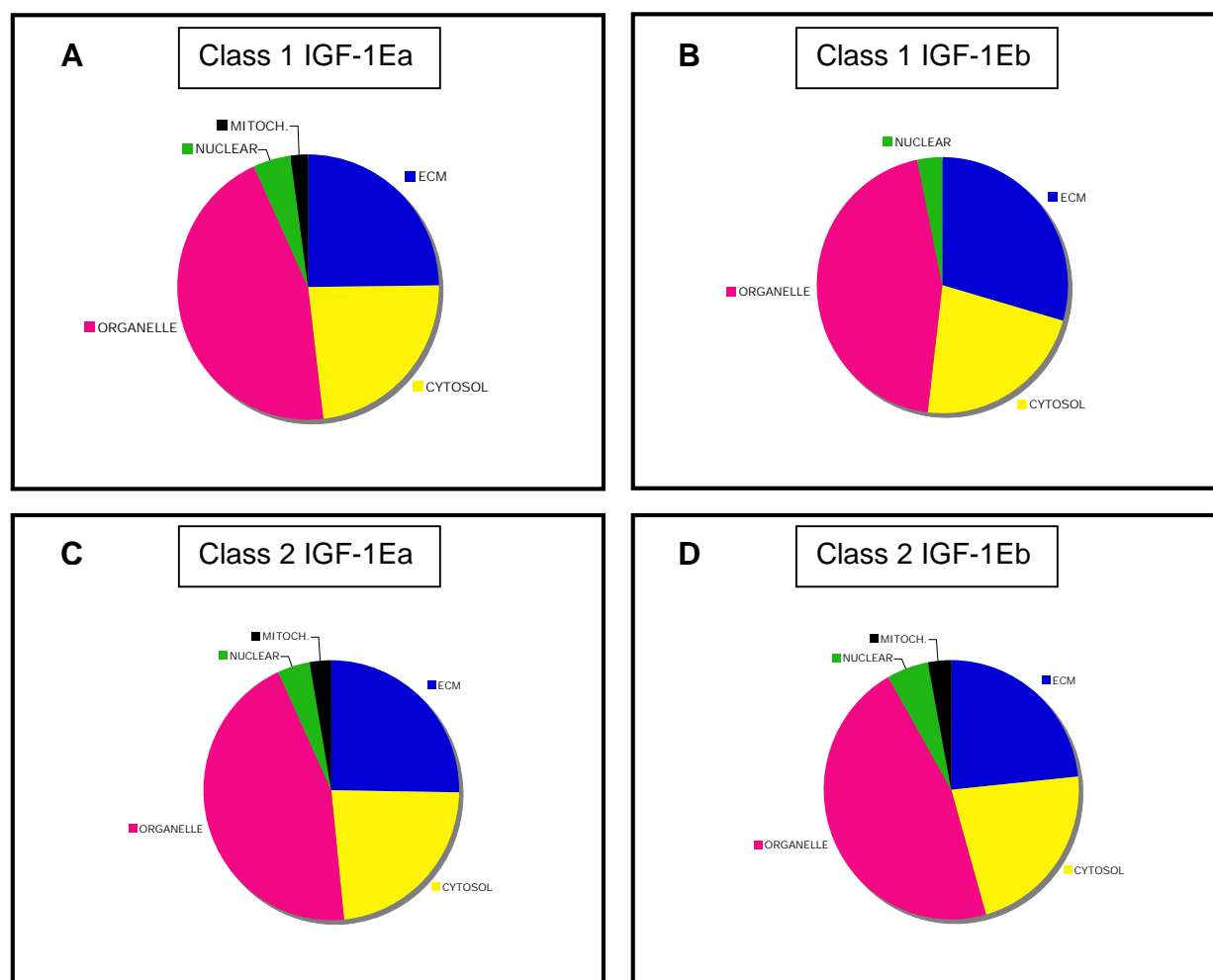


Figure 3.24 Distribution of regulated genes by cellular localization. The genes that were regulated (either up- or down-regulated) in each IGF1-isoform transgenic were pooled and classified by cellular localization according to their Gene Ontology annotations (available at www.Affymetrix.com). The values in each pie chart therefore represent the total number of regulated genes scored as belonging to each compartment. **A** MLC/Class 1 IGF-1Ea **B** MLC/Class 1 IGF-1Eb **C** MLC/Class 2 IGF-1Ea **D** MLC/Class 2 IGF-1Eb

To just name some examples, an interesting candidate identified as being unique to MLC/Class 1 IGF-1 Ea transgenic samples is forkhead box O3a (FOXO3A), which is a downstream target of Insulin/IGF1-Akt pathway and has been shown to impede muscle growth both in cardiac and skeletal muscle [62, 301]. Foxo3A can also stimulate expression of IGFBP1 in response to insulin signaling [302] and was found 2.8-fold down-regulated specifically in the MLC/Class 1 IGF-1 Ea transgenic samples. An interesting candidate gene found to be 2.74-fold up-regulated in MLC/Class 1 IGF-1Eb animals is the matrix metalloproteinase 7 (MMP7), which has been associated with processing of an important regulator of IGF1 function, i.e. IGFBP5 [303]. In MLC/Class 2 IGF-1Ea animals the Bcl2-like 2 mRNA, which was 2.05-fold down-regulated, represents an attractive candidate belonging to the family of Bcl-proteins that regulate cell death and that could play a key role in disease states [304, 305]. Although we could identify genes showing altered expression solely in the MLC/Class 2 IGF-1Eb, they did not appear as solid candidate of interest. However, a

stringent analysis of up- or down-regulated genes can offer the opportunity to explore molecular players previously unnoted to the current view of IGF1 isoform function. Therefore, consolidation of our analysis by thorough confirmation of identified targets should be a prerequisite for further speculation on the potential underlying mechanisms.

A general observation was that more genes were down-regulated in the different IGF-1 transgenic samples and that there was little overlap of differentially expressed genes among the different IGF-1 isoforms. In order to have a preliminary overview of potentially common mediators of IGF1-isoform-specific functions, we lowered the cut off of the filtered genes and analyzed the lists of only those genes that presented opposing trends of expression in Class 1 vs. Class 2, or in Ea vs. Eb isoforms. The list of such genes (see table B5 and B6) is less stringent, but highlights a group of genes that in both IGF1Ea isoform transgenic models show a trend opposed to the one of the IGF1Eb isoform transgenic models. These genes include putative candidates involved in regulating signal transduction, such as endothelin converting enzyme and proteins associated to Rho and G-protein activity, as well as proteins relevant for muscle function, such as a cardiac myosin isoform, integrin subunits and cGMP-dependent protein kinase. Due to the intrinsic significance of gene profiling analysis, and to the lower cut off value chosen for this analysis, these genes are potentially useful to elaborate a working hypothesis able to explain at least some of the phenotypes common to the IGF1Ea transgenic models; however, further validation of the candidates will be necessary before formulating such hypothesis.

The analysis described above, although only valid as initial assessment of the data, is useful to identify solid targets to confirm and possibly link to the different phenotypes. However, one could take an alternative approach. With increasing demand from researchers for tools that allow to analyze large sets of data (coming from gene expression analyses or other means of high throughput screenings), more sophisticated network analysis tools have been developed. These software platforms rely on an underlying knowledge database in which every node (gene of interest) is connected to any other node by either direct or indirect relationships (such as being a downstream/upstream regulator, a phosphorylating enzyme, a binding partner and so on). By screening the filtered array of probe sets through these network interaction repositories, it is possible to identify groups of genes that, although being differentially regulated outside of specific stringency criteria, nevertheless belong to a coherent biochemical/molecular pathway. By identifying and grouping genes with altered expression in this way, we can gain a consistent overview of the significance of those candidate genes. Of course, the more comprehensive the database of knowledge, the more

solid the analysis can be. Ingenuity Inc. (www.ingenuity.com) offers such a tool and we had the possibility to run these data via a trial account.

In order to validate our approach we selected a network related to IGF1R function, included additional elements (such as NF- κ B related genes) and compared the results by overlapping the expression ratios relative to each of the four transgenic models (Figure C1 in the appendix). The results were impressively promising. Targets such as the IGFBPs, which are important regulators of IGF1 function and which were not highlighted in our previous analysis because of their lower level of expression changes (below 1.9-fold up- or down-regulated), are now embedded in a coherent network and appear to be selectively and differentially deregulated in the four animal models. At the same time this view highlights other genes with different levels of regulation, which could be interesting targets for further studies, such as IGF-2, GH or the IGFBP-related gene Cyr61 (Figures C2-C5 in the appendix)

3.3.11c Kinetworks™ Phospho-site screen

The Kinetworks™ Phospho-site screen provides both qualitative and semi-quantitative analysis of the expression and phosphorylation states of protein kinases. For analysis of the IGF-1 isoform transgenic muscles, the Kinetworks™ Phospho-site screen KPSS 4.1 was chosen, because it provides a broad overview of the phosphorylation of a set of kinases known to be downstream of the IGF-1R (Table 4). This tool was used to gain a broad overview of the protein kinases that might be involved in the signal transduction pathways mediated by different IGF-1 isoform.

Whole quadriceps samples, isolated in duplicates from two transgenic mice per transgenic line were sent for analysis. The quadriceps muscles from one negative littermate for each line were pooled for comparison (total n=4). The complete processing of the samples was performed by the Kinetworks™ service (further information is available on the Kinexus webpage: www.kinexus.ca and more specifically on <http://www.kinexus.ca/KPSS.htm>).

Results obtained by this high throughput screen are shown in Figure 3.25 A-F. The first pathway of interest was the PI(3)-kinase/Akt pathway (Figure 3.25 A), where GSK-3 α and -3 β , mTOR, PDK1, and Akt1 were analyzed for their phosphorylation state. In addition, members of the S6-kinase family, p85^{S6K}, p70^{S6K} and ribosomal S6 protein-serine kinase (RSK1/2/3) were part of the screen (Figure 3.25 B). Notably, most of the values were not significantly changed, thus only tendencies can be described for this pathway. In the presence of both Class 1 isoforms protein phosphorylation was consistently down-regulated or did not change (MLC/Class 1 IGF-1Ea: GSK-3 α : -8%, GSK-3 β : -29%, PDK1: -28%, Akt1: -

26%; MLC/Class 1 IGF-1Eb: GSK-3 α : -6%, GSK-3 β : 2%, PDK1: -35%, Akt1: -19%). Class 2 isoforms in contrast up-regulated the phosphorylation of these protein-kinases (ML/Class 2 IGF-1Ea: GSK-3 α : 32%, GSK-3 β : -35%, PDK1: 4%, Akt1: 12%; MLC/Class 2 IGF-1Eb: GSK-3 α : 30%, GSK-3 β : 55%, PDK1: 18%, Akt1: 50%). The only exception was mTOR phosphorylation, which was up-regulated by both Ea-containing isoforms (MLC/Class 1 IGF-1Ea: 32% and MLC/Class 2 IGF-1Ea: 18%), while unchanged in samples over-expressing the two Eb-containing isoforms (MLC/Class 1 IGF-1Eb: 2% and MLC/Class 2 IGF-1Eb: 2%). These results point towards a preferential activation of the PI(3)-kinase/Akt pathway by isoforms containing a Class 2 signal peptide, while Class 1 isoforms do not seem to activate those molecules.

Interestingly this trend does not apply to the S6-kinases, which are also downstream of the PI(3)-kinase (Figure 3.25 B). p85^{S6K} (S6K2) phosphorylation of residues T444 and S447 was significantly down-regulated by MLC/Class 1 IGF-1Ea (-64%, p=0.01), MLC/Class 2 IGF-1Ea (-58%, p=0.01), and MLC/Class 1 IGF-1Eb (-71%, p=0.003), while the 17% decrease in MLC/Class 2 IGF-1Eb samples was not significant. Phosphorylation of residue T412 of S6K2 instead was unchanged in presence of MLC/Class 2 IGF-1Ea (-1%) and increased by the other three IGF-1 isoforms (MLC/Class 1 IGF-1Ea: 30%, MLC/Class 1 IGF-1Eb: 121%, MLC/Class 2 IGF-1Eb: 218%). Even though these results were not significant, our findings suggest a preferential phosphorylation of residue T412 in these latter three transgenic lines. Analysis of p70^{S6K} (S6K1) phosphorylation showed a strong induction in presence of IGF-1 isoforms MLC/Class 1 IGF-1Ea (299%), MLC/Class 2 IGF-1Ea (635%), and MLC/Class 2 IGF-1Eb (606%), while p70^{S6K} was not present in WT and MLC/Class 1 IGF-1Eb samples. The induction seen in the first three transgenic lines again did not reach significance, but allows speculations about a preferential activation of p70^{S6K} over p85^{S6K}.



KINEXUS

Appendix F

KINETWORKS™ PHOSPHO-SITE SCREEN 4.1

Catalog Number KPSS – 4.1

KPSS-4.1 tracks the following forty (40) phosphorylation sites in phosphoproteins with antibodies that recognize phosphorylated epitopes:

No.	Abbreviation	Full Name of Protein	Epitope(s)
1.	4E-BP1	eIF4E binding protein 1	S65
2.	AMPK α	AMP-activated protein kinase alpha	T172
3.	B23	B23 (nucleophosmin)	S4
4.	Bmx (Etk)	Eph-like tyrosine kinase	Y40
5.	BTK	Bruton's tyrosine kinase	Y223
6.	CaMK2	Calcium/calmodulin-dependent kinase 2	T286
7.	CDK1	Cyclin-dependent kinase 1	T161
8.	CDK1	Cyclin-dependent kinase 1	Y15
9.	ERK1	Extracellular signal-regulated kinase 1	T202/Y204
10.	ERK2	Extracellular signal-regulated kinase 2	T185/Y187
11.	GSK3 α	Glycogen synthase kinase-3 alpha	S21
12.	GSK3 β	Glycogen synthase kinase-3 beta	S9
13.	IKK α	Inhibitor-kappa-B kinase alpha	S180
14.	IKK β	Inhibitor-kappa-B kinase beta	S181
15.	LYN	Lyn	Y507
16.	MAPKAPK-2	MAP kinase activated protein kinase 2	T334
17.	MEK 1/2	MAP kinase kinase 1/2	S217/S221
18.	MKK 3/6	MAP kinase kinase 3/6	S189/207
19.	MNK1	MAP kinase interacting kinase 1	T197/T202
20.	mTOR	The mammalian target of rapamycin (FRAP)	S2448
21.	p38 MAPK	p38 alpha MAP kinase	T180/Y182
22.	p70S6K	p70 S6 kinase	T389
23.	p70S6K	p70 S6 kinase	T421/T424
24.	p90 RSK	90 kDa ribosomal S6 kinase	S381
25.	p90 RSK	90 kDa ribosomal S6 kinase	T573
26.	PKD1	Phosphoinositide-dependent protein kinase 1	S241
27.	PKB α (Akt1)	Protein kinase B alpha	T308
28.	PKC α / β	Protein kinase C alpha/beta	T638
29.	PKC δ	Protein kinase C delta	T505
30.	PKC θ	Protein kinase C theta	T538
31.	PKC ζ / λ	Protein kinase C zeta/lambda	T410/T403
32.	PKC μ	Protein kinase mu (Protein kinase D)	S916
33.	PP1 α	Type 1 protein phosphatase alpha	T320
34.	PRK1	PKC-related kinase 1	T778
35.	PRK2	PKC-related kinase 2	T816
36.	RAF	RAF proto-oncogene serine/threonine protein kinase	S259
37.	RB	Retinoblastoma protein	S780
38.	RB	Retinoblastoma protein	S807/S811
39.	SYK	Spleen tyrosine kinase	Y352
40.	ZAP 70	Zeta-chain (TCR) associated protein kinase	Y319

Y = tyrosine S = serine T = threonine

4SE28– Customer Information Package

14

Kinexus Bioinformatics Corporation

Table 4 List of kinases screened by the Kinetworks™ Phospho-site screen

Finally, phosphorylation of RSK1/2/3 revealed a significant increase for both Ea-containing isoforms (MLC/Class 1 IGF-1Ea: 91%, $p=0.02$ and MLC/Class 2 IGF-1Ea: 60%, $p=0.02$), while the induction by both Eb-containing isoforms was not significant (MLC/Class 1 IGF-1Eb: 42% and MLC/Class 2 IGF-1Eb: 21%). The significant results obtained for both Ea-containing isoforms do raise the possibility that these IGF-1 variants might transmit part of their hypertrophic signal via RSK1/2/3.

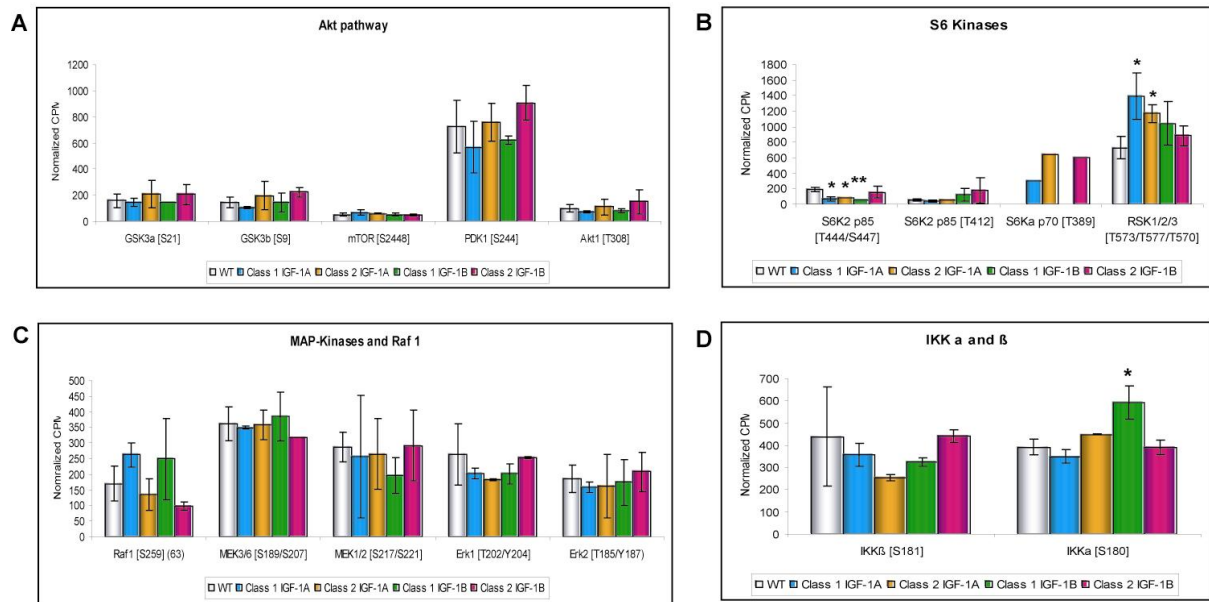


Figure 3.25 Kinetworks™ Phospho-site screen. The entire processing of samples was performed by the Kinetworks™ service: Transgenic quadriceps samples from two one-month-old animals per genotype have been sent for analysis together with one negative littermate from each line (total n=4). **A** Results for members of the Akt pathway. No significant changes were observed. **B** Screening results for members of the S6-kinase family. Significant changes were only seen for specific residues of S6K p85. **C** Members of the MAP-kinase pathway were not significantly influenced by IGF-1 isoform over-expression. **D** Phosphorylation level of IKK α and β . MLC/Class 1 IGF-1Eb significantly increased IKK α -phosphorylation (p=0.01).

The other major pathway downstream of the IGF-1R is the MAP-kinase pathway. Raf-1, as the most upstream kinase, MAPK-Erk protein-serine kinase (MEK) 3/6 and MEK1/2, Erk1, and Erk2 were analyzed for their phosphorylation state by the Kinetworks™ Phospho-site screen (Figure 3.25 C). None of the results obtained for this part of the screen were significant and most of the results displayed enormous variations and therefore did not show major phosphorylation-mediated changes. However, phosphorylation of Raf1 was increased only in response to Class 1 IGF-1 isoforms (MLC/Class 1 IGF-1Ea: 55% and MLC/Class 1 IGF-1Eb: 48%), while both Class 2 IGF-1Ea isoforms showed a decrease (MLC/Class 2 IGF-1Ea: -19% and MLC/Class 2 IGF-1Eb: -42%). MEK3/6 displayed minor differences (MLC/Class 1 IGF-1Ea: -3%; MLC/Class 2 IGF-1Ea: -1%; MLC/Class 1 IGF-1Eb: 6%; MLC/Class 2 IGF-1Eb: -12%), MEK1/2 levels were highly variable and no pattern of Class or E-peptide-specificity could be noted (MLC/Class 1 IGF-1Ea: -9%; MLC/Class 2 IGF-1Ea: -8%; MLC/Class 1 IGF-1Eb: -31%; MLC/Class 2 IGF-1Eb: 55%). Erk1 phosphorylation was down-regulated in all different IGF-1 isoform transgenic samples (MLC/Class 1 IGF-1Ea: -23%; MLC/Class 2 IGF-1Ea: -31%; MLC/Class 1 IGF-1Eb: -23%; MLC/Class 2 IGF-1Eb: -3%), while Erk2 activation was decreased in MLC/Class 1 IGF-1Ea (-23%), MLC/Class 2 IGF-1Ea (-12%), and MLC/Class 1 IGF-1Eb (-5%) transgenic lines, but was slightly up-regulated in MLC/Class 2 IGF-1Eb (12%). Although the lack of significance in these changes

precludes any definitive involvement of this pathway, the data exclude a pronounced up-regulation of Erk1 and Erk 2 in response to any of the IGF-1 isoforms.

Other kinases screened by using the KinetworksTM approach, that were not part of the major pathways described for IGF-1 are not described within this work, since they were not significantly changed. The only remaining significant result to be described here was obtained for phosphorylation of Ikk α . Levels were moderately changed by MLC/Class 1 IGF-1Ea (-11%), MLC/Class 2 IGF-1Ea (14%), and MLC/Class 2 IGF-1Eb (-0.5%), while MLC/Class 1 IGF-1Eb significantly up-regulated Ikk α -phosphorylation by 51% (Figure 3.25 D). IKK β phosphorylation was not significantly affected by any of the IGF-1 isoform transgenes, but was slightly decreased (MLC/Class 1 IGF-1Ea: -18%, MLC/Class 2 IGF-1Ea: -42%) or unchanged (MLC/Class 2 IGF-1Eb: 0.6%).

In summary, results described above point towards Class 2 IGF-1 isoforms signaling through the classical PI(3)-kinase pathway, since they showed an increase in Akt1, PDK-1, and GSK-3 α and -3 β phosphorylation, while Class 1 IGF-1 isoforms did not. The analysis of the S6-kinases as further downstream targets of this pathway, revealed an induction of p70^{S6K} – phosphorylation in MLC/Class 1 IGF-1Ea, MLC/Class 2 IGF-1Ea, and MLC/Class2 IGF-1Eb samples, while p70^{S6K} was absent in MLC/Class 1 IGF-1Eb samples. RSK1/2/3 S6-kinases-phosphorylation was increased in response to all IGF-1 isoforms, but only Ea-peptide containing isoforms (MLC/Class 1 IGF-1Ea and MLC/Class 2 IGF-1Ea) values reached significance. The MAP-kinase pathway was not regulated to a significant extent, but showed increased levels of Raf1-phosphorylation for both Class 1 IGF-1 isoform transgenic lines (MLC/Class 1 IGF-1Ea and MLC/Class 1 IGF-1Eb). Unexpectedly, phosphorylation of Ikk α was significantly increased in MLC/Class 1 IGF-1Eb samples, an effect that was not previously described as being regulated by IGF-1 in resting skeletal muscle previously.

Taken together, a high variation was observed, which makes interpretation of these results difficult. It should be noted that due to the high cost of different lines to be screened, only duplicates could be sent for each transgenic line, which makes the significance of these findings statistically questionable. Especially when interpreting results for MLC/Class 1 IGF-1Ea and comparing them to a previously performed KinetworksTM analysis on MLC/mIGF-1 animals [261], the different nature of the transgenic line has to be taken in account for the experiments described in this chapter.

3.3.11d The calcineurin pathway

In the last few years the calcineurin (Cn) pathway has been controversially implicated in the mediation of the hypertrophic response in skeletal muscle (compare section 1.4.5.5). Especially because previous work on the mIGF-1 (= rat Class 1 IGF-1Ea) transgene implicated Cn in mediating skeletal muscle hypertrophy [77, 282], the role of Cn isoforms in the different IGF-1 isoform transgenic mice was investigated.

To discover changes in expression of the three calcineurin A-subunit isoforms A α , A β 1, and A β 2, quantitative RT-PCR was performed on quadriceps RNA (n=3) of male WT and each IGF-1 isoform transgenic line. Analyzed was performed with primers specific for CnA α , CnA β 1, and CnA β 2 (section 2.1.14). Results shown in Figure 3.26 A-C demonstrated that none of these isoforms was changed significantly in any of the IGF-1 isoform transgenic mice. On the contrary, a tendency towards a down-regulation of CnA α (Figure 3.26 A) and CnA β 2 (Figure 3.26 C) was noticed, while the expression of CnA β 1 was slightly up-regulated in the presence of both Class 1 IGF-1 isoforms (MLC/mIGF-1: 16% and MLC/Class 1 IGF-1Eb: 6%). MLC/Class 2 IGF-1Ea showed a 32% decrease of CnA β 1 mRNA and MLC/Class 2 IGF-1Eb showed a 162% increase. This strong increase was accompanied by a very high standard deviation (51 ± 44 molecules/ng), which has to be taken in account for final conclusions (Figure 3.26 B).

To further confirm these results, the expression of the Cn downstream target Gata-2 was assessed by Northern blot analysis. Gata-2 has been shown to be up-regulated in response to IGF-1 in the MLC/mIGF-1 mice [77] and to be involved in mediation of cardiac hypertrophy [275]. Northern blot analysis was performed on RNA of the quadriceps muscle from six-months-old male WT and transgenic mice from every IGF-1 isoform transgenic line. No differences were detected in Gata-2 mRNA expression levels between two WT and the transgenic samples (Figure 3.26 D and E), further suggesting that other pathways are involved in IGF-1-mediated hypertrophy.

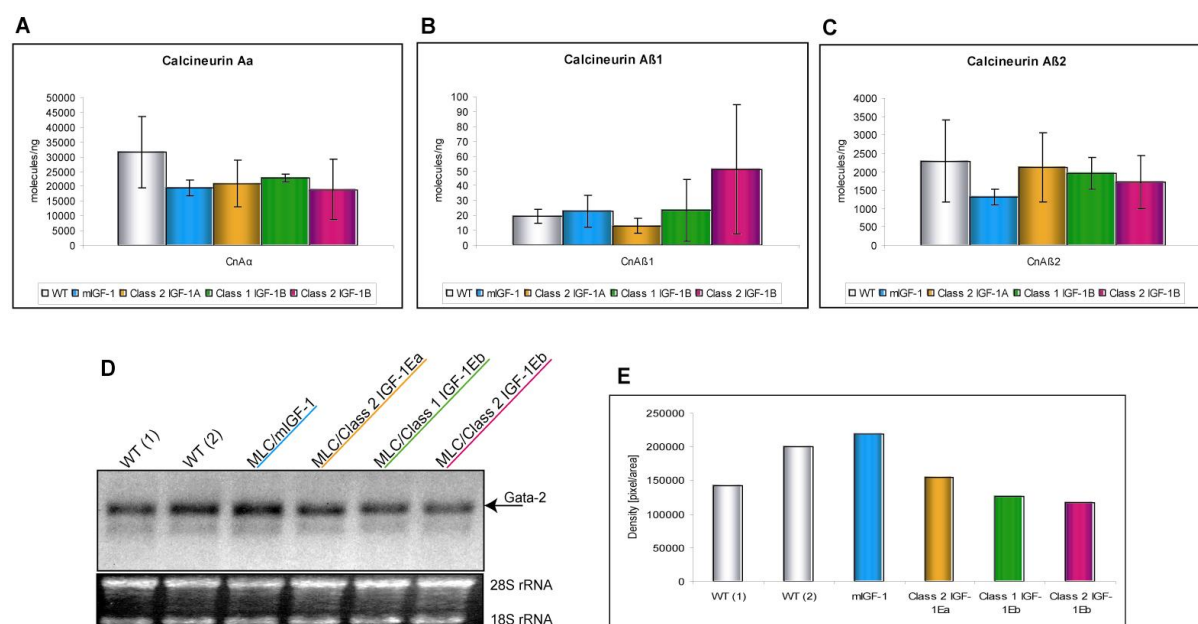


Figure 3.26 The calcineurin pathway in IGF-1 isoform transgenic skeletal muscle. A-C RNA from three-months-old male quadriceps muscle of transgenic mice from every line and from age-matched WT animals of the same sex (n=3 for all) was used for quantitative RT-PCR to determine changes of CnA isoforms in response to IGF-1 isoform over-expression. None of the IGF-1 isoform transgenic lines induced changes in CnAα (A), CnAβ1 (B) or CnAβ2 (C) expression. D Northern blot analysis of GATA-2 expression in six-months-old WT (n=2) and transgenic mice (n=1). 10µg of total RNA were isolated from the quadriceps muscle and GATA-2 was detected with a specific probe. E Density of bands detected by Northern blot. No major differences could be detected for any of the transgenic IGF-1 isoform lines.

3.4 Regeneration of IGF-1 isoform transgenic muscle

Skeletal muscle is one of the tissues in the body that has the intrinsic capacity to regenerate and adapt to environmental changes. With the onset of age and/or disease, this capacity decreases or is even lost, leading to atrophy and paralysis of skeletal muscle (described in detail in section 1.2.1 and 1.2.2). Based on recent findings showing that mIGF-1 had beneficial effects on many disease states associated with skeletal muscle (compare section 1.2), the obvious question of how other IGF-1 isoforms would affect regeneration of skeletal muscle arose and was addressed in this chapter. Since such investigations represent only a portion of the work for this thesis, the results presented in the following chapter have to be considered preliminary. Thus, we aimed to provide preliminary evidence of IGF-1 isoform regenerative capacities. The MLC/mIGF-1 transgenic animals have not been included in the histological analysis of cardiotoxin (CTX)-injured muscle, since the regenerative capacities of this line are well described (see above). However, for comparative reasons, MLC/mIGF-1 samples were analyzed on the molecular level with the other lines.

Skeletal muscle injury was achieved by CTX injections into the TA and quadriceps muscle of male three-months-old WT and transgenic animals (n=4 for each genotype and time point). CTX is a snake venom, which leads to depolarization of muscle fibers resulting in necrosis of

those cells. Skeletal muscle samples were taken two, five, and ten days after injections. The TA muscle was used for histological analysis, while quadriceps samples were kept for RNA and protein analysis. Only injuries of similar size were chosen for comparative analysis.

3.4.1 Histological analysis of regeneration in IGF-1 isoform transgenic mice

To evaluate changes in the regenerative capacity of the different IGF-1 isoform transgenic lines after CTX-induced injury, the TA muscle sections of WT and transgenic mice were stained by trichrome staining, which allows the visualization of skeletal muscle fibers, nuclei, as well as fibrotic tissue, by staining collagen. Representative pictures are shown in Figure 3.27. After two days of CTX injection muscle fibers underwent massive necrosis, indicated by the comparable damaged structures and the invasion of mononuclear cells at the site of injury that marks the initiation of the inflammation process. The comparison of the muscle phenotype between the different IGF-1 isoform transgenic lines and the WT did not show any differences at two days after injury.

After five days of CTX injury, the WT muscle showed a strong inflammatory response, reflected in the dense population of intracellular spaces by mononuclear cells (Figure 3.27 middle panel). At this stage of regeneration, new muscle fibers start forming and can be identified by centrally localized nuclei. The WT muscle displayed a considerable amount of regenerating fibers that were still quite small and closely surrounded by mononuclear cells. In contrast, TA muscles of MLC/Class 2 IGF-1Ea transgenic animals showed newly forming fibers of much bigger size and less mononuclear cells, determined by more intracellular space. In addition, many newly formed fibers contained up to three nuclei already, while the majority of WT fibers only contained one central nucleus. This indicates that the regeneration process in MLC/Class 2 IGF-1Ea proceeded faster. Overall, the morphology of the regenerating muscle appeared to be improved by the presence of this IGF-1 isoform transgene. Similarly, MLC/Class 1 IGF-1Eb muscle sections displayed a more ordered morphology with more free intracellular space. In comparison to the WT and also to MLC/Class 2 IGF-1Ea samples, muscles of MLC/Class 1 IGF-1Eb animals had more smaller new fibers, rather than bigger new fibers as seen in MLC/Class 2 IGF-1Ea animals. The regenerating fibers did not have more than two nuclei and were only slightly increased in size when compared to WT controls. MLC/Class 2 IGF-1Eb samples instead had a similar or even slightly stronger inflammatory response when compared to the WT, but nevertheless displayed a visible increase in the amount of fibers present in the injured area. The size of the new myofibers showed a mild increase but did not reach the size of MLC/Class 2 IGF-1Ea fibers and the majority of those fibers contained only one central nucleus.

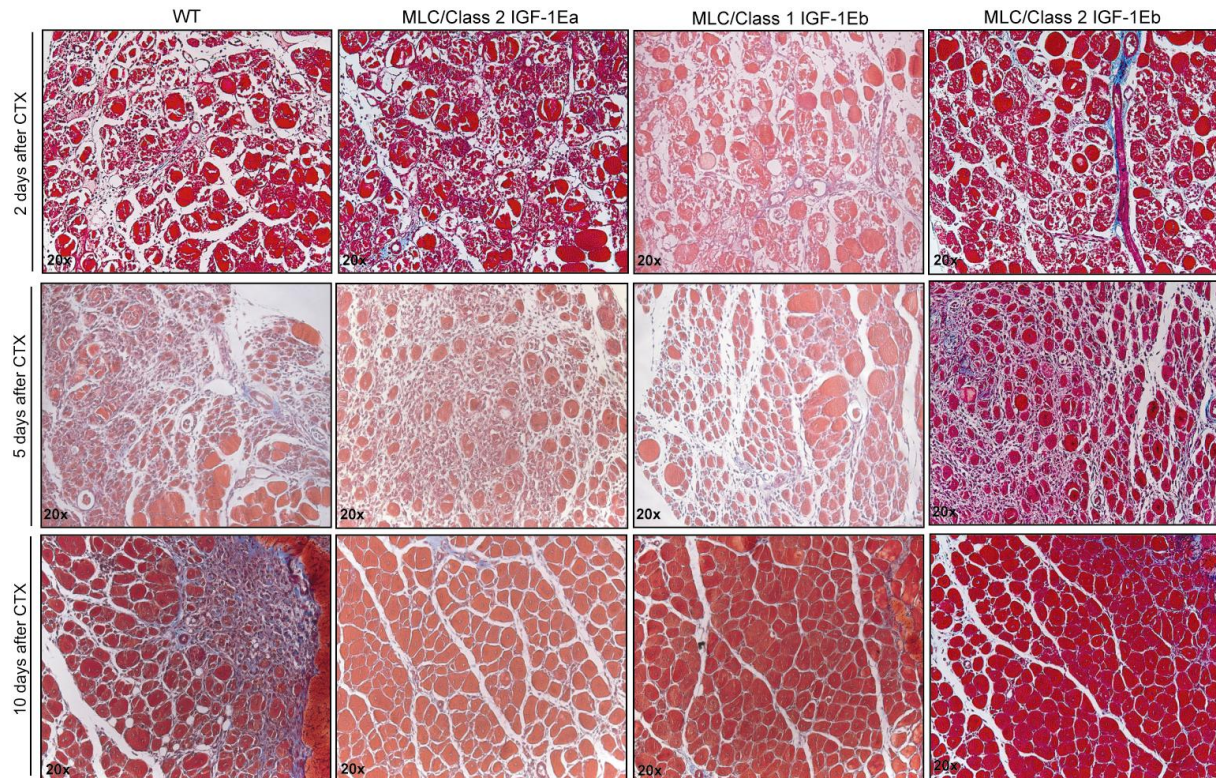


Figure 3.27 Histological analysis of CTX-injected skeletal muscle. Three-month-old male WT and transgenic mice ($n=4$ for each genotype and time point) were subjected to CTX injury. Samples were taken at two, five, and ten days after injury. 8 μ m transverse sections of the TA muscle were cut and stained with trichrome staining. The mid region of the injury was identified for each injury and pictures were taken at a 20x magnification (corresponds to 200x, considering a 10x magnification of the camera). Representative pictures of samples for two days after injection are shown in the upper panel, five day samples are represented in the middle panel, and the lower panel shows the muscle morphology ten days after CTX injection.

Finally, all muscles were analyzed ten days after CTX injection to evaluate the capacity of the different IGF-1 isoforms to restore the muscle phenotype (Figure 3.27 lower panel). In the WT samples, many fibers had reached almost normal size, but other regions of the regenerated area displayed large islands of inflammatory cells, many small fibers, and accumulation of fibrotic tissue. In comparison to the WT regenerated muscle, the three IGF-1 isoform transgenic lines uniformly displayed a more normal morphology: fibers reached normal size without leaving much space between the fibers. Only a very small amount of mononuclear cells was observed and there was no accumulation of these cells as seen in the WT samples.

Taken together, this preliminary analysis of tissue morphology after CTX injury revealed an improved regeneration process in every transgenic line analyzed. MLC/Class 2 IGF-1Ea displayed larger fibers containing between one and three nuclei at day five after injury, MLC/Class 1 IGF-1Eb and MLC/Class 2 IGF-1Eb showed more fibers when compared to WT and also to MLC/Class 2 IGF-1Ea. After ten days of regeneration, all transgenic lines displayed similar improvements in muscle morphology that appeared to be closer to the

normal muscle morphology when compared to the WT, indicating that the presence of the different IGF-1 isoforms each resulted in enhanced regeneration.

3.4.2 Changes in endogenous IGF-1 isoform expression in response to injury

IGF-1 isoforms have been implicated in the regenerative response to exercise- and stretch-induced injury previously [209-211] and have therefore been included in the present regeneration study for several reasons. First, this allowed the comprehensive analysis of WT IGF-1 isoform expression in response to muscle injury, which previously has been focused on Class 1 IGF-1Ea and Class 1 IGF-1Eb expression analysis. Second, endogenous IGF-1 levels of IGF-1 isoform transgenic lines were monitored and compared to the WT expression of the same isoform and time point after injury to evaluate if over-expression of certain IGF-1 isoforms had a feedback effect on the endogenous IGF-1 isoform expression pattern after CTX injury.

This analysis was performed by quantitative RT-PCR on RNA samples isolated from the quadriceps muscle of injured WT and transgenic animals (n=3 for all genotypes and time points). Three uninjured controls were included for every genotype. Analysis of endogenous Class 1 IGF-1Ea in the WT background revealed a non-significant increase of 111% at day two after injury, and a significant and pronounced increase of this isoform at day five and day ten after injection (209% at day five ($p=0.003$) and 664% at day ten ($p=0.001$) when compared to uninjured controls (Figure 3.28 A). Class 2 IGF-1Ea molecules displayed a similar but less pronounced pattern of increased expression, culminating in a significant induction after ten days of regeneration (604%, $p=0.005$). Notably, expression of this isoform was generally lower than Class 1 IGF-1Ea expression (Figure 3.28 B).

Class 1 IGF-1Eb and Class 2 IGF-1Eb isoforms instead showed very high variability with generally low expression profiles and were therefore not significantly changed throughout the process of regeneration. The only exception was a transient and significant up-regulation of Class 2 IGF-1Eb molecules at day five after injury (111%, $p=0.02$) (Figure 3.28 C and D). Despite the high variability, a mild induction of the two Eb-containing isoforms that was comparable throughout the different time points was observed.

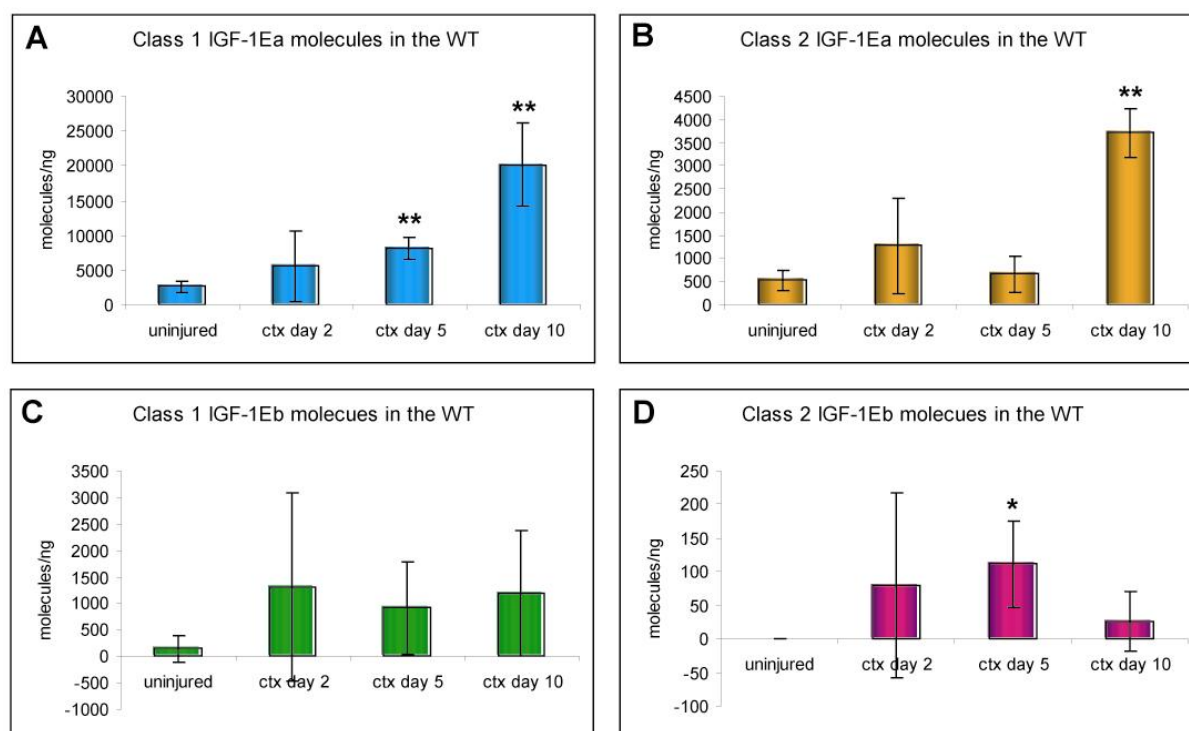


Figure 3.28 Expression of endogenous IGF-1 isoforms in WT CTX-injected muscle. Three-months-old male quadriceps RNA from WT and transgenic mice (n=3 for all) was used for quantitative RT-PCR analysis of CTX-injury induced changes in endogenous IGF-1 isoform expression. **A** Class 1 IGF-1Ea RNA was significantly induced at day five ($p=0.003$) and day ten ($p=0.001$) after CTX-injection. **B** Class 2 IGF-1Ea RNA showed a similar trend as seen for Class 1 IGF-1Ea RNA, but was only significantly increased after ten days of regeneration ($p=0.005$). **C** Class 1 IGF-1Eb did not show significant changes in response to injury, but a tendentious increase was noted. **D** Class 2 IGF-1Eb was transiently and significantly induced at day five after injury ($p=0.02$).

In summary, the analysis of the WT expression pattern of IGF-1 isoforms upon injury revealed a pronounced up-regulation of both Ea-peptide-containing isoforms throughout the process of regeneration, reaching highest induction levels at day ten after injury. The two Eb-containing isoforms instead, showed mild induction upon injury without being significant. The only exception was a transient up-regulation of Class 2 IGF-1Eb at day five after injury.

The WT expression pattern of IGF-1 isoforms was then compared to the expression pattern of endogenous isoforms in the different IGF-1 isoform transgenic animals. The line over-expressing the analyzed isoform of interest was not included in the analysis, as endogenous isoform levels were masked by the over-expression of the transgene. Results for endogenous Class 1 IGF-1Ea expression revealed no significant changes for line MLC/Class 2 IGF-1Ea throughout the regeneration process (Figure 3.29 A). Analysis of line MLC/Class 1 IGF-1Ea showed a significant ($p=0.03$) up-regulation of this isoform in uninjured MLC/Class 1 IGF-1Eb animals, an effect that was described in section 3.3.5. At day two after injury, when many myofibers are destroyed this up-regulation is decreased, but an elevation of Class 1 IGF-1Ea mRNA was still visible (123%), but not significant anymore. Five days after injection, MLC/Class 1 IGF-1Eb samples were again significantly increased by 154% ($p=0.001$), while at day ten the 9% increase of Class 1 IGF-1Ea mRNA was no longer significant (Figure 3.29

A), due to up-regulation of this isoform in the WT upon injury. Since values were compared to the WT expression of the same day, where Class 1 IGF-1Ea transcripts are increased by 664%, this increase is not significant.

MLC/Class 2 IGF-1Eb samples showed no significant changes at day two and ten after injury, but significantly up-regulated Class 1 IGF-1Ea mRNA at day five when compared to the WT sample of the same time point (77%, $p=0.04$) (Figure 3.29 A).

Taken together, endogenous Class 1 IGF-1Ea expression patterns observed in the WT were not influenced by over-expression of Class 2 IGF-1Ea, but showed a significant increase at day five after injury for Lines MLC/Class 1 IGF-1Eb and MLC/Class 2 IGF-1Eb.

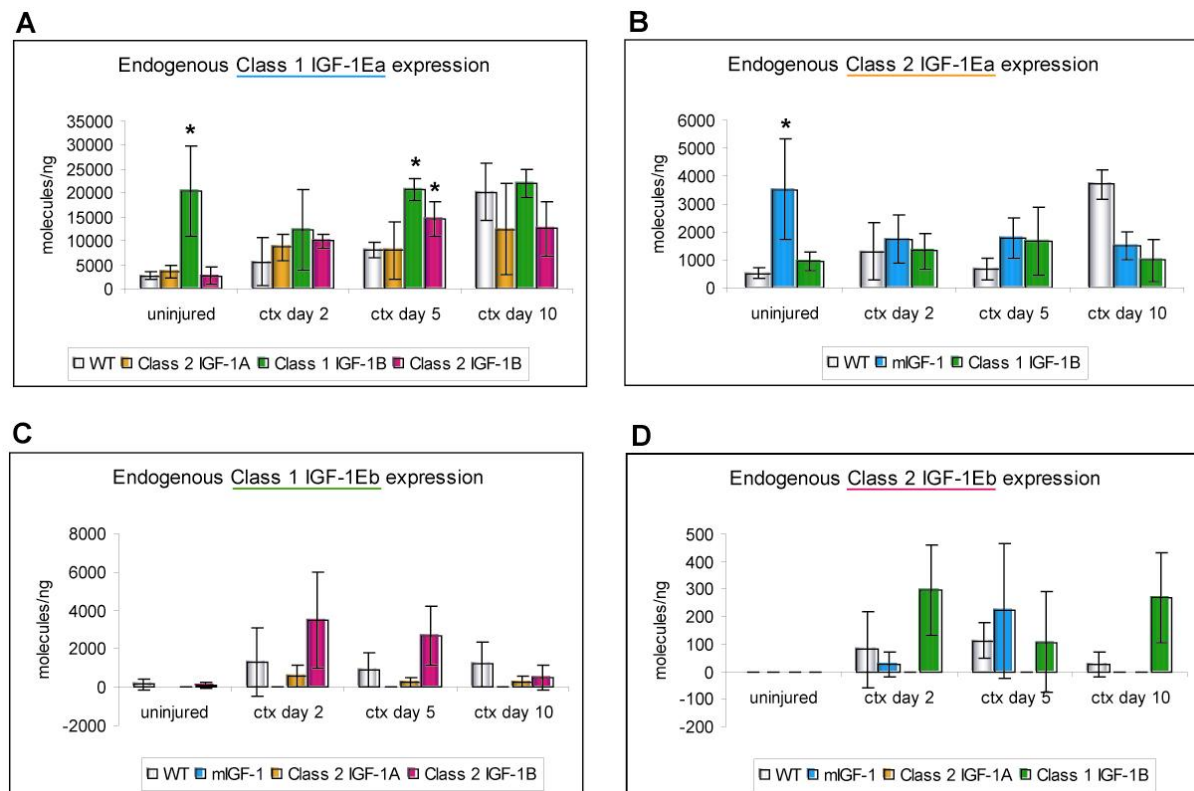


Figure 3.29 Influence of IGF-1 isoform transgenes on endogenous isoform expression after CTX-injury. Three-months-old male quadriceps RNA from WT and transgenic mice ($n=3$ for all) was used for quantitative RT-PCR analysis of injury-induced changes in endogenous IGF-1 isoform expression in the background of IGF-1 isoform over-expression. All values were compared to WT values of the same time point to evaluate if IGF-1 isoform over-expression influenced the normal WT expression pattern of IGF-1 isoforms after injury. **A** Analysis of endogenous Class 1 IGF-1Ea molecules revealed significant changes at day five after injury for Lines MLC/Class 1 IGF-1Eb ($p=0.001$) and MLC/Class 2 IGF-1Eb ($p=0.04$). **B** Endogenous Class 2 IGF-1Ea expression was not influenced in MLC/mIGF-1 and MLC/Class 1 IGF-1Eb animals after injury. **C** Endogenous levels of Class 1 IGF-1Ea were not significantly changed. **D** Endogenous Class 2 IGF-1Eb mRNA was also not altered in the background of any of the transgenes.

The expression analysis of endogenous Class 2 IGF-1Ea revealed a significant increase in MLC/mIGF-1 animals, an effect that was described in section 3.3.5. During the time-course

of regeneration neither line MLC/mlIGF-1 nor line MLC/Class 1 IGF-1Eb had a significant influence of the endogenous expression pattern of Class 2 IGF-1Ea (Figure 3.29 B). However, an increase was noticed at day five post-injury (169% in MLC/mlIGF-1 animals and 152% in MLC/Class 1 IGF-1Eb animals) and a decrease was observed for both transgenic lines at day ten, where MLC/mlIGF-1 decreased Class 2 IGF-1Ea mRNA levels by 59% and MLC/Class 1 IGF-1Eb by 73%. MLC/Class 2 IGF-1Eb values displayed a standard deviation that was too high and therefore was not considered here.

In summary, no significant alterations of endogenous Class 2 IGF-1Ea expression was observed in response to the MLC/mlIGF-1 and MLC/Class 1 IGF-1Eb transgenes.

The evaluation of endogenous expression of Class 1 IGF-1Eb and Class 2 IGF-1Eb (Figure 3.29 C and D) showed no significant changes in response to the Class 1 IGF-1Ea transgene (mlIGF-1) and the Class 2 IGF-1Ea transgene. In the background of MLC/Class 2 IGF-1Eb a non-significant increase of Class 1 IGF-1Eb RNA was observed throughout the regeneration process (Figure 3.29 C), while in the background of MLC/Class 1 IGF-1Eb endogenous Class 2 IGF-1Eb was elevated upon injury (Figure 3.29 D), but again not reaching significance.

3.4.3 Expression of calcineurin isoforms in response to injury

Recently the catalytic subunit CnA β 1 isoform of CnA β , which lacks the auto-inhibitory domain (compare section 1.4.5.5), has been implicated in regeneration of skeletal muscle (Enrique Lara-Pezzi, manuscript submitted). This isoform was shown to be up-regulated in response to injury and over-expression of this isoform in skeletal muscle of transgenic mice led to enhanced regeneration and reduced fibrosis in response to CTX-injury (Enrique Lara-Pezzi, manuscript submitted). This same isoform of CnA β has also been shown to be induced in the regenerating muscle tissues of a mouse model of ALS, when crossed to the MLC/mlIGF-1 transgenic line, indicating a role for CnA β 1 in regeneration [78]. To determine if the different IGF-1 isoforms had an influence on CnA isoform expression upon injury, CnA α , CnA β 1 and β 2 isoforms were analyzed at all time points after injury.

This analysis was performed by quantitative RT-PCR on RNA samples isolated from the quadriceps muscle of injured WT and transgenic animals (n=3) for all genotypes and time points). Three uninjured controls were included for every genotype.

In the WT background, CnA α expression was not significantly changed upon injury (Figure 3.30 A) and no changes to the WT expression were significant in the background of the different IGF-1 isoform transgenes. Analysis of CnA β 1 RT-PCRs confirmed the previously

established up-regulation of CnA β 1 upon injury in the WT background (54% at day two, 93% at day five, and 116% at day 10 after CTX-injection) compared to the uninjured control animals, even though these values were not significant due to high standard variations (Figure 3.30 B). Interestingly, this trend was not observed for the IGF-1 isoform transgenic lines MLC/mlIGF-1, MLC/Class 2 IGF-1Ea and MLC/Class 1 IGF-1Eb, where CnA β 1 levels actually decreased in comparison to WT levels of the same time point, without reaching significance. The only exception was line MLC/Class 2 IGF-1Eb, which up-regulated CnA β 1 mRNA at all time points after CTX injury when compare to WT levels of the same time points (240% at day two, 230% at day five, and 120% at day 10 after injury). Only the 240% increase at day two reached significance ($p=0.02$), since the standard error was very high for five day and 10 day samples of this IGF-1 transgenic line (day five WT: 38 ± 20 molecules/ng, transgene: 124 ± 67 molecules/ng; day 10 WT molecules/ng: 42 ± 26 molecules/ng, transgene: 93 ± 84 molecules/ng).

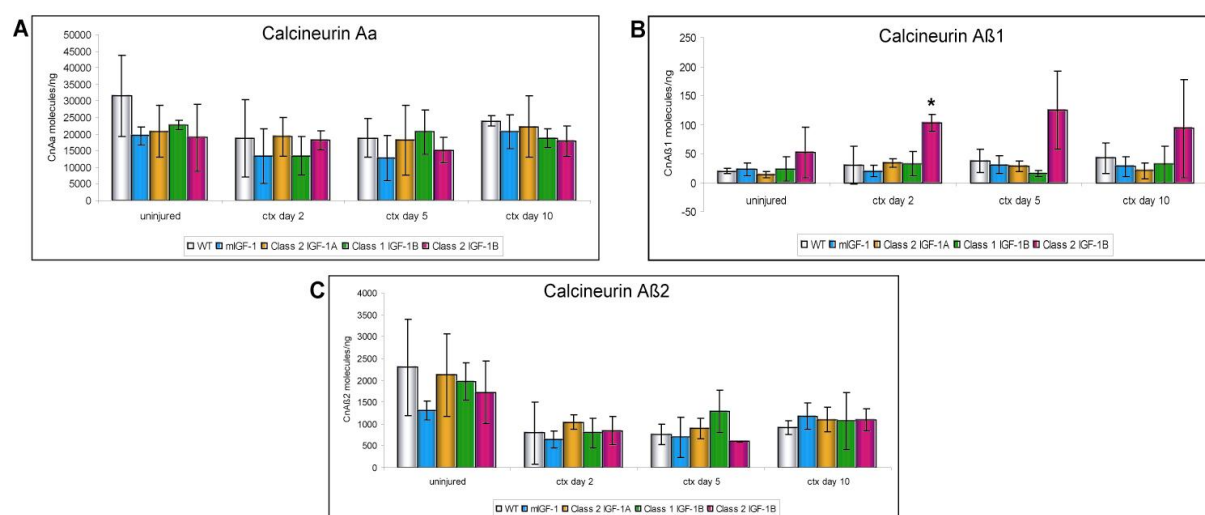


Figure 3.30 Expression of calcineurin isoforms in CTX-injured transgenic muscles. Quantitative RT-PCR was performed on three-month-old CTX-injected male mice of WT and transgenic origin. RNA was isolated from the quadriceps muscle of uninjured mice, as well as injured mice two, five, and ten days after injection ($n=3$ per genotype and time point). **A** RT-PCR for CnA α showed no differences between WT and transgenic animals. **B** Analysis of CnA β 1 expression revealed a significant increase at day two of regeneration for line MLC/Class 2 IGF-1Eb, while other IGF-1 isoform transgenic lines did not show significant changes. **C** CnA β 2 expression was also not changed in the background of IGF-1 isoform over-expression.

RT-PCR analysis of CnA β 2 revealed a non-significant decrease of this isoform upon injury in the WT situation (day two: -65%, day five: -67%, and day ten: -60) when compared to non-injured controls (Figure 3.30 C). In the presence of the different IGF-1 isoforms this situation was unchanged, leading to a similar decrease of this isoform upon injury as seen in the WT background.

In summary, CnA α and CnA β 2 WT expression levels decreased upon injury and this situation was unchanged in the background of the different IGF-1 isoform transgenes. CnA β 1

expression was induced in the WT upon injury, an effect that was even more pronounced in the background of the MLC/Class 2 IGF-1Eb transgene, even though this increase was only significant at day two post-injury. The other IGF-1 isoforms did not significantly change in comparison to the WT situation, but showed a tendency towards a mild down-regulation.

4 Discussion

Much research and effort has been invested to evaluate the enormous variety of effects that IGF-1 has on different cells types and tissues of the body at all stages of pre-and postnatal development. An impressive body of knowledge has been accumulated in the last two decades, but surprisingly the existence of many isoforms that are generated from the IGF-1 gene was not taken into account for the majority of the studies on IGF-1 function, even though their transcription was already reported 20 years ago. Only recently has the field begun to appreciate that the different IGF-1 isoforms have specialized functions, which might explain the pleiotropic effects of IGF-1 on proliferation, differentiation and survival. In the last couple of years, research has focused on the potential therapeutic application of IGF-1 in treating many skeletal muscle diseases and therefore the need for evaluating IGF-1 isoform function has become a crucial prerequisite for developing IGF-1 based therapies. A comprehensive comparison of IGF-1 isoform function is long overdue and is described in the present thesis. The work presented here documents the diverse effects of IGF-1 isoforms on skeletal muscle, and will have major implications on therapy-oriented research. This study also provides a comprehensive basis for further investigations into mechanisms that underlie these differential effects. In addition, we succeeded in cloning an IGF-1 isoform variant that was thought to be absent from mouse tissues.

4.1 The rodent En-peptide

Section 3.1 described the cloning of a Class 2 IGF-1 isoform containing an E-peptide splice variant that has previously not been reported to be present in rodents. Although the possible existence of this isoform was predicted from the sequence, transcripts could not be detected by Northern blot analysis, which led to the assumption that this isoform was not transcribed in rat liver {Shimatsu, 1987 #29}. With the availability of more sensitive methods to detect mRNA transcripts (amplification by RT-PCR from mouse liver mRNA), we succeeded in cloning a Class 2 IGF-1 isoform that contained an exon 4-5 splice variant, which has been described to give rise to the Eb-peptide in humans. Since the Eb-peptide in rodents corresponds to the Ec-peptide in humans, we termed this version En-peptide, to avoid further confusion.

Until now the rodent exon 5 has been considered to be a 52 bp cassette exon (in contrast to a terminal exon giving rise to a functional 3'-UTR), while the human exon 5 represents a terminal exon, encoding a stop codon and a 3'-UTR. With the description of the Ec-peptide in

humans, where exon 5 is spliced to exon 4 and 6, it became clear that also the human exon 5 can become a cassette exon, if a cryptic 5'-donor splice site is used [208]. With the cloning of the exon 4-5 splice variant in mice, this model will need to be revised for rodents as well.

In humans, splicing of the exon 4-5-6 variant (encoding the Ec-peptide in humans) occurs by use of a cryptic IGF₆₃₃ donor splice site located 49 bp downstream from the 5' end of exon 5. The sequence of this donor splice site deviates from the vertebrate 5'-donor splice site consensus and failure to use this cryptic IGF₆₃₃ donor splice site results in the exon 4-5 splice variant (corresponds to the human Eb-peptide) [208]. A possible reason for the low expression of the exon 4-5 splice variants in rodents might be the strength of the 5'-splice donor site. When comparing the 3'exon5:5'intron boundary to the vertebrate 5'-donor splice site consensus AG:AGTAAGT, the rat sequence matches by five out of six bases, the mouse sequence matches by four out of six bases, and the human sequence matches only by three out of six bases (Figure 4.1). These polymorphisms might alter the strength of the donor splice site and influence the splicing machinery. Because the rat donor splice site shows the highest match to the vertebrate 5'-donor splice site consensus, it is less likely to be overseen by the splicing machinery. In addition, the rat intron sequence following the 52 bp cassette exon contains 4 purine-rich repeats (GGAAG) within 300 bp downstream of the 5'-donor splice site, which have been shown to enhance splicing in the bovine GH gene [306]. Finally, the sequence downstream of the 5'-donor splice site contains only one AATATA polyadenylation signal, which might not be strong enough to compete with the stronger 5'-donor splice site.

Vertebrate 5'-donor splice site 3'-exon 5:5'intron 5 boundary con- sensus comparison	
consensus	AG:GTAAGT
RAT	AG:GT G AGT
MOUSE	AG:GA GAGC
HUMAN	AG:GT TGGC

Figure 4.1 Vertebrate 5'-donor splice site comparison. Red marks the bases that are different from the consensus sequence.

The observation that the En-peptide variant could only be detected in Class 2 IGF-1 mRNAs and showed weak expression only in mouse liver suggests a specialized, possibly endocrine

function for this isoform, which might need specific stimuli to be induced. However, since the rodent En-peptide lacks sequences that have been demonstrated to be important for human Eb-peptide function (compare section 3.1) [199, 296], further analysis will be necessary to evaluate the function of this splice variant in rodents.

4.2 The effects of IGF-1 on myoblast proliferation

Numerous studies have described IGF-1 as a mitogen, a function that is well established (reviewed extensively in [215, 297]). Since the majority of studies described in the literature applied commercially available mature IGF-1 to treat cells exogenously, the present *in vitro* study was designed to define if the mitogenic effect of IGF-1 were specific to a certain isoform or if they can be observed in response to all the six different isoforms analyzed here.

The *in vitro* experiments were performed using a doxycycline-inducible system of IGF-1 isoform expression in L6E9 cells, a rat myogenic cell line that does not express endogenous IGF-1 (described in section 3.2). The analysis suggests that Class 1 and Class 2 IGF-1Ea isoforms do not stimulate proliferation of myoblasts as efficiently as IGF-1 isoforms that contain the Eb-peptide. This conclusion was drawn from observations of the transfected cells upon shift from growth medium (GM) to differentiation medium (DM), where IGF-1 isoforms containing the Eb-peptide displayed a delayed exit from the cell cycle and underwent an additional round of replication as has been reported using recombinant, fully processed IGF-1 [307]. In addition, IGF-1 isoforms that contain the Ea-peptide, especially Class 1 and Class 2 IGF-1Ea, displayed weak levels of histone H3 phosphorylation as a maker of mitotic activity, while Eb-peptide containing isoforms showed higher levels of phospho-H3. These findings suggest a link between IGF-1Eb isoforms and proliferation and IGF-1Ea isoforms and differentiation (discussed in detail below). A possible role for an Eb-peptide-containing isoform in stimulating proliferation of myoblasts was reported previously [308], but was accompanied by a block in differentiation, which was not seen in the present study (discussed below).

Notably, none of the over-expressed prepro-variants of IGF-1 were processed to pro-IGF-1Ea/Eb or mature IGF-1 during proliferation. This observation makes it difficult to link the present findings to previous studies, where mature IGF-1 was used to determine IGF-1 mediated effects on proliferation. However, it suggests that the entire prepro-peptide, including signal- and Eb-peptide, influenced proliferation of myoblasts in this system. The possibility that L6E9 cells are not equipped to process IGF-1 due to the lack of endogenous

IGF-1 expression can be excluded, since processing was observed at later stages during differentiation (discussed below).

These findings also shed light on the outstanding question of whether the IGF-1 isoforms are active or properly localized without cleavage of the signal or E-peptides. Since the transgenic mice in the present study were designed for post-mitotic expression of IGF-1, the relevance of these results in cell culture to the role of specific pro-peptides on myoblast proliferation *in vivo* remains to be determined. Nevertheless, the data presented here strongly indicate that the entire IGF-1 prepro-peptide does not need processing to be active, and raise the possibility that specificity of IGF-1 function might be determined by processing status, or by the presence of isolated E-peptide once the prepro-peptide is cleaved.

4.3 Effects of IGF-1 isoforms on myoblast differentiation and muscle growth

4.3.1 *In vitro* effects of IGF-1 isoforms

IGF-1 effects on the differentiation of skeletal myoblasts are well described and largely attributed to the fact that IGF-1 can activate the myogenin gene, one of the MDFs that is most directly associated with terminal differentiation of skeletal muscle [309]. In addition, *in vitro* and *in vivo* studies have described increased myofiber size upon IGF-1 treatment or over-expression. In one such case recombinant IGF-1 (corresponding to mature IGF-1) was administered exogenously to L6E9 cells, which resulted in an increased size of differentiated fibers [307]. Also C2C12 cells showed a hypertrophic phenotype when stably transfected with IGF-1 (isoform was not indicated) or treated with IGF-1 [310]. Other groups employed specific isoforms, overall the Class 1 IGF-1 Ea isoform of either human [287] or rat origin [77, 278] *in vitro* and *in vivo*. Coleman et al. demonstrated enhanced fusion in stably transfected C2C12 cells, while Musaro et al. showed hypertrophic growth of stably transfected cells *in vitro* and of transgenic skeletal muscle *in vivo*. On the other hand, an unpublished study on transgenic mice over-expressing the mature version of IGF-1 in skeletal muscle did not show hypertrophy of myofibers (reviewed in [300]). Yet another group applied the IGF-1Eb isoform (Class was not indicated) or a synthetic Eb-peptide alone, to demonstrate that this isoform actually blocked differentiation in C2C12 cells and might act through another receptor [308]. Finally, a very recent report described the viral-mediated expression of Class 1 IGF-1Ea and Class 1 IGF-1Eb and showed that viral injection of both IGF-1 isoforms in young (two-weeks-old) animals resulted in hypertrophic muscles, while injection of older animals (six-months-old) only resulted in hypertrophy of Class 1 IGF-1Ea injected muscles [311]. This report

concluded that Class 1 IGF-1Eb was effective in promoting hypertrophy only in young muscles.

The present study described a comprehensive comparison of the different effects of the four main IGF-1 isoforms *in vitro* and *in vivo*. The approach is unprecedented in that it provides comparable transgene expression from the same regulatory elements that drive expression specifically in skeletal muscle of transgenic mice and provide expression throughout the life of the animals from embryonic day E9.5. The selection of isoforms used in this study (defined combination of signal peptide and E-peptide) provides valuable information and distinguishes it from many previous studies that lacked information of the precise isoform employed.

The *in vitro* data described in section 3.2 revealed an enhancement of differentiation for cells transfected with Class 1 IGF-1Ea that culminated in the formation of hypertrophied myofibers. Interestingly, cells transfected with Class 2 IGF-1Ea showed normal differentiation kinetics but nevertheless showed an increased size of differentiated fibers after day three of differentiation. L6E9 cultures transfected with the Eb-peptide containing isoforms of IGF-1 showed a delay in the differentiation process and the formation of normally sized muscle fibers, suggesting that IGF-1 isoforms containing the Eb-peptide do not play a role in mediating IGF-1 induced hypertrophy. Moreover, cells transfected with 22-IGF-1Ea revealed a third phenotype, since they showed fibers that were comparable to control fibers although an early initiation of the differentiation process was indicated by a stronger up-regulation of myogenin in comparison to the mock control cells and cells transfected with other IGF-1 isoforms after one day of differentiation. Notably, after two days of differentiation all isoforms uniformly up-regulated myogenin and MEF2C in comparison to mock controls, indicating that the myogenic program was efficiently induced by all of the IGF-1 isoforms.

These findings confirm earlier publications that demonstrated a hypertrophic response to the Class 1 IGF-1Ea isoforms, but contradict a study mentioned above, which claimed that IGF-1Eb or the Eb-peptide alone could block differentiation [308], since in the present study all the different isoforms containing the Eb-peptide up-regulated markers of myocyte maturation and differentiated into myotubes. A possible reason for this observation is that Yang et al. used an IGF-1Eb peptide that presumably did not contain a signal peptide and a synthetic Eb-peptide. The signal peptide most likely plays an important role in directing IGF-1 isoforms to the desired compartment of the cell and thereby also determines IGF-1 processing and IGF-1 function. This possibility is supported by two observations: first, IGF-1 isoform processing in the system described here only occurred upon shift to DM, indicating that initially the entire prepro-peptide has a function (as mentioned above), and second, that the

induction of IGF-1 isoform processing upon early differentiation might determine their function during differentiation. Thus, the availability of IGF-1Eb (without signal peptide) or the Eb-peptide alone might influence the cells differently. However, since it cannot be excluded that the IGF-1Eb peptide used by Yang et al. contained a signal peptide, differences seen might also be due to the different cell lines used. The significance of a synthetic Eb-peptide is also questionable, since alone it is apparently very unstable, and in that study was stabilized by amino acids substitutions and polyethylene glycol addition, therefore side effects from these modifications cannot be excluded.

The *in vitro* findings presented here also show for the first time that Class 2 IGF-1Ea is also capable of inducing cell hypertrophy. In contrast, the three different IGF-1Eb isoforms do not display enlarged fiber sizes. These findings implicate that the Ea-peptide is important for mediating a hypertrophic response, while the presence of the Eb-peptide is not involved in mediating such an effect. Clearly, context is critical, since the 22-IGF-1Ea isoform, with a truncated signal peptide, did not lead to a hypertrophic phenotype of transfected cells. At this point further research is needed to evaluate why this isoform behaves differently. It is possible that the 22 amino acid signal peptide directs this isoform to a different sub-cellular localization, which might result in less efficient secretion or differential binding of this isoform to the different IGFBPs.

4.3.2 *In vivo* effects of IGF-1 isoforms

In order to comprehensively compare IGF-1 isoform function *in vivo*, six transgenic mouse lines over-expressing the six main IGF-1 isoforms have been generated. Selected founders from different transgenic lines were chosen on the bases of high and comparable expression. High to moderate skeletal muscle-specific expression was seen for each transgene, depending on the specific skeletal muscle group analyzed: fast muscles showed higher transgene expression levels due to the fast fiber restriction of the MLC regulatory elements.

For further analysis, priority was given to the main IGF-1 isoforms expressed in mouse liver: MLC/Class 2 IGF-1Ea, MLC/Class 1 IGF-1Eb, and MLC/Class 2 IGF-1Eb. Since line MLC/Class 1 IGF-1Ea was lost due to breeding problems early in this study, the well-characterized MLC/mIGF-1 line, generated by Antonio Musaro [77] was used for further comparative work. This line carries the same transgene as used for generating the MLC/Class 1 IGF-1Ea line (Class 1 IGF-1Ea), but of rat rather than mouse origin, and contains the same MLC 1/3-derived regulatory sequences to drive transgene expression. Further, comparative expression analysis between the different transgenic lines revealed variable differences in IGF-1 transgene expression on the transcriptional level, which were

nevertheless translated into comparable protein levels. This observation implies a threshold for IGF-1 protein translation that is not dependent on absolute transcription levels.

In correlation with the *in vitro* findings described in section 4.3.1, detailed analysis of skeletal muscle phenotype and physiological performance revealed striking muscle hypertrophy in line MLC/Class 2 IGF-1Ea. This was reflected by an increase in CSA of fast, intermediate, and slow fibers in the TA and EDL muscle. The increase of skeletal muscle fiber CSA was accompanied by a significant increase of skeletal muscle wet weight and a pronounced increase in force generation of fast but not slow skeletal muscle groups, confirming functional hypertrophy. The transgenic MLC/Class 2 IGF-1Ea animals also showed increased body weight at all ages studied, which can be correlated to the pronounced increase of fast skeletal muscle wet weight, since distal organs were not affected in their weight. Interestingly, the phenotype observed in these animals was more pronounced compared to the MLC/mlIGF-1 line, reflected in a stronger increase of skeletal muscle weight and physiological performance, as well as in a consistent, but small relative increase in overall bodyweight. These results highlight a strong connection between IGF-1Ea isoforms and induction of hypertrophy in skeletal muscle.

The fact that the MLC/Class 1 IGF-1Ea transgene increased endogenous levels of Class 2 IGF-1Ea raises the possibility that hypertrophy in these animals is predominately due to the Class 2 IGF-1Ea isoform. This is supported by the fact that the increase in endogenous Class 1 IGF-1Ea induced by the MLC/Class 1 IGF-1Eb transgene did not result in a hypertrophic response. It also appears that only Class 1 isoforms can influence endogenous IGF-1 expression, since endogenous IGF-1 levels were unaffected in transgenic lines over-expressing Class 2 IGF-1 isoforms. Thus the crosstalk between exogenous and endogenous IGF-1 isoforms must be taken into consideration when interpreting the results of any over-expression studies.

The two lines over-expressing the Ea-peptide-containing isoforms Class 1 IGF-1Ea (mlIGF-1) and Class 2 IGF-1Ea also showed a modest, but significant up-regulation of total circulating levels of IGF-1, which was not the case for transgenic lines over-expressing IGF-1 isoforms containing the Eb-peptide. Notably, the increase of total serum IGF-1 remained significant in MLC/Class 2 IGF-1Ea mice at the age of six months, while levels were still elevated, but no longer significant in MLC/mlIGF-1 mice. In either case, the total IGF-1 elevation did not lead to an increase in the weight of visceral organs, such as heart, brain, liver, kidney or spleen at all ages analyzed for both lines, indicating that the mild increase of serum IGF-1 did not disturb other organ systems. The assay used for these experiments included a step to strip

off IGF-binding proteins and therefore does not reflect levels of free, bioavailable IGF-1. An attempt to analyze the level of free IGF-1 in control and transgenic animals using the same assay failed to give conclusive results. Thus, is it difficult to determine at this point whether the modest elevation of total serum IGF-1 in these animals has any biological significance. A recent study on the SIS2 mice (over-expressing human Class 1 IGF-1Ea) demonstrated that hIGF-1 was detectable in the circulation, without changing total levels of IGF-1. An unpublished study on MLC/mlIGF-1 serum levels (Shavlakadze et al., unpublished) demonstrated no changes at three months of age, contradicting the results presented here. Finally, another unpublished study on the Rsk α -actin/hIGF-1 mice (over-expressing mature IGF-1 of human origin), revealed a strong increase of total serum IGF-1, which resulted in an increase of seminal vesicles in 24-months-old male mice (Shavlakadze et al., unpublished). However, in the last case mature IGF-1 was fused to the signal peptide of somatostatin, which is normally found in the circulation (compare section 1.5) and therefore most likely directs this version of IGF-1 to the circulation as well. Controversial claims in the literature and a large discrepancy of circulating IGF-1 levels in different mouse strains (reviewed in detail in [151]) underscore the need for caution in interpreting the relevance of these measurements. When using sensitive assays such as ELISA, which are routinely used to determine serum IGF-1 levels, it is crucial to consider that results can only be compared in a reliable way, if the samples have been screened using the same calibrators and controls in the same assay. Most importantly, different assays using different antibodies for IGF-1 detection can give different results and should not be compared. For this reason only relative changes were considered in the present study. They suggest that IGF-1 isoforms containing the Ea-peptide could enter the circulation, since this has been observed for the SIS2, the MLC/Class 2 IGF-1Ea, and the MLC/mlIGF-1 mice, at least in the present study. Since no correlation with the signal peptide was seen (Class 1 versus Class 2), the Ea-peptide might therefore determine if an isoform is secreted to the circulation or not. This could be mediated by the binding to certain IGFBPs, an issue that has not been addressed in the present study, but will be necessary in the future. Notably, this approach could not determine whether the over-expressed transgene itself was secreted or led to the induction of endogenous IGF-1 secretion.

In contrast to the phenotype seen in MLC/mlIGF-1 and MLC/Class 2 IGF-1Ea mice, both transgenic lines that over-express Eb-containing isoforms (MLC/Class 1 IGF-1Eb and MLC/Class 2 IGF-1Eb) displayed only a mild increase of skeletal muscle mass, accompanied by a small shift towards a higher proportion of larger fibers in the fast muscles that did not result in a consistent increase of fiber CSA. These modest changes did not result in physiological improvements of muscle performance and did not affect the overall bodyweight

of these animals. The *in vitro* and *in vivo* results presented for both Eb-peptide-containing isoforms demonstrate for the first time that these versions of IGF-1 do not play a role in mediating IGF-1 induced functional hypertrophy of skeletal muscle *in vivo*.

These findings stand in contrast to a very recent report that analyzed the differential effects of Class 1 IGF-1Ea versus Class 1 IGF-1Eb in skeletal muscle, using rAAV viral injection of these isoforms under the control of the same MLC1/3 regulatory elements applied in the present study [311]. Viral-mediated expression of both Class 1 IGF-1Ea and Class 1 IGF-1Eb resulted in a mild increase of muscle mass ($12\pm 2\%$ for Class 1 IGF-1Ea and $7\pm 2\%$ for Class 1 IGF-1Eb) after two months of injection of the viruses into the TA and EDL muscles of two-weeks-old mice and was maintained up until four months post-injection. The author concluded a hypertrophic phenotype in response to both isoforms, without an increase of force-related physiological parameters. Critical evaluation of this report reveals that the hypertrophic phenotype was only determined by measuring the muscle weight. No histological analysis was performed to prove an increase of the CSA of fibers in the injected muscles and no correlation was seen with an increase in muscle strength. Injections of the same viral constructs in six-months-old animals resulted in a 5% increase of muscle mass in animals injected with Class 1 IGF-1Ea viruses at four months post-injury, while no differences were seen at this age in muscles injected with Class 1 IGF-1Eb viruses. Thus, the mild increase in muscle mass most likely reflected a modest shift towards a higher content of bigger fibers, as observed for MLC/Class 1 IGF-1Eb animals in the present study, and did not represent a hypertrophic phenotype. Although discrepancies in the experimental design of the two studies must be considered (C57B1/6 versus FVB backgrounds, different mode of delivery and time-line of transgene expression) the conclusion that Class 1 IGF-1Eb promotes hypertrophy in growing animals is unlikely to hold in light of the present study, where the Class 1 IGF-1Eb transgene produced from embryonic day E9.5 onwards did not lead to a significant increase in fiber size, even though a modest weight increase was observed. This is supported by the comparable phenotype of MLC/Class 1 IGF-1Eb and MLC/Class 2 IGF-1Eb transgenic mice, neither of which display a consistent significant weight increase or a consistent increase in fiber CSA.

4.4 IGF-1 signaling in response to different IGF-1 isoforms

The detailed description of IGF-1-mediated intracellular signaling in section 1.4.5 underscores the complex and inter-connected nature of these interactions, as well as the confusion that still exists in the literature. Three main pathways have been implicated for different functions of IGF-1: first, the MAP-kinase pathway, which has mainly been connected

to the proliferative response to IGF-1 [242] and reviewed in [297], second, the PI(3)-kinase pathway, which has been linked to myoblast differentiation (reviewed in [215]), hypertrophy of skeletal muscle [61], survival (reviewed in [257]), and prevention of atrophy [60, 61], and third, the calcineurin pathway, which is also connected to myoblast differentiation [39, 278] and controversially suggested to mediate the hypertrophic response to IGF-1 [39, 61, 282, 310].

Results presented here demonstrated that over-expression of the four main IGF-1 isoforms in skeletal muscle *in vivo* similarly resulted in activation of the IGF-1R, without influencing the transcription of the IGF-1R gene. However, the efficiency of IGF-1R activation varied amongst the IGF-1 isoforms, with MLC/Class 2 IGF-1Ea samples providing the strongest signal. Even though MLC/Class 2 IGF-1Ea displayed the most pronounced phenotype in skeletal muscle, the stronger activation of the IGF-1R cannot be correlated to the stronger phenotype, since also MLC/Class 2 IGF-1Eb animals, which do not show such a strong phenotype, also demonstrated an increased phosphorylation of IGF-1R. Thus, other components downstream of the IGF-1R are likely to govern the hypertrophic response.

Analysis of differential activation of MAP-kinase family members during growth *in vitro* revealed subtle changes for samples transfected with the Class 1 IGF-1Ea and the Class 2 IGF-1Ea isoforms: Class 2 IGF-1Ea transfected cultures decreased phospho-JNK1 levels, while increased phospho-Erk1 and 2 levels were observed in cultures transfected with Class 1 IGF-1Ea. The significance of these changes is not clear, since they cannot be correlated to the phenotype of the cells discussed in section 4.2. Since the Eb-containing isoforms showed prolonged proliferation it is perhaps surprising that Class 1 IGF-1Ea, which actually showed less effect of proliferation, was the only isoform up-regulating Erk 1 and 2. A broader screen of molecules implicated in the proliferative response to IGF-1 will be needed in the future to further dissect the mechanism, whereby IGF-1 isoforms control the proliferative response.

The cellular response to the post-mitotic over-expression of IGF-1 isoforms *in vivo* did not involve the MAP-kinase pathway, as revealed by the Kinetworks™ Phospho-site screen. This is in agreement with previous studies on skeletal muscle-specific IGF-1 transgenic animals, and a recent publication describing a down-regulation of MAP-kinase kinase (MEK) 1 and 2 and MEK 3 and 6 in response to the MLC/mIGF-1 transgene [261], also supports the results presented here. Interestingly, the Kinetworks™ analysis presented here and previously [261] revealed a trend towards Raf-1 phosphorylation for both Class 1 transgenic lines. In light of recent findings linking p21 activated kinase (PAK1)-mediated Raf-1 phosphorylation to mitochondrial translocation of Raf-1 and phosphorylation of BAD [274], this phosphorylation

of Raf-1 might be connected to an activation of survival pathways, although its relevance in healthy and unchallenged mice used here remains to be determined.

Analysis of the PI(3)-kinase pathway *in vitro* demonstrated a similar increase in phosphorylated Akt and its downstream target S6 ribosomal protein in response to each IGF-1 isoform. Ubiquitous activation of Akt in the cell transfection experiments may be an artifact of doxycycline induction, which is stressful for the cells. Thus, activation of Akt in cell culture could be attributed to the fortuitous induction of survival pathways, which are not implicated in the analysis of transgenic animals that were not challenged in any way. Indeed, analysis of this pathway *in vivo* revealed up-regulation of PI(3)-kinase pathway members such as Akt1, PDK1, and GSK-3 α and β only in Class 2 IGF-1 transgenic mice. This is corroborated by a recent study demonstrating that Akt was not regulated in response to the mIGF-1 transgene in MLC/mIGF-1 mice [261], supporting the conclusion that Class 1 isoforms did not influence Akt activity. Similar evidence comes from analysis of cardiac-specific mIGF-1 transgenic mice, where no activation of Akt was detected (Santini et al., manuscript submitted).

Not all aspects of IGF-1 intracellular signaling are as consistent between studies. Activation of the known downstream effectors of the PI(3)-pathway, such as the induction of p70^{S6K}, was documented in MLC/Class 1 IGF-1Ea, MLC/Class 2 IGF-1Ea and MLC/Class 2 IGF-1Eb transgenic animals, confirming previous analysis for the mIGF-1 transgene [261]. However, phosphorylation of PDK-1 in mIGF-1 transgenic mice [261] was not observed in the present study, where Class 2 but not Class 1 IGF-1Ea isoforms led to up-regulation of PDK-1. Conversely, significant induction of RSK1/2/3 in MLC/Class 1 IGF-1Ea and MLC/Class 2 IGF-1Ea transgenic animals was not seen in MLC/mIGF-1 animals [261]. These discrepancies may stem from variables in experimental design such as the number and ages of animals analyzed, potential subtle differences in rat versus mouse transgenes, and the reliability of the KineteworksTM screen results, which were not always confirmed by Western blot (data not shown). In addition, signaling analysis *in vivo* is biased by the variety of cell types present in skeletal muscle. It will also be of interest to repeat these analyses on mice that have been challenged with exercise, injury or disease such as the *mdx* mouse model for DMD, which may enhance differences of IGF-1 isoform-mediated signaling. For example, Akt phosphorylation absent in steady state conditions of MLC/mIGF-1 animals [261], could be induced in the background of muscular dystrophy in *mdx*/mIGF-1 animals [90], and in conditions of cardiac cachexia following myocardial infarction [46].

Notably, analysis of the calcineurin pathway clearly demonstrated that none of the transgenic lines activated any of the calcineurin isoforms and no changes in GATA-2, a downstream

target of calcineurin, was observed. Although involvement of calcineurin in mediating the hypertrophic response to the MLC/mlIGF-1 transgene has been suggested *in vitro* [282] and *in vivo* [77], subsequent studies suggested that calcineurin was not implicated in mediating an IGF-1 mediated hypertrophic response in skeletal muscle [39, 61]. The latter two reports employed recombinant (fully processed) IGF-1; the present study further documents that calcineurin is not implicated in mediating the hypertrophic response of IGF-1Ea isoforms.

In summary, the present study serves to emphasize the complexity of the IGF-1 signaling system and to provide a firm base for deeper analysis. One issue that merits further study is the regulation of the different IGF-1 isoforms by the different IGFBPs and the effect this might have on phenotype and signaling. The structure of different E-peptides may direct the binding of IGF-1 protein to different IGFBPs, a likely mechanism whereby IGF-1 isoforms might achieve their target specificity and influence downstream intracellular signaling. From the Ingenuity pathway analysis performed on the Affymetrix data, it is clear that the IGF-1 isoforms themselves differentially regulate IGFBP availability (up- or down-regulation), further highlighting the importance of these IGF-1 regulator proteins and the presence of feedback loops in the system. The two different approaches described in section 3.3.11b are extremely valuable, since they highlight that fact that analysis using only one approach with a certain cut off of regulated genes might miss important connections between a differential stimulus (in our case different IGF-1 isoforms) and the downstream transcriptional regulation in an overall connected network of genes. Candidate genes identified with both approaches may serve as potential candidates involved in the IGF-1 isoform-induced response in the future. In this respect the Affymetrix analysis provides a different approach, as it reflects a genomic response to IGF-1 isoform over-expression. Taken together with snap-shots of protein activation provided by the Kinetworks™ Phospho-site screen, the steady-state status of gene expression afforded by transcriptional profiling provides valuable information about the basic regulatory units that can govern IGF-1 isoform-induced phenotypes.

Another area of future research will be the control of IGF-1 prepro-peptide processing as well as the glycosylation of the Ea-peptide, which as the present study demonstrates, is highly regulated in skeletal muscle. An early *in vitro* study on the relation between the length of the signal peptide and the glycosylation of the Ea-peptide [186] demonstrated that IGF-1Ea isoforms containing the longest (48 amino acids) signal peptide, did not undergo post-translational glycosylation. However, in the present work, a band-shift presumably reflecting the molecular weight increase caused by glycosylation was observed for all Ea-containing isoforms, providing the first evidence that IGF-1Ea isoform-glycosylation is differently regulated *in vivo*. These distinct and separable phenotypic variations described for the IGF-1

isoform transgenic mice will inform the future design of better tools, more specific experiments and new approaches to tackle these outstanding questions in IGF-1 research.

4.5 Effects of IGF-1 isoforms on regeneration of skeletal muscle

Although skeletal muscle maintains an intrinsic capacity to regenerate after work-induced damage and injury, it gradually loses this capacity in many disease states, but also in unavoidable conditions like aging. Endogenous IGF-1 levels decrease with age, which is considered one of the reasons for the reduced capacity of skeletal muscle regeneration. Supplemental administration of Class 1 IGF-1Ea (mIGF-1) by muscle-specific transgenesis or muscle-specific viral-mediated delivery has enhanced regenerative capacity of aged skeletal muscle, providing evidence for the beneficial effect of IGF-1 in skeletal muscle repair [76, 77]. More recently it has been shown that the mIGF-1 transgene also attenuates skeletal muscle degeneration and promotes regeneration in disease models of Duchene Muscular Dystrophy (DMD) and Amyotrophic Lateral Sclerosis (ALS), where supplemental mIGF-1 transgene expression reduced myofiber breakdown and necrosis [90], protected against free radical induced damage [78], and promoted regeneration [130]. The mIGF-1-enhanced regeneration of skeletal muscle involves stimulating satellite cell proliferation, as well as the recruitment of progenitor cells intrinsic to the muscle and from the circulation (reviewed in [110], compare section 1.2.9).

The work in the thesis is especially important in light of IGF-1-based therapies, which have long been in the center of interest. Depending on the disease condition, it might be preferable to protect the muscle and at the same time increase muscle mass. For other applications it might be preferable to protect the muscle without inducing muscle hypertrophy. Therefore it is crucial to determine if IGF-1 isoforms that do not display skeletal muscle hypertrophy bear a similar regenerative capacity described for the MLC/mIGF-1.

The preliminary results described in section 3.4 demonstrated an improved regeneration process in response to CTX-injections in every IGF-1 transgenic line. However, the morphological analysis suggests differences in the initial regenerative response. While MLC/Class 2 IGF-1Ea displayed larger fibers containing between one and three nuclei at day five after injury, MLC/Class 1 IGF-1Eb and MLC/Class 2 IGF-1Eb showed more fibers when compared to WT and also to MLC/Class 2 IGF-1Ea. After ten days of regeneration, all transgenic lines displayed similar improvements in muscle morphology than the WT,

indicating that the presence of the different IGF-1 isoforms each resulted in enhanced regeneration, despite potential differences in the mechanisms involved. These findings suggest that IGF-1 isoforms can improve regeneration by either enhancing the growth of newly forming fibers (Class 2 IGF-1Ea) or by stimulating the proliferation of satellite cells and potentially other stem cell types (Class 1 IGF-1Eb and Class 2 IGF-1Eb). A connection between Eb-peptide-containing isoforms and proliferation was also suggested by the *in vitro* experiments discussed earlier (compare section 4.2) and has been proposed in the literature [210, 214, 308]. Since the design of the transgenic expression cassette only provides post-mitotic expression of the IGF-1Eb transgenes, these findings also imply that both IGF-1Eb isoforms could be secreted from intact fibers and act in a paracrine way to stimulate proliferation of myogenic precursor cells.

Another result presented here describes the effects of CTX-induced injury on the endogenous gene in a WT or transgenic background (compare section 3.4.2). The expression pattern of endogenous IGF-1 isoforms upon injury revealed a pronounced up-regulation of both Ea-peptide-containing isoforms throughout the process of regeneration, reaching highest induction levels at day ten after injury, while both Eb-containing isoforms showed mild induction upon injury without being significant. The only exception was a transient up-regulation of Class 2 IGF-1Eb at day five after injury. Similar observations were described for IGF-1Ea and IGF-1Eb (the signal peptides were not defined) in previous studies on exercised-induced damage in skeletal muscle [210, 214]. However, the present study extends the previous ones in that both Class 1 and Class 2 IGF-1 isoforms with the different E-peptide combinations were screened. Moreover, the present work shows that both IGF-1Ea isoforms are implicated in the regeneration process in response to CTX injections in the WT muscle. Furthermore, although the two models of injury are very different, these findings suggest that the IGF-1Eb up-regulation reported by earlier studies [210, 214] actually corresponds to the Class 2 version of IGF-1Eb, raising the possibility that “MGF” might originate from transcription initiation in exon 2.

In the IGF-1 transgenic background, both Eb-peptide-containing isoforms significantly up-regulated endogenous Class 1 IGF-1Ea after five days of regeneration when compared to WT levels, although MLC/Class 1 IGF-1Eb animals showed endogenous Class 1 IGF-1Ea up-regulation without injury as well (compare section 3.3.5). However, these findings indicate that the Class 1 IGF-1Ea isoform might be necessary to promote the regenerative process. None of the other transgenic lines induced significant changes in the endogenous IGF-1 isoform expression patterns observed in the WT.

Recently, a naturally occurring calcineurin A splice variant, CnA β 1, has been shown to promote regeneration in response to CTX injury when over-expressed in the skeletal muscle of transgenic mice, while over-expression of CnA α worsened the regenerative response (Lara-Pezzi E., manuscript submitted). The same study showed that the CnA β 1 isoform is normally induced upon injury, while CnA α and CnA β 2 are down-regulated in response to such damage. CnA β 1 has also been shown to be up-regulated by mIGF-1 in the background of the SOD1 mouse (mIGF-1/SOD1), which serves a model for ALS [78] This isoform is not induced in healthy MLC/mIGF-1 animals, suggesting that its induction is specific to certain detrimental stimuli. Interestingly, up-regulation of the CnA β 1 isoform was observed specifically in the MLC/Class 2 IGF-1Eb animals at every time point post-injury, while none of the other IGF-1 isoforms, including MLC/mIGF-1, regulated the expression of CnA β 1. This suggests that Class 2 IGF-1Eb induces a specific response that differs from the other IGF-1 isoforms. The enhanced regenerative response seen for transgenic CnA β 1 animals has been linked to modulation of the inflammatory response and to a reduction of fibrosis (Lara-Pezzi E., manuscript submitted). Very preliminary results obtained by RT-PCR, not included in this thesis, point towards a similar mechanism in the MLC/Class 2 IGF-1Eb animals, where MCP-1 (a marker for macrophages that induces the recruitment of inflammatory cells) was elevated two days post-injury and significantly increased at five days post-injury, and IL-10, an anti-inflammatory cytokine, was increased at two, five, and ten days post-injury. Collagen I was analyzed to determine the fibrotic response and was shown to be down-regulated at day ten post-injury. In contrast, analysis of these markers revealed no conclusive changes in response to the other IGF-1 isoforms. These results further implicate Class 2 IGF-1Eb in inducing a specific response that discriminates this isoform from the other IGF-1 isoforms in promoting the regeneration process. Further investigation of these findings with more quantitative and molecular evidence will be necessary to determine whether the specific role of Class 2 IGF-1Eb can be confirmed and consistently connected to CnA β 1 up-regulation.

4.6 Future perspectives

The present study revealed a clear connection between the IGF-1 Ea-peptide and mediation of a hypertrophic phenotype in skeletal muscle. This increase in myofiber size was accompanied by an increase of the force generation and strength of the muscles affected. In contrast, the presence of the Eb-peptide in IGF-1 isoforms was not connected to an induction of skeletal muscle hypertrophy, and even though a mild increase of muscle mass was seen, this did not result in an increase in force generation or strength. Analysis of the regenerative capacity of IGF-1 isoforms in response to injury revealed that each IGF-1 isoform led to an improvement of the regeneration process that seemed to be mediated by an increased

number of fibers in response to both Eb-peptide-containing isoforms. The mechanism by which IGF-1 isoforms mediated these findings are not clear at this point and will have to be addressed in detail in the future to further understand the beneficial effects of IGF-1.

One of the possible tools that will prove useful in the future is the generation of doxycycline-inducible IGF-1 transgenic mice that allow the induction of IGF-1 at a chosen time point specifically in skeletal muscle. This will be especially useful to investigate whether IGF-1 is needed at a certain time to enhance regeneration and whether IGF-1 isoforms can have different effects if the expression is induced later in life of the transgenic animal. Inducible-mIGF-1 transgenic animals have been generated by Ekaterina Semenova in Nadia Rosenthal's laboratory and I generated inducible Class 1 IGF-1Eb animals, as well as the skeletal muscle-specific MLC/rtTA mouse line (compare section 2.1.5.2). Generation of inducible Class 2 IGF-1 animals is planned for future studies. Although the tools were developed during this thesis, the time schedule did not allow studying those animals in the end. In light of the results discussed in section 4.5, it will be of interest to include Class 2 IGF-1Eb in further studies.

Other approaches to further investigate the beneficial effects of IGF-1 isoform over-expression skeletal muscle have already been initiated for line MLC/Class 2 IGF-1Ea in collaboration with Professor Miranda Grounds (University of Western Australia, Perth, Australia). The MLC/Class 2 IGF-1Ea animals are currently crossed to the *mdx* mice, a model of Duchenne muscular dystrophy, to evaluate if this isoform can have similar effects as described for the MLC/mIGF-1 animals, such as protection from necrosis [90, 91], reduction of fibrotic tissue [90], and thereby enhance regeneration of the myopathic muscles. In the future, similar experiments are planned for Class 1 IGF-1Eb and /or Class 2 IGF-1Eb, to compare the beneficial effects of an isoform that is capable to induce hypertrophy and enhanced regeneration (one of the Ea-peptide-containing isoforms) to the effects of an IGF-1 isoforms that does not induce hypertrophy, but nevertheless improves the regenerative response (one of the Eb-peptide-containing isoforms). These experiments will be especially important, since some disease conditions do not require the overall increase of muscle mass, but still an enhanced regeneration. One of the major questions concerning muscular dystrophies in this respect is if the improvement of skeletal muscle regeneration and morphology seen in the *mdx*/mIGF-1 animals was in part due to an increase of the muscle mass as well, or if the stimulation of the regenerative response and the protection from necrosis is enough to induce the observed improvements. If so, induction an overall increase of muscle mass (up to 40%) [90] may not be necessary in future strategies to treat muscular dystrophy.

Another project that has been initiated in the Rosenthal laboratory is a profound investigation into the role of the six main IGF-binding proteins in the different IGF-1 isoform transgenic mice. This is a crucial point, which has not been addressed in the present thesis, but is clearly one of the factors that can determine IGF-1 isoform function *in vivo*.

In summery, different roads can be taken from this point to continue our approach of clarifying the role of different IGF-1 isoforms. On the background of the differential phenotypes described here, more functional, as well as mechanistic experiments can be preformed on the way to discover the right version of IGF-1 for treatment of a certain disease. The examples given in this section only provide a few possible directions that can be taken, but clearly show the significance of the present thesis, which finally constitutes a solid bases for selecting the IGF-1 isoform candidate for further therapy-based research.

Appendix A: List of Abbreviations

aa	Amino acid
AChR	Acetylcholin receptor
ALS	Acid-labile subunit
ALS	Amyotrophic lateral sclerosis
ATP	Adenosine triphosphate
Bcl	B-cell lymphoma
bFGF	basic fibroblast growth factor
bHLH	basic Helix-Loop-Helix
BMP-4	Bone morphogenic protein-4
CaMK	Calcium/calmodulin-dependent kinase
Cn	Calcineurin
CSA	Cross-sectional area
CsA	Cyclosporin A
CTX	Cardiotoxin
DHPR	Dihydropyridine receptor
DM	Dermamyotome
DM	Differentiation
DMD	Duchenne muscular dystrophy
DMSO	Dimethyl sulfoxide
DPC	Dystrophin-associated protein complex
EDL	Extensor digitorum longus
EFP	Epididymis fat pat
EGF	Epidermal growth factor
E-peptide	Extension-peptide
Erk	Extracellular regulated kinase
FBS	Fetal bovine serum
FGF	Fibroblast growth factor
GH	Growth hormone
GM	Growth medium
GPE	Glycyl-prolyl-glutamate
Grb-2	Growth factor receptor-bound protein-2
GSK-3	Glucose synthase-kinase-3
IGF-1	Insulin-like growth factor-1
IGF-1R	Insulin-like growth factor-1 receptor
IGFBP	Insulin-like growth factor binding protein
IP	Immunoprecipitation
IRS	Insulin receptor substrate
LM	Lateral mesoderm
MAFbx	Muscle atrophy F box = Atropin-1
MAP-kinase	Mitogen activated protein-kinase
MCK	Muscle creatine kinase
MDF	Myogenic determination factor
MEF	Myocyte enhancing factor

MEK	MAPK-Erk protein-serine kinase
MGB	Major groove binding
MGF	Mechano growth factor (= IGF-1Eb)
MLC	Myosin light chain
MRF-4	Myogenic regulatory facto-4
mTOR	Mammalian Target of rapamycin
MURF-1	Muscle ring finger-1
MyHC	Myosin heavy chain
NADH-TR	Nicotinamide adenine inucleotide nitro blue Tetrazolium
NBT	Nitro blue tetrazolium
Nc	Notochord
NF-ATc	Nuclear factor of activated T-cells
NT	Neural tube
ORF	Open reading frame
PAK	p21-activated kinase
PBS	Phosphate-buffered saline
PDGF	Platelet-derived growth factor
PDK-1	Phosphoinisitol-dependent kinase
PEG	Polyethylene glycol
PHAS	Phosphorylated heat- and acid-stable protein
PI(3)-kinase	Phosphatidylinositol-3-kinase
PK	Proteinase K
PKC	Protein kinase C
PVDF	Polyenyldine difluoride
Rb	Retinoblastoma protein
ROS	Reactive oxygen species
RSK	Ribosomal S6 protein-serine kinase
RT	Room temperature
rtTA	Reverse tetracycline trans-activator
Sc	Sclerotome
SH2/3	src-homology-2 /-3 domain
SHC	src-homolgy contining
Shh	Sonic hedgehog
Sm	Somite
SOD1	Superoxide dismutase-1
Sos	Sons of sevenless
SP	Side population
TA	Tibialis anterior
TAE	Tris-acetate-EDTA buffer
TBE	Tris-borate-EDTA buffer
TGF- β	Transforming growth factor- β
TNF α	Tumor necrosis factor α
TSB	Transform storage buffer
UTR	Untranslated region
VEGF	Vascular endothelial growth factor
(v/v)	Volume per volume

WT	Wildtype
(w/v)	Weight per volume

Appendix B: Affymetrix analysis

GENE NAME	1EA	1EB	2EA	2EB
insulin-like growth factor 1	25.52 *	3.32	15.69	1.80
zinc finger protein, subfamily 1A, 1 (Ikaros)	2.91 *	2.79 *	2.07 *	2.55 *
DIX domain containing 1	2.82	2.00 *	2.29	3.29
TGFB-induced factor 2	2.34	1.46	1.44 *	1.69
solute carrier family 16 (monocarboxylic acid transporters), member 11	2.30	1.32 *	-1.22 *	-1.40
sarcolipin	2.15 *	1.11	-1.49 *	1.19 *
Bcl2-interacting killer-like	2.14	1.26	1.08 *	1.64
colony stimulating factor 3 receptor (granulocyte)	2.11	1.44	2.39	-1.13 *
RIKEN cDNA 9130019O22 gene putative zinc-finger containing protein	1.94	1.69	1.05 *	-2.50
hyaluronan mediated motility receptor (RHAMM)	1.91	1.20	1.05	1.35
pterin 4 alpha carbinolamine dehydratase/dimerization cofactor of hepatocyte nuclear factor 1 alpha (TCF1) 1	-1.91 *	1.07 *	-1.09 *	1.58
Sjogren syndrome antigen B	-1.98	-1.11	-1.44	-1.10 *
src homology 2 domain-containing transforming protein C1	-2.01	1.04	1.37	1.14
elongation factor Tu GTP binding domain containing 2	-2.02	1.12	-1.47	-1.08
synaptotagmin III	-2.04 *	1.02 *	-1.77	1.14
RNA binding motif protein, X chromosome, mRNA	-2.06	-1.85	-1.16 *	1.17 *
Expressed sequence AW538196 (AW538196), mRNA	-2.08	1.12 *	1.20	-1.13 *
RIKEN cDNA 5730466C23 gene	-2.11	1.27	-1.02	1.40
phenylalanine-tRNA synthetase-like, alpha subunit	-2.12	1.17	1.20	-1.74
---	-2.12	-1.18	-1.18	-1.93
RIKEN cDNA 1810057C19 gene	-2.17	-1.72	1.07	-1.50 *
melanoma antigen, family A, 7	-2.26	-2.04	1.12	1.75
plakophilin 3	-2.27	-1.52	-1.38 *	-1.25 *
solute carrier organic anion transporter family, member 1c1	-2.28	-1.33	1.53	-1.36 *
3-hydroxybutyrate dehydrogenase (heart, mitochondrial)	-2.36	-1.50	-1.04	1.55
contactin associated protein-like 2	-2.36	1.17	1.10	-1.13
forkhead box N4	-2.51	-2.09	-1.43	-1.87
forkhead box O3a	-2.83	-1.19 *	1.12 *	-1.26
reproductive homeobox on X chromosome, 9	-2.89	1.15	-1.00	-1.66 *
serine (or cysteine) peptidase inhibitor, clade D, member 1	-2.96	-1.00	1.08	-2.92 *
lysyl oxidase-like 4	-3.04	1.25	1.02	-1.08
CD28 antigen	-3.10	1.01	-1.54	1.14
solute carrier family 35 (UDP-galactose transporter), member 2	-3.35	1.67	1.35	-1.25
aldo-keto reductase family 1, member C18	-3.67	-1.76 *	-1.39 *	1.48
CD28 antigen	-6.46 *	1.18	-1.14	1.02
solute carrier family 35, member A5	-6.63	-1.84	-1.25	-1.23

Table B1 MLC/Class 1 IGF-1Ea list of up- and down-regulated genes. A selection of genes that were either up- or down-regulated by 1.9-fold. Genes in bold are unique for the Class 1 IGF1-1Ea transgenic samples, i.e. they scored an increase or decrease of 1.9-fold in the Class 1 IGF-1Ea transgenic while at the same time scoring less than 1.3-fold up- or down-regulation in the other three transgenic models. The presence of a star on the right of some values indicates a higher variability of the signal intensity between the two RNA samples analyzed for each model.

GENE NAME	1 EA	1 EB	2 EA	2 EB
insulin-like growth factor 1	25.52 *	3.32	15.69	1.80
zinc finger protein, subfamily 1A, 1 (Ikaros)	2.91 *	2.79 *	2.07 *	2.55 *
matrix metalloproteinase 7	1.01	2.74 *	-1.14	-1.54
bromodomain adjacent to zinc finger domain, 1B	2.14 *	2.68	-1.21	1.65 *
Monoclonal antiidiotypic antibody IgK (hypervariable region) mRNA	1.54 *	2.01	1.14 *	1.39
DIX domain containing 1	2.82	2.00 *	2.29	3.29
CEA-related cell adhesion molecule 1	1.11	1.96	1.46	1.79
N-terminal Asn amidase, mRNA (cDNA clone MGC:29106 IMAGE:5037501)	1.53	1.95	1.22	1.78
T-cell receptor beta, variable 13	1.64	1.94	1.25	2.03
protein tyrosine phosphatase, non-receptor type 13	-1.41	-1.90	-1.18	1.13
Kruppel-like factor 4 (gut)	-1.11	-1.93	-1.63	-1.07
CD3 antigen, zeta polypeptide	1.05	-1.93	-1.20	1.02
cytidine monophospho-N-acetylneuraminic acid hydroxylase	-1.11 *	-1.93	-1.80	-1.02
ecotropic viral integration site 5	1.12	-1.94	-2.29 *	-2.40 *
uroplakin 1A	-1.08 *	-1.96	1.21	1.19
RNA binding motif protein, X chromosome, mRNA	1.07	-1.96	-1.14	-1.03
presenilin 2	-1.22	-1.97	-1.05	1.32
heat shock protein 1B	-1.02	-1.98	1.16 *	-1.98
fascin homolog 1, actin bundling protein	1.15	-1.99	1.18	1.09
deoxyuridine triphosphatase	1.29	-2.03	-1.10	1.31
sodium channel, nonvoltage-gated 1 beta	-1.04 *	-2.03	-1.07	-1.00
melanoma antigen, family A, 7	-2.26	-2.04	1.12	1.75
Ras association (RalGDS/AF-6) domain family 7	-1.81 *	-2.05 *	-1.21	-1.15
peroxisome biogenesis factor 16	1.38	-2.07	-1.56 *	-1.88
forkhead box N4	-2.51	-2.09	-1.43	-1.87
RIKEN cDNA 1200007D18 gene	1.14 *	-2.11	-1.15	-1.18
SH3 multiple domains 1	1.05 *	-2.11	1.22	-1.10
membrane metallo endopeptidase	1.01	-2.11 *	1.08	-1.14
neuron specific gene family member 2	1.31	-2.12	1.09	-1.21
Ros1 proto-oncogene	1.37 *	-2.13	1.04	1.25
glutamate receptor, ionotropic, NMDA2D (epsilon 4)	1.26	-2.23	-1.58	-1.18
heat shock protein 1A	1.02	-2.25	1.37	-1.88
nuclear factor of kappa light polypeptide gene enhancer in B-cells 2, p49/p100	-1.28 *	-2.46	-2.35	-2.09
DNA segment, Chr 7, ERATO Doi 462, expressed	-1.09 *	-2.61	-1.53 *	-1.06
immunoglobulin superfamily, member 4B	1.00	-2.82	1.47	-1.23 *
target of myb1-like 1 (chicken)	1.42	-2.98 *	-1.56 *	-1.02
myo-inositol oxygenase	-1.35 *	-3.17	-1.06	-1.23 *
RIKEN cDNA 5730507H05 gene	-1.21 *	-4.58	-4.22	-2.61 *

Table B2 MLC/Class 1 IGF-1Eb list of up- and down-regulated genes. A selection of genes that were either up- or down-regulated by 1.9-fold. Genes in bold are unique for the Class 1 IGF1-1Eb transgenic samples, i.e. they scored an increase or decrease of 1.9-fold in the Class 1 IGF-1Eb transgenic while at the same time scoring less than 1.3-fold up- or down-regulation in the other three transgenic models. The presence of a star on the right of some values indicates a higher variability of the signal intensity between the two RNA samples analyzed for each model.

GENE NAME	1 EA	1 EB	2 EA	2 EB
insulin-like growth factor 1	25.52 *	3.32	15.69	1.80
colony stimulating factor 3 receptor (granulocyte)	2.11	1.44	2.39	-1.13 *
gap junction membrane channel protein alpha 1	-1.03	1.13	2.33	-1.07
adaptor-related protein complex AP-4, mu 1	1.39	1.89	2.29	3.29
DIX domain containing 1	2.82	2.00 *	2.29	3.29
beta-site APP-cleaving enzyme 2	1.89	-1.32	2.27	-1.16 *
shroom	-1.07 *	-1.10 *	2.09	-2.63 *
zinc finger protein, subfamily 1A, 1 (Ikaros)	2.91 *	2.79 *	2.07 *	2.55 *
serine (or cysteine) peptidase inhibitor, clade A, member 3A	1.23 *	1.30	1.97	1.11
carbonic anhydrase 5a, mitochondrial	1.82	1.31 *	1.94	-1.02 *
FK506 binding protein 5 (immunophilin)	1.03 *	1.18 *	1.93	1.18
deltex 2 homolog (Drosophila)	1.09 *	-1.01	1.91	1.81
transmembrane protein 54	1.08	-1.18	-1.94	1.24
Slit-like 2 (Drosophila)	-1.30	-1.09	-1.95	-1.20
RNA binding motif protein, X chromosome, mRNA	-1.07	-1.16	-1.95	1.18
chloride channel CLIC-like 1	-1.14 *	-1.12	-1.99	-1.16
cytochrome P450, family 2, subfamily b, polypeptide 10	-1.03	-1.27 *	-2.02	-1.07
Bcl2-like 2	-1.30	1.00	-2.05 *	1.21
RIKEN cDNA 2310043L02 gene	1.25	1.39	-2.09	1.10
splicing factor proline/glutamine rich	-1.14	-1.42	-2.09	-1.18
phosphatidylserine synthase 2	-1.47 *	-1.02 *	-2.12	1.09
tRNA nucleotidyl transferase, CCA-adding, 1	-1.55	1.14	-2.14	1.36 *
C79248: similar to platelet-activated factor acetylhydrolase (PAF-AH)	1.50	-1.53	-2.15	-1.43
DnaJ (Hsp40) homolog, subfamily C, member 18	-1.34	-1.23	-2.16	-1.02
calcium regulated heat stable protein 1	1.20	1.09 *	-2.23	1.44
B-cell CLL/lymphoma 6, member B	1.20	-1.32 *	-2.25	1.36 *
cerebellin 1 precursor protein	-1.20	-1.34 *	-2.27	-1.64
CEA-related cell adhesion molecule 2	1.75 *	-1.58	-2.31	2.11 *
proteasome (prosome, macropain) 26S subunit, ATPase, 6	-1.41	1.12	-2.31	1.18
suppressor of cytokine signaling 3	-1.06	-1.25 *	-2.31	1.29 *
NF-kB 2, p49/p100	-1.28 *	-2.46	-2.35	-2.09
cell division cycle associated 3	1.30	-1.18 *	-2.42	1.14
tissue factor pathway inhibitor	1.18	-1.03 *	-2.46	1.21 *
cyclic AMP-regulated phosphoprotein, 21	1.52	-1.01	-2.52 *	-1.36
mutY homolog (E. coli)	1.15	-1.13 *	-2.54	-1.46
apoptosis antagonizing transcription factor	-1.04	1.36	-2.56 *	-1.08 *
integrin alpha 5 (fibronectin receptor alpha)	-1.81 *	-1.04	-2.66	1.18
calsyntenin 3	1.15	-1.76 *	-2.71	1.20
SRY-box containing gene 4 (Sox4), mRNA	1.68	-1.41 *	-2.85	1.21
coagulation factor VII	1.31	1.11 *	-2.86	1.09
aldehyde dehydrogenase 2, mitochondrial	-1.71 *	-1.12	-3.06	-1.51
tetraspan 1	-1.71	1.14	-3.12	-2.03 *
myelin basic protein expression factor 2, repressor	-1.85 *	1.03	-3.36 *	-1.06
Ubiquitin specific peptidase 7 (Usp7), mRNA	-1.31	-2.27 *	-3.39	-1.48 *
Notch-regulated ankyrin repeat protein	-1.18	1.14	-3.51 *	-1.11 *
scaffold attachment factor B2	-1.41 *	-1.65 *	-3.78	-2.41
zinc finger protein 503	1.12	-1.65 *	-3.94	-2.09 *
per-pentamer repeat gene	1.35	-1.06 *	-4.03	-1.27
thyroid stimulating hormone, beta subunit	1.07	1.17 *	-4.03 *	1.12
contactin associated protein-like 2	1.71	1.39	-5.11	1.37
splA/ryanodine receptor domain and SOCS box containing 4	1.45	1.40	-7.87 *	1.58

Table B3 MLC/Class 2 IGF-1Ea list of up- and down-regulated genes. A selection of genes that were either up- or down-regulated by 1.9-fold. Genes in bold are unique for the Class 2 IGF1-1Ea transgenic samples, i.e. they scored an increase or decrease of 1.9-fold in the Class 2 IGF-1Ea transgenic while at the same time scoring less than 1.3-fold up- or down regulation in the other three transgenic models. The presence of a star on the right of some values indicates a higher variability of the signal intensity between the two RNA samples analyzed for each model.

GENE NAME	1 EA	1 EB	2 EA	2 EB
DIX domain containing 1	2.82	2.00 *	2.29	3.29
adaptor-related protein complex AP-4, mu 1	1.39	1.89 *	2.29	3.29
zinc finger protein, subfamily 1A, 1 (Ikaros)	2.91 *	2.79 *	2.07 *	2.55 *
homeodomain interacting protein kinase 2	1.35	1.33	1.43	2.34
WAP four-disulfide core domain 2	1.23 *	-1.05 *	-1.02 *	2.18
CEA-related cell adhesion molecule 2	1.75 *	-1.58	-2.31	2.11 *
ferritin mitochondrial	1.63	1.58	1.18	2.07
T-cell receptor beta, variable 13	1.64	1.94	1.25	2.03
EH-domain containing 1	1.14	-1.26	1.33	-1.93
angiopoietin-like 1	-1.29	1.03	1.09	-1.93 *
heat shock protein 1B	-1.02	-1.98	1.16 *	-1.98
homeo box C5	1.02	1.17	1.42	-1.99
tetraspan 1	-1.71	1.14	-3.12	-2.03 *
Rho GTPase activating protein 4	1.10 *	-1.80	1.32	-2.04
nuclear factor of kappa light polypeptide gene enhancer in B-cells 2, p49/p100	-1.28 *	-2.46	-2.35	-2.09
RNA binding motif protein, X chromosome, mRNA	1.40	-1.20	1.01 *	-2.09
ephrin B3	-1.13	1.00 *	1.29	-2.09
transmembrane protein 45b	-1.18	-1.04	-1.09	-2.13
erythroid associated factor	1.07	-1.51 *	1.47	-2.18
procollagen, type II, alpha 1	-1.16	1.05	-1.59	-2.23 *
sphingomyelin phosphodiesterase 2, neutral	-1.13 *	-1.64 *	1.22	-2.23
PKD2 interactor, golgi and endoplasmic reticulum associated 1	-1.00	-1.03 *	1.22	-2.30
scaffold attachment factor B2	-1.41 *	-1.65 *	-3.78	-2.41
phosphoenolpyruvate carboxykinase 1, cytosolic	-1.17 *	-1.00	1.15	-2.49
RIKEN cDNA 9130019O22, putative zinc finger protein	1.94	1.69	1.05 *	-2.50
mast cell protease 5	1.30	-1.34	1.13	-2.61 *
Shroom	-1.07 *	-1.10 *	2.09	-2.63 *
endothelin 1	-1.08 *	1.02	-1.10	-2.67 *
serine (or cysteine) peptidase inhibitor, clade D, member 1	-2.96	-1.00	1.08	-2.92 *
potassium channel, subfamily K, member 7	1.29	-1.23	-1.07	-3.12
myosin, light polypeptide 4	-1.20 *	-1.12	-1.83 *	-3.21
major urinary protein 1 and 3	-1.13 *	1.05 *	-1.01	-3.38
cofactor required for Sp1 transcriptional activation, subunit 6	-1.92 *	-1.20	-1.71 *	-3.58
RIKEN cDNA 5730410I19 gene	1.05	-1.32	-1.18	-3.96
Sulfiredoxin 1 homolog (S. cerevisiae) (Srxn1), mRNA	1.01	-1.45	1.45	-4.44

Table B4 MLC/Class 2 IGF-1Eb list of up- and down-regulated genes. A selection of genes that were either up- or down-regulated by 1.9-fold. Genes in bold are unique for the Class 2 IGF1-1Eb transgenic samples, i.e. they scored an increase or decrease of 1.9-fold in the Class 2 IGF-1Eb transgenic while at the same time scoring less than 1.3-fold up- or down regulation in the other three transgenic models. The presence of a star on the right of some values indicates a higher variability of the signal intensity between the two RNA samples analyzed for each model.

GENE NAME	1 Ea	1 Eb	2 Ea	2 Eb
melanoma antigen, family A, 7	-2.26	-2.04	1.12	1.75
DNA segment, Chr 2, ERATO Doi 63, expressed	-2.05 *	-1.58	1.01	1.61
transmembrane channel-like gene family 1	-1.89 *	-1.31	1.33	1.17
cofactor required for Sp1 transcriptional activation, subunit 2	-1.49 *	-1.84 *	1.01	1.19
potassium voltage-gated channel, shaker-related subfamily, member 1	-1.63 *	-1.56 *	1.06	1.14
potassium voltage-gated channel, shaker-related subfamily, beta member 1	-1.53	-1.35	1.04	1.25
melanophilin	-1.45	-1.46 *	1.12	1.09
growth differentiation factor 11	-1.47	-1.33	1.04	1.03
3-hydroxybutyrate dehydrogenase (heart, mitochondrial)	-2.36	-1.50	-1.04	1.55
small EDRK-rich factor 1	-2.06	-1.85	-1.16 *	1.17 *
6-phosphofructo-2-kinase/fructose-2,6-biphosphatase 3	-1.60	-1.74 *	-1.17 *	1.08
PHD finger protein 2	-1.74	-1.30	1.22	-1.14
protein kinase C, gamma	-1.34	-1.32	-1.21 *	1.46
Ras association (RalGDS/AF-6) domain family 7	-1.81 *	-2.05 *	-1.21	-1.15
toll-like receptor 9	1.43	1.59	1.11 *	-1.02
ubiquitination factor E4B, UFD2 homolog (S. cerevisiae)	1.62	1.53	-1.03	1.08 *
syndecan 3	1.57 *	1.53	-1.37	1.10
Immunoglobulin kappa light variable region (IgKV gene)	1.90	1.36	1.02	-1.64 *
protocadherin beta 8	1.35	1.31	-1.30 *	-1.00
apolipoprotein B editing complex 3	1.41	1.41	-1.06 *	-1.10
Syntaxin 5A, mRNA (cDNA clone MGC:25518 IMAGE:3487476)	1.40	1.48	-1.12	-1.03
RIKEN cDNA 9130019O22 gene	1.94	1.69	1.05 *	-2.50
antigen identified by monoclonal antibody Ki 67	1.46	1.32	-1.11	-1.23
bleomycin hydrolase	1.36	1.32	-1.35	-1.29
keratin associated protein 5-1	1.52 *	1.52 *	-1.07	-1.38
zinc finger protein 30	1.45	1.52	-1.41 *	-1.38
hyaluronidase 3	1.42 *	2.14 *	-1.15	-1.23
midasin homolog (yeast)	1.72	1.30 *	-1.67 *	-1.32 *
solute carrier family 16 (monocarboxylic acid transporters), member 11	2.30	1.32 *	-1.22 *	-1.40

Table B5 List of up- and down-regulated genes only in response to Class 1 isoforms. A selection of genes, that were either up- or down-regulated by 1.3-fold only in the Class 1 IGF-1-expressing transgenic samples. The presence of a star on the right of some values indicates a higher variability of the signal intensity between the two RNA samples analyzed for each model.

GENE NAME	1 Ea	1 Eb	2 Ea	2 Eb
cyclin D1	1.31	1.04	-2.13 *	-1.89 *
interleukin 4 receptor, alpha	1.47 *	1.26	-1.56	-1.83
phosphatidylinositol glycan, class O	1.19 *	1.47	-1.58	-1.80 *
Prkr interacting protein 1 (IL11 inducible)	1.37 *	1.20 *	-1.35 *	-1.41 *
ADP-ribosylation factor 3	1.21	1.08	-1.32 *	-1.68
protein tyrosine phosphatase, receptor type, C	1.47	1.12	-1.31	-1.36
REX4, RNA exonuclease 4 homolog (S. cerevisiae)	1.10	1.05	-1.53	-1.31
DEAD (Asp-Glu-Ala-Asp) box polypeptide 39	1.20	1.00	-1.35	-1.33
A kinase (PRKA) anchor protein 10	1.02	1.14 *	-1.38	-1.31 *
cyclic AMP-regulated phosphoprotein, 21	1.52	-1.01	-2.52 *	-1.36
TSC22 domain family, member 1	-1.04	1.12 *	-2.20 *	-1.45 *
procollagen, type II, alpha 1	-1.16	1.05	-1.59	-2.23 *
neurobeachin-like 2	1.16	-1.05	-1.53	-1.84 *
lactate dehydrogenase 3, C chain, sperm specific	1.11	-1.18	-1.50	-1.85 *
progesterone receptor membrane component 2	-1.14	1.35	-1.31 *	-1.71 *
isopentenyl-diphosphate delta isomerase	1.02	-1.07	-1.54	-1.71
deiodinase, iodothyronine, type II	1.02	-1.01	-1.40	-1.77
tumor protein D52-like 1	1.06	-1.28	-1.50	-1.82
cDNA sequence BC002059	1.01	-1.08	-1.73	-1.41
annexin A2	-1.01	1.22	-1.39	-1.45 *
dystrobrevin alpha	1.18	-1.10	-1.53	-1.42
ring finger and FYVE like domain containing protein	-1.07	1.09	-1.49	-1.47
myosin, light polypeptide 4	-1.20 *	-1.12	-1.83 *	-3.21
poly (A) polymerase alpha	-1.02	-1.19	-1.69	-1.60 *
DNA segment, Chr 6, ERATO Doi 47, expressed	-1.04	-1.29	-1.88	-1.46 *
leucine-zipper-like transcriptional regulator, 1	-1.15	-1.24	-1.69	-1.51
HIV-1 Rev binding protein-like	-1.12	-1.15	-1.52	-1.52
hypoxia inducible factor 1, alpha subunit	1.21 *	1.07	1.36	1.76 *
alcohol dehydrogenase 1 (class I)	1.05	1.05	1.61	1.34
mitogen-activated protein kinase kinase kinase kinase 5	1.15 *	1.02 *	1.44	1.63 *
phosphatidylinositol-3-phosphate/phosphatidylinositol 5-kinase, type III	1.14 *	-1.15 *	1.33	1.62
X-linked myotubular myopathy gene 1	-1.41 *	1.10	1.55 *	1.37
deltex 2 homolog (Drosophila)	1.09 *	-1.01	1.91	1.81
decapping enzyme, scavenger	-1.29	-1.41	1.39	1.38

Table B6 List of up- and down-regulated genes only in response to Class 2 isoforms. A selection of genes that were either up- or down-regulated by 1.3-fold only in the Class 2 IGF-1-expressing transgenic samples. The presence of a star on the right of some values indicates a higher variability of the signal intensity between the two RNA samples analyzed for each model.

GENE NAME	1 Ea	2 Ea	1 Eb	2 Eb
CD28 antigen	-3.10	-1.54	1.01	1.14
proteasome (prosome, macropain) 26S subunit, ATPase, 6	-1.41	-2.31	1.12	1.18
synaptotagmin III	-2.04 *	-1.77	1.02 *	1.14
src homology 2 domain-containing transforming protein C3	-1.61	-1.66 *	1.17	1.07
myelin basic protein expression factor 2, repressor	-1.85 *	-3.36 *	1.03	-1.06
asparagine-linked glycosylation 1 homolog	-1.36	-1.31	1.01	1.30
myosin, heavy polypeptide 6, cardiac muscle, alpha	-1.37	-1.32	1.06	1.21 *
integrin alpha 5 (fibronectin receptor alpha)	-1.81 *	-2.66	-1.04	1.18
NADH dehydrogenase (ubiquinone) 1 alpha subcomplex 10	-1.42 *	-3.14 *	-1.10 *	1.12
phosphatidylserine synthase 2	-1.47 *	-2.12	-1.02 *	1.09
elongation factor Tu GTP binding domain containing 2	-2.02	-1.47	1.12	-1.08
RecQ protein-like	-1.70 *	-1.66	-1.09	1.19 *
regulator of G-protein signaling 5	-1.37	-1.83	-1.03	1.27
zinc finger, FYVE domain containing 19	-1.40 *	-1.67	1.19 *	-1.06
Rho GTPase activating protein 21	-1.46	-1.50 *	-1.04 *	1.02
protein kinase, cGMP-dependent, type I	-1.47	-2.32 *	-1.23 *	-1.17
DnaJ (Hsp40) homolog, subfamily C, member 18	-1.34	-2.16	-1.23	-1.02
Sjogren syndrome antigen B	-1.98	-1.44	-1.11	-1.10 *
ring finger protein 11	-1.50	-1.69	-1.06	-1.11
neutral sphingomyelinase (N-SMase) activation associated factor	-1.33	-1.74	-1.01	-1.05
tumor necrosis factor receptor superfamily, member 19	-1.37	-1.78	-1.10	-1.06
enhancer of yellow 2 homolog (Drosophila)	-1.49	-1.61	-1.11	-1.11
ATPase, H ⁺ transporting, lysosomal accessory protein 2	-1.45	-1.38	-1.02	-1.02
CDC42 effector protein (Rho GTPase binding) 3	-1.42 *	-1.46	-1.10	-1.02
methylenetetrahydrofolate dehydrogenase (NAD ⁺ dependent)	-1.31	-1.47	-1.04	-1.04
GTP binding protein 4	-1.49	-1.37	-1.14	-1.12
ADP-ribosylation factor-like 6 interacting protein 6	-1.42 *	-1.44	-1.09	-1.29
fibroblast growth factor 11	-1.36	-1.50	-1.23	-1.28
RAS related protein 1b	-1.33	-1.36	-1.23	-1.11
Rho GTPase activating protein 5	1.65	1.30	1.11	1.20
upregulated during skeletal muscle growth 1	1.40	1.47	1.17	1.04 *
sushi domain containing 4	1.45	1.43	1.16	1.04
growth factor receptor bound protein 2-associated protein 3	1.48	1.42	1.02	1.08 *
SH3-domain GRB2-like 2	1.32	1.76 *	1.22 *	1.02
trace amine-associated receptor 1	1.32	1.77	1.10	1.15
DNA segment, Chr 9, ERATO Doi 720, expressed	1.53	1.65	1.05	1.29
keratin complex 1, acidic, gene 24	1.88	1.56	1.05 *	1.27
leucine rich repeat containing G protein coupled receptor 5	1.91 *	1.58 *	1.24	1.02
adaptor protein with pleckstrin homology and src	1.38	1.57	-1.03	1.08
RASD family, member 2	1.66	1.40	1.16 *	-1.01
synaptotagmin XII	1.31	1.62	1.09	-1.09
laminin, beta 3	1.37	1.56	1.17	-1.33 *
midasin homolog (yeast)	1.58	1.56 *	1.01	-1.11
ankyrin repeat and SOCS box-containing protein 6	1.53 *	1.70 *	-1.04	1.02
CEA-related cell adhesion molecule 2	1.32	1.85	-1.54	1.06
Rho GDP dissociation inhibitor (GDI) gamma	1.32	1.32	-1.27	-1.06
mbt domain containing 1	1.32	1.35	-1.31	-1.02 *
endothelin converting enzyme 2	1.38	1.52	-1.23 *	-1.06
expressed in non-metastatic cells 6, protein	1.64	1.50	-1.18 *	-1.01
phosphatidylinositol membrane-associated 1	1.53	1.61 *	-1.21 *	-1.05 *
lin 7 homolog b (C. elegans)	1.34	1.41	-1.60	-1.10
beta-site APP-cleaving enzyme 2	1.89	2.27	-1.32	-1.16 *
proline rich protein HaeIII subfamily 1	3.83 *	2.99 *	-1.42	-1.09

Table B7 List of up- and down-regulated genes only in response to Ea isoforms. A selection of genes that were either up- or down-regulated by 1.3-fold only in the IGF-1Ea-expressing transgenic samples. The presence of a star on the right of some values indicates a higher variability of the signal intensity between the two RNA samples analyzed for each model.

GENE NAME	1 Ea	2 Ea	1 Eb	2 Eb
Sulfiredoxin 1 homolog (S. cerevisiae) (Srxn1), mRNA	1.01	1.45	-1.45	-4.44
heat shock protein 1A	1.02	1.37	-2.25	-1.88
mast cell protease 5	1.30	1.13	-1.34	-2.61 *
CD52 antigen	1.35 *	-1.13 *	-2.13 *	-3.99
Rho GTPase activating protein 4	1.10 *	1.32	-1.80	-2.04
lactalbumin, alpha	1.45	1.26 *	-1.63 *	-1.91 *
erythroid associated factor	1.07	1.47	-1.51 *	-2.18
activating transcription factor 3	1.01	1.34	-1.83	-1.41
leucine-rich repeat kinase 1	1.30	1.02	-1.48	-1.71 *
Immunoglobulin A heavy chain variable region (IGHV gene), clone WJ17	1.34 *	1.04	-1.50 *	-1.63 *
heat shock protein 1B	-1.02	1.16 *	-1.98	-1.98
sphingomyelin phosphodiesterase 2, neutral	-1.13 *	1.22	-1.64 *	-2.23
early B-cell factor 3	1.01	-1.09	-1.39	-1.69
transient receptor potential cation channel, subfamily M, member 7	-1.06	1.00	-1.55	-1.49 *
thyrotroph embryonic factor	-1.13	1.07	-1.30	-1.67
DNA segment, Chr 16, ERATO Doi 472, expressed	1.07	-1.04	-1.31	-1.34
solute carrier family 5 (choline transporter), member 7	-1.15	-1.05	-1.57	-1.69
chemokine (C-C motif) ligand 6	-1.04	-1.07	-1.66 *	-1.39
cholinergic receptor, nicotinic, alpha polypeptide 4	-1.26 *	-1.08	-1.77 *	-1.50
ribosomal protein S9	-1.24	-1.15	-1.36	-1.76
RIKEN cDNA 4631403P03 gene	-1.05	-1.09	-1.31	-1.36 *
EGF-like-domain, multiple 9	-1.24	-1.20	-1.35	-1.55
RER1 retention in endoplasmic reticulum 1 homolog (S. cerevisiae)	1.01	-1.03	1.32	1.61
scratch homolog 1, zinc finger protein (Drosophila)	-1.01 *	1.19 *	1.48	1.76
eukaryotic translation initiation factor 3, subunit 6 interacting protein	1.02 *	-1.35	1.31	1.85

Table B8 List of up- and down-regulated genes only in response to Eb isoforms. A selection of genes that were either up- or down-regulated by 1.3-fold only in the IGF-1Eb-expressing transgenic samples. The presence of a star on the right of some values indicates a higher variability of the signal intensity between the two RNA samples analyzed for each model.

Appendix C: Ingenuity pathway analysis

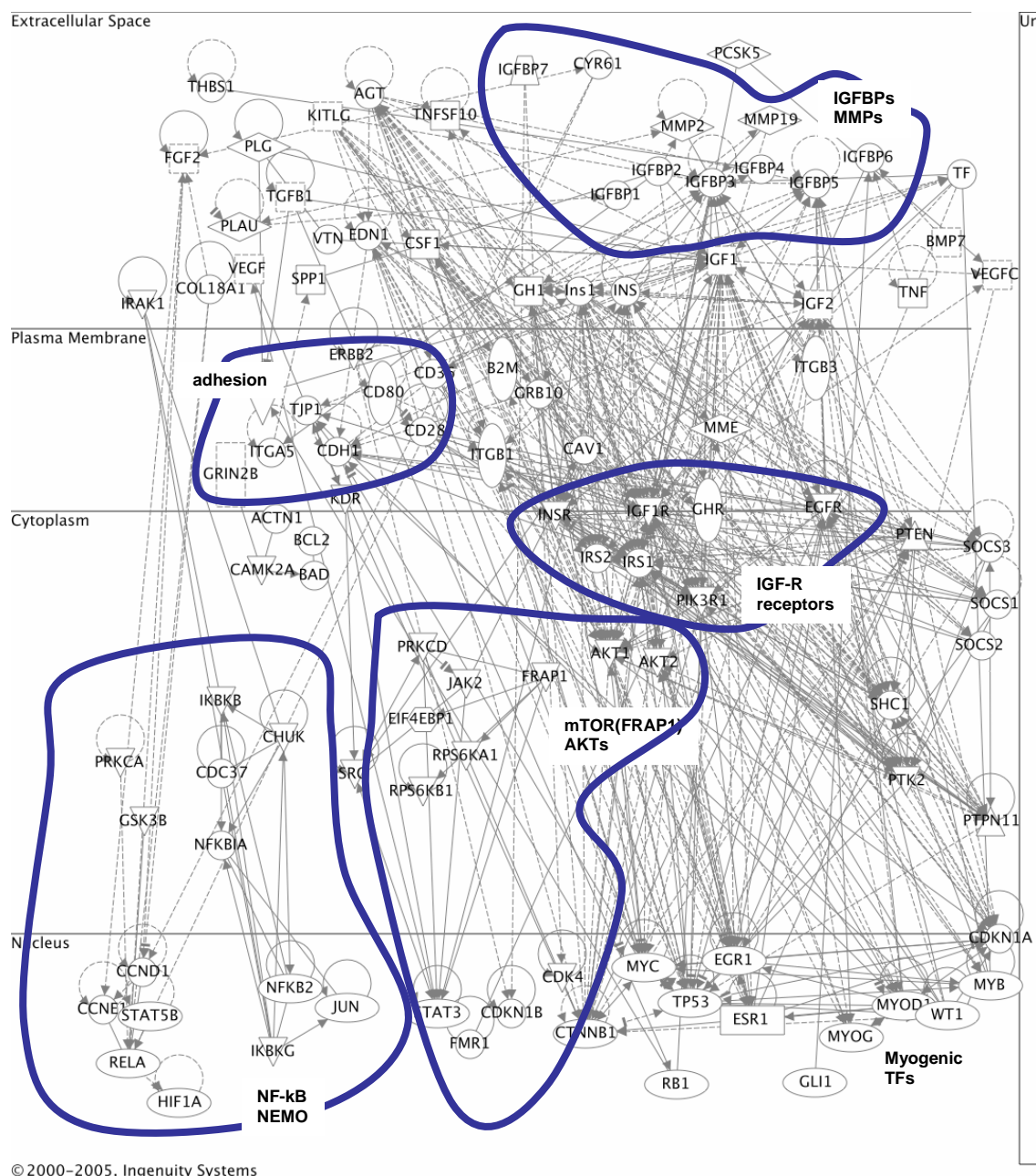


Figure C1 Example of an IGF-1 network constructed with Ingenuity. The interaction network related to IGF-1 was built according to the information available at Ingenuity Inc. The different circles highlight genes involved or related to NF- κ B, mTOR/Akt or IGF-1 receptor pathways, as well as to adhesion function, extracellular IGFBPs and metalloproteases.

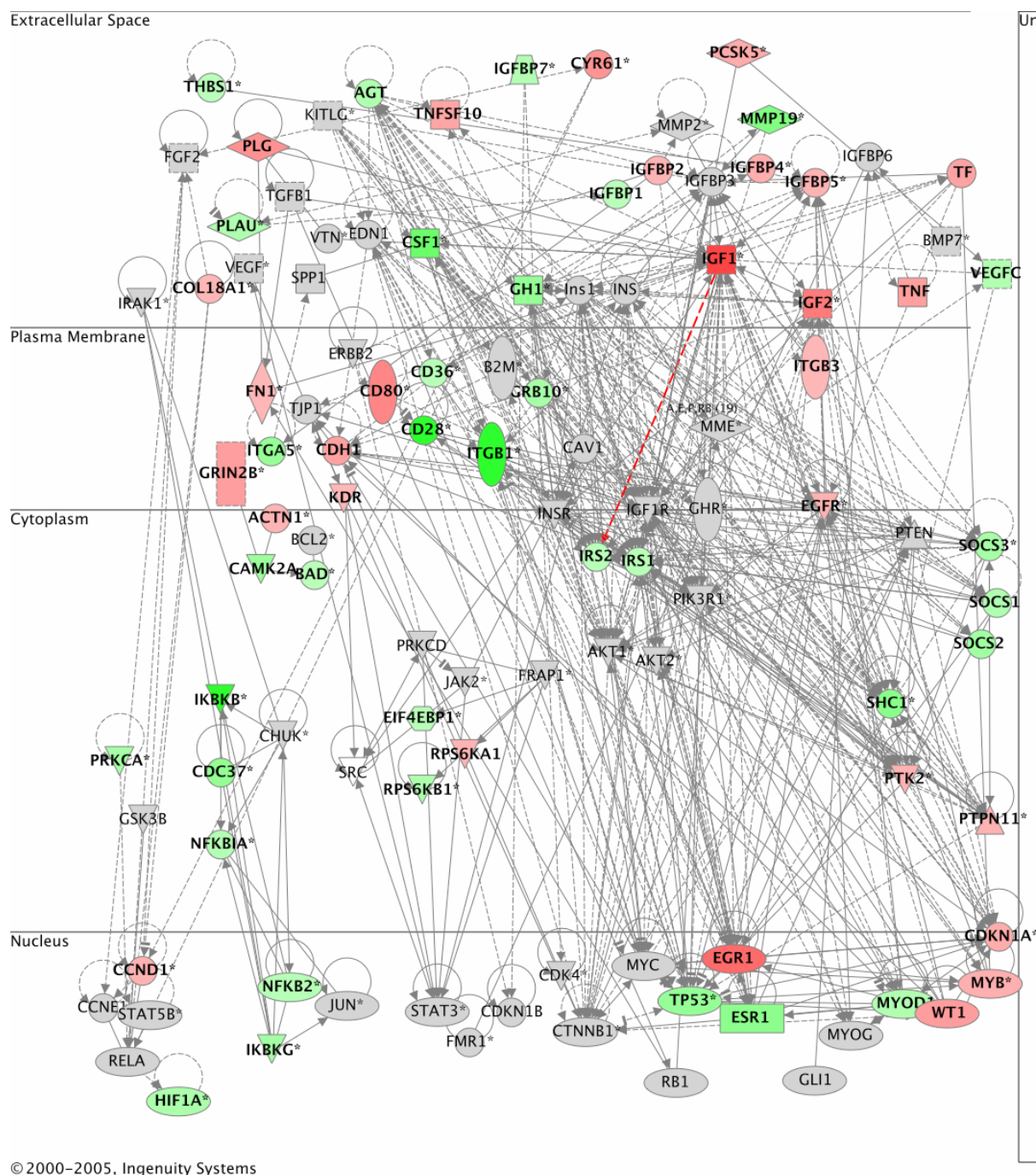


Figure C2 MLC/Class 1 IGF-1Ea overlay of regulated genes in the Ingenuity IGF-1 network. Genes that are either up-regulated (red) or down-regulated (green) at least 1.3-fold in Class 1 IGF-1Ea transgenic muscles, compared to WT, were mapped against the IGF-1 network built by using the Ingenuity Pathway Analysis software platform.

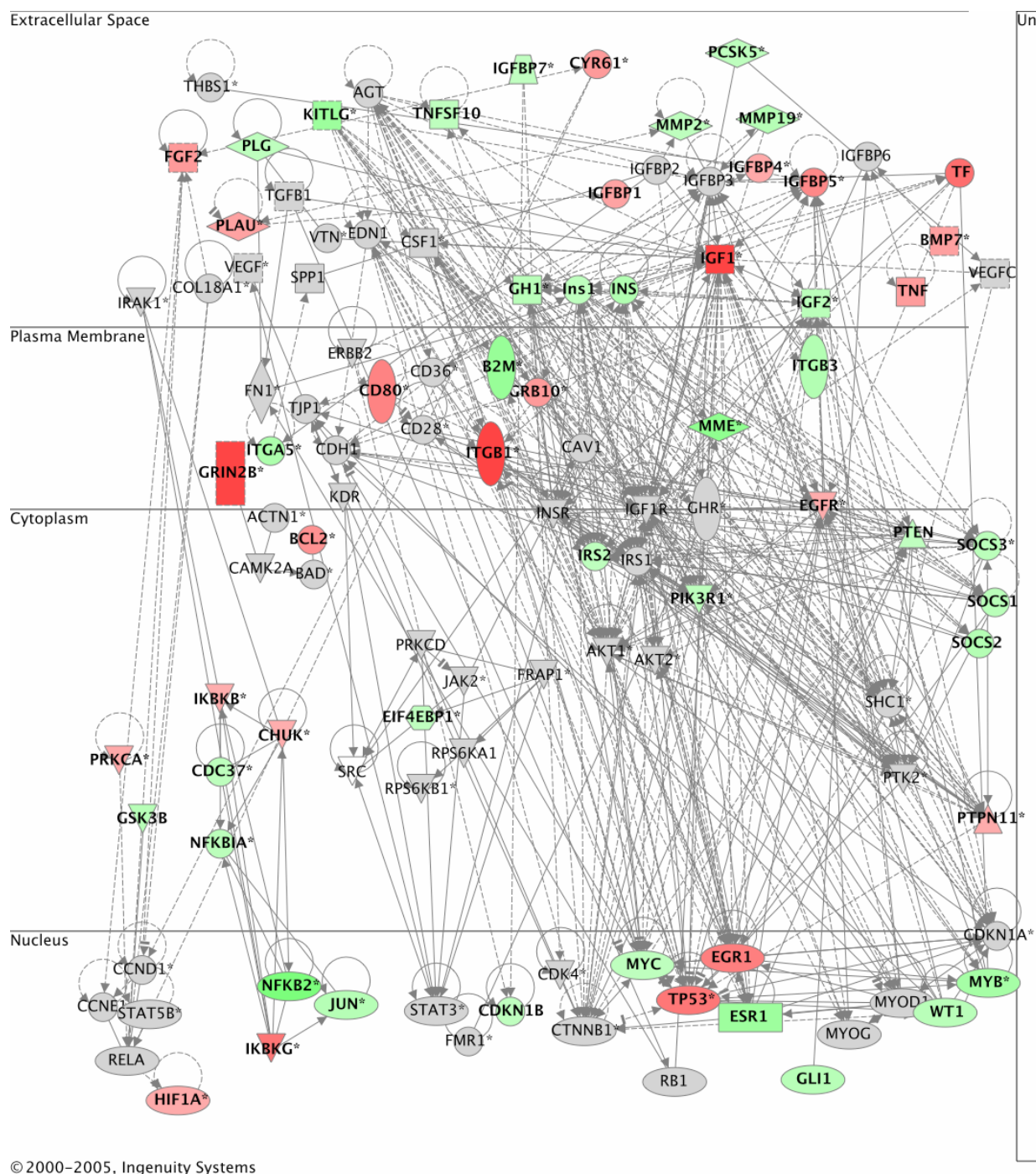


Figure C3 MLC/Class 1 IGF-1Eb overlay of regulated genes in the Ingenuity IGF-1 network. Genes that are either up-regulated (red) or down-regulated (green) at least 1.3-fold in Class 1 IGF-1Eb transgenic muscles, compared to WT, were mapped against the IGF-1 network built by using the Ingenuity Pathway Analysis software platform.

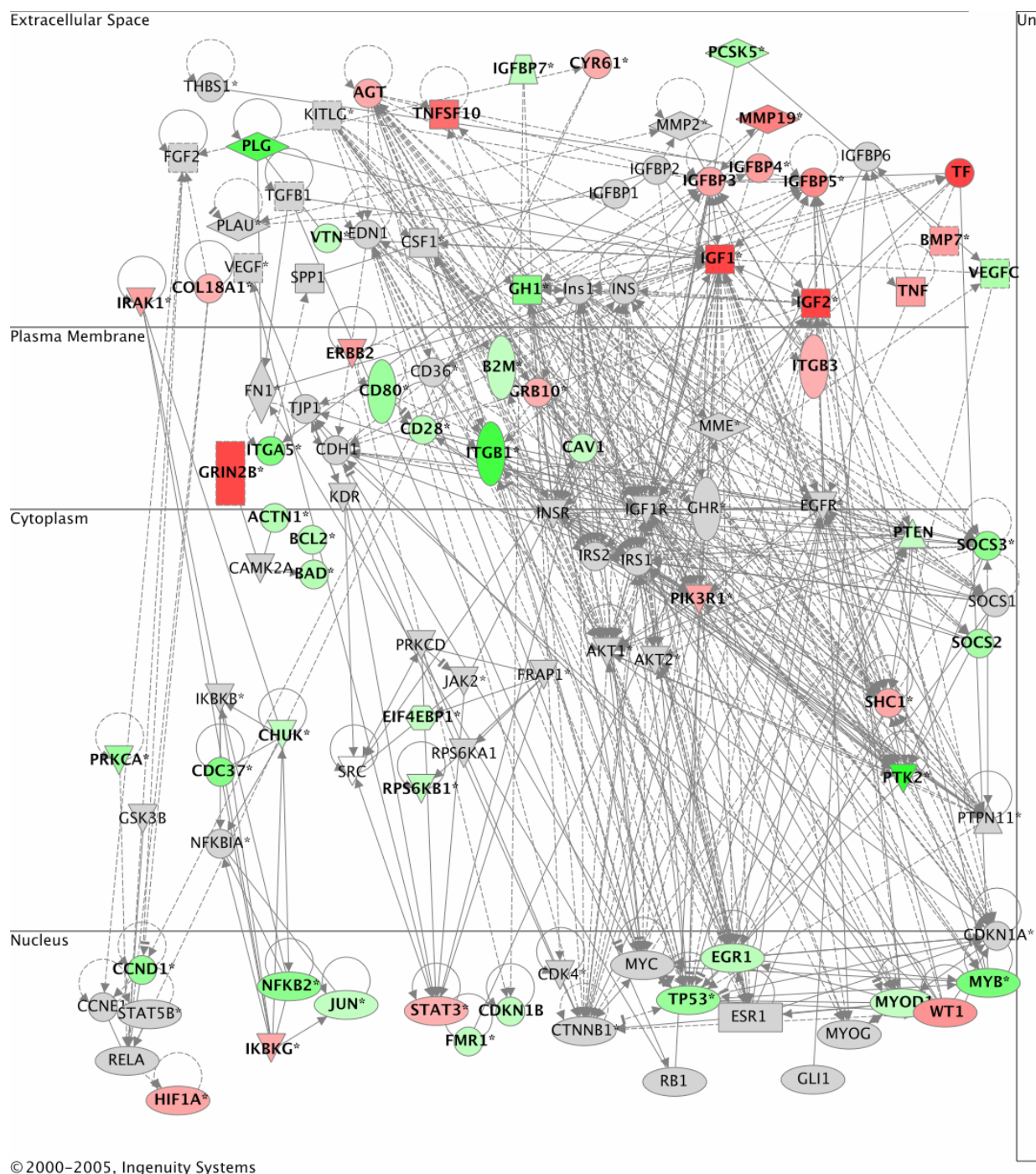


Figure C4 MLC/Class 2 IGF-1Ea overlay of regulated genes in the Ingenuity IGF-1 network. Genes that are either up-regulated (red) or down-regulated (green) at least 1.3-fold in Class 2 IGF-1Ea transgenic muscles, compared to WT, were mapped against the IGF1 network built by using the Ingenuity Pathway Analysis software platform.

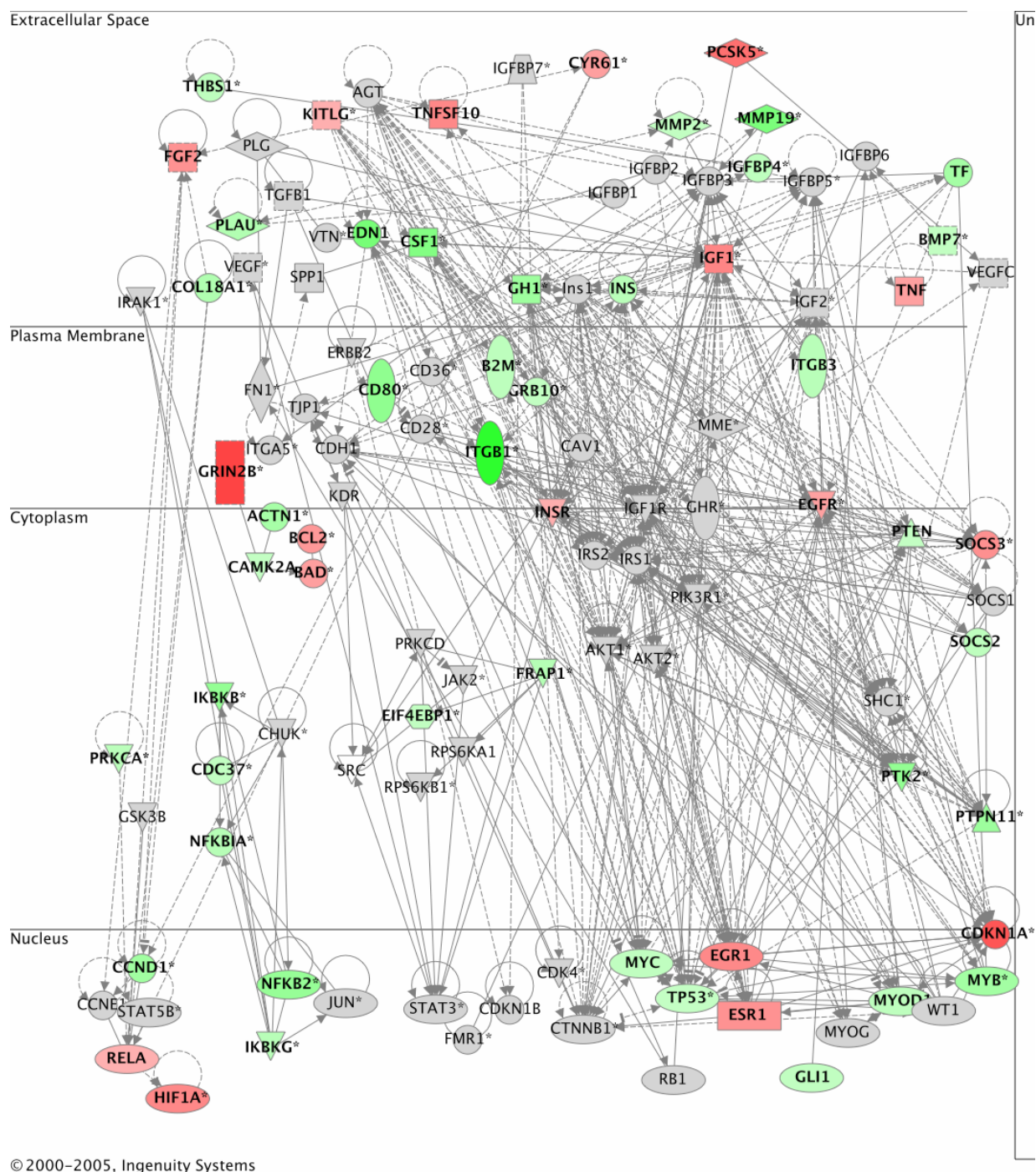


Figure C5 MLC/Class 2 IGF-1Eb overlay of regulated genes in the Ingenuity IGF-1 network. Genes that are either up-regulated (red) or down-regulated (green) at least 1.3 fold in Class 2 IGF-1Eb transgenic muscles, compared to WT, were mapped against the IGF1 network built by using the Ingenuity Pathway Analysis software platform.

Table C1 List of Ingenuity gene abbreviations

ACTN1	<i>actinin, alpha 1</i>	INSR	<i>insulin receptor</i>
AGT	<i>angiotensinogen</i>	IRAK1	<i>interleukin-1 receptor-associated kinase 1</i>
AKT1	<i>thymoma viral proto-oncogene 1</i>	IRS1	<i>insulin receptor substrate 1</i>
AKT2	<i>thymoma viral proto-oncogene 2</i>	IRS2	<i>insulin receptor substrate 2</i>
B2M	<i>beta-2 microglobulin</i>	ITGA5	<i>integrin alpha 5</i>
BAD	<i>Bcl-associated death promoter</i>	ITGB1	<i>integrin beta 1</i>
BCL2	<i>B-cell leukemia/lymphoma 2</i>	ITGB3	<i>integrin beta 3</i>
BMP7	<i>bone morphogenetic protein 7</i>	JAK2	<i>Janus kinase 2</i>
CAMK2A	<i>calcium/calmodulin-dependent protein kinase II alpha</i>	JUN	<i>Jun oncogene</i>
CAV1	<i>caveolin, caveolae protein 1</i>	KDR	<i>kinase insert domain protein receptor</i>
CCND1	<i>cyclin D1</i>	KITLG	<i>kit ligand</i>
CCNE1	<i>cyclin E1</i>	MME	<i>membrane metallo endopeptidase</i>
CD28	<i>CD28 antigen</i>	MMP19	<i>matrix metalloproteinase 19</i>
CD36	<i>CD36 antigen</i>	MMP2	<i>matrix metalloproteinase 2</i>
CD80	<i>CD80 antigen</i>	MYB	<i>MYB (myeloblastosis oncogene)</i>
CDC37	<i>cell division cycle 37 homolog</i>	MYC	<i>c-myc</i>
CDH1	<i>cadherin 1</i>	MYOD1	<i>MyoD</i>
CDK4	<i>cyclin-dependent kinase 4</i>	MYOG	<i>myogenin</i>
CDKN1A	<i>cyclin-dependent kinase inhibitor 1A (P21)</i>	NFKB2	<i>nuclear factor of kappa light polypeptide gene enhancer in B-cells 2, p49/p100</i>
CDKN1B	<i>cyclin-dependent kinase inhibitor 1B (P27)</i>	NFKBIA	<i>nuclear factor of kappa light chain gene enhancer in B-cells inhibitor, alpha</i>
CHUK	<i>conserved helix-loop-helix ubiquitous kinase</i>	PCSK5	<i>proprotein convertase subtilisin/kexin type 5</i>
COL18A1	<i>procollagen, type XVIII, alpha 1</i>	PIK3R1	<i>phosphatidylinositol 3-kinase, regulatory subunit</i>
CSF1	<i>colony stimulating factor 1 (macrophage)</i>	PLAU	<i>plasminogen activator, urokinase</i>
CTNNB1	<i>beta-catenin</i>	PLG	<i>plasminogen</i>
CYR61	<i>cysteine rich protein 61 (IGFBP10)</i>	PRKCA	<i>protein kinase C, alpha</i>
EDN1	<i>endothelin 1</i>	PRKCD	<i>protein kinase C, delta</i>
EGFR	<i>epidermal growth factor receptor</i>	PTEN	<i>phosphatase and tensin homolog</i>
EGR1	<i>early growth response 1</i>	PTK2	<i>Focal Adhesion Kinase</i>
EIF4EBP1	<i>eukaryotic translation initiation factor 4E binding protein 1</i>	PTPN11	<i>protein tyrosine phosphatase, non-receptor type 11</i>
ERBB2	<i>v-erb-b2 erythroblastic leukemia viral oncogene homolog 2</i>	RB1	<i>retinoblastoma 1</i>
ESR1	<i>estrogen receptor 1 (alpha)</i>	RELA	<i>v-rel reticuloendotheliosis viral oncogene homolog A</i>
FGF2	<i>fibroblast growth factor 2</i>	RPS6KA1	<i>ribosomal protein S6 kinase polypeptide 1</i>
FMR1	<i>fragile X mental retardation syndrome 1 homolog</i>	RPS6KB1	<i>ribosomal protein S6 kinase, polypeptide 1</i>
FN1	<i>fibronectin 1</i>	SHC1	<i>src homology 2 domain-containing transforming protein C1</i>
FRAP1	<i>mTOR</i>	SOCS1	<i>suppressor of cytokine signaling 1</i>
GH1	<i>growth hormone</i>	SOCS2	<i>suppressor of cytokine signaling 2</i>
GHR	<i>growth hormone receptor</i>	SOCS3	<i>suppressor of cytokine signaling 3</i>
GLI1	<i>GLI-Kruppel family member GLI1</i>	SPP1	<i>secreted phosphoprotein 1</i>
GRB10	<i>growth factor receptor bound protein 10</i>	SRC	<i>src</i>
GRIN2B	<i>glutamate receptor, ionotropic, NMDA2B</i>	STAT3	<i>STAT 3</i>
GSK3B	<i>glycogen synthase kinase 3 beta</i>	STAT5B	<i>STAT 5B</i>
HIF1A	<i>hypoxia inducible factor 1, alpha subunit</i>	TF	<i>transferrin</i>
IGF1	<i>insulin-like growth factor 1</i>	TGFB1	<i>transforming growth factor, beta 1</i>
IGF1R	<i>insulin-like growth factor I receptor</i>	THBS1	<i>thrombospondin 1</i>
IGF2	<i>insulin-like growth factor 2</i>	TJP1	<i>tight junction protein 1</i>
IGFBP1	<i>insulin-like growth factor binding protein 1</i>	TNF	<i>tumor necrosis factor</i>
IGFBP2	<i>insulin-like growth factor binding protein 2</i>	TNFSF10	<i>tumor necrosis factor (ligand) superfamily</i>
IGFBP3	<i>insulin-like growth factor binding protein 3</i>	TP53	<i>transformation related protein 53</i>
IGFBP4	<i>insulin-like growth factor binding protein 4</i>	VEGF	<i>vascular endothelial growth factor A</i>
IGFBP5	<i>insulin-like growth factor binding protein 5</i>	VEGFC	<i>vascular endothelial growth factor C</i>
IGFBP6	<i>insulin-like growth factor binding protein 6</i>	VTN	<i>vitronectin</i>
IGFBP7	<i>insulin-like growth factor binding protein 7</i>	WT1	<i>Wilms tumor homolog</i>
IKBKB	<i>inhibitor of kappaB kinase beta</i>		
IKBKG	<i>inhibitor of kappaB kinase gamma</i>		
INS	<i>insulin II</i>		
Ins1	<i>insulin I</i>		

Bibliography

1. Buckingham, M., *Skeletal muscle formation in vertebrates*. Curr Opin Genet Dev, 2001. **11**(4): p. 440-8.
2. Pourquie, O., *Vertebrate somitogenesis*. Annu Rev Cell Dev Biol, 2001. **17**: p. 311-50.
3. Arnold, H.H. and T. Braun, *Genetics of muscle determination and development*. Curr Top Dev Biol, 2000. **48**: p. 129-64.
4. Christ, B. and C.P. Ordahl, *Early stages of chick somite development*. Anat Embryol (Berl), 1995. **191**(5): p. 381-96.
5. Wolpert, L., et al., *Principles of Development*. 1998, Oxford: Current Biology. 484.
6. Bailey, P., T. Holowacz, and A.B. Lassar, *The origin of skeletal muscle stem cells in the embryo and the adult*. Curr Opin Cell Biol, 2001. **13**(6): p. 679-89.
7. Pourquie, O., et al., *Lateral and axial signals involved in avian somite patterning: a role for BMP4*. Cell, 1996. **84**(3): p. 461-71.
8. Amthor, H., B. Christ, and K. Patel, *A molecular mechanism enabling continuous embryonic muscle growth - a balance between proliferation and differentiation*. Development, 1999. **126**(5): p. 1041-53.
9. Ordahl, C.P. and N.M. Le Douarin, *Two myogenic lineages within the developing somite*. Development, 1992. **114**(2): p. 339-53.
10. Edmondson, D.G. and E.N. Olson, *Helix-loop-helix proteins as regulators of muscle-specific transcription*. J Biol Chem, 1993. **268**(2): p. 755-8.
11. Buckingham, M., *Making muscle in mammals*. Trends Genet, 1992. **8**(4): p. 144-8.
12. Rudnicki, M.A., et al., *Inactivation of MyoD in mice leads to up-regulation of the myogenic HLH gene Myf-5 and results in apparently normal muscle development*. Cell, 1992. **71**(3): p. 383-90.
13. Braun, T., et al., *Targeted inactivation of the muscle regulatory gene Myf-5 results in abnormal rib development and perinatal death*. Cell, 1992. **71**(3): p. 369-82.
14. Nabeshima, Y., et al., *Myogenin gene disruption results in perinatal lethality because of severe muscle defect*. Nature, 1993. **364**(6437): p. 532-5.
15. Hasty, P., et al., *Muscle deficiency and neonatal death in mice with a targeted mutation in the myogenin gene*. Nature, 1993. **364**(6437): p. 501-6.
16. Kablar, B., et al., *MyoD and Myf-5 differentially regulate the development of limb versus trunk skeletal muscle*. Development, 1997. **124**(23): p. 4729-38.
17. Kablar, B. and M.A. Rudnicki, *Skeletal muscle development in the mouse embryo*. Histol Histopathol, 2000. **15**(2): p. 649-56.
18. Weintraub, H., *The MyoD family and myogenesis: redundancy, networks, and thresholds*. Cell, 1993. **75**(7): p. 1241-4.
19. Tajbakhsh, S., et al., *Differential activation of Myf5 and MyoD by different Wnts in explants of mouse paraxial mesoderm and the later activation of myogenesis in the absence of Myf5*. Development, 1998. **125**(21): p. 4155-62.
20. Palmer, C.M. and M. Rudnicki, *The myogenic regulatory factors*. IN: Advances in Developmental Biology and Biochemistry: Stem cells and cell signalling in skeletal myogenesis; Sassoon, D.A. (ed.) Elsevier Science, 2002: p. pp. 1-32.
21. Pirskanen, A., J.C. Kiefer, and S.D. Hauschka, *IGFs, insulin, Shh, bFGF, and TGF-beta1 interact synergistically to promote somite myogenesis in vitro*. Dev Biol, 2000. **224**(2): p. 189-203.
22. Seed, J. and S.D. Hauschka, *Temporal separation of the migration of distinct myogenic precursor populations into the developing chick wing bud*. Dev Biol, 1984. **106**(2): p. 389-93.
23. Mauro, A., *Satellite cells of skeletal muscle fibers*. J Biophys Biochem Cytol, 1961. **9**: p. 493-495.
24. Partridge, T., *Reenthronement of the muscle satellite cell*. Cell, 2004. **119**: p. 447-448.
25. Clark, K.A., et al., *Striated muscle cytoarchitecture: an intricate web of form and function*. Annu Rev Cell Dev Biol, 2002. **18**: p. 637-706.

26. Bonnemann, C.G. and N.G. Laing, *Myopathies resulting from mutations in sarcomeric proteins*. Curr Opin Neurol, 2004. **17**(5): p. 529-37.
27. Burkin, D.J. and S.J. Kaufman, *The alpha7beta1 integrin in muscle development and disease*. Cell and Tissue Research, 1999. **296**(1): p. 183-90.
28. Grounds, M.D., L. Sorokin, and J. White, *Strength at the extracellular matrix-muscle interface*. Scand J Med Sci Sports, 2005. **15**(6): p. 381-91.
29. Blake, D.J., et al., *Function and genetics of dystrophin and dystrophin-related proteins in muscle*. Physiol Rev, 2002. **82**(2): p. 291-329.
30. Michele, D.E. and K.P. Campbell, *Dystrophin-glycoprotein complex: post-translational processing and dystroglycan function*. J Biol Chem, 2003. **278**(18): p. 15457-60.
31. Engel, A., and B.Banker, *Myology Basic and Clinical*. 1986: McGraw-Hill Book Company.
32. Shavlakadze, T.a.M.D.G., *Therapeutic interventions for age-related muscle wasting: importance of innervation and exercise for preventing sarcopenia*. In: Modulating aging and longevity, 2003: p. 139-166.
33. Schiaffino, S. and G. Salvati, *Molecular diversity of myofibrillar proteins: isoforms analysis at the protein and mRNA level*. in: Meth. in Cell Biol., 1997. **i**: p. 349-369.
34. Buonanno, A. and N. Rosenthal, *Molecular control of muscle diversity and plasticity*. Dev Genet, 1996. **19**(2): p. 95-107.
35. Roy, R.R., et al., *Modulation of myonuclear number in functionally overloaded and exercised rat plantaris fibers*. J Appl Physiol, 1999. **87**(2): p. 634-42.
36. Paul, A.C. and N. Rosenthal, *Different modes of hypertrophy in skeletal muscle fibers*. J Cell Biol, 2002. **156**(4): p. 751-60.
37. Rosenblatt, J.D., D. Yong, and D.J. Parry, *Satellite cell activity is required for hypertrophy of overloaded adult rat muscle*. Muscle & Nerve, 1994. **17**: p. 608-613.
38. Semsarian, C., et al., *Insulin-like growth factor (IGF-I) induces myotube hypertrophy associated with an increase in anaerobic glycolysis in a clonal skeletal-muscle cell model*. Biochem J, 1999. **339**(Pt 2)(1 Pt 1): p. 443-51.
39. Rommel, C., et al., *Mediation of IGF-1-induced skeletal myotube hypertrophy by PI(3)K/Akt/mTOR and PI(3)K/Akt/GSK3 pathways*. Nat Cell Biol, 2001. **3**(11): p. 1009-13.
40. Jacquemin, V., et al., *IGF-1 induces human myotube hypertrophy by increasing cell recruitment*. Exp Cell Res, 2004. **299**(1): p. 148-58.
41. Barton-Davis, E.R., Shiturma, D.I., Sweeney, H.L., *Contribution of satellite cells to IGF-I induced hypertrophy of skeletal muscle*. Acta Physiol. Scand., 1999. **167**: p. 301-305.
42. Lowe, D.A. and S.E. Alway, *Stretch-induced myogenin, MyoD, and MRF4 expression and acute hypertrophy in quail slow-tonic muscle are not dependent upon satellite cell proliferation*. Cell Tissue Res, 1999. **296**(3): p. 531-9.
43. Rennie, M.J., H. Wackerhage, E.E. Spangenburg, and F.W. Booth, *Control of the size of the human muscle mass*. Annu Rev Physiol, 2004. **66**: p. 799-828.
44. Criswell, D.S., et al., *Overexpression of IGF-I in skeletal muscle of transgenic mice does not prevent unloading-induced atrophy*. Am J Physiol, 1998. **275**(3 Pt 1): p. E373-9.
45. Gutmann, E., *The denervated muscle*. Vol. 486pp. 1962, Prague: Publishing house of the Czechoslovak Academy of Sciences.
46. Schulze, P.C., et al., *Transgenic overexpression of locally acting insulin-like growth factor-1 inhibits ubiquitin-mediated muscle atrophy in chronic left-ventricular dysfunction*. Circ Res, 2005. **97**(5): p. 418-26.
47. Gomes, M.D., et al., *Atrogin-1, a muscle-specific F-box protein highly expressed during muscle atrophy*. Proc Natl Acad Sci U S A, 2001. **98**(25): p. 14440-5.
48. Fang, C.H., B.J. Li, C.J. Wray, and P.O. Hasselgren, *Insulin-like growth factor-1 inhibits lysosomal and proteasome-dependent proteolysis in skeletal muscle after burn injury*. J Burn Care Rehabil, 2002. **23**: p. 318-325.
49. Fang, C.H., et al., *Insulin-like growth factor I reduces ubiquitin and ubiquitin-conjugating enzyme gene expression but does not inhibit muscle proteolysis in septic rats*. Endocrinology, 2000. **141**(8): p. 2743-51.

50. Chrysis, D. and L.E. Underwood, *Regulation of components of the ubiquitin system by insulin-like growth factor I and growth hormone in skeletal muscle of rats made catabolic with dexamethasone*. *Endocrinology*, 1999. **140**(12): p. 5635-41.
51. Price, S.R., J.L. Bailey, X. Wang, C. Jurkowitz, B.K. England, X. Ding, L.S. Phillips, and W.E. Mitch, *Muscle wasting in insulinopenic rats results from activation of the ATP-dependent, ubiquitin-proteasome proteolytic pathway by a mechanism including gene-transcription*. *J Clin Invest*, 1996. **98**: p. 1703-1708.
52. Baracos, V.E., et al., *Activation of the ATP-ubiquitin-proteasome pathway in skeletal muscle of cachectic rats bearing a hepatoma*. *Am J Physiol*, 1995. **268**(5 Pt 1): p. E996-1006.
53. Gonzalez-Cadavid, N.F., et al., *Organization of the human myostatin gene and expression in healthy men and HIV-infected men with muscle wasting*. *Proc Natl Acad Sci U S A*, 1998. **95**(25): p. 14938-43.
54. Lynch, G., T. Shavlakadze, and M. Grounds, *Evaluation of strategies to reduce age-related skeletal muscle wasting*. *IN Aging interventions and therapies*, ed. S. Rattan. 2005, Singapore: World Scientific publishers.
55. Goldberg, A.L., et al., *Hormonal regulation of protein degradation and synthesis in skeletal muscle*. *Fed Proc*, 1980. **39**(1): p. 31-6.
56. Wing, S.S., and A.L. Goldberg, *Glucocorticoids activate the ATP-ubiquitin-dependent proteolytic system in skeletal muscle during fasting*. *Am J Physiol*, 1993. **264**: p. E668-676.
57. Kettelhut, I.C., et al., *Regulation of different proteolytic pathways in skeletal muscle in fasting and diabetes mellitus*. *Braz J Med Biol Res*, 1994. **27**(4): p. 981-93.
58. Argiles, J.M., S.H. Meijsing, J. Pallares-Trujillo, X. Guirao, and F.J. Lopez-Soriano, *Cancer cachexia: a therapeutic approach*. *Med Res Rev*, 2001. **21**: p. 83-101.
59. Lecker, S.H., et al., *Multiple types of skeletal muscle atrophy involve a common program of changes in gene expression*. *Faseb J*, 2004. **18**(1): p. 39-51.
60. Latres, E., A.R. Amini, A.A. Amini, J. Griffiths, F.J. Martin, Y. Wei, H.C. Lin, G.D. Yancopoulos, D.J. Glass, *IGF-1 inversely regulates atrophy-induced genes via the PI3/Akt/mTOR pathway*. *J Biol Chem*, 2004. **280**: p. 2737-44.
61. Bodine, S.C., et al., *Akt/mTOR pathway is a crucial regulator of skeletal muscle hypertrophy and can prevent muscle atrophy in vivo*. *Nat Cell Biol*, 2001. **3**(11): p. 1014-9.
62. Sandri, M., et al., *Foxo transcription factors induce the atrophy-related ubiquitin ligase atrogin-1 and cause skeletal muscle atrophy*. *Cell*, 2004. **117**(3): p. 399-412.
63. Stitt, T.N., D. Drujan, B.A. Clarke, F. Panaro, Y. Timofeyva, W.O. Kline, M. Gonzalez, G.D. Yancopoulos, D.J. Glass, *The IGF-1/PI3K/Akt pathway prevents expression of muscle atrophy-induced ubiquitin ligases by inhibiting FOXO transcription factors*. *Mol Cell*, 2004. **14**: p. 395-403.
64. Song, Y.H., et al., *Muscle-specific expression of IGF-1 blocks angiotensin II-induced skeletal muscle wasting*. *J Clin Invest*, 2005. **115**(2): p. 451-8.
65. Musaro, A. and N. Rosenthal, *Transgenic mouse models of muscle aging*. *Exp Gerontol*, 1999. **34**(2): p. 147-56.
66. Morley, J.E., et al., *Sarcopenia*. *J Lab Clin Med*, 2001. **137**(4): p. 231-43.
67. Booth, F.W. and D.S. Criswell, *Molecular events underlying skeletal muscle atrophy and the development of effective countermeasures*. *Int J Sports Med*, 1997. **18**(Suppl 4): p. S265-9.
68. Alnaqueeb, M., and Goldspink, G., *Changes in fibre type, number, and diameter in developing and aging muscle*. *J Anat*, 1987. **153**: p. 31-34.
69. Musaro, A., et al., *Enhanced expression of myogenic regulatory factors in aging skeletal muscle*. *Exp. Cell Res.*, 1995. **221**: p. 241-248.
70. Carmeli, E., R. Coleman, and A.Z. Reznick, *The biochemistry of aging muscle*. *Exp Gerontol*, 2002. **37**(4): p. 477-89.
71. Linton, S., M.J. Davies, and R.T. Dean, *Protein oxidation and ageing*. *Exp Gerontol*, 2001. **36**(9): p. 1503-18.

72. Matsuo, M., *Age-related alterations in antioxidant defense*. In: B.P. Yu (Ed.), *Free Radical in Aging*. Boca Raton, FL: CRC, 1993: p. pp 143-181.
73. Rosen, D.R., et al., *Mutations in Cu/Zn superoxide dismutase gene are associated with familial amyotrophic lateral sclerosis*. *Nature*, 1993. **362**(6415): p. 59-62.
74. Gurney, M.E., et al., *Motor neuron degeneration in mice that express a human Cu,Zn superoxide dismutase mutation*. *Science*, 1994. **264**(5166): p. 1772-5.
75. Velasco, B., et al., *Growth hormone gene expression and secretion in aging rats is age dependent and not age-associated weight increase related*. *Endocrinology*, 1998. **139**(3): p. 1314-20.
76. Barton-Davis, E.R., et al., *Viral mediated expression of insulin-like growth factor I blocks the aging-related loss of skeletal muscle function*. *Proc Natl Acad Sci U S A*, 1998. **95**(26): p. 15603-7.
77. Musaro, A., et al., *Localized Igf-1 transgene expression sustains hypertrophy and regeneration in senescent skeletal muscle*. *Nat Genet*, 2001. **27**(2): p. 195-200.
78. Dobrowolny, G., et al., *Muscle expression of a local Igf-1 isoform protects motor neurons in an ALS mouse model*. *J Cell Biol*, 2005. **168**(2): p. 193-9.
79. Clarkson, P.M. and M.J. Hubal, *Exercise-induced muscle damage in humans*. *Am J Phys Med Rehabil*, 2002. **81**(11 Suppl): p. S52-69.
80. Lieber, R.L. and J. Friden, *Mechanisms of muscle injury gleaned from animal models*. *Am J Phys Med Rehabil*, 2002. **81**(11 Suppl): p. S70-9.
81. Teague, B.N. and J.A. Schwane, *Effect of intermittent eccentric contractions on symptoms of muscle microinjury*. *Med Sci Sports Exerc*, 1995. **27**(10): p. 1378-84.
82. McCully, K.K. and J.A. Faulkner, *Injury to skeletal muscle fibers of mice following lengthening contractions*. *J. Appl. Physiol.*, 1985. **59**: p. 547-559.
83. Brooks, S. and J. Faulkner, *Contraction induced injury: Recovery of skeletal muscles in young and old mice*. *Am. J. Physiol.*, 1990. **258**(Cell Physiol 7): p. C436-C442.
84. Tsivitse, S.K., et al., *Downhill running in rats: influence on neutrophils, macrophages, and MyoD+ cells in skeletal muscle*. *Eur J Appl Physiol*, 2003. **90**(5-6): p. 633-8.
85. Hansen-Smith, F.M. and B.M. Carlson, *Cellular responses to free grafting of the extensor digitorum longus muscle of the rat*. *J Neurol Sci*, 1979. **41**(2): p. 149-73.
86. Roberts, P., et al., *Initiation and duration of myogenic precursor cell replication in transplants of intact skeletal muscles: an autoradiographic study in mice*. *Anat Rec*, 1989. **224**(1): p. 1-6.
87. Engel, A.G. and C. Franzini-Armstrong, eds. *Myology: Basic and Clinical*. 2 ed., ed. W.J. Lamsback and M. Navrozov. Vol. 1. 1994, McGraw-Hill: New York. 1129.
88. Mitchell, C.A., J.K. McGeachie, and M.D. Grounds, *Cellular differences in the regeneration of murine skeletal muscle: a quantitative histological study in SJL/J and BALB/c mice*. *Cell Tissue Res*, 1992. **269**(1): p. 159-66.
89. Couteaux, R., J.C. Mira, and A. d'Albis, *Regeneration of muscles after cardiotoxin injury. I. Cytological aspects*. *Biol Cell*, 1988. **62**(2): p. 171-82.
90. Barton, E.R., et al., *Muscle-specific expression of insulin-like growth factor I counters muscle decline in mdx mice*. *J Cell Biol*, 2002. **157**(1): p. 137-48.
91. Shavlakadze, T., et al., *Targeted expression of insulin-like growth factor-I reduces early myofiber necrosis in dystrophic mdx mice*. *Mol Ther*, 2004. **10**(5): p. 829-43.
92. Carlson, B.M., *The regeneration of minced muscles*. 1972, Basel: Krager.
93. Grounds, M.D. and J.K. McGeachie, *Myogenic cell replication in minced skeletal muscle isografts of Swiss and BALBc mice*. *Muscle Nerve*, 1990. **13**(4): p. 305-13.
94. Robertson, T.A., J.M. Papadimitriou, and M.D. Grounds, *Fusion of myogenic cells to the newly sealed region of damaged myofibres in skeletal muscle regeneration*. *Neuropathol Appl Neurobiol*, 1993. **19**(4): p. 350-8.
95. McGeachie, J.K. and M.D. Grounds, *Initiation and duration of muscle precursor replication after mild and severe injury to skeletal muscle of mice. An autoradiographic study*. *Cell Tissue Res*, 1987. **248**(1): p. 125-30.
96. Papadimitriou, J.M., et al., *The process of new plasmalemma formation in focally injured skeletal muscle fibers*. *J Struct Biol*, 1990. **103**(2): p. 124-34.

97. Robertson, T.A., et al., *The role of macrophages in skeletal muscle regeneration with particular reference to chemotaxis*. Exp Cell Res, 1993. **207**(2): p. 321-31.
98. Schmalbruch, H., *Muscle regeneration: fetal myogenesis in a new setting*. Bibl Anat, 1986(29): p. 126-53.
99. Hansen-Smith, F.M., B.M. Carlson, and K.L. Irwin, *Revascularization of the freely grafted extensor digitorum longus muscle in the rat*. Am J Anat, 1980. **158**(1): p. 65-82.
100. Roberts, P., and J.K. McGeachie, *The influence of revascularisation, vasoactive drugs and exercise on the regeneration of skeletal muscle, with particular reference to muscle transplantation*. BAM, 1992. **2**: p. 5-16.
101. Roberts, P. and J.K. McGeachie, *Endothelial cell activation during angiogenesis in freely transplanted skeletal muscles in mice and its relationship to the onset of myogenesis*. J Anat, 1990. **169**: p. 197-207.
102. Smythe, G.M., et al., *Adeno-associated virus-mediated vascular endothelial growth factor gene therapy in skeletal muscle before transplantation promotes revascularization of regenerating muscle*. Tissue Eng, 2002. **8**(5): p. 879-91.
103. Watson, A.C. and A.R. Muir, *Failure of free muscle grafts in dogs*. Br J Plast Surg, 1976. **29**(1): p. 27-33.
104. Markley, J.M., J.A. Faulkner, and B.M. Carlson, *Regeneration of skeletal muscle after grafting in monkeys*. Plast Reconstr Surg, 1978. **62**(3): p. 415-22.
105. Lavine, D.M. and T.A. Cochran, *The failure to survive of autogenous free grafts of whole gracilis muscles in dogs*. Plast Reconstr Surg, 1976. **58**(2): p. 221-7.
106. Tidball, J.G., *Inflammatory cell response to acute muscle injury*. Med Sci Sports Exerc, 1995. **27**(7): p. 1022-32.
107. Pizza, F.X., et al., *Neutrophils injure cultured skeletal myotubes*. Am J Physiol Cell Physiol, 2001. **281**(1): p. C335-41.
108. Husmann, I., et al., *Growth factors in skeletal muscle regeneration*. Cytokine Growth Factor Rev, 1996. **7**(3): p. 249-58.
109. Wiendl, H., R. Hohlfeld, and B.C. Kieseier, *Immunobiology of muscle: advances in understanding an immunological microenvironment*. Trends Immunol, 2005. **26**(7): p. 373-80.
110. Mourkioti, F. and N. Rosenthal, *IGF-1, inflammation and stem cells: interactions during muscle regeneration*. Trends Immunol, 2005. **26**(10): p. 535-42.
111. Chazaud, B., et al., *Satellite cells attract monocytes and use macrophages as a support to escape apoptosis and enhance muscle growth*. J Cell Biol, 2003. **163**(5): p. 1133-43.
112. Prisk, V. and J. Huard, *Muscle injuries and repair: the role of prostaglandins and inflammation*. Histol Histopathol, 2003. **18**(4): p. 1243-56.
113. Irintchev, A., et al., *Expression pattern of M-cadherin in normal, denervated, and regenerating mouse muscles*. Developmental Dynamics, 1994. **199**(4): p. 326-37.
114. Cornelison, D.D. and B.J. Wold, *Single-cell analysis of regulatory gene expression in quiescent and activated mouse skeletal muscle satellite cells*. Developmental Biology, 1997. **191**(2): p. 270-83.
115. Cornelison, D.D., et al., *Syndecan-3 and syndecan-4 specifically mark skeletal muscle satellite cells and are implicated in satellite cell maintenance and muscle regeneration*. Dev Biol, 2001. **239**(1): p. 79-94.
116. Oustanina, S., G. Hause, and T. Braun, *Pax7 directs postnatal renewal and propagation of myogenic satellite cells but not their specification*. Embo J, 2004. **23**(16): p. 3430-9.
117. Grounds, M.D., *Towards understanding skeletal muscle regeneration*. Pathol Res Pract, 1991. **187**(1): p. 1-22.
118. Asakura, A., et al., *Myogenic specification of side population cells in skeletal muscle*. J Cell Biol, 2002. **159**(1): p. 123-34.
119. Deasy, B.M., R.J. Jankowski, and J. Huard, *Muscle-derived stem cells: characterization and potential for cell-mediated therapy*. Blood Cells Mol Dis, 2001. **27**(5): p. 924-33.
120. Qu-Petersen, Z., et al., *Identification of a novel population of muscle stem cells in mice: potential for muscle regeneration*. J Cell Biol, 2002. **157**(5): p. 851-64.

121. Young, H.E., et al., *Human reserve pluripotent mesenchymal stem cells are present in the connective tissues of skeletal muscle and dermis derived from fetal, adult, and geriatric donors*. Anat Rec, 2001. **264**(1): p. 51-62.
122. McKinney-Freeman, S.L., et al., *Muscle-derived hematopoietic stem cells are hematopoietic in origin*. Proc Natl Acad Sci U S A, 2002. **99**(3): p. 1341-6.
123. Fukada, S., et al., *Muscle regeneration by reconstitution with bone marrow or fetal liver cells from green fluorescent protein-gene transgenic mice*. J Cell Sci, 2002. **115**(Pt 6): p. 1285-93.
124. LaBarge, M.A. and H.M. Blau, *Biological progression from adult bone marrow to mononucleate muscle stem cell to multinucleate muscle fiber in response to injury*. Cell, 2002. **111**(4): p. 589-601.
125. Goodell, M.A., *Multipotential stem cells and 'side population' cells*. Cytotherapy, 2002. **4**(6): p. 507-8.
126. Corbel, S.Y., et al., *Contribution of hematopoietic stem cells to skeletal muscle*. Nat Med, 2003. **9**(12): p. 1528-32.
127. Brazelton, T.R., M. Nystrom, and H.M. Blau, *Significant differences among skeletal muscles in the incorporation of bone marrow-derived cells*. Dev Biol, 2003. **262**(1): p. 64-74.
128. White, J.a.M.D.G., *Harnessing the therapeutic potential of myogenic stem cells*. Cytotechnology, 2003. **41**: p. 153-164.
129. Torrente, Y., et al., *Human circulating AC133(+) stem cells restore dystrophin expression and ameliorate function in dystrophic skeletal muscle*. J Clin Invest, 2004. **114**(2): p. 182-95.
130. Musaro, A., et al., *Stem cell-mediated muscle regeneration is enhanced by local isoform of insulin-like growth factor 1*. Proc Natl Acad Sci U S A, 2004. **101**(5): p. 1206-10.
131. Seale, P., A. Asakura, and M.A. Rudnicki, *The potential of muscle stem cells*. Dev Cell, 2001. **1**(3): p. 333-42.
132. Carlson, B.M., *Muscle regeneration in amphibians and mammals: passing the torch*. Dev Dyn, 2003. **226**: p. 167-181.
133. Le Roith, D., et al., *The somatomedin hypothesis: 2001*. Endocr Rev, 2001. **22**(1): p. 53-74.
134. Jones, J., and Clemmons, DR., *Insulin-like growth factors and their binding proteins: biological actions*. Endo Rev, 1995. **16**: p. 3-34.
135. Clemmons, D.R., et al., *Role of insulin-like growth factor binding proteins in modifying IGF actions*. Ann N Y Acad Sci, 1993. **692**: p. 10-21.
136. Twigg, S.M. and R.C. Baxter, *Insulin-like growth factor (IGF)-binding protein 5 forms an alternative ternary complex with IGFs and the acid-labile subunit*. J Biol Chem, 1998. **273**(11): p. 6074-9.
137. Twigg, S.M., K.V. Hardman, and R.C. Baxter, *A purified bovine serum albumin preparation contains an insulin-like growth factor (IGF) binding protein-3 fragment that forms ternary complexes selectively with IGF-II and the acid-labile subunit*. Growth Horm IGF Res, 2000. **10**(4): p. 215-23.
138. Ricort, J.M., *Insulin-like growth factor binding protein (IGFBP) signalling*. Growth Horm IGF Res, 2004. **14**(4): p. 277-86.
139. Murphy, L.J., *Insulin-like growth factor-binding proteins: functional diversity or redundancy?* J Mol Endocrinol, 1998. **21**(2): p. 97-107.
140. Rajkumar, K., et al., *Growth retardation and hyperglycemia in insulin-like growth factor binding protein-1 transgenic mice*. Endocrinology, 1995. **136**(9): p. 4029-34.
141. Hoeflich, A., et al., *Overexpression of insulin-like growth factor-binding protein-2 in transgenic mice reduces postnatal body weight gain*. Endocrinology, 1999. **140**(12): p. 5488-96.
142. Modric, T., et al., *Phenotypic manifestations of insulin-like growth factor-binding protein-3 overexpression in transgenic mice*. Endocrinology, 2001. **142**(5): p. 1958-67.

143. Bienvenu, G., et al., *Insulin-like growth factor binding protein-6 transgenic mice: postnatal growth, brain development, and reproduction abnormalities*. Endocrinology, 2004. **145**(5): p. 2412-20.
144. Salih, D.A., et al., *Insulin-like growth factor-binding protein 5 (Igfbp5) compromises survival, growth, muscle development, and fertility in mice*. Proc Natl Acad Sci U S A, 2004. **101**(12): p. 4314-9.
145. Kricker, J.A., C.L. Towne, S.M. Firth, A.C. Herington, and Z. Upton, *Structural and functional evidence for the interaction of insulin-like growth factors (IGF) and IGF-binding proteins with vitronectin*. Endocrinology, 2003. **144**: p. 2807-2815.
146. Hyde, C., et al., *Insulin-like growth factors (IGF) and IGF-binding proteins bound to vitronectin enhance keratinocyte protein synthesis and migration*. J Invest Dermatol, 2004. **122**(5): p. 1198-206.
147. Loechel, F., et al., *ADAM 12-S cleaves IGFBP-3 and IGFBP-5 and is inhibited by TIMP-3*. Biochem Biophys Res Commun, 2000. **278**(3): p. 511-5.
148. Arai, T., et al., *Heparin, heparan sulfate, and dermatan sulfate regulate formation of the insulin-like growth factor-I and insulin-like growth factor-binding protein complexes*. J Biol Chem, 1994. **269**(32): p. 20388-93.
149. Upton, Z., et al., *Identification of vitronectin as a novel insulin-like growth factor-II binding protein*. Endocrinology, 1999. **140**(6): p. 2928-31.
150. Winn, N., et al., *Insulin-like growth factor isoforms in skeletal muscle aging, regeneration, and disease*. Cold Spring Harb Symp Quant Biol, 2002. **67**: p. 507-18.
151. Shavlakadze, T., et al., *Reconciling data from transgenic mice that overexpress IGF-I specifically in skeletal muscle*. Growth Horm IGF Res, 2005. **15**(1): p. 4-18.
152. Daughaday, W.H., et al., *Somatomedin: proposed designation for sulphation factor*. Nature, 1972. **235**(5333): p. 107.
153. Svoboda, M.E., et al., *Purification of somatomedin-C from human plasma: chemical and biological properties, partial sequence analysis, and relationship to other somatomedins*. Biochemistry, 1980. **19**(4): p. 790-7.
154. Isaksson, O.G., J.O. Jansson, and I.A. Gause, *Growth hormone stimulates longitudinal bone growth directly*. Science, 1982. **216**(4551): p. 1237-9.
155. Isaksson, O.G., et al., *Mechanism of the stimulatory effect of growth hormone on longitudinal bone growth*. Endocr Rev, 1987. **8**(4): p. 426-38.
156. Schlechter, N.L., et al., *A direct growth effect of growth hormone in rat hindlimb shown by arterial infusion*. Am J Physiol, 1986. **250**(3 Pt 1): p. E231-5.
157. D'Ercole, A., Applewhite, G., and Underwood, L., *Evidence that somatomedin is synthesized by multiple tissues in the fetus*. Dev Biol, 1980. **75**: p. 315-328.
158. Lupu, F., J.D. Terwillinger, K. Lee, G.V. Segre, A. Egstradiadis, *Roles of growth hormone an insulin-like growth factor-1 in mouse postnatal growth*. Dev Biol, 2001. **229**: p. 141-162.
159. D'Ercole, A.J.a.A.S.C., *Editorial review: the case of local versus endocrine IGF-1 action: the jury is still out*. Growth Horm IGF Res, 2001. **11**: p. 261-265.
160. D'Ercole, A.J., *Actions of IGF system proteins from studies of transgenic and gene knockout models*. In: Rosenfeld R, Roberts Jr. CT (eds) The IGF System. Humana Press, Totowa, 1999: p. pp 545-577.
161. DeChiara, T.M., A. Efstratiadis, and E.J. Robertson, *A growth-deficiency phenotype in heterozygous mice carrying an insulin-like growth factor II gene disrupted by targeting*. Nature, 1990. **345**(6270): p. 78-80.
162. Powell-Braxton, L., et al., *IGF-I is required for normal embryonic growth in mice*. Genes Dev, 1993. **7**(12B): p. 2609-17.
163. Liu, J., Baker, J., Perkins, AS., Robertson, EJ, and Efstratiadis, A., *Mice carrying null mutations of the genes encoding insulin-like growth factor I (IGF-I) and type I IGF receptor (IGF-Ir)*. Cell, 1993. **75**: p. 59-72.
164. Baker, J., Liu, JP., Robertson, EJ., and Efstratiadis, A., *Role of insulin-like growth factors in embryonic and post-natal growth*. cell, 1993. **75**: p. 73-90.
165. Liu, J.L., A. Grindberg, H. Westphal, B. Sauer, D. Accili, M. Karas, and D. LeRoith, *Insulin-like growth factor-1 affects perinatal lethality and postnatal development in a*

- gene dosage-dependent manner: manipulation using the Cre/LoxP system in transgenic mice. *Mol Endocrinol*, 1998. **12**: p. 1452-1462.
166. Sjogren, K., et al., *Liver-derived IGF-I is the principal source of IGF-I in blood but is not required for postnatal body growth in mice*. *Proc. Natl. Acad. Sci. USA*, 1999. **96**: p. 7088-7092.
167. Yakar, S., et al., *Normal growth and development in the absence of hepatic insulin-like growth factor I*. *Proc Natl Acad Sci U S A*, 1999. **96**(13): p. 7324-9.
168. Le Roith, D., L. Scavo, and A. Butler, *What is the role of circulating IGF-I?* *Trends Endocrinol Metab*, 2001. **12**(2): p. 48-52.
169. Yakar, S., et al., *Liver-specific igf-1 gene deletion leads to muscle insulin insensitivity*. *Diabetes*, 2001. **50**(5): p. 1110-8.
170. Rinderknecht, E. and R.E. Humbel, *The amino acid sequence of human insulin-like growth factor I and its structural homology with proinsulin*. *J Biol Chem*, 1978. **253**(8): p. 2769-76.
171. Duguay S.J., J.L.-Z., D.F. Steiner, *Mutational analysis of the insulin-like growth factor-I prohormone processing site*. *J. Biol. Chem.*, 1995. **279**: p. 17566-17574.
172. Delafontaine P., H.L., D.G. Harrison, K.E. Bernstein, *Sequence of a cDNA encoding dog insulin-like growth factor-1*. *Gene*, 1993. **130**: p. 305-306.
173. Francis G.L., F.M.U., F.J. Ballard, K.A. McNeil, J.C. Wallace, *Insulin-like growth factor-1 and 2 in bovine colostrum. Sequences and biological activities compared with those of a potent truncated form*. *Biochem J*, 1988. **251**: p. 95-103.
174. Francis G.L., K.A.M.N., J.C. Wallace, F.J. Ballard, P.C. Owens, *Sheep insulin-like growth factor I and II: Sequence, activities and assays*. *Endocrinology*, 1989. **124**: p. 1173-1183.
175. Francis G.L., P.C.O., K.A. McNeil, J.C. Wallace, F.J. Ballard, *Purification, amino acid sequence and assay cross-reactivities of porcine insulin-like growth factor-I and II*. *J Endocrinol*, 1989. **122**: p. 681-687.
176. Shimatsu, A., and Rotwein, P., *Mosaic evolution of the insulin-like growth factors: organization, sequence, and expression of the rat insulin-like growth factor I gene*. *The Journal of Biological Chemistry*, 1987. **262**(16): p. 7894-7900.
177. Bell, G.I., et al., *Sequences of liver cDNAs encoding two different mouse insulin-like growth factor I precursors*. *Nucleic Acids Res*, 1986. **14**(20): p. 7873-82.
178. Sara V.R., C.C.-S., K. Drakenberg et al., *The biological role of truncated insulin-like growth factor-1 and the tripeptide gpe in the central nervous system*. *Ann N Y Acad Sci*, 1993. **692**: p. 183-191.
179. Carlsson-Skwrut, C., et al., *A comparison of the biological activity of the recombinant intact and truncated insulin-like growth factor 1 (IGF-1)*. *Biochim Biophys Acta*, 1989. **1011**(2-3): p. 192-7.
180. Sara, V.R., et al., *Identification of Gly-Pro-Glu (GPE), the aminoterminal tripeptide of insulin-like growth factor 1 which is truncated in brain, as a novel neuroactive peptide*. *Biochem Biophys Res Commun*, 1989. **165**(2): p. 766-71.
181. Rotwein, P., Pollock, K.M., Didier, D.K., and Krivi, G.G., *Organization and sequence of the human insulin-like growth factor gene*. *J Biol Chem*, 1986. **261**: p. 4828-4832.
182. Shimatsu, A. and P. Rotwein, *Sequence of two rat insulin-like growth factor I mRNAs differing within the 5' untranslated region*. *Nucleic Acids Res*, 1987. **15**(17): p. 7196.
183. Bucci, C., et al., *Nucleotide sequence of a genomic fragment of the rat IGF-I gene spanning an alternate 5' non coding exon*. *Nucleic Acids Res*, 1989. **17**(9): p. 3596.
184. Tobin, G., et al., *A novel human insulin-like growth factor I messenger RNA is expressed in normal and tumor cells*. *Mol Endocrinol*, 1990. **4**(12): p. 1914-20.
185. Adamo, M., Ben-Hur, H., LeRoith, D., Roberts, C.T., Jr., *Transcription initiation in the two leader exons of the rat IGF-I gene occurs from disperse versus localized sites*. *Biochem Biophys Res Comm*, 1991. **176**: p. 887-893.
186. Simmons, J.G., et al., *Multiple transcription start sites in the rat insulin-like growth factor-I gene give rise to IGF-I mRNAs that encode different IGF-I precursors and are processed differently in vitro*. *Growth Factors*, 1993. **9**(3): p. 205-21.

187. Yang, H., et al., *Alternative leader sequences in insulin-like growth factor I mRNAs modulate translational efficiency and encode multiple signal peptides*. Mol Endocrinol, 1995. **9**(10): p. 1380-95.
188. Roberts, C., Jr., Lasky, SR., Lowe, WL., JR., Seamon, WT., and LeRoith, D., *Molecular cloning of rat insulin-like growth factory I complementary deoxyribonucleic acids, differential messenger ribonucleic acid processing and regulation by growth hormone in extrahepatic tissue*. Mol Endocrinol, 1987. **1**: p. 243-248.
189. Lund, P.K., E.C. Hoyt, and J.J. Van Wyk, *The size heterogeneity of rat insulin-like growth factor-I mRNAs is due primarily to differences in the length of 3'-untranslated sequence*. Mol Endocrinol, 1989. **3**(12): p. 2054-61.
190. Le Bouc, Y., et al., *Complete characterization of the human IGF-I nucleotide sequence isolated from a newly constructed adult liver cDNA library*. FEBS Lett, 1986. **196**(1): p. 108-12.
191. Adamo, M.L., et al., *Regulation of start site usage in the leader exons of the rat insulin-like growth factor-I gene by development, fasting, and diabetes*. Mol Endocrinol, 1991. **5**(11): p. 1677-86.
192. Jansen, E., et al., *Identification of multiple transcription start sites in the human insulin-like growth factor-I gene*. Mol Cell Endocrinol, 1991. **78**(1-2): p. 115-25.
193. Holthuizen, E., et al., In: *Modern Concepts of Insulin-like Growth Factors* (E.Spencer, ed.); Elsevier, New York, 1991: p. pp. 733-736.
194. Adamo, M.L., et al., *Transcription initiation in the two leader exons of the rat IGF-I gene occurs from disperse versus localized sites*. Biochem Biophys Res Commun, 1991. **176**(2): p. 887-93.
195. Bach, M.A., et al., *Alternative splicing produces messenger RNAs encoding insulin-like growth factor-I prohormones that are differentially glycosylated in vitro*. Mol Endocrinol, 1990. **4**(6): p. 899-904.
196. Jansen, M., et al., *Sequence of cDNA encoding human insulin-like growth factor I precursor*. Nature, 1983. **306**(5943): p. 609-11.
197. Rotwein, P., *Two insulin-like growth factor I messenger RNAs are expressed in human liver*. Proc Natl Acad Sci USA, 1986. **83**: p. 77-81.
198. Chew, S.L., et al., *An alternatively spliced human insulin-like growth factor-I transcript with hepatic tissue expression that diverts away from the mitogenic IBE1 peptide*. Endocrinology, 1995. **136**(5): p. 1939-44.
199. Tan, D.S., A. Cook, and S.L. Chew, *Nucleolar localization of an isoform of the IGF-I precursor*. BMC Cell Biol, 2002. **3**: p. 17.
200. Hepler, J.E., J.J. Van Wyk, and P.K. Lund, *Different half-lives of insulin-like growth factor I mRNAs that differ in length of 3' untranslated sequence*. Endocrinology, 1990. **127**(3): p. 1550-2.
201. Roberts, C.T., Jr., et al., *Rat IGF-I cDNA's contain multiple 5'-untranslated regions*. Biochem Biophys Res Commun, 1987. **146**(3): p. 1154-9.
202. LeRoith, D., amd Roberts, CT., Jr., *At the cutting edge. Insulin-like growth factor I (IGF-1): a molecular basis for endocrine versus local action*. Molecular and Cellular Endocrinology, 1991. **77**: p. C57-C61.
203. Carlsson-Skwirut, C., et al., *Isolation and characterization of variant IGF-1 as well as IGF-2 from adult human brain*. FEBS Lett, 1986. **201**(1): p. 46-50.
204. Sara, V.R., et al., *Characterization of somatomedins from human fetal brain: identification of a variant form of insulin-like growth factor I*. Proc Natl Acad Sci U S A, 1986. **83**(13): p. 4904-7.
205. Lowe, W.L., Jr., et al., *Differential expression of alternative 5' untranslated regions in mRNAs encoding rat insulin-like growth factor I*. Proc Natl Acad Sci U S A, 1987. **84**(24): p. 8946-50.
206. Adamo, M., et al., *Insulin-like growth factor I messenger ribonucleic acids with alternative 5'-untranslated regions are differentially expressed during development of the rat*. Endocrinology, 1989. **124**(6): p. 2737-44.

207. Shemer, J., et al., *Tissue-specific transcription start site usage in the leader exons of the rat insulin-like growth factor-I gene: evidence for differential regulation in the developing kidney*. Endocrinology, 1992. **131**(6): p. 2793-9.
208. Lowe, W.L., Jr., et al., *Distribution and regulation of rat insulin-like growth factor I messenger ribonucleic acids encoding alternative carboxyterminal E- peptides: evidence for differential processing and regulation in liver*. Mol Endocrinol, 1988. **2**(6): p. 528-35.
209. McKoy, G., et al., *Expression of insulin growth factor-1 splice variants and structural genes in rabbit skeletal muscle induced by stretch and stimulation*. J Physiol, 1999. **516**(Pt 2): p. 583-92.
210. Hameed M., R.W.O., M. Cobbold, G. Goldspink, S.D. Harridge, *Expression of insulin-like growth factor-1 in young and old human skeletal muscle after high endurance exercise*. J. Physiology, 2003. **547**: p. 247-254.
211. Yang, S., et al., *Cloning and characterization of an IGF-1 isoform expressed in skeletal muscle subjected to stretch*. J Muscle Res Cell Motil, 1996. **17**(4): p. 487-95.
212. Haddad F., G.R.A., *Selected contribution: Acute cellular and molecular responses to resistance exercise*. J Appl Physiol, 2002. **93**: p. 394-403.
213. Yang, S.F., G.Goldspink, *Different roles of the Igf-1 Ec peptide (mgf) and mature Igf-1 in myoblast proliferation and differentiation*. FEBS Lett, 2002. **522**: p. 156-160.
214. Hill, M., G. Goldspink, *Expression and splicing of the insulin-like growth factor gene in rodent muscle is associated with muscle satellite (stem) cell activation following local tissue damage*. J Physiol, 2003. **549**: p. 409-418.
215. Florini, J., D. Ewton, and S. Coolican, *Growth hormone and the insulin-like growth factor system in myogenesis*. Endocrine Rev., 1996. **17**: p. 481-517.
216. Florini, J., Ewton, D., and Magri, K., *Hormones, growth factors, and myogenic differentiation*. Ann Rev Physiol, 1991. **53**: p. 201-216.
217. Stewart, C., Rotwein, P., *Growth, differentiation, and survival: multiple physiological functions for insulin-like growth factors*. Physiological Reviews, 1996. **76**(4): p. 1005-1026.
218. Fryburg, D.A., *Insulin-like growth factor I exerts growth hormone- and insulin-like actions on human muscle protein metabolism*. Am J Physiol, 1994. **267**(2 Pt 1): p. E331-6.
219. Fryburg, D.A., et al., *Insulin and insulin-like growth factor-I enhance human skeletal muscle protein anabolism during hyperaminoacidemia by different mechanisms*. J Clin Invest, 1995. **96**(4): p. 1722-9.
220. Florini, J.R., et al., *Biphasic concentration dependency of stimulation of myoblast differentiation by somatomedins*. Am J Physiol, 1986. **250**(5 Pt 1): p. C771-8.
221. Rosenthal, S. and Z.-Q. Cheng, *Opposing early and late effects of insulin growth factor I on differentiation and the cell cycle regulatory retinoblastoma protein in skeletal myoblasts*. Proc. Natl. Acad. Sci. USA, 1995. **92**: p. 10307-10311.
222. Engert, J., Berglund, EB., and Rosenthal, N., *Proliferation precedes differentiation in IGF-I stimulated myogenesis*. The Journal of Cell Biology, 1996. **135**(2): p. 431-440.
223. Stiles, C.D., et al., *Dual control of cell growth by somatomedins and platelet-derived growth factor*. Proc Natl Acad Sci U S A, 1979. **76**(3): p. 1279-83.
224. Rubin, R. and R. Baserga, *Insulin-like growth factor-I receptor. Its role in cell proliferation, apoptosis, and tumorigenicity*. Lab Invest, 1995. **73**(3): p. 311-31.
225. Adesanya, O.O., et al., *Insulin-like growth factor 1 is required for G2 progression in the estradiol-induced mitotic cycle*. Proc Natl Acad Sci U S A, 1999. **96**(6): p. 3287-91.
226. Ullrich, A., et al., *Insulin-like growth factor I receptor primary structure: comparison with insulin receptor suggests structural determinants that define functional specificity*. Embo J, 1986. **5**(10): p. 2503-12.
227. Werner, H., et al., *The insulin-like growth factor I receptor: molecular biology, heterogeneity, and regulation*. In: LeRoith D (eds) Insulin-like Growth Factors: Molecular and Cellular Aspects. CRC Press, Boca Raton, 1991: p. pp 17-47.
228. Frattali, A.L., J.L. Treadway, and J.E. Pessin, *Transmembrane signaling by the human insulin receptor kinase. Relationship between intramolecular beta subunit trans- and*

- cis*-autophosphorylation and substrate kinase activation. J Biol Chem, 1992. **267**(27): p. 19521-8.
229. Frattali, A.L. and J.E. Pessin, *Relationship between alpha subunit ligand occupancy and beta subunit autophosphorylation in insulin/insulin-like growth factor-1 hybrid receptors*. J Biol Chem, 1993. **268**(10): p. 7393-400.
230. Treadway, J.L., et al., *Transdominant inhibition of tyrosine kinase activity in mutant insulin/insulin-like growth factor I hybrid receptors*. Proc Natl Acad Sci U S A, 1991. **88**(1): p. 214-8.
231. Treadway, J.L., et al., *Assembly of insulin/insulin-like growth factor-1 hybrid receptors in vitro*. J Biol Chem, 1989. **264**(36): p. 21450-3.
232. Treadway, J.L., A.L. Frattali, and J.E. Pessin, *Intramolecular subunit interactions between insulin and insulin-like growth factor 1 alpha beta half-receptors induced by ligand and Mn/MgATP binding*. Biochemistry, 1992. **31**(47): p. 11801-5.
233. Bailyes, E.M., et al., *Insulin receptor/IGF-I receptor hybrids are widely distributed in mammalian tissues: quantification of individual receptor species by selective immunoprecipitation and immunoblotting*. Biochem J, 1997. **327**(Pt 1): p. 209-15.
234. Soos, M.A., C.E. Field, and K. Siddle, *Purified hybrid insulin/insulin-like growth factor-I receptors bind insulin-like growth factor-I, but not insulin, with high affinity*. Biochem J, 1993. **290**(Pt 2): p. 419-26.
235. Nissley, S.P., W. Kiess, and M.M. Sklar, *The insulin-like growth factor II/ mannose 6-phosphate receptor*. In: LeRoith D (eds) *Insulin-like Growth Factors: Molecular and Cellular Aspects*. CRC Press, Boca Raton, 1991: p. pp 111-150.
236. Ludwig, T., et al., *Mouse mutants lacking the type 2 IGF receptor (IGF2R) are rescued from perinatal lethality in Igf2 and Igf1r null backgrounds*. Dev Biol, 1996. **177**(2): p. 517-35.
237. Morgan, D.O., et al., *Insulin-like growth factor II receptor as a multifunctional binding protein*. Nature, 1987. **329**(6137): p. 301-7.
238. Butler, A.A., et al., *Insulin-like growth factor-I receptor signal transduction: at the interface between physiology and cell biology*. Comp Biochem Physiol B Biochem Mol Biol, 1998. **121**(1): p. 19-26.
239. White, M.F., *The IRS-signalling system: a network of docking proteins that mediate insulin action*. Mol Cell Biochem, 1998. **182**(1-2): p. 3-11.
240. Craparo, A., T.J. O'Neill, and T.A. Gustafson, *Non-SH2 domains within insulin receptor substrate-1 and SHC mediate their phosphotyrosine-dependent interaction with the NPEY motif of the insulin-like growth factor I receptor*. J Biol Chem, 1995. **270**(26): p. 15639-43.
241. Tartare-Deckert, S., et al., *Evidence for a differential interaction of SHC and the insulin receptor substrate-1 (IRS-1) with the insulin-like growth factor-I (IGF-I) receptor in the yeast two-hybrid system*. J Biol Chem, 1995. **270**(40): p. 23456-60.
242. Coolican, S., Samuel, D.S., Ewton, D.Z., McWade, F.J., and Florini, J.R., *The mitogenic and myogenic actions of insulin-like growth factors utilize distinct signaling pathways*. The Journal of Biological Chemistry, 1997. **272**(10): p. 6653-6662.
243. Bennett, A.M. and N.K. Tonks, *Regulation of distinct stages of skeletal muscle differentiation by mitogen-activated protein kinases*. Science, 1997. **278**(5341): p. 1288-91.
244. Giorgetti, S., et al., *The insulin and insulin-like growth factor-I receptor substrate IRS-1 associates with and activates phosphatidylinositol 3-kinase in vitro*. J Biol Chem, 1993. **268**(10): p. 7358-64.
245. Tartare-Deckert, S., et al., *Interaction of the molecular weight 85K regulatory subunit of the phosphatidylinositol 3-kinase with the insulin receptor and the insulin-like growth factor-1 (IGF- I) receptor: comparative study using the yeast two-hybrid system*. Endocrinology, 1996. **137**(3): p. 1019-24.
246. Kaliman, P., et al., *Phosphatidylinositol 3-kinase inhibitors block differentiation of skeletal muscle cells*. J Biol Chem, 1996. **271**(32): p. 19146-51.

247. Kaliman, P., et al., *Insulin-like growth factors require phosphatidylinositol 3-kinase to signal myogenesis: dominant negative p85 expression blocks differentiation of L6E9 muscle cells*. Mol Endocrinol, 1998. **12**(1): p. 66-77.
248. Pinset, C., et al., *Wortmannin inhibits IGF-dependent differentiation in the mouse myogenic cell line C2*. C R Acad Sci III, 1997. **320**(5): p. 367-74.
249. Weintraub, H., et al., *The myoD gene family: nodal point during specification of the muscle cell lineage*. Science, 1991. **251**(4995): p. 761-6.
250. Lassar, A.B., S.X. Skapek, and B. Novitch, *Regulatory mechanisms that coordinate skeletal muscle differentiation and cell cycle withdrawal*. Curr Opin Cell Biol, 1994. **6**(6): p. 788-94.
251. Olson, E.N., M. Perry, and R.A. Schulz, *Regulation of muscle differentiation by the MEF2 family of MADS box transcription factors*. Dev Biol, 1995. **172**(1): p. 2-14.
252. Black, B.L. and E.N. Olson, *Transcriptional control of muscle development by myocyte enhancer factor-2 (MEF2) proteins*. Annu Rev Cell Dev Biol, 1998. **14**: p. 167-96.
253. Lawlor, M.A. and P. Rotwein, *Coordinate control of muscle cell survival by distinct insulin-like growth factor activated signaling pathways*. J Cell Biol, 2000. **151**(6): p. 1131-40.
254. Lawlor, M.A. and P. Rotwein, *Insulin-like growth factor-mediated muscle cell survival: central roles for Akt and cyclin-dependent kinase inhibitor p21*. Mol Cell Biol, 2000. **20**(23): p. 8983-95.
255. Guo, K., et al., *MyoD-induced expression of p21 inhibits cyclin-dependent kinase activity upon myocyte terminal differentiation*. Mol Cell Biol, 1995. **15**(7): p. 3823-9.
256. Halevy, O., et al., *Correlation of terminal cell cycle arrest of skeletal muscle with induction of p21 by MyoD*. Science, 1995. **267**(5200): p. 1018-21.
257. Datta, S.R., A. Brunet, M.E. Greenberg, *Cellular survival: a play in three Akts*. Genes Dev, 1999. **13**: p. 2905-2927.
258. Florini, J.R. and D.Z. Ewton, *Highly specific inhibition of IGF-I-stimulated differentiation by an antisense oligodeoxyribonucleotide to myogenin mRNA. No effects on other actions of IGF-T*. J Biol Chem, 1990. **265**(23): p. 13435-7.
259. Tamir, Y. and E. Bengal, *Phosphoinositide 3-kinase induces the transcriptional activity of MEF2 proteins during muscle differentiation*. J Biol Chem, 2000. **275**(44): p. 34424-32.
260. Lai, K.M., M.Gonzalez, W.T. Poueymirou, W.O. Kline, E. Na, E. Zlotchenko, T.N. Stitt, A.N. Economides, G.D. Yancopoulos, D.J. Glass, *Conditional activation of Akt in adult skeletal muscle induces rapid hypertrophy*. Mol Cell Biol, 2004. **24**: p. 9295-9304.
261. Song, Y.H., et al., *Insulin-like growth factor I-mediated skeletal muscle hypertrophy is characterized by increased mTOR-p70S6K signaling without increased Akt phosphorylation*. J Investig Med, 2005. **53**(3): p. 135-42.
262. Sandri, M., U. Carraro, M. Podhorska-Okolov, C. Rizzi, P. Arslan, D. Monti, C. Franceschi, *Apoptosis, DNA damage and ubiquitin expression in normal and mdx muscle fibers after exercise*. FEBS Lett, 1995. **373**: p. 291-295.
263. Brunet, A., A. Bonni, M.J. Zigmond, M.Z. Lin, P. Jou, L.S. Hu, M.J. Anderson, K.C. Arden, J. Blenis, M.E. Greenberg, *Akt promotes cell survival by phosphorylating and inhibiting a Forkhead transcription factor*. Cell, 1999. **96**: p. 857-868.
264. Datta, S.R., et al., *Akt phosphorylation of BAD couples survival signals to the cell-intrinsic death machinery*. Cell, 1997. **91**(2): p. 231-41.
265. del Peso, L., et al., *Interleukin-3-induced phosphorylation of BAD through the protein kinase Akt*. Science, 1997. **278**(5338): p. 687-9.
266. Gross, A., *BCL-2 proteins: regulators of the mitochondrial apoptotic program*. IUBMB Life, 2001. **52**(3-5): p. 231-6.
267. Zimmermann, K.C., C. Bonzon, and D.R. Green, *The machinery of programmed cell death*. Pharmacol Ther, 2001. **92**(1): p. 57-70.
268. Minshall, C., et al., *IL-4 and insulin-like growth factor-I inhibit the decline in Bcl-2 and promote the survival of IL-3-deprived myeloid progenitors*. J Immunol, 1997. **159**(3): p. 1225-32.

269. Minshall, C., et al., *Phosphatidylinositol 3'-kinase, but not S6-kinase, is required for insulin-like growth factor-I and IL-4 to maintain expression of Bcl-2 and promote survival of myeloid progenitors*. J Immunol, 1999. **162**(8): p. 4542-9.
270. Parrizas, M. and D. LeRoith, *Insulin-like growth factor-1 inhibition of apoptosis is associated with increased expression of the bcl-xL gene product*. Endocrinology, 1997. **138**(3): p. 1355-8.
271. Parrizas, M., A.R. Saltiel, and D. LeRoith, *Insulin-like growth factor 1 inhibits apoptosis using the phosphatidylinositol 3'-kinase and mitogen-activated protein kinase pathways*. J Biol Chem, 1997. **272**(1): p. 154-61.
272. Peruzzi, F., et al., *Multiple signaling pathways of the insulin-like growth factor 1 receptor in protection from apoptosis*. Mol Cell Biol, 1999. **19**(10): p. 7203-15.
273. Sasaoka, T., et al., *Shc is the predominant signaling molecule coupling insulin receptors to activation of guanine nucleotide releasing factor and p21ras-GTP formation*. J Biol Chem, 1994. **269**(14): p. 10734-8.
274. Jin, S., Zhuo Y., Guo W., Field G., *p21-activated Kinase 1 (Pak1)-dependent Phosphorylation of Raf-1 Regulates Its Mitochondrial Localization, Phosphorylation of BAD, and Bcl-2 Association*. J. Biol. Chem., 2005. **280**(26): p. 24698-24705.
275. Olson, E.N.a.R.S.W., *Calcineurin signaling and muscle remodeling*. Cell, 2000. **101**: p. 689-692.
276. Guerini, D. and C.B. Klee, *Cloning of human calcineurin A: evidence for two isozymes and identification of a polyproline structural domain*. Proc Natl Acad Sci U S A, 1989. **86**(23): p. 9183-7.
277. Crabtree, G.R., *Generic signals and specific outcomes: signaling through Ca²⁺, calcineurin, and NF-AT*. Cell, 1999. **96**(5): p. 611-4.
278. Musaro, A., and Rosenthal, N., *Maturation of the myogenic program is induced by post-mitotic expression of IGF-I*. Mol Cell Biol, 1999. **19**(4): p. 3115-24.
279. Semsarian, C., et al., *Skeletal muscle hypertrophy is mediated by a Ca²⁺-dependent calcineurin signalling pathway*. Nature, 1999. **400**(6744): p. 576-81.
280. Dunn, S.E., E.R. Chin, and R.N. Michel, *Matching of calcineurin activity to upstream effectors is critical for skeletal muscle fiber growth [In Process Citation]*. J Cell Biol, 2000. **151**(3): p. 663-72.
281. Friday, B.B., V. Horsley, and G.K. Pavlath, *Calcineurin activity is required for the initiation of skeletal muscle differentiation*. J Cell Biol, 2000. **149**(3): p. 657-66.
282. Musaro, A., et al., *IGF-1 induces skeletal myocyte hypertrophy through calcineurin in association with GATA-2 and NF-ATc1*. Nature, 1999. **400**(6744): p. 581-5.
283. Davis, E., C.H. Jensen, H.D. Schroder, F. Farnir, T. Shay-Hadfield, A. Kliem, N. Cockett, M. Georges, C. Charlier, *Ectopic expression of DLK1 protein in skeletal muscle of padumnal heterozygotes causes the callipyge phenotype*. Curr Biol, 2004. **14**: p. 1858-1862.
284. Naya, F.J., et al., *Stimulation of slow skeletal muscle fiber gene expression by calcineurin in vivo*. J Biol Chem, 2000. **275**(7): p. 4545-8.
285. Musaro, A. and N. Rosenthal, *Maturation of the myogenic program is induced by postmitotic expression of insulin-like growth factor I*. Mol Cell Biol, 1999. **19**(4): p. 3115-24.
286. Wesselborg, S., D.A. Fruman, J.K. Sagoo, B.E. Bierer, S.J. Burakoff, *Identification of a physical interaction between calcineurin and nuclear factor of activated T cells (NFATp)*. J Biol Chem, 1996. **271**: p. 1274-1277.
287. Coleman, M., DeMayo, F., Yin, KC., Lee, HM., Geske, R., Montgomery, C., and Schwartz, R.J., *Myogenic vector expression of insulin-like growth factor I stimulate myocyte differentiation and myofiber hypertrophy in transgenic mice*. The Journal of Biological Chemistry, 1995. **270**(20): p. 12109-12116.
288. Reiss, K., Cheng, W., Ferber, A., Kajstura, J., Li, P., Li, B., Olivetti, G., Homcy, C.J., Baserga, R., Anversa, P., *Overexpression of insulin-like growth factor-I in the heart is coupled with myocyte proliferation in transgenic mice*. Proc Natl Acad Sci USA, 1996. **93**: p. 8630-8635.

289. Li, Q., Li, B., Wang, X., Leri, A., Jana, KP., Liu, Y., Kajstura, J., Baserga, R., and Anversa, P., *Overexpression of insulin-like growth factor-I in mice protects from myocyte death after infarction attenuating ventricular dilation, wall stress, and cardiac hypertrophy*. J Clin Invest, 1997. **100**: p. 1991-1999.
290. Gossen, M.a.H.B., *Tight control of gene expression in mammalian cells by tetracycline-responsive promoters*. PNAS USA, 1992. **89**(12): p. 5547-51.
291. Baron, U.a.H.B., *Tet repressor-based system for regulated gene expression in eukaryotic cells: principles and advances*. Methods Enzymol, 2000. **327**: p. 401-421.
292. Bonin, A.L., M. Gossen, and H. Bujard, *Photinus pyralis luciferase: vectors that contain a modified luc coding sequence allowing convenient transfer into other systems*. Gene, 1994. **141**(1): p. 75-7.
293. Baron, U., et al., *Co-regulation of two gene activities by tetracycline via a bidirectional promoter*. Nucleic Acids Res, 1995. **23**(17): p. 3605-6.
294. Andersen, J., *In: Atlas of skeletal muscle pathology*. 1985: Lancaster:MTP press limited. p168.
295. Sue, S.C., et al., *Heparin binding stabilizes the membrane-bound form of cobra cardiotoxin*. J Biol Chem, 2002. **277**(4): p. 2666-73.
296. Siegfried, J.M., et al., *A mitogenic peptide amide encoded within the E peptide domain of the insulin-like growth factor IB prohormone*. Proc Natl Acad Sci U S A, 1992. **89**(17): p. 8107-11.
297. Florini, J.R.a.D.Z.E., *IGFs, muscle growth, and myogenesis*. Diabetes Reviews, 1995. **3**(1): p. 73-92.
298. Hendzel, M.J., et al., *Mitosis-specific phosphorylation of histone H3 initiates primarily within pericentromeric heterochromatin during G2 and spreads in an ordered fashion coincident with mitotic chromosome condensation*. Chromosoma, 1997. **106**(6): p. 348-60.
299. Fiorotto, M.L., R.J. Schwartz, and M.C. Delaughter, *Persistent IGF-1 overexpression in skeletal muscle transiently enhances DNA accretion and growth*. Faseb J, 2003. **17**: p. 59-60.
300. Shavlakadze, T., N.Winn, N. Rosenthal, and M. Grounds, *Reconciling data from transgenic mice that overexpress IGF-1 specifically in skeletal muscle*. Growth Horm IGF Res, 2005. **15**: p. 4-18.
301. Skurk, C., et al., *The FOXO3a transcription factor regulates cardiac myocyte size downstream of AKT signaling*. J Biol Chem, 2005. **280**(21): p. 20814-23.
302. Hall, R.K., et al., *Regulation of phosphoenolpyruvate carboxykinase and insulin-like growth factor-binding protein-1 gene expression by insulin. The role of winged helix/forkhead proteins*. J Biol Chem, 2000. **275**(39): p. 30169-75.
303. Hemers, E., et al., *Insulin-like growth factor binding protein-5 is a target of matrix metalloproteinase-7: implications for epithelial-mesenchymal signaling*. Cancer Res, 2005. **65**(16): p. 7363-9.
304. Dominov, J.A., et al., *Pro- and anti-apoptotic members of the Bcl-2 family in skeletal muscle: a distinct role for Bcl-2 in later stages of myogenesis*. Dev Dyn, 2001. **220**(1): p. 18-26.
305. Dominov, J.A., et al., *Muscle-specific BCL2 expression ameliorates muscle disease in laminin {alpha}2-deficient, but not in dystrophin-deficient, mice*. Hum Mol Genet, 2005. **14**(8): p. 1029-40.
306. Sun, Q., et al., *General splicing factor SF2/ASF promotes alternative splicing by binding to an exonic splicing enhancer*. Genes Dev, 1993. **7**(12B): p. 2598-608.
307. Engert, J.C., E.B. Berglund, and N. Rosenthal, *Proliferation precedes differentiation in IGF-I-stimulated myogenesis*. J Cell Biol, 1996. **135**(2): p. 431-40.
308. Yang, S.Y. and G. Goldspink, *Different roles of the IGF-I Ec peptide (MGF) and mature IGF-I in myoblast proliferation and differentiation*. FEBS Lett, 2002. **522**(1-3): p. 156-60.
309. Florini, J.R., D.Z. Ewton, and S.L. Roof, *Insulin-like growth factor-I stimulates terminal myogenic differentiation by induction of myogenin gene expression*. Mol Endocrinol, 1991. **5**(5): p. 718-24.

310. Semsarian, C., et al., *Insulin-like growth factor (IGF-I) induces myotube hypertrophy associated with an increase in anaerobic glycolysis in a clonal skeletal-muscle cell model*. Biochem J, 1999. **339 (Pt 2)**: p. 443-51.
311. Barton, E.R., *Viral expression of Insulin-like Growth Factor-I isoforms promotes different responses in skeletal muscle*. J Appl Physiol, 2006.